

SETTLEMENT OF DRY COHESIONLESS
SOIL DEPOSITS
UNDER EARTHQUAKE INDUCED LOADING

by

Jamal I Ramadan

A Dissertation Presented to the
FACULTY OF THE GRADUATE SCHOOL
UNIVERSITY OF SOUTHERN CALIFORNIA
In Partial Fulfillment of the
Requirements for the Degree
DOCTOR OF PHILOSOPHY
(CIVIL ENGINEERING)

December 2007

Copyright 2007

Jamal Ibrahim Ramadan

DEDICATION

This work is dedicated to my father Ibrahim, my mother Hana, my sisters Feryal and her family, Gada, Fadia and to my wife Monica, without their love and support, it could have never been attempted, much less completed.

ACKNOWLEDGEMENTS

From beginning to end, my career as a doctoral candidate has spanned over many years. To fully thank everyone involved in making this project possible would require a second volume at least as large as the document before the reader. If I have left anyone off this list please realize that you are only missing from this page, not from my mind. My deepest appreciation goes to my advisor, Doctor Geoffrey R. Martin for the patience, advice, understanding and professionalism that he demonstrated throughout the process of bringing this document to end. My gratitude also goes to the members of my dissertation committee, Dr. M. D. Trifunac, for his guidance, Dr. L. Carter Wellford and Dr. Hung Leung Wong for their encouragement and Dr. Frank Corsetti and his department of Earth Science for his help in the mineralogy and grains shape analysis. My deepest appreciation goes to Dr. Mladen Vucetic and Dr. Chu-Chung Hsu for helping me using their soil testing laboratory at UCLA and, Dr. Jonathan Stewart and his team, Dr. Daniel Whang and Dr. Pendo Duku For providing me with the database they documented and conducting more laboratory testing when needed and also to Dr. Ricardo Dobry and Dr. Tarek Abdoun for their guidance and for their insights and recommendations. Special thanks go to Lester Fruth at Leighton and Associates for allowing me the use of their laboratory. A special word of thanks goes to the staff members in the Department of Civil Engineering at the University of Southern California.

A special word of thanks also goes to the peoples at Earth Mechanics and in particular to Mike Kapuskar.

I would like also to thank my fellow graduate students for their friendship, input, and support over the years. This group includes, but is certainly not limited to, Qui P., Nick Mace, Andy Dodds, Jianping Hu, Yang Soo Lee, Liping Yan, Fang Lui, Nazila Moukarram and Hossein Ataei.

And very special thanks to the special person who has made it possible for me to achieve my goal, my wife Monica.

TABLE OF CONTENTS

DEDICATION	ii
ACKNOWLEDGEMENTS.....	iii
LIST OF TABLES	ix
LIST OF FIGURES	x
LIST OF SYMBOLS	xviii
ABSTRACT	xx
Chapter 1 INTRODUCTION	1
1.1 Earthquake Induced Settlement	1
1.2 Compacted Structural Fills	2
1.3 Observed Behavior of Structural Fills During Earthquakes	2
1.4 Motivation for the Present Study	5
1.5 Objectives of the Investigation	5
1.6 Outline of this Document.....	7
Chapter 2 PREVIOUS RESEARCH ON SETTLEMENT OF DRY OR PARTIALLY SATURATED SAND	9
2.1 Introduction.....	9
2.2 Silver and Seed (1971).....	9
2.3 Seed and Silver (1972).....	12
2.4 Youd (1972).....	14
2.5 Pyke et al. (1975)	15
2.6 Martin et. al (1975)	17
2.7 Tokimatsu and Seed (1987)	18
Chapter 3 THE COMPUTER PROGRAM DESRA	21
3.1 Introduction.....	21
3.2 DESRA-MUSC Program.....	21
3.3 Energy-Transmitting Boundary	26
3.4 Volumetric Changes Analysis During Drained Non-Uniform Cyclic Loading.....	28
3.5 A Review of Martin et al. Constitutive Model	31
3.6 Hardening Parameters	33
3.7 Pore-Water Pressure Increase During Undrained Tests.....	37

Chapter 4	THE LABORATORY TESTING PROGRAM	39
4.1	Significance of Dynamic and Cyclic Soil Behavior Parameters in Civil Engineering	39
4.2	Simulation of Field Conditions by Direct Simple Shear Testing	40
4.3	Characterization of Dynamic and Cyclic Behavior	43
4.3.1	Definition of Parameters	43
4.3.2	Modulus Reduction Curve, G_s versus γ_c , Presented in a Semi-Log Format	45
4.3.3	Normalized Modulus Reduction Curve, G/G_{max} versus γ_c , Presented in a Semi-Log Format.....	46
4.3.4	Equivalent Viscous Damping Ratio Curve, λ versus γ_C , Presented in a Semi-Log Format	46
4.3.5	Vertical Settlement Strain, ε_v , versus Number of Cycles, N	47
4.4	Scope of the Experimental Investigation	48
4.4.1	Soil Samples Tested and Analyzed.....	48
4.4.2	Types of Cyclic and Dynamic Direct Simple Shear Tests Conducted	49
4.4.3	Types of Classification of Tests Conducted	49
4.4.4	Cyclic and Dynamic Testing Equipment	50
4.4.5	Standard NGI Direct Simple Shear Test	51
4.4.6	Boundary Conditions in NGI Type Simple Shear Test.....	55
4.5	Brief Review of two Theoretical Studies on the Stress and Strain Distributions in the Simple Shear Specimen	57
4.6	Review of Some Experimental Studies on Stress Distribution.....	59
4.7	Examples Direct Simple Shear (DSS-L) test results.....	60
4.7.1	Synthesis of Modulus Reduction and Damping Results From Tests... ..	64
4.7.2	Identification and Inspection of The Cyclic Stress-Strain Loops	65
4.8	Organization of the Data Into the "Microsoft Excel" Worksheet Files	66
4.9	Input of the Data Into the Database	66
4.10	Soils Tested.....	68
4.10.1	Preparation of Specimen	71
4.10.2	Grain Size Characteristics	72
4.10.3	Maximum and Minimum Void Ratios	72
4.10.4	Specific Gravity	73
4.10.5	Cyclic Simple Shear Testing.....	73
4.10.6	Uniformity of Loadings.....	75
4.10.7	Components of Loadings	75
4.10.8	Factors Affecting Cyclic Response of Soil	76
4.10.9	Specimen Size	76
4.10.10	Shape of the Loading Pattern	77
Chapter 5	DEVELOPMENT OF DATA BASE.....	78
5.1	Introduction.....	78
5.2	Data Presentation	79

5.2.1	Data Obtained From Previous Studies	79
5.2.2	Tested Sands	82
5.2.3	UCLA Test Program Data.....	84
Chapter 6	MINERALOGY AND PARTICLE CHARACTERISTICS ANALYSIS	88
6.1	Introduction.....	88
6.2	X-Ray Powder Diffraction Method	89
6.2.1	Electromagnetic Properties of X-Rays.....	92
6.2.2	X-Rays and Crystalline Solids	93
6.2.3	How Diffraction Patterns are Made	94
6.2.4	Purpose of X-Ray Diffraction	95
6.2.5	Instrumentation	98
6.2.6	Deriving Bragg's Law	100
6.3	Results of X-Ray powder Diffraction analysis	102
6.4	Petrographic Analysis	103
6.4.1	The Nature of Polarised Light.....	105
6.4.2	Double Refraction	106
6.4.3	Common Minerals in Igneous Rocks:.....	106
6.5	Results of Petrographic Analysis	108
Chapter 7	GRAIN PACKING OF SPHERES	115
7.1	Introduction.....	115
7.2	Theory	118
7.3	Maximum and Minimum Dry Densities of Cohesionless Soils.....	120
7.4	Homogeneous Sphere Models	121
7.5	Heterogeneous Sphere Models	123
7.6	Theoretical Packing	127
7.7	Experimental Packing	128
7.8	Ternary and Quarternary Packing	130
7.9	Optimum Grain-Size Relations for Dense Packing	133
7.10	Maximum Void Ratios of Spherical Particles	135
7.11	Effects of Fines in Sands with Non-Spherical Particles	137
7.12	Experimental Study.....	139
7.13	Procedures for Minimum and Maximum void ratios.....	140
7.14	Santamarina et.al Studies(2004)	141
Chapter 8	DATA ANALYSIS PROCEDURE AND RESULTS	143
8.1	Tests Evaluated in Terms of Sand Type or Characteristics	144
8.2	Tests Evaluated in Terms of the Mineral Composition of Sand.....	145
8.3	Tests Evaluated in Terms of Grains Size and Shape	147
8.4	Grain Size Distribution and Grain Shape.....	149
8.5	Tests Evaluated in Terms of Soil Relative Density	151
8.5.1	Tests Evaluated in Terms of Soil Overconsolidation Ratio	152
8.5.2	Tests Evaluated in Terms of Applied Shear Strain	153

8.6	Overall Evaluation of the Results	154
8.7	Settlement of Sands in Term of Mineral Composition	155
8.8	Settlement of Non-Plastic Silty Sands	157
8.9	Effect of Fines Content	160
8.10	Effect of Over Consolidation Ratio	164
Chapter 9	PARAMETRIC ANALYSES USING DESRA-MUSC	166
9.1	Introduction.....	166
9.2	Settlement Analysis using the Computer Program DESRA-MUSC.	167
9.3	Errors in Tokimatsu and Seed Procedure.....	172
9.3.1	Effect of Sand Type or Characteristics	172
9.3.2	Effect of the Equivalent Number of Cycles Concept.....	176
9.4	Discussion on Implications for Liquefaction Analysis	178
9.4.1	Pore-Water Pressure Increase During Undrained Tests.....	178
9.4.2	Liquefaction Resistance of Sands	180
9.4.3	Settlement and Liquefaction of Four Types of Sands.....	181
9.5	Recommendations for a Settlement Design Approach	183
9.5.1	Design Approach Using DESRA or DESRA-MUSC With Time History Input	183
9.5.2	Design Approach Using a Modified Tokimatsu and Seed Procedure	185
Chapter 10	SUMMARY AND CONCLUSIONS	186
10.1	The objective of Research.....	186
10.2	Research Findings and Recommendations	187
10.3	Recommendations for Future Research	189
REFERENCES	190
APPENDICES	196
Appendix A	DATABASE FOR NEVADA SAND.....	197
Appendix B	DATABASE FOR SILICA #30 SAND	198
Appendix C	DATABASE FOR CLEAN SAND, (QUARTZ, DR= 60%).....	199
Appendix D	DATABASE FOR CLEAN MATERIALS SAND (DR =60%).....	200
Appendix E	DATABASE FOR SEVERAL SAND (DR =40%)	201
Appendix F	SOILS WITH FINES PARAMETERS	202
Appendix G	VOLUME CHANGE CONSTANTS.....	203
Appendix H	X-RAY DIFFRACTION RESULTS	204
Appendix I	THIN SECTION RESULTS.....	212

LIST OF TABLES

Table 4-1	Index properties of tested sand.....	69
Table 4-2	Index Properties of previous history tested sands	69
Table 4-3	Index Properties of UCLA tested sands	70
Table 6-1	Mineral composition of sands	102
Table 6-2	Mineral composition of sands	114
Table 8-1	Sand- Silt mixtures used by in the UCLA testing program.....	161
Table 9-1	Values of C1, C2, C3 and C4 for the three relative densities	168

LIST OF FIGURES

Figure 1-1	Site locations where fill movements caused significant damage during Northridge earthquake (Stewart et al., 2001)	4
Figure 2-1	Effect of Relative Density on Settlement in 10 Cycles.....	11
Figure 2-2	Effect of relative density on settlement of dry sand (Silver and Seed, 1971).....	11
Figure 2-3	Settlement-number-of-cycles-relationships for DR = 60%) Silver and Seed, 1971)	12
Figure 2-4	Soil profile Analyzed by Silver and Seed (1971) and by Tokimatsu and Seed (1987).....	13
Figure 2-5	Relationship between shear modulus and shear strain for sand (Seed et al.1984).....	13
Figure 2-6	Comparison of vertical strains at 10 cycles for Ottawa sand (Youd, 1972) and Crystal Silica sand (Silver and Seed, 1971) at $D_r = 80\%$	15
Figure 2-7	Comparison of settlements of sand from shaking table tests performed (a) Under unidirectional and bi-directional stress-controlled loading and (b) Under three-directional stress-controlled loading (Pyke et al., 1975).....	16
Figure 2-8	Reduction factor to estimate the variation of the cyclic shear stress	20
Figure 2-9	Relationship between volumetric strain ratio and earthquake magnitude for dry sands. (After Tokimatsu and Seed, 1987)	20
Figure 3-1	Effect of number of stress cycles on shear modulus-shear strain relationship for medium dense Silica sand ($D_r = 60\%$) (After Silver and Seed 1971)	22
Figure 3-2	The Iwan model.....	25
Figure 3-3	Typical stress-strain loop from the Iwan model.....	26
Figure 3-4	Incremental volumetric strain curves (After Martin et al. 1975)	29
Figure 3-5	Volumetric Strain Curves for Constant Cyclic Shear Strain Amplitude tests (After Martin et al. 1975)	29
Figure 3-6	Settlement Data from Cyclic Simple Shear Tests (Pyke 1973)	30

Figure 3-7	Incremental Volumetric Strain Curves.....	32
Figure 3-8	Volumetric Strain curves versus Number of Cycles	33
Figure 3-9	The Effect of Cyclic Shear Strain Amplitude and Volumetric Strain on Drained Stress-Strain Relationship (Martin et al.1975).....	35
Figure 3-10	The Effect of Cyclic Shear Strain Amplitude and Volumetric Strain on Drained Shear Modulus-Shear Strain Relationship (Martin et al.1975).....	35
Figure 3-11	Variation of the G_{max} and τ_{max} versus the volumetric change	36
Figure 4-1	Idealized stress- strain conditions of a soil element during earthquakes	41
Figure 4-2	Multi-degree-of freedom lumped parameter model representation of horizontally layered soil deposit shaken at the base by a vertically propagating horizontal shear wave.....	42
Figure 4-3	Idealized cyclic stress-strain loop	42
Figure 4-4	Definition of the equivalent viscous damping ratio, λ	44
Figure 4-5	Modulus reduction and damping curves	45
Figure 4-6	Incremental volumetric change versus number of cycles (Pyke 1975).....	47
Figure 4-7	Applied shear strain history for three cyclic strain controlled tests	48
Figure 4-8	Variation of vertical strain with number of cycles	48
Figure 4-9	View of the NGI direct simple shear device with hydraulic actuator at the UCLA Soil Dynamics Laborator.....	52
Figure 4-10	The NGI simple shear device at UCLA with the description of components.....	53
Figure 4-11	Illustration of the principles of testing with the NGI direct simple shear device	54
Figure 4-12	View of the specimen setup after shearing in a static test.....	55
Figure 4-13	Simple shear and pure shear conditions	56
Figure 4-14	Stress distribution on the specimen boundaries and corresponding resultant forces (Vucetic and Lacasse, 1982).....	56

Figure 4-15	Normal stress distribution at specimen boundary (Lucks et al., 1972)	58
Figure 4-16	Typical stress- strain plot obtained with the DSS-L	60
Figure 4-17	Example of shear strain time history results for Silica sand	61
Figure 4-18	Example of shear stress time history results for Silica sand	61
Figure 4-19	Example of volumetric strain time history results for Silica sand	62
Figure 4-20	Example of cyclic loops for Silica Sand	62
Figure 4-21	Example of shear strain versus vertical displacement.....	63
Figure 4-22	Example of shear strain versus number of cycles	63
Figure 4-23	Example of horizontal load versus number of cycles.....	64
Figure 4-24	Example of vertical displacement versus number of cycles.....	64
Figure 4-25	Degradation of G/G_{max} versus shear strain.....	65
Figure 4-26	Vibrating Table and Mold used in computing e_{min} (ASTM 4353).....	74
Figure 5-1	Vertical Settlement versus the number of Cycles	80
Figure 5-2	Vertical Settlement versus the number of Cycles (Pyke 1975).....	80
Figure 5-3	Vertical Settlement versus the number of Cycles (Bathia,1980)	81
Figure 5-4	Vertical Settlement versus the number of Cycles (Chung 2004)	81
Figure 5-5	Size distribution of Nevada and Silica # 30 sands	83
Figure 5-6	Vertical Settlement versus the number of Cycle (OCR=1, $\gamma=0.1\%$).....	83
Figure 5-7	Vertical Settlement versus the number of Cycle (OCR=1, $\gamma=0.1\%$).....	84
Figure 5-8	Vertical Settlement versus the number of Cycles (Stewart 2004).....	85
Figure 5-9	Variation of volumetric strain with cyclic shear strain for Newhall Sand	86
Figure 5-10	Variation of volumetric strain with cyclic shear strain for Pacoima 3 Sand.....	86

Figure 5-11	Variation of volumetric strain with cyclic shear strain for Flint 16 Sand.....	86
Figure 5-12	Effect of silt content on seismic compression of Silica host sand.....	87
Figure 5-13	Effect of silt content on seismic compression of NSF host sand	87
Figure 6-1	Electromagnetic spectrum. The colors of the visible range of the spectrum are abbreviated violet (V), indigo (I), blue (B), green (G), yellow (Y), orange (O), and red (R).....	93
Figure 6-2	A schematic of X-ray diffraction	94
Figure 6-3	Reflection of x-rays from two planes of atoms in a solid	96
Figure 6-4	X-ray diffraction pattern for Silica #2 Sand.....	97
Figure 6-5	X-ray diffraction pattern for NSF Sand.....	98
Figure 6-6	Schematic of an X-ray powder diffractometer	99
Figure 6-7	Deriving Bragg's Law using the reflection geometry and applying trigonometry. The lower beam must travel the extra distance (AB + BC) to continue traveling parallel and adjacent to the top beam.	101
Figure 6-8	Thin Section	104
Figure 6-9	The Polarising Microscope.....	105
Figure 6-10	Quartz	107
Figure 6-11	Plagioclase.....	107
Figure 6-12	Calcite.....	108
Figure 6-13	Sphericity and Roundness chart Diagonal dotted line correspond to constant particle regularity $\rho = (R+S)/2$ (Santamarina et al.2004.....	110
Figure 6-14	Silica 0 Sand.....	110
Figure 6-15	Silica 1 Sand.....	111
Figure 6-16	F-110 Sand	111
Figure 6-17	Flint 16 Sand	112
Figure 6-18	Pacoima 1 Sand, Microcline Feldspar Grain.....	112

Figure 6-19	Newhall Volcanic Fragments Sand	113
Figure 6-20	NSF Metamorphic Fragment Foliation Sand	113
Figure 6-21	Post Office Feldspar Sand	113
Figure 7-1	(a) Simple Cubic, Packing fraction=0.52; (b) Body Centered Cubic, Packing fraction=0.68; (c) Face Centered Cubic Packing fraction=0.74	117
Figure 7-2	Envelope geometries and elementary cells for different types of spheremodels. A: and B: Cubic densest packing (density of elementary cell approx. 0.78). C: and D: Hexagonal densest packing (density of elementary cell approx. 0.91). E: Continuous three-size densest packing (density of elementary cell approx. 0.78). F: Fractal three-size densest packing (density of elementary cell approx. 0.96); (A to D after Leppmeier, 1997).....	118
Figure 7-3	Volume fraction vs. aspect ratio for prolate (○), oblate (□), and aspherical (◇) ellipsoids	118
Figure 7-4	Number of contact points vs. aspect ratio for prolate (○), oblate (□) ellipsoids and aspherical (◇) ellipsoids.....	118
Figure 7-5	Theoretical packing of mono-sized spheres, (a) simple packing, (b) single stagger, (c) double stagger, (d) tetrahedral	122
Figure 7-6	Schematic diagram of theoretical variation of minimum void ratio in binary packing with % fines (Lade, 1998)	123
Figure 7-7	Shematic diagram of filling void between large particles with smaller particles (Lade 1998).....	124
Figure 7-8	Schematic diagram of increasing % fines from B to C,(Lade 1998)	124
Figure 7-9	Effect of % fines and ratio of diameters of large and small spherical steel shot on e_{min} (Lade 1998).....	125
Figure 7-10	Minimum void ratio versus the ratio of large diameter to the small diameter (Lade 1998)	125
Figure 7-11	Theoretical and experimental grain size distribution to produce the densest possible quaternary packing of spherical particles (Mc Geary 1961).....	126
Figure 7-12	Variation of maximum and minimum void ratio for binary mixtures of particles (Lade 1998).....	126

Figure 7-13	Random homogeneous single-layer sphere models after a volume increase of 10%: A: Random single-size sphere model. B: Random fractal three-size sphere model, showing the incomplete filling of the interstitial spaces with the use of the same number of spheres as the symmetric fractal model. C: Random continuous three-size sphere model. Note the similar occupation of the available volume of models A, and B, and the settlement effect of model C in the same available volume.	131
Figure 7-14	Symmetric single-layer sphere models for densest packing within a constant volume. A: Hexagonal densest packing, single-size sphere model. B: Fractal three-size sphere model (Appolonian Packing). C: Continuous three-size sphere model.	132
Figure 7-15	Random heterogeneous single-layer sphere models with 10% of weak spheres (dark colour). The weak grains are distributed randomly. Models A, B, and C compare to Figure 7-13.	133
Figure 7-16	Variation of grains particle size and shape – important factors for packing density.....	139
Figure 7-17	Effect of particle shape on extreme void ratios (natural sands with $C_u \leq 2.5$).	142
Figure 8-1	Settlement of 18 types of sands under uniform cyclic loading.	144
Figure 8-2	Settlement of sands under uniform cyclic loading.....	145
Figure 8-3	Grain size distribution.....	146
Figure 8-4	Settlement of sands under uniform cyclic loading.....	146
Figure 8-5	Settlement of sands under uniform cyclic loading.....	147
Figure 8-6	Settlement of sands under uniform cyclic loading.....	148
Figure 8-7	Grain distribution curves for Flint 13 and 16.....	148
Figure 8-8	F-110 (top), Nevada (middle) and F-110 (bottom).....	150
Figure 8-9	Settlement of Nevada sand under uniform cyclic loading and with OCR =1 and OCR = 4.	152
Figure 8-10	Settlement of Silica # 30 sand under uniform cyclic loading and OCR =1 and OCR= 4.	153

Figure 8-11	Settlement versus shear strain, %	153
Figure 8-12	Typical Variation of Void ratio	154
Figure 8-13	Settlement of pure quartz sand ($D_r = 60\%$) versus $e - e_{min}$	156
Figure 8-14	Settlement of materials sand ($D_r = 60\%$) versus $e - e_{min}$	156
Figure 8-15	Settlement of all sands ($D_r = 60\%$) versus ($e - e_{min}$)	157
Figure 8-16	Variation of Index Void Ratios with Silt Content, Vulcan Host Sand (right) Silica #2 Host Sand (left)	159
Figure 8-17	$e - e_{min}$ versus fine content for Vulcan Host Sand (Stewart et.al, 2004) ..	162
Figure 8-18	$e - e_{min}$ versus fine content for Silica #2 Host sand (Stewart et.al, 2004)	162
Figure 8-19	Settlement of sands versus ($e - e_{min}$) for Vulcan Host sand and For Silica #2 Host Sand	163
Figure 8-20	Settlement of sands versus ($e - e_{min}$)	164
Figure 8-21	Settlement of sands versus ($e - e_{min}$) for OCR= 1,2 and 4	165
Figure 9-1	Volumetric Strain curves versus Number of Cycles for constant shear strain amplitude of 0.1 %.	167
Figure 9-2	Soil profile Analyzed by Tokimatsu and Seed (1987)	169
Figure 9-3	Relationship between shear modulus and shear strain for sand	169
Figure 9-4	Effect of Relative Density on Settlement in 10 Cycles (Silver and Seed 1971)	170
Figure 9-5	Settlement versus depth for relative density ($D_r = 45\%$)	170
Figure 9-6	Settlement versus depth for relative density ($D_r = 60\%$)	171
Figure 9-7	Settlement versus depth for relative density ($D_r = 80\%$)	171
Figure 9-8	Grain size distribution	173
Figure 9-9	Earthquake magnitude versus equivalent number of cycles (Seed et al. 1975)	173

Figure 9-10	Three ground motion used in the parametric studies, El-Centro (top), Pacoima Dam (middle) and Northridge (bottom)	174
Figure 9-11	Settlement versus depth using El Centro earthquake (Dr=60%).....	175
Figure 9-12	Settlement versus depth using San Fernando earthquake (Dr=60%).....	175
Figure 9-13	Settlement versus depth using Northridge earthquake (Dr = 60 %)	176
Figure 9-14	Settlement versus depth for NSF sand (Dr = 60%).....	177
Figure 9-15	Settlement versus depth for F-110 sand (Dr=60%).....	177
Figure 9-16	Settlement versus depth for S1 sand (Dr=60%)	178
Figure 9-17	Experimental Loading-Unloading Curve for Nevada Sand	181
Figure 9-18	Settlement of Four Types of Sands	182
Figure 9-19	One- Dimensional Unloading Curves for Four Types of Sands	182
Figure 9-20	Computed Results for Number of Cycles causing Liquefaction for Four Types of Sands.....	183

LIST OF SYMBOLS

D_r = relative density

e = void ratio

f = frequency of cyclic loading

G_{\max} = maximum shear modulus at small strain

G_s = secant shear modulus

G_s/G_{\max} = normalized shear modulus

LL = Atterberg liquid limit

N = number of cycles

OCR = overconsolidation ratio

PI = LL - PL = plasticity index

PL = Atterberg plastic limit

S = degree of saturation

u = pore water pressure

ε_v = vertical axial strain

γ = shear strain

γ_c = cyclic shear strain amplitude

$\Delta\varepsilon_v$ = change of vertical axial strain

σ_h = total horizontal stress

$\sigma'_h = \sigma_h - u$ = effective horizontal stress

σ_v = total vertical stress

σ'_v = effective vertical stress

τ = shear stress

τ_c = cyclic shear stress amplitude

ABSTRACT

The earthquake induced settlement of cohesionless sand or silty sands, has been the source of significant structural damage to bridges and buildings in past earthquakes.

The procedure for evaluating the settlement of dry sands during earthquake ground shaking developed by Tokimatsu and Seed (1987) is widely used in engineering practice.

The method recognizes that seismic settlement is controlled by earthquake induced cyclic shear strain amplitudes but was developed using experimental data based on cyclic laboratory tests on only one sand. In addition, the procedure is based on simplifying assumptions approximating earthquake site response, namely the concept of an equivalent number of uniform shear strain amplitude cycles with depth varying amplitude.

This study evaluates a simplified version of a constitutive model for the settlement of sands under non-uniform time varying cyclic shear strain amplitudes (originally developed by Martin et al. (1975)) in combination with a nonlinear site response program as a means of determining the earthquake induced settlement of sands in a more rigorous manner. Compilation of existing and new cyclic simple shear laboratory tests on several different sands also shows that settlements can be significantly greater or less than the data adopted for the Tokimatsu and Seed procedure. Constitutive model parameters adopted for the settlement analyses are shown to depend on the value of $e - e_{\min}$ (where e is the void ratio) for a given relative density.

The results of the research clearly illustrate settlement sensitivity to sand particle characteristics. A simple approach based on void ratio parameters to characterize settlement potential and the new analytical methodology adopted as a design approach, overcomes the limitations of the Tokimatsu and Seed methodology. These parameters when combined with a time history site response analysis form the basis for the proposed new design methodology.

A basic understanding of volume change behavior under cyclic loading as described above is also fundamental to the understanding of liquefaction behavior of saturated sands under undrained conditions as reported by Martin et. al, 1975. The research also illustrates and reinforces this basic understanding.

CHAPTER 1

INTRODUCTION

1.1 Earthquake Induced Settlement

Earthquakes can cause considerable settlements in deposits of cohesionless soils. In the 1971 San Fernando earthquake for example, settlements of 4 to 6 in. have been reported under a building on spread footing on a 40 ft deep sand fill (Seed and Silver 1972). Settlement of approximately 2 in. was noted in other areas after the same earthquake. Ground settlements resulting from ground shaking during earthquakes are rarely uniformly distributed and cause differential settlements in structures which can be a major cause of damage. Settlement is the term commonly used to describe the volume change, which sometimes occurs in sands during seismic loading. While most frequently associated with cohesionless soils and dynamic loadings, it has been reported in many types of soils under both dynamic and static loadings. The settlement of sands during earthquakes has occurred throughout recorded history, and certainly before that, however it was not until the early 1960's that scientific research into the subject began in earnest. Since the 1964 Anchorage, Alaska, and Niigata, Japan earthquakes, great strides have been made in understanding the mechanisms behind settlement and the conditions that make soils susceptible to it.

The behavior of dry sand deposits subjected to earthquake type of loadings may involve highly nonlinear stress-strain relationships and large deformations such as the settlement of the ground surface due to the densification of sand layers. In many cases the ground motions developed in a soil deposit during an earthquake may be attributed primarily to

the upward propagation of shear waves from an underlying rock formation, If the ground surface, the rock surface and the boundaries between layers are essentially horizontal, the lateral extent of the deposit has no influence on the response, and the deposit may be considered as a one-dimensional shear beam.

1.2 Compacted Structural Fills

Structural fills are earth structures that are placed to create level building pads for building construction. In hillside areas, these fills are generally constructed in wedge shapes and placed along hillsides or are placed in canyons. There are a number of processes that can lead to deformations of compacted structural fills. Static, long-term processes include hydro-compression, consolidation, and slope creep (e.g., Lawton et al., 1989; Brandon et al., 1990). Seismic processes include seismic slope instability and seismic compression (e.g., Stewart et al., 2001). Deformations resulting from the above processes can be damaging to the building structures, and hence engineers generally design fills so as to minimize future ground deformations. Such analysis procedures are well developed for static processes (e.g., Houston et al., 1988 for hydro-compression), but significant work remains to be done before reliable ground deformation analysis procedures can be developed for seismic applications.

1.3 Observed Behavior of Structural Fills During Earthquakes

The performance of structural fills during earthquakes has been documented both in general field reconnaissance and in detailed studies of specific sites. The reconnaissance work involves observing the general characteristics of ground deformations across many sites. The detailed studies involve more intensive examination of the geotechnical and

damage characteristics at a few specific sites (e.g., Pyke et al., 1975; Stewart et al., 2004). The focus here is on the general reconnaissance work to establish the motivation for this research. The performance of structural fills during earthquakes has been documented following the 1906 San Francisco, 1971 San Fernando, and 1994 Northridge earthquakes. Lawson (1908) summarized observations of ground cracking in hillside areas from the 1906 San Francisco earthquake by noting, “roadways and artificial embankments were particularly susceptible to cracks.” After the 1971 San Fernando earthquake, McClure (1973) noted the influence of fills on damage patterns, particularly when residences were constructed over cut/fills contacts. This study found that ground failure occurred on a higher percentage of sites that were on fill or cut and fill than those sites which were on cut or natural grade and dwellings on cut and fill or fill had more relative damage than dwellings on cut or natural grade. After the 1994 Northridge earthquake, Stewart et al. (2001) documented locations of about 250 sites where fill movements caused damage. As shown in Figure 1-1, concentrated damage occurred on the north flank of the Santa Monica Mountains, along the north rim of the San Fernando Valley, and in the Santa Clarita Valley area. Other affected areas include isolated portions of the south flank of the Santa Monica Mountains and portions of Simi Valley. The data in Figure 1-1 can be used to roughly evaluate the levels of shaking that were required during the Northridge earthquake for seismic compression of fills to be a significant problem. Areas with significant damage such as Sherman Oaks, the northern San Fernando Valley, and Santa Clarita had peak accelerations in the range of 0.4 to 0.8 g (Chang et al., 1996), whereas outlying areas where incidents of seismic compression induced damage are relatively

sparse (e.g., Calabasas, Universal City) had levels of shaking < 0.4 g. Based on analyses of typical fill geometries reported in Stewart et al. (2001), approximate levels of peak shear strain corresponding to those acceleration levels are generally on the order of $> 0.1\%$ in the areas with damage and $< 0.1\%$ in areas without significant damage. Those shear strain levels can be contrasted with volumetric threshold shear strains (i.e., the shear strains below which no volume change would be expected) of $\gamma_{tv} = 0.01-0.02\%$ for sands and $\gamma_{tv} = 0.04-0.09\%$ for clays having $PI = 30$ (Hsu and Vucetic, 2004).

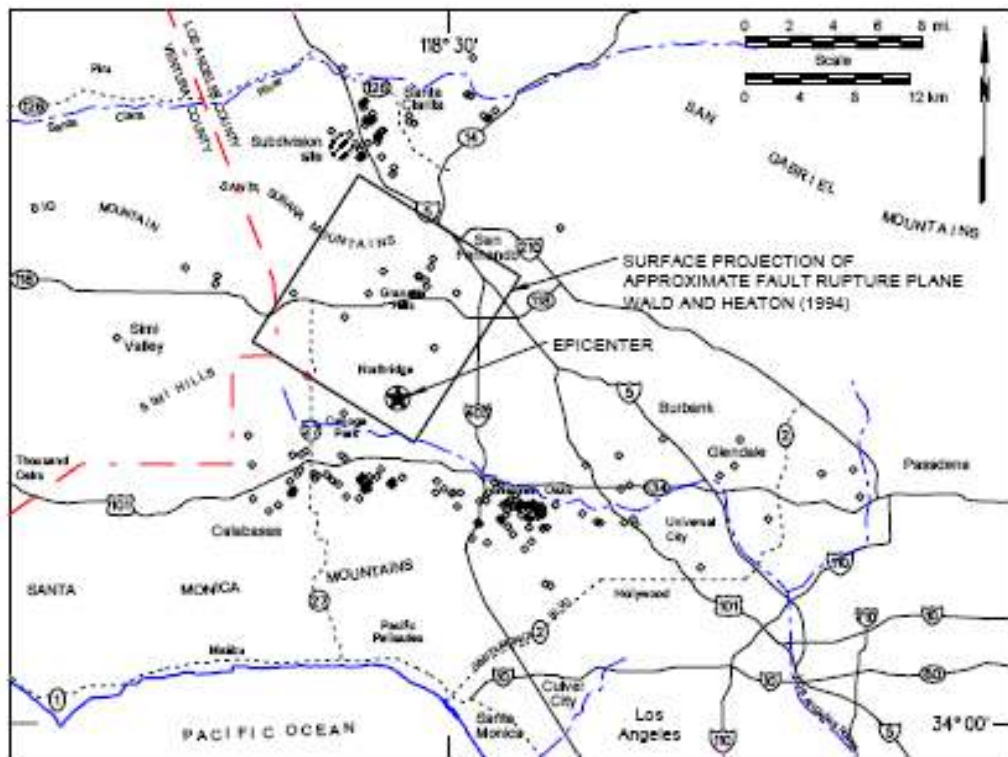


Figure 1-1 Site locations where fill movements caused significant damage during Northridge earthquake (Stewart et al., 2001)

Typical damage patterns at the mapped fill deformation sites included:

Cracks near cut/fill contacts: typically < 8 cm of lateral extension and 3 cm of localized differential settlement relative to cut Lateral extension in fill pad: observed in the form of tensile cracking parallel to the top of the slope, which typically caused 3-10 cm of horizontal or vertical offsets.

Differential settlement on fills surfaces: observed as cracks with vertical offsets and tilted floors and swimming pools.

Slope-face bulging: characterized by movement of surface drains running cross-slope (terrace drains) and down-slope (down drains)

1.4 Motivation for the Present Study

There has been an increasing demand within the engineering profession for settlement analysis procedures under ground shaking. Existing methods for estimating settlement susceptibility are limited in their applicability, because they only apply for a few specific soil characteristics. Accordingly, there is a major research need for laboratory testing to develop relations between volumetric strains, applied shear strains and number of strain cycles (termed a volumetric strain material model) that cover a broad range of soil types.

1.5 Objectives of the Investigation

The principal objective of this research was to perform laboratory simple shear testing to provide insight into the seismic settlement of sands, and then to develop volumetric strain material models for those soils. Test data for a total of 18 different clean sands was compiled including tests performed by author and test data developed by other researchers. Sands were also tested to characterize the effect of sand compositional factors (mineralogy, gradation and particle shape on vertical strain from seismic

settlement. The sands were selected to span a range of material gradation, particle size and particle shape, and. specimens were prepared to varying levels of relative density.

The many assumptions and simplifications inherent in the method of Tokimatsu and Seed (1987) lead to many questions as to the reliability of the design procedure. Two of the key assumptions relate to site response simplifications and the limited test data (one normally consolidated sand) on which the method is based. A further objective of this research program is to address these concerns by:

- a) Evaluating the test data described above to determine a method to account for sand type on settlement behavior.
- b) Simplifying the constitutive model developed by Martin et al.(1975) in the nonlinear site response program DESRA and conducting analyses to assess the sensitivity of settlement to earthquake time histories
- c) Developing a robust design methodology to overcome the limitations of the Tokimatsu and Seed methodology knowing that the settlement of sands depends on the induced shear strain, the relative density, the grain mineralogy and the over consolidation ratio as discussed below.
- d) Recommendations for revised settlement design and analysis procedures using time history approaches

It is important to note that a basic understanding of volume change behavior under drained cyclic loading as described above is fundamental to the understanding of liquefaction behavior of saturated sands under undrained conditions. The mechanics of

liquefaction on a particulate scale is uniquely linked to the mechanics of volume change as described by Martin et al.(1975).

This experimental and analytical research program will play a key and complementary role in meeting other objectives in terms of:

- Understanding the mechanics of site settlement behavior under earthquake loading, including the role of lateral stress increases.
- Validating the nonlinear site response methodology for evaluating site settlement under earthquake loading.
- Establishing a sound basis for improved analysis and design procedures of settlement evaluation in practice. Providing preliminary liquefaction test data where a complementary volume change database has been established.

1.6 Outline of this Document

Following this introductory section, Chapter 2 presents the results of a literature review performed to learn what is currently understood about the mechanism of settlement of sandy soils. Next, Chapter 3 discusses the DESRA program which is going to be used in this research when performing parametric studies, Chapter 4 consists of a discussion of the soils tested, a brief review of cyclic simple shear testing and the factors which affect it, and a detailed review of the cyclic simple shear test methodology used in this study. It also discusses the details of all the tested sands and the details of their characteristic parameters. Chapter 5 presents the development of the database consisting of the existing database and then the new database developed as a part of this research and finally the database contributed by a UCLA research team. Chapter 6 describes the results of

mineralogy analysis of all the sands which was performed using the X-ray diffraction method and the thin slide method and their effects on the settlement of sandy soils. One global theory is presented and used to reconcile the differences found in the literature. Chapter 7 presents the findings of the effects grain size and their shape on the settlement of sandy soils. Chapter 8 discusses the result of the analysis and presents a theory that can explain the reason behind the difference in sand behavior during ground shaking. Chapter 9 presents the results of parametric studies using DESRA and examines how the findings of this study may impact the manner in which simplified settlement analyses are performed in engineering practice. Chapter 10 presents a summary of conclusions drawn from this study and suggestions for further studies in this area. A series of appendices containing the results of the cyclic shear tests and of the mineralogy tests follow Chapter 10.

CHAPTER 2

PREVIOUS RESEARCH ON SETTLEMENT OF DRY OR PARTIALLY SATURATED SAND

2.1 Introduction

Earthquakes can cause considerable settlements in deposits of cohesionless soils. In the San Fernando earthquake of February 9, 1971, Settlements of 4 to 6 in were reported under a building on spread footing on 50 ft deep sand fill. Settlements of up to 2 in were noted in other areas. Studies by (Silver and Seed (1971), Youd (1972), Seed and Silver (1972), and Pyke et al. (1975)) were conducted to investigate various aspects of settlement resulting from ground shaking during earthquakes and were largely motivated by the above case history. These studies led to the advancement of semi-empirical approaches for design. These studies and additional study by Youd (1972) are discussed below.

2.2 Silver and Seed (1971)

The original studies of settlement of dry sand were performed by Silver and Seed (1971) who used laboratory testing to investigate the volumetric strains induced in dry, clean sands undergoing cyclic loading with zero mean (static) shear stress. Silver and Seed (1971) and Seed and Silver (1972) performed strain-controlled simple shear testing using an NGI-type device on dry quartz sand (Crystal Silica No. 20). The specimens were prepared by dry pluviating a reweighed amount of sand, and then vibrating it to a specified height such that the target density ($DR = 45, 60, \text{ and } 80\%$) was achieved. The tests were performed by first applying a specified vertical stress to the specimen (values

of $\sigma'_v = 500, 200$ and 400 psi), and then subjecting the specimens to a uniform cyclic shear strain amplitude that varied from $\gamma_c = 0.01$ to 0.5% . Continuous readings of vertical deformation were made that enabled vertical strains to be evaluated as a function of the number of strain cycles (N). Figure 2-1 shows a summary of test results at $N = 15$ cycles of loading for the three relative densities. The vertical strain was seen to increase with cyclic shear strain amplitude, and to decrease with increasing relative density. The vertical strains were found to be negligible below a limiting value of shear strain. Denoted γ_{tv} this limiting strain has since come to be known as the volumetric threshold shear strain (Vucetic, 1994). Typical values of threshold shear strains for sands are $\gamma_{tv} = 0.01$ to 0.02% (Hsu and Vucetic). Silver and Seed (1971) suggested a procedure for estimating the probable settlements of non-saturated sands caused by earthquakes. Their procedure requires the establishment of the stress-strain, damping, and volume change characteristics by means of simple shear tests and the use of an analytical procedure in order to evaluate the shear strain history at any depth in a soil deposit and finally the use of their charts to compute the settlement after transforming the irregular shear strain history into an equivalent number of uniform cycles. Knowing that a soil element at any depth may be considered subjected to a known overburden pressure and a given number of cycles of a horizontal shear strain, Silver and Seed concluded that the vertical settlement resulting from these strain applications could be measured directly by subjecting a representative sample of soil to the field loading conditions in a simple shear device. Their studies showed that the settlement of dry sands due to cyclic loading is a function of:

- The relative density of the soil
- The magnitude of the cyclic shear strain
- The number of strain cycles.

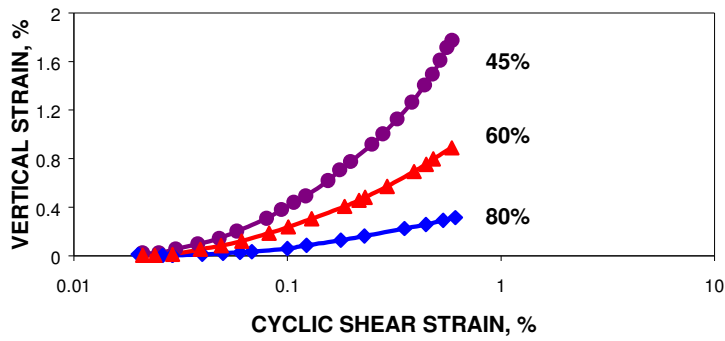


Figure 2-1 Effect of Relative Density on Settlement in 10 Cycles (Silver and Seed 1971)

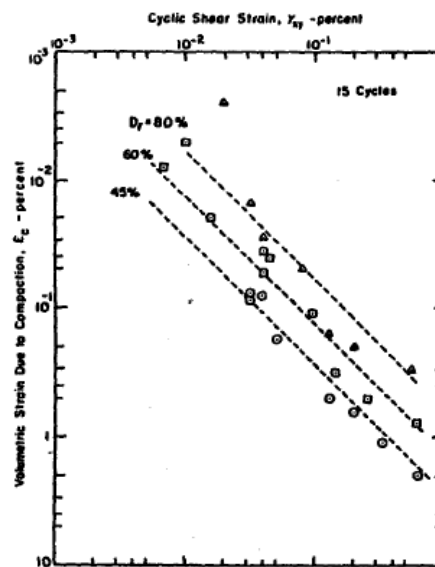


Figure 2-2 Effect of relative density on settlement of dry sand (Silver and Seed, 1971)

The dependence of vertical strain on the number of strain cycles was relatively consistent for all test results, as shown in Figure 2-3. These results demonstrate a characteristic feature of seismic compression, which is that a significant fraction of the overall volumetric strain occurs within the first few cycles (e.g., 50% of the volumetric strain at 15 cycles occurs within the first 3 cycles), and relatively little deformation occurs for $N > 100$. Several suites of tests were performed at different vertical stresses σ'_v , but vertical strain was found to not be significantly affected by σ'_v .

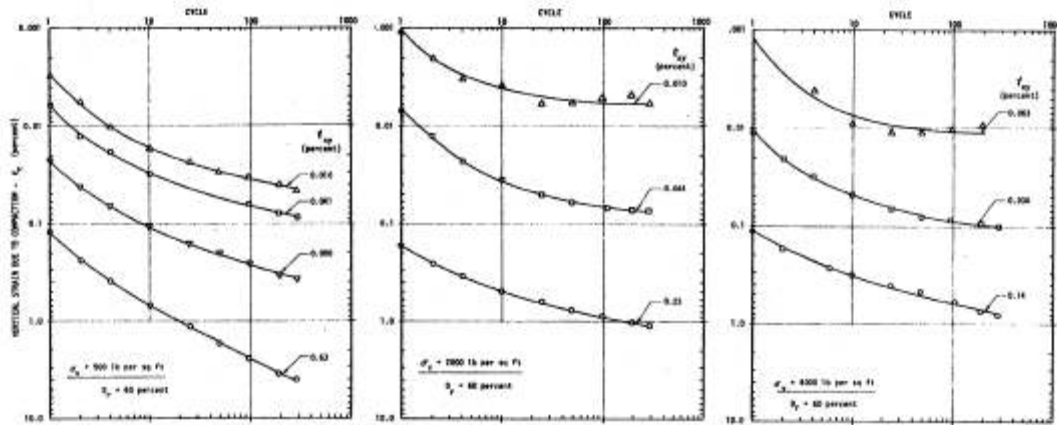


Figure 2-3 Settlement-number-of-cycles-relationships for DR = 60%)
Silver and Seed, 1971)

2.3 Seed and Silver (1972)

Seed and Silver (1972) used the technique described above to compute the settlement in 50-ft deposit of sand with a relative density of 45% shown in Figure 2-4. The deposit was subjected to a maximum base acceleration of 0.35 g resulting in maximum surface acceleration of 0.45g during the San Fernando earthquake of 1971.

The shear modulus used shown by the middle curve in Figure 2-5 was expressed by the relationship:

$$G = 1000k_m\sigma_v^m$$

Where σ_v = the applied vertical confining pressure; m = an exponent; and K_m = a coefficient whose value varies with the shear strain. The computed settlement was about 2.7 in.

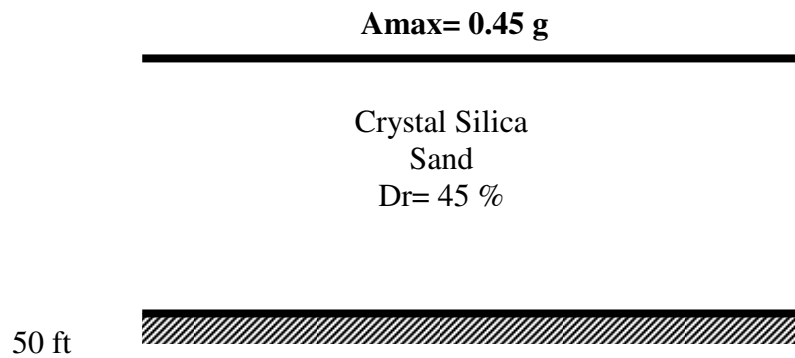


Figure 2-4 Soil profile Analyzed by Silver and Seed (1971) and by Tokimatsu and Seed (1987)

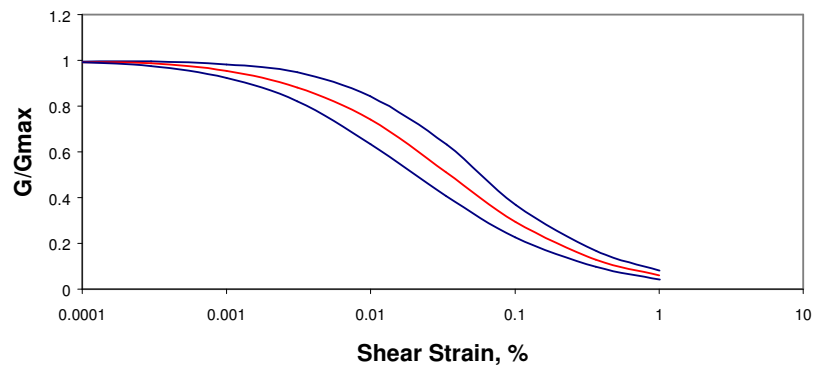


Figure 2-5 Relationship between shear modulus and shear strain for sand (Seed et al.1984)

2.4 Youd (1972)

Youd (1972) investigated seismic compression of Ottawa sand using simple shear laboratory testing with an NGI-type device. The specimens were prepared by pouring sand into a membrane and in some cases, vibrating the top cap to densify the specimen. Youd performed one subset of tests on specimens that were saturated, consolidated under vertical stresses of $\sigma'_v = 5, 48$ and 192 kN/m^2 , and then sheared under drained conditions. Volume change was monitored by a water column (equipped with a pressure transducer) that was connected to the specimen. A second subset of tests was performed using air-dry specimens. In both subsets of tests, specimens were generally prepared to relative densities of $DR = 70\text{--}80\%$. For each test, sinusoidal loading was applied at a constant frequency that was varied from test-to-test across the range of $f = 0.2$ to 1.9 Hz . During an individual test, shear strain amplitudes varied somewhat with time as a result of compliance in the load cell. Accordingly, applied shear strains were reported as a range rather than as a unique value. The results of selected tests on Ottawa sand are presented in

Figure 2-6, with the Silver and Seed results also indicated for comparison. The Ottawa sand results confirm the finding of Silver and Seed that vertical strains increase with increasing shear strain, but the vertical strains are systematically higher (by factors of 4 to 6) than those of Silver and Seed for Crystal Silica No. 20 sand. The reasons for this difference are unknown. The results of Youd's tests investigating saturation and frequency of loading effects revealed no significant influence of either factor.

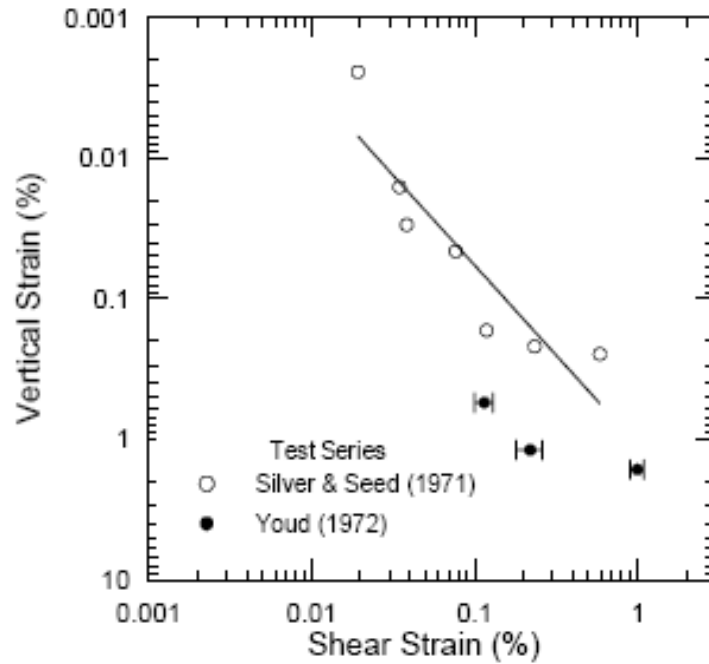


Figure 2-6 Comparison of vertical strains at 10 cycles for Ottawa sand (Youd, 1972) and Crystal Silica sand (Silver and Seed, 1971) at $D_r = 80\%$.

2.5 Pyke et al. (1975)

Pyke et al. (1975) investigated the seismic compression of dry Monterey No. 0 sand using large-scale specimens tested on a shaking table. The disk-shaped specimens were prepared to $DR = 40, 60,$ and 80% by raining sand from a spreader box into a 7.6 cm deep form, temporarily mounted on top of the shaking table. The form was slightly overfilled and the excess sand was removed with a screed. The specimens had sloping lateral boundaries, which were enclosed by a rubber membrane. Vertical stresses were applied by the weight of a steel cap (7.7 kN/m^2) placed on top of the sand and vacuum

pressures applied to the specimen. All testing was performed under stress-controlled conditions, and the shear strains that occurred during the tests were not reported. The intent of the shaking table tests by Pyke et al. (1975) was to evaluate the effect of multidirectional shaking (two horizontal directions and one vertical). The results of unidirectional, bi-directional (two horizontal directions of shaking), and tri-directional (two horizontal and one vertical direction of shaking) are compared in (Figure 2-7 a). Based on the results, Pyke et al. surmised that the settlements caused by the combined horizontal motions are about equal to the sum of the settlements caused by the horizontal stresses acting separately. Since peak accelerations in two horizontal directions are often similar, Pyke et al. recommended that settlements under bi-directional shear generally be taken as about twice those under unidirectional shear. Moreover, as indicated by the results in (Figure 2-7b), Pyke et al. found that vertical accelerations superimposed on horizontal accelerations could cause an additional increase in the settlements of as much as 50%.

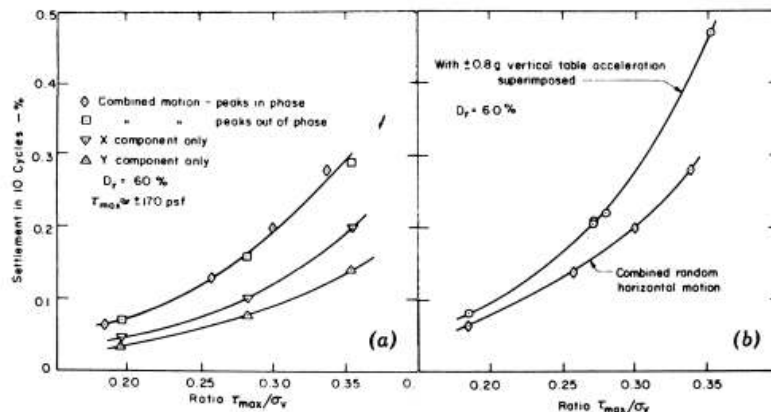


Figure 2-7 Comparison of settlements of sand from shaking table tests performed
 (a) Under unidirectional and bi-directional stress-controlled loading and
 (b) Under three-directional stress-controlled loading (Pyke et al., 1975)

Pyke et al. computed the settlement for the Joseph Jensen Filtration Plant of the Metropolitan Water District of Southern California located in the Granada Hills area of the San Fernando Valley (Figure 2-4). The site was made of 50 ft compacted fill overlying an alluvial layer of 5 ft. They used the record obtained at Pacoima Dam S74⁰ W after modifying it to remove the Effects of the topography at the site of the dam site. Their analysis consisted of using a one-dimensional lumped- mass model in order to obtain the shear strain-time history and then, the use of the relationship between settlements in 10 cycles versus the cyclic shear strain that they established using cyclic simple shear tests. The result of their analysis showed a settlement of 1.6 in. when unilateral shaking is considered.

2.6 Martin et. al (1975)

Martin et al. (1975) performed a detailed study of volumetric change in sand subjected to cyclic shear strains. They showed that the increment in volumetric strain depends on the shear strain amplitude and the total volumetric strain accumulated during the previous cycles of shear strain. Also the volumetric strain amplitude for a given number of cycles is proportional to the cyclic strain amplitude. The analytical expression for volumetric strain increment is given by:

$$\Delta\varepsilon_{vd} = c_1(\gamma - c_2\varepsilon_{vd}) + \frac{c_3\varepsilon_{vd}^2}{(\gamma + c_4\varepsilon_{vd})}$$

Where c_1 , c_2 , c_3 and c_4 are four constant to be determined from two or three constant strain amplitude cyclic tests. $\Delta\varepsilon_{vd}$, ε_{vd} and γ are respectively the incremental

volumetric strain, the accumulated volumetric strain and the shear strain all expressed as percentage.

They used Crystal Silica No.20 sand with a relative density of 45%. Further discussion of the constitutive model is given in paragraph 3.5 and 3.6.

2.7 Tokimatsu and Seed (1987)

Tokimatsu and Seed (1987) used the same soil profile shown in Figure 2-4 to compute the settlement using a simplified method that does not require a dynamic analysis of the soil deposit.

Knowing that the primary factor controlling settlement in dry sands is the cyclic shear strain, they estimated these values at any depth in a soil deposit as follow:

$$\gamma_{eff} = \frac{\tau_{av}}{G_{eff}} = \frac{\tau_{av}}{G_{max} \cdot \left(\frac{G_{eff}}{G_{max}} \right)}$$

Where G_{max} = Shear modulus at low strain,

G_{eff} = Effective shear modulus at induced strain level,

τ_{av} = Average cyclic shear stress at the corresponding depth.

The average cyclic shear strain can be computed using the following relationship:

$$\tau_{av} = 0.65 \cdot \frac{a_{max}}{g} \cdot \sigma_o \cdot r_d$$

where a_{max} is the maximum horizontal acceleration at the ground surface,

σ_o is the overburden pressure at the considered depth and

r_d is a stress reduction factor that varies from a value of 1 at the ground surface to a value of 0.9 at a depth of 30-ft.

G_{\max} was computed using the relationship proposed by Seed and Idriss (1971).

Having determined the effective shear strain at the considered level, the relationships between the volumetric strains and shear strain proposed by Silver and Seed (1971) is then used to compute the settlement. These relationships, which are applicable only for case involving 15 equivalent uniform cycles that represent an earthquake of magnitude 7.5, were extended to different magnitudes. The results of their study, which they multiplied by a factor of 2 to account for the effect of multidirectional shaking, produced an estimated settlement of 3.6 in.

In summary, all of these procedures, and in particular, the most commonly used, Tokimatsu and Seed (1987) have the following limitations:

- There are based on one set of data (Silica Sand No: 20)
- They assume that the soil deposit is normally consolidated.

They require the transformation of the non-uniform shear strain history into an equivalent number of uniform cycles knowing the earthquake magnitude (Seed et al. 1975a) The use of an empirical relationship to estimate the average shear strain in a given layer (Figure 2-8). The use of the chart developed by Silver and Seed (1971) which was developed for 15 uniform cyclic shear strain which is representative of an earthquake of magnitude 7.5. For earthquakes of different magnitude, they propose to use a correlation factor as shown in

Figure 2-9.

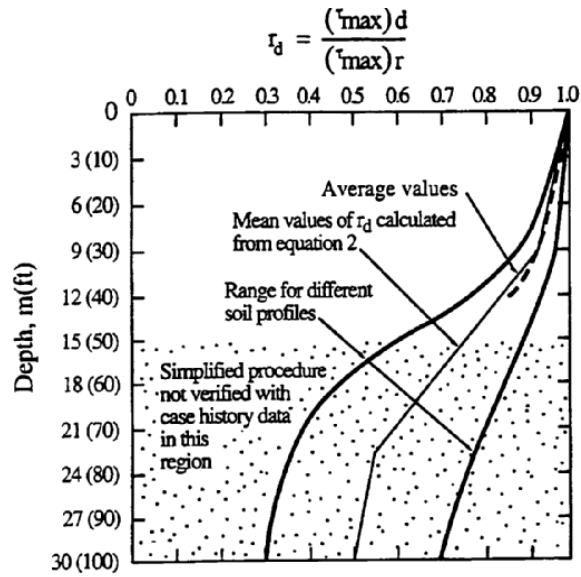


Figure 2-8 Reduction factor to estimate the variation of the cyclic shear stress (Silver and Seed 1971)

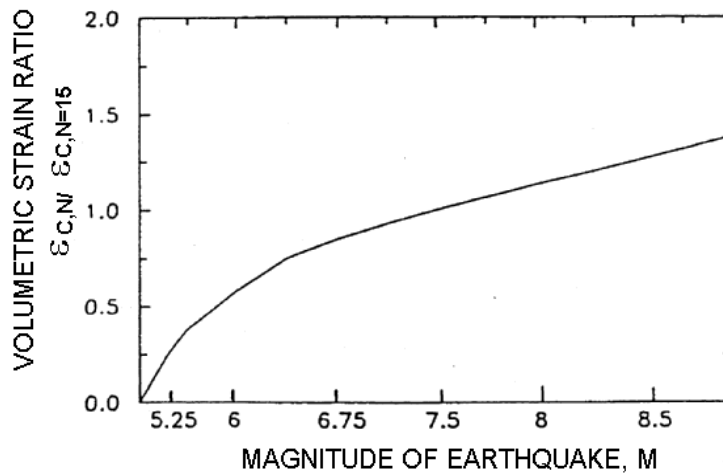


Figure 2-9 Relationship between volumetric strain ratio and earthquake magnitude for dry sands. (After Tokimatsu and Seed, 1987)

CHAPTER 3

THE COMPUTER PROGRAM DESRA

3.1 Introduction

To accomplish the research objectives, the constitutive model developed by Martin et al. (1975) will be used in numerical analyses. The model is incorporated in the one-dimensional nonlinear site response DESRA-MUSC (Qiu 1998). DESRA-MUSC is a modified version of DESRA (Lee and Finn 1978) and is discussed below.

3.2 DESRA-MUSC Program.

DESRA-MUSC (Qui, 1988), an existing one-dimensional dynamic effective stress analysis computer program for soil deposit with an energy-transmitting boundary is to be used to compute the probable settlement in dry sand deposits subjected to earthquake loading. Knowing that the major factors controlling induced settlement in dry sand are the magnitude of the cyclic shear strain induced in the sand by the earthquake shaking and the number of strain cycles, the program determines the non-linear soil response including the time-history of shear strains at any required depth and uses the incremental shear-volume coupling equation for sand under simple shear loading proposed by Martin et al. (1975). The program also accounts for the increase in the shear modulus with number of cycles using the accumulated volumetric strain as a hardening parameter. This aspect was reported by Silver and Seed (1971) as shown in Figure 3-1. Their finding was that “there was a slight increase in the shear modulus for increasing number of stress cycles for the entire range of confining pressures investigated. They also noted that this

increase is greatest in the first 10 cycles, after which changes in modulus are relatively small". Seed and Silver (1972) and by Tokimatsu and Seed (1987) neglected this aspect when they developed their procedures. One of the main advantages of the program is that it can be easily used and it does not require the use of charts, tables, and diagrams. It allows an expeditious analysis of soil profiles with numerous layers. Its application to a case study shows a good agreement with the settlement observed at the site.

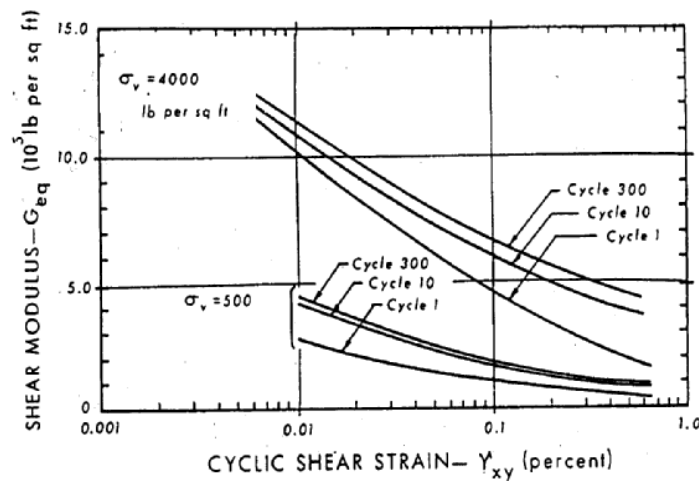


Figure 3-1 Effect of number of stress cycles on shear modulus-shear strain relationship for medium dense Silica sand ($D_r = 60\%$) (After Silver and Seed 1971)

DESRA-MUSC is restricted for the case of horizontally layered dry and saturated sand deposits shaken by horizontal shear waves propagating vertically upwards. The method is based on a set of constitutive laws, which take into account important factors that are known to affect the response of dry and saturated sands to earthquake loading. Those factors include the variation of shear stiffness with shear strain amplitude, the assumption of volume change in dry sand, the generation and dissipation of pore pressure in saturated sand and hysteretic damping and hardening effects. The initial shear stress-shear strain

loading curve, “the backbone curve”, is represented by the Iwan model (1964), which incorporates an array of elasto-plastic elements to simulate a given nonlinear backbone, curve and provides hysteretic damping automatically. There are many advantages of using a physical or mechanical model, and these advantages are:

It provides the means for a non-iterative time domain solution, which can be used for arbitrary cyclic loading such as earthquakes.

It allows a yielding or failure criterion to be incorporated so that the seismic response of soft soil sites can be realistically analyzed without the need for a stress cut off to achieve the yielding characteristics.

It can duplicate many properties observed in the laboratory or produced by other soil models without difficulty.

These abilities improve the non-linear behavior modeling, and they provide a means for comparative studies, which will lead to a better understanding of the influence of variations in nonlinear properties.

The Iwan model is based on the assumption that a general hysteretic system may be thought of as consisting of a large number of ideal elasto-plastic elements having different yielding levels. Iwan mechanical model is simulated by a set of spring and slip elements. It satisfies the Masing criteria, which describes the material hysteresis characteristics often associated with soil behavior. The model can fit experimental results to a great degree by simply increasing the number of elements.

In general, there are two forms of the Iwan model. One is a parallel-series combination of springs and Coulomb sliders. The other is a series-parallel combination of spring and

Coulomb sliders. These two forms are generally similar in their characteristics, except that the parallel-series form is more suitable for strain-controlled loading, while the other which was incorporated into DESRA-MUSC is more suitable for stress-controlled loading.

For the series-parallel system (Figure 3-2), the friction element represented by Coulomb slider remains locked until the applied stress exceeds the yielding stress, which is the Coulomb resistance, R . If the m^{th} element yields, the stress remains R_m during yielding. The excess portion of the stress is absorbed by the spring in the same element. The strain of each element for the loading procedure can be expressed as:

$$\gamma_m = \begin{cases} 0 & 0 \leq \tau \leq R_m \\ \frac{\tau - R_m}{K_m} & \tau \geq R_m \end{cases} \quad \text{for } m = 1, 2, 3, \dots$$

The unloading will not cause any change on the element strain until it unloads by $-2R_m$, at which $\tau = K_m \gamma_m - R_m$. The spring releases the energy stored during previous loading and the elastic strain recovers to zero at $\sigma = -R_m$. If the reversal loading continues in the other direction, the strain is expressed as:

$$\gamma_m = \frac{\tau - (-R_m)}{K_m} \quad \text{For } \tau < R_m$$

A typical stress-strain loop generated by the Iwan model at different strain amplitudes is shown in

Figure 3-3. It can be observed that the tangent modulus decreases as the strain increases. However, the tangent modulus at each reversal point is the same as the one of the initial loading curve corresponding to zero strain. It can also be observed that the peak point of

each hysteretic loop is on the backbone curve. These characteristics observed in the Iwan model are observed in many experimental results (Taylor and Larkin, 1978). The hysteretic loops generated by the Iwan model satisfy the Masing criteria. The model also memorizes the past loading history and follows the loading curve associated with the appropriate load reversal point automatically. By choosing the appropriate values of the spring stiffness K_m and the Coulomb resistance R_m , we can model a very broad range of material behavior as observed in laboratory experiments. The accuracy of the model depends on the number of elements. Joyner et al. (1975) chose an Iwan system with 50 elements. They defined the following 51 values of Coulomb resistance normalized by the soil shear strength:

$$\begin{cases} R_m = 0 & m = 1 \\ R_m = 0.025(0.5)^{6-m} & 2 \leq m \leq 6 \\ R_m = 0.025(m - 5) & 7 \leq m \leq 44 \\ R_m = 1 - 0.025(0.5)^{m-44} & 45 \leq m \leq 51 \end{cases}$$

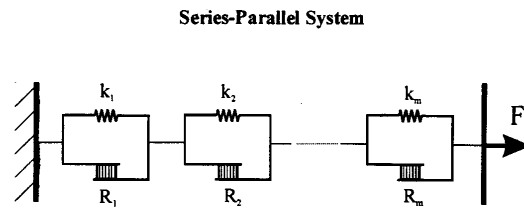


Figure 3-2 The Iwan model

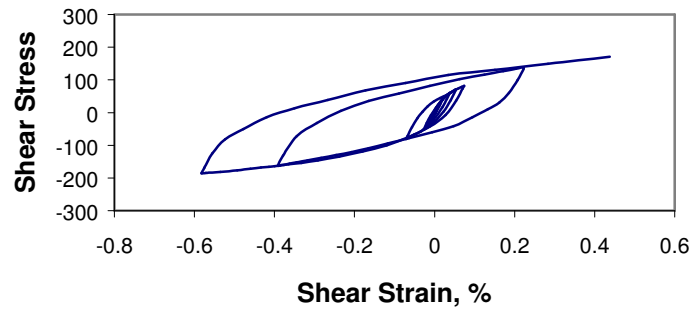


Figure 3-3 Typical stress-strain loop from the Iwan model

3.3 Energy-Transmitting Boundary

In order to take into account the effect of the finite stiffness of the underlying soil and to allow the energy to radiate back into the underlying half space medium, a transmitting boundary condition applied on the bottom of the soil column under consideration, was incorporated in the program DESRA-MUSC. This is in contrast with the assumption of infinitely rigid base of the soil deposit, where motion is prescribed, does not allow any energy of the vibrating soil deposit to radiate back into the underlying medium. The transmitting boundary condition that was suggested by Joyner et al. (1975) allows the energy to propagate up and down through the boundary. The method basically evaluates the shear stress, τ_B , being transmitted across the boundary between the soil deposit and the underlying medium. This underlying medium is assumed to be elastic and the propagating shear waves are plane waves traveling vertically. If U is the horizontal displacement of a material particle located at depth z , then,

$$\tau = G_E \frac{\delta U}{\delta z}$$

Where $G_E = \rho_E V_s^2$ is the shear modulus of the underlying soil. If U^i, V^i and U^r, V^r are the displacement and velocity component due to the incident and reflected waves respectively. Then,

$$U^i = U^i(z + V_s t)$$

And

$$U^r = U^r(z - V_s t)$$

Where V_s is the shear wave velocity in the underlying medium. The shear stress developed on the interface due to the shear wave excitation is:

$$\tau_B = G_B \left(\frac{\delta U^i}{\delta z} + \frac{\delta U^r}{\delta z} \right) = G_B \left(\frac{V^{iB}}{V_s} - \frac{V^{rB}}{V_s} \right)$$

The particle velocity on the boundary is the sum of both velocities of the incident and reflected waves:

$$V_B = V^{iB} + V^{rB} = \frac{\delta U^i}{\delta z} V_s - \frac{\delta U^r}{\delta z} V_s$$

Where V_B is the particle velocity at the boundary, V^{iB} and V^{rB} are the particle velocity component at the boundary due respectively to the incident and reflected wave.

The resulting shear stress at the boundary is:

$$\tau_B = \rho_E V_s (2V^{iB} - V_B)$$

3.4 Volumetric Changes Analysis During Drained Non-Uniform Cyclic Loading

As mentioned in paragraph 2.6, Martin et al. (1975) performed a detailed study of volumetric change in sand subjected to cyclic shear strains. They showed that the increment in volumetric strain depends on the shear strain amplitude and the total volumetric strain accumulated during the previous cycles of shear strain. Also the volumetric strain amplitude for a given number of cycles is proportional to the cyclic strain amplitude. The analytical expression for volumetric strain increment is given by:

$$\Delta\varepsilon_{vd} = c_1(\gamma - c_2\varepsilon_{vd}) + \frac{c_3\varepsilon_{vd}^2}{(\gamma + c_4\varepsilon_{vd})}$$

Where c_1 , c_2 , c_3 and c_4 are four constant to be determined from two or three constant strain amplitude cyclic tests. $\Delta\varepsilon_{vd}$, ε_{vd} and γ are respectively the incremental volumetric strain, the accumulated volumetric stain and the shear strain all expressed as percentage (Figure 3-4).

They used Crystal Silica No.20 sand with a relative density of 45%. It also should be noted that the volumetric strains computed by the above equation were in perfect agreement with measured strains over a wide range of strain.

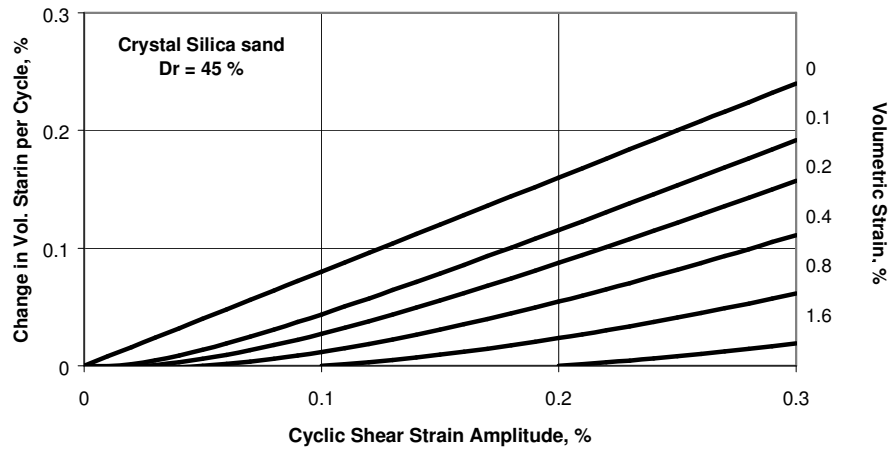


Figure 3-4 Incremental volumetric strain curves (After Martin et al. 1975)

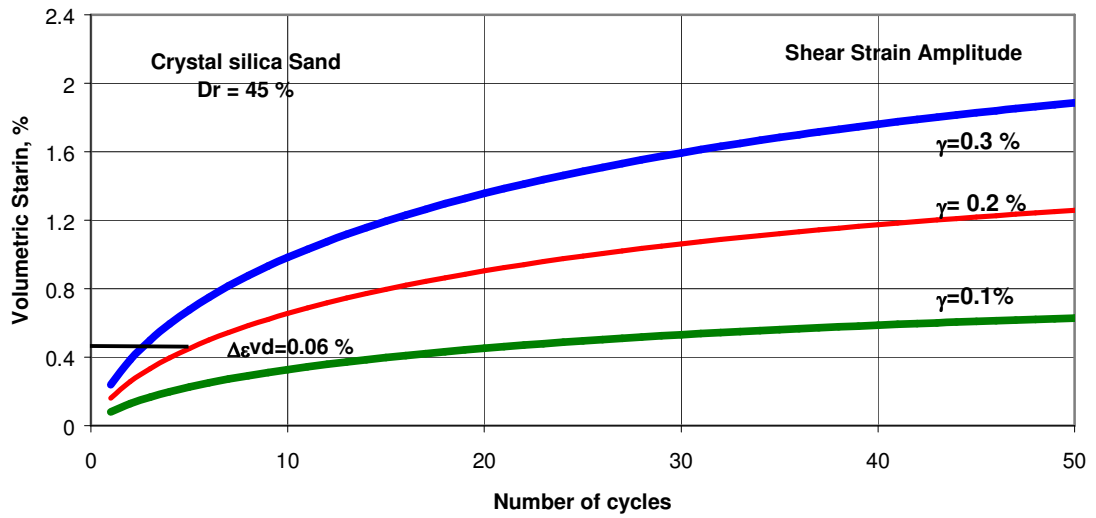


Figure 3-5 Volumetric Strain Curves for Constant Cyclic Shear Strain Amplitude tests (After Martin et al. 1975)

The basis of the method developed for predicting the volumetric strains during irregular shear strain amplitude sequences from the constant shear strain amplitude shown above, can be explained as follows (Martin et al. (1975):

Let it be assumed that after N cycles of non-uniform shear strain amplitude sequence, the volumetric strain has accumulated to 0.4 % and that the shears strain amplitude of the (N+1)Th cycle is 0.2 % (Figure 3-5). Thus, the volumetric strain increment for the that cycle can be determined by finding the intersection of the horizontal line of $\epsilon_{vd} = 0.4 \%$ with the curve $\gamma = 0.2 \%$ and measuring the value of volumetric strain increment appropriate to a further cycle width on the 0.2 % shear strain curve. The empirical method described above is based on the fact that experimental observation (Figure 3-6) shows that for shear strain in the range of 0.3 %, the volumetric strain is proportional to the shear strain.

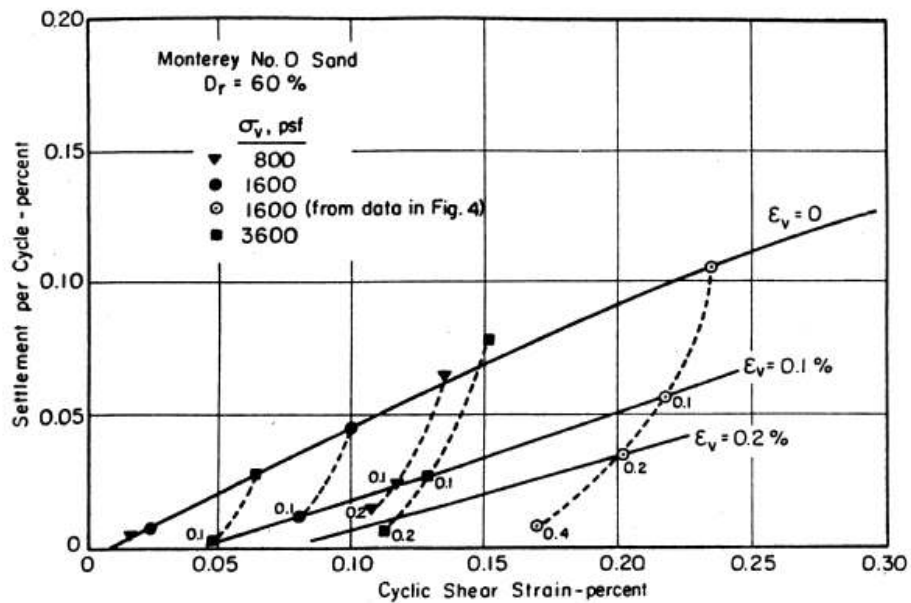


Figure 3-6 Settlement Data from Cyclic Simple Shear Tests (Pyke 1973)

3.5 A Review of Martin et al. Constitutive Model

A review of the above empirical expression, which contains four parameters, showed that these are not unique and that they are very difficult to evaluate. A parametric simplification was performed as part of this research as follow:

When the shear strain is zero, the incremental volumetric strain must be zero also and thus:

$$\Delta \varepsilon_{vd} = c_1(0 - c_2 \varepsilon_{vd}) + \frac{c_3 \varepsilon_{vd}^2}{(0 + c_4 \varepsilon_{vd})} = 0$$

$$\Delta \varepsilon_{vd} = \frac{-c_1 c_2 c_4 \varepsilon_{vd}^2 + c_3 \varepsilon_{vd}^2}{c_4 \varepsilon_{vd}} = 0$$

$$c_1 c_2 c_4 = c_3$$

Hence the revised expression for the incremental volumetric strain is:

$$\Delta \varepsilon_{vd} = c_1 \gamma \left(1 - \frac{c_2 \varepsilon_{vd}}{\gamma + c_3 \varepsilon_{vd}} \right)$$

Figure 3-7 and Figure 3-8 show respectively the volumetric strain contours versus shear strain and the volumetric strain versus number of cycles computed using the two expressions mentioned above. The above analytical expression of volumetric strain increment can be further simplified by replacing it with another expression with only two parameters as follows:

$$\Delta \varepsilon_{vd} = c_1 \gamma \left(1 - \frac{c_1 \varepsilon_{vd}}{\gamma + c_2 \varepsilon_{vd}} \right)$$

Where c_1 is the slope of the $\varepsilon_{vd}=0$ line as defined by Martin et.al (1975) and c_2 is a constant obtained by selecting any point of intersection of any contour with the shear

strain axis ($\Delta\varepsilon_{vd} = 0$) and substituting for the value of γ in the above equation. The empirical expression described above is unique. The nature of the curves is asymptotic, because the volumetric strain increment must eventually become zero at a given time where the volumetric strain becomes constant.

$$\Delta\varepsilon_{vd} = c_1\gamma\left(1 - \frac{c_1\varepsilon_{vd}}{\gamma + c_2\varepsilon_{vd}}\right) = 0$$

$$\frac{c_1\gamma^2 + c_1c_2\gamma\varepsilon_{vd} - c_1^2\gamma\varepsilon_{vd}}{\gamma + c_2\varepsilon_{vd}} = 0$$

$$c_1\gamma(\gamma + \varepsilon_{vd}(c_2 - c_1)) = 0$$

$$\boxed{\varepsilon_{vd\max} = \frac{\gamma}{c_1 - c_2}}$$

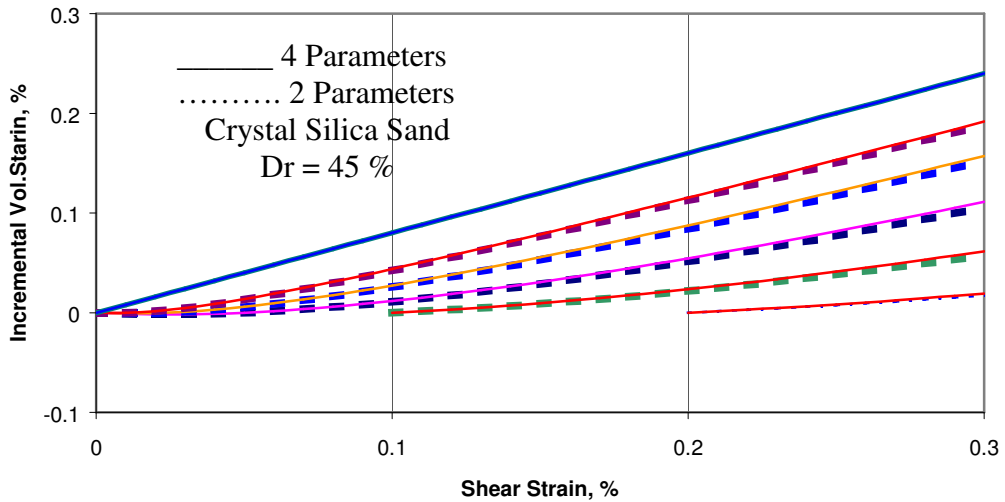


Figure 3-7 Incremental Volumetric Strain Curves

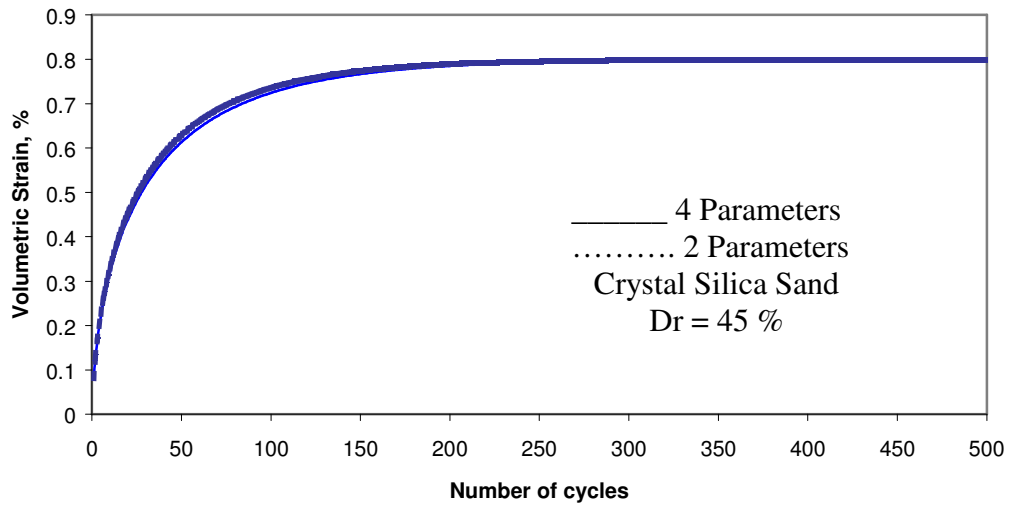


Figure 3-8 Volumetric Strain curves versus Number of Cycles

3.6 Hardening Parameters

Many materials strain harden under repetitive loading. The strain hardening law is of primary importance, as it is the key for understanding the cyclic behavior of the material.

Martin et al. (1975) presented a new empirical strain hardening law to describe the increase in shear stiffness of dry sand during cyclic simple shear loading. A relationship was developed between the shear stress-shear strain amplitude as a function of the accumulated volumetric strain and shear strain amplitude. The equation is of the form:

$$\tau = \frac{\gamma(\sigma'_v)^{1/2}}{a + b\gamma}$$

Where $a = A_1 - \frac{\epsilon_{vd}}{A_2 + A_3\epsilon_{vd}}$ and $b = B_1 - \frac{\epsilon_{vd}}{B_2 + B_3\epsilon_{vd}}$

A_1, A_2, A_3, B_1, B_2 and B_3 are six constant to be determined from experimental data.

In order to enable this relationship to be incorporated in DESRA, Finn, Lee, and Martin (1975) expressed the maximum shear modulus and maximum shear stress in the n th cycle as a function of the initial maximum shear modulus and maximum shear stress and thus reduced the number of constants to four as follows:

$$G_{mn} = G_{mo} \left(1 + \frac{\varepsilon_{vd}}{H_1 + H_2 \varepsilon_{vd}} \right)$$

$$\tau_{mn} = \tau_{mo} \left(1 + \frac{\varepsilon_{vd}}{H_3 + H_4 \varepsilon_{vd}} \right)$$

Where H_1 and H_2 are respectively $(A_1 A_2)$ and $(A_1 A_3 - 1)$

H_3 and H_4 are respectively $(B_1 B_2)$ and $(B_1 B_3 - 1)$

G_{mn} and τ_{mn} are respectively the maximum shear modulus and maximum shear stress at the n^{th} cycle, G_{mo} and τ_{mo} are the maximum shear modulus and maximum shear stress at the beginning of the test. Figure 3-9 shows the variation of the shear stress with both shear strain and volumetric strain as reported by Martin et al. (1975). Figure 3-10 shows the variation of the shear modulus with shear strain amplitude and accumulated volumetric strain, which is evaluated from the ratio of shear stress to shear strain amplitude for any cycle of loading.

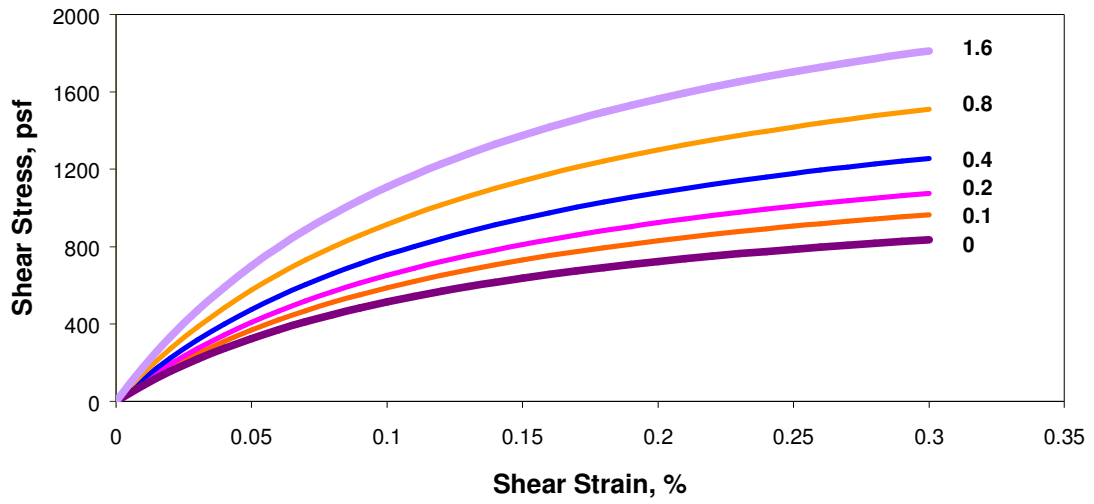


Figure 3-9 The Effect of Cyclic Shear Strain Amplitude and Volumetric Strain on Drained Stress-Strain Relationship (Martin et al.1975)

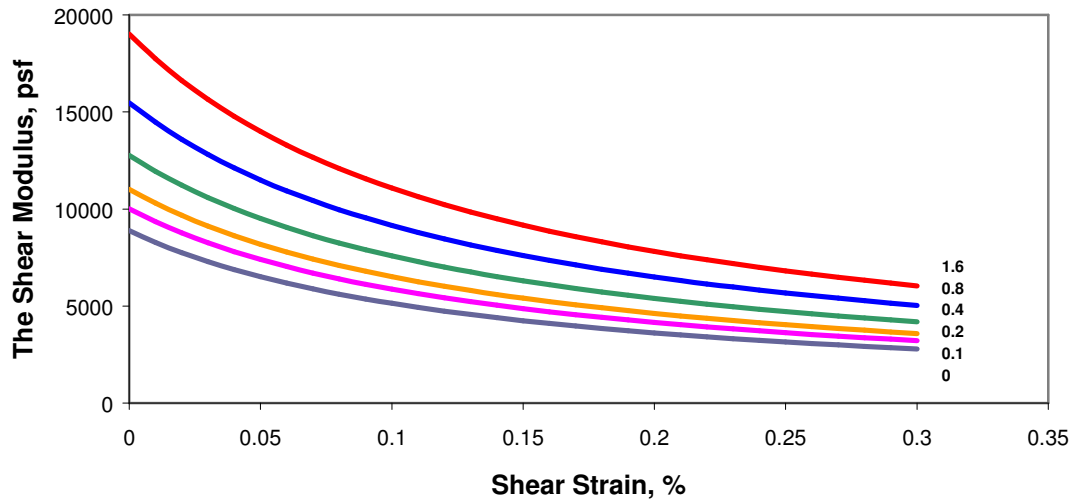


Figure 3-10 The Effect of Cyclic Shear Strain Amplitude and Volumetric Strain on Drained Shear Modulus-Shear Strain Relationship (Martin et al.1975)

Figure 3-11 shows the variation of the maximum shear modulus and the maximum shear stress with volumetric strain for shear strain amplitude of 0.3 %. It appears that their variation can be assumed linear and similar; hence, the six parameters can be replaced by only one parameter. Hence, the revised empirical expression for the increase in shear stiffness and shear stress is:

$$G_{mn} = G_{mo} \left(1 + \frac{\varepsilon_{vd}}{M_1}\right)$$

$$\tau_{mn} = \tau_{mo} \left(1 + \frac{\varepsilon_{vd}}{M_1}\right)$$

Where $M_1=1.48$ for the Crystal Silica sand with relative density of 45 %.

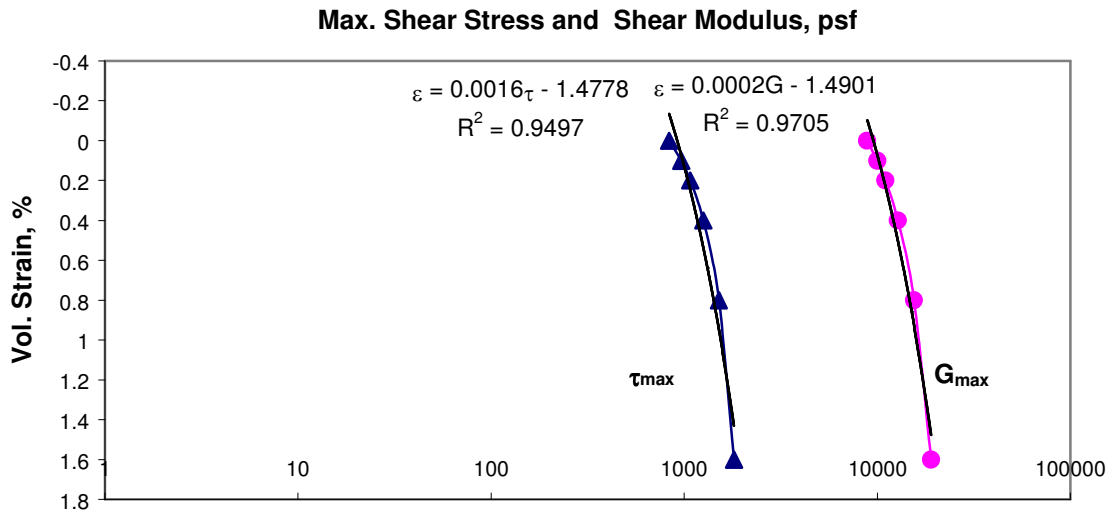


Figure 3-11 Variation of the G_{max} and τ_{max} versus the volumetric change

3.7 Pore-Water Pressure Increase During Undrained Tests.

As previously discussed, Martin et al., (1975) presented a detailed study of the volumetric changes in sand subjected to cyclic shear strains and proposed an empirical function to compute the incremental volumetric strain $\Delta\varepsilon_{vd}$ in dry sand as follows:

$$\Delta\varepsilon_{vd} = c_1(\gamma - c_2\varepsilon_{vd}) + \frac{c_3\varepsilon_{vd}^2}{(\gamma + c_4\varepsilon_{vd})}$$

Where c_1 , c_2 , c_3 and c_4 are four constant to be determined from two or three constant strain amplitude cyclic tests. $\Delta\varepsilon_{vd}$, ε_{vd} and γ are respectively the incremental volumetric strain, the accumulated volumetric strain and the shear strain all expressed as percentage.

They also proposed an analytical function to express the incremental pore water pressure in saturated sand, which can be described as follows:

Let us assume that a sample of saturated sand is subjected to one cycle of loading in a drained simple shear test, and let us assume that $\Delta\varepsilon_{vd}$ is the net volumetric strain increment due to slip at grain contacts and corresponding to the decrease in volume occurring during that cycle. For undrained conditions, it is reasonable to assume that slip at grain contacts resulting in volumetric strain increment $\Delta\varepsilon_{vd}$ will occur. However, the slip deformation must transfer some of the vertical stress carried by the intergranular forces to the more incompressible water. The increase in pore water pressure will result in decrease in vertical effective stress, which results in the release of recoverable volumetric $\Delta\varepsilon_{vr} = \frac{\Delta u}{E_r}$ strain stored by elastic deformation at grain contacts. For

volumetric compatibility, we must have:

Change in volume of voids = net change in volume of sand structure.

$$\frac{\Delta u \cdot n_e}{K_w} = \Delta \varepsilon_{vd} - \frac{\Delta u}{E_r}$$

$$\Delta u = \frac{\Delta \varepsilon_{vd}}{\frac{1}{E_r} + \frac{n_e}{K_w}}$$

Where Δu = residual pore water pressure increment; K_w = bulk modulus of water; n_e = porosity of the sample; E_r = tangent modulus of the one-dimensional unloading curve at a point corresponding to the initial vertical effective stress.

For saturated samples and assuming incompressible water, the equation becomes:

$$\Delta u = E_r \Delta \varepsilon_{vd}$$

Where the unloading modulus was reasonably fitted to a function of the form:

$$E_r = \frac{(\sigma'_v)^{1-m}}{mk(\sigma'_{v0})^{n-m}}$$

Where E_r is the unloading modulus of 1-D unloading curve at a point corresponding to the initial vertical effective stress and m, n, k are three controlling parameters.

These expressions are also incorporated in DESRA to compute the response of saturated sand.

CHAPTER 4

THE LABORATORY TESTING PROGRAM

4.1 Significance of Dynamic and Cyclic Soil Behavior Parameters in Civil Engineering

Soil deposits supporting civil engineering structures can be subjected to cyclic and dynamic loads by earthquakes, pile driving, traffic, explosions, machine foundations, ocean wave storms, and other causes. The cyclic loading is defined here as a repetitive loading while the dynamic loading is defined as a fast monotonic loading. The response of soil deposits and supporting structures to such loads depends to a large extent on the cyclic stress-strain characteristic of soil in shear. Consequently, for a successful and safe design of the civil engineering structures and their foundations, it is essential to know stress-strain properties of the foundation soil. Such soil properties are given in terms of a number of parameters that can be obtained either from field or laboratory testing.

There are several types of geotechnical laboratory tests that are typically used in today's practice to simulate field stress-strain conditions and provide designers with cyclic and dynamic soil parameters. They are: triaxial test, simple shear test, torsional shear test (solid or hollow cylinder), and resonant column test. Among these tests, the simple shear test stands out as the one that simulates field conditions in a relatively large number of problems in the most direct way, as discussed below. That is why the Simple shear test is used in this study to evaluate the whole range of dynamic and cyclic soil properties and parameters.

4.2 Simulation of Field Conditions by Direct Simple Shear Testing

Simple shear testing has become increasingly relevant because of both the greater awareness of the importance of stress-strain anisotropy in geotechnical problems and its simplicity relative to triaxial testing. Since the development of early simple shear device prototypes, including the cylindrical SGI type (Kjellman, 1955), the rectangular Cambridge type (Roscoe, 1953) and the cylindrical NGI type (Bjerrum and Landva, 1966), the interest in the test has grown. The apparatus is designed for the testing of soil specimens under the conditions of simple shear strains, which can reasonably well simulate the pure shear stress conditions. These conditions cannot be obtained directly with other standard laboratory testing methods, and yet they are applicable to a number of common field situations such as: horizontal portions of the slope failure surface and foundation bearing capacity failure surface, behavior of soil surrounding vertically loaded piles, etc. In soil dynamics, in particular, the role of simple shear testing is significant. In the cyclic simple shear test, the stress-strain conditions correspond rather closely to those occurring during the propagation of shear waves through soil deposits. A typical example of the pure shear stress conditions pertaining to a geotechnical earthquake engineering problem that can be simulated in the simple shear device is presented in Figure 4-1. The figure shows an idealized situation of vertically propagating seismic shear waves. In the analyses of seismic site response, the vertically propagating shear waves are considered the most important, because the resulting horizontal shaking of ground surface causes most of the damage to civil engineering structures. One-dimensional site response analysis is used to solve the problem of vertical propagation of horizontal shear waves (SH waves) through a horizontally layered soil

deposit. Horizontal soil layer behavior is approximated as a nonlinear shear moduli and damping parameters to characterize soil properties. This approach provides results that compare well with field measurements and is widely used in engineering practice. Non-linear site response analysis is employed by integrating the equation of motion of multi degree of freedom soil as shown in Figure 4-2. A non-linear constitutive relation is used to represent the hysteretic behavior of soil during cyclic loading. The simplest constitutive relations use a model relating shear stress to shear strain, whereby the backbone curve is represented by a hyperbolic function. Strain dependent modulus degradation curves are used to define the backbone curve. The Masing criteria and extended Masing criteria define unloading–reloading criteria and behavior under general cyclic loading. The geometry and stress-strain conditions of the element in Figure 4-1 resemble those generated in the simple shear test. These conditions and associated parameters are systematically described below.

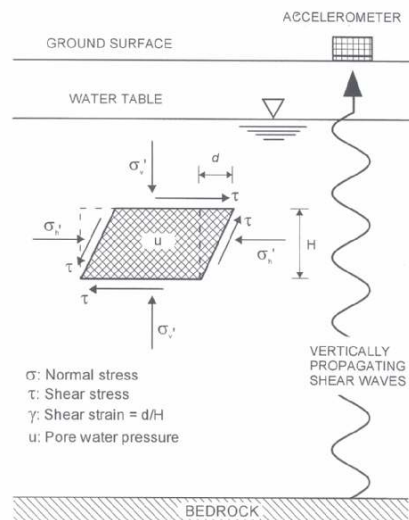


Figure 4-1 Idealized stress- strain conditions of a soil element during earthquakes

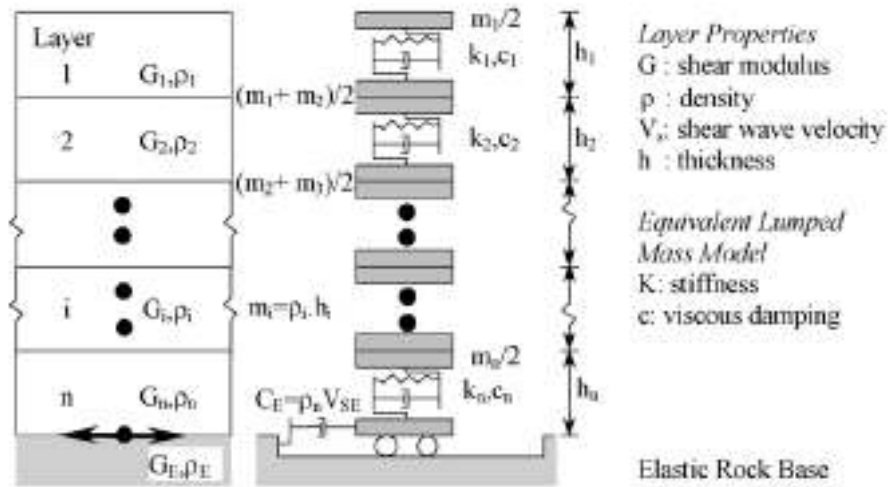


Figure 4-2 Multi-degree-of freedom lumped parameter model representation of horizontally layered soil deposit shaken at the base by a vertically propagating horizontal shear wave.

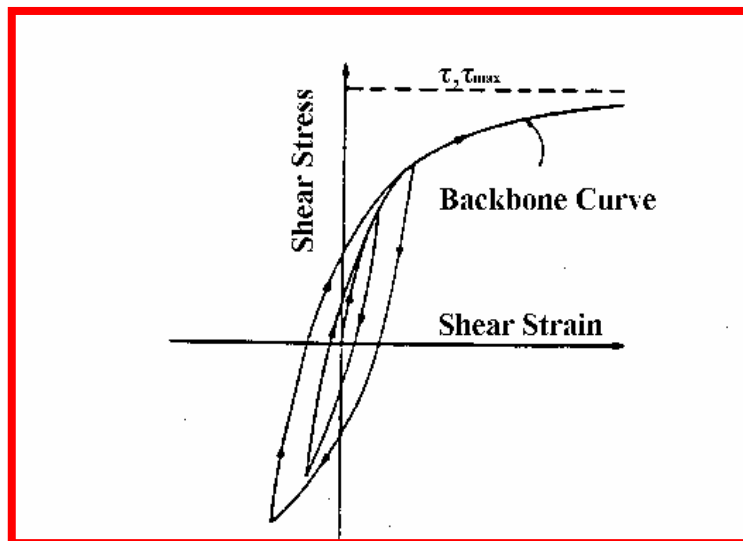


Figure 4-3 Idealized cyclic stress-strain loop

4.3 Characterization of Dynamic and Cyclic Behavior

In order to understand the simple shear test results, the parameters employed to describe them must be defined first.

4.3.1 Definition of Parameters

In Figure 4-3, an idealized cyclic stress-strain loop representative of the loops typically obtained in a cyclic simple shear test is presented. This loop describes the stress-strain behavior of the element presented in Figure 4-1 above. As shown in these two figures, such cyclic behavior and boundary conditions can be characterized with the following parameters:

σ_v = total vertical stress

σ'_v = effective vertical stress

u = pore water pressure

σ_h = total horizontal stress

$\sigma'_h = \sigma_h - u$ = effective horizontal stress

γ = shear strain

γ_c = cyclic shear strain amplitude

τ = shear stress

τ_c = cyclic shear stress amplitude

G_{\max} = maximum shear modulus at small strain

G_s = secant shear modulus

From the loops such as that in Figure 4-3, the parameter called the equivalent viscous damping ratio λ , can be determined as well. The definition λ of used in this report is illustrated in Figure 4-4. The ratio λ is expressed by the equation:

$$\lambda = \Delta w / 2\pi\tau_0\gamma_0, \text{ where } \Delta w = \text{area of the loop.}$$

In soil dynamics and geotechnical earthquake engineering practice, the cyclic soil behavior is conveniently characterized by several relationships which combine some of the above parameters, These relationships will be described in the following sections

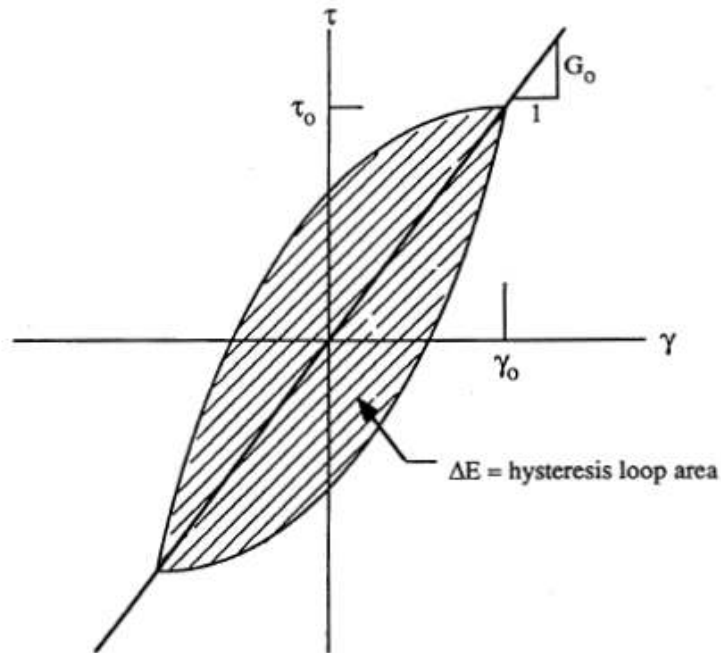


Figure 4-4 Definition of the equivalent viscous damping ratio, λ

4.3.2 Modulus Reduction Curve, G_s versus γ_c , Presented in a Semi-Log Format

The evaluation of the reduction of secant shear modulus, G_s , with γ_c is very important in soil dynamics. The secant shear modulus, G_s , is often used as a constant modulus in linear wave propagation and lumped parameter system dynamic analyses.

In Figure 4-5 a, an example of a modulus reduction curve is presented. The presentation in the semi-log format was originally suggested by Seed and Idriss (1970). Such a semi-log presentation emphasizes the modulus reduction in the range of strains, which are usually dominant in the soil dynamics and geotechnical earthquake engineering problems.

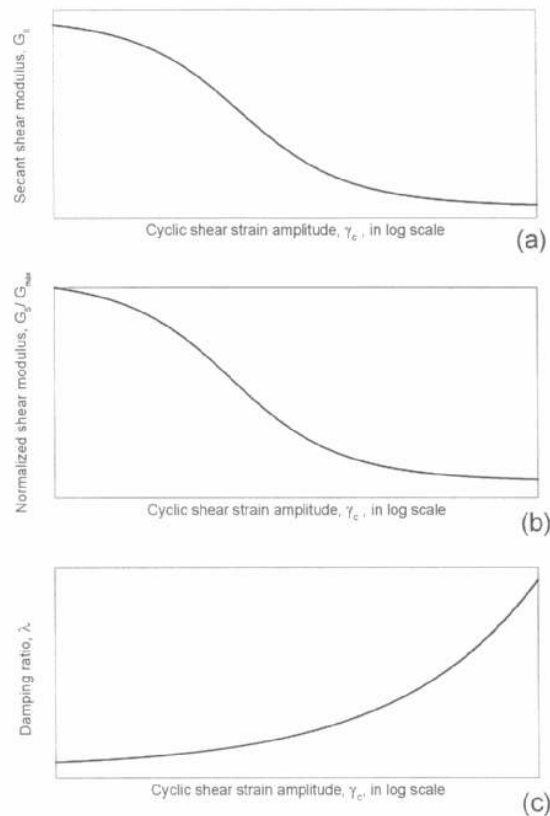


Figure 4-5 Modulus reduction and damping curves

4.3.3 Normalized Modulus Reduction Curve, G/G_{\max} versus γ_c , Presented in a Semi-Log Format.

Considering that variation of both G_s and G_{\max} depends more or less on the same parameters, such as confining or vertical stress, σ_v , overconsolidation ratio, OCR, and void ratio (Dobry And Vucetic, 1987), in particular in the range of small γ_c , it is convenient to present the reduction of G_s modulus in the normalized form with respect to G_{\max} , i.e., in the G_s/G_{\max} versus γ_c format. Consequently, the shape of the normalized modulus reduction curve, G/G_{\max} versus γ_c , depends predominantly on the type of soil, instead of the parameters just listed. An example of the G/G_{\max} versus γ_c modulus reduction curve is presented in Figure 4-5 b.

4.3.4 Equivalent Viscous Damping Ratio Curve, λ versus γ_c , Presented in a Semi-Log Format

The evaluation of the variation of the equivalent viscous damping ratio, λ , with γ_c is also very important in soil dynamics. Just like G_s modulus, damping ratio λ is often used in wave propagation and lumped parameter system dynamic analyses. The equivalent viscous damping ratio, λ , describes the critical damping ratio, of a one-degree-of freedom system subjected to a harmonic forcing function having the natural frequency *of* the system. The definition of λ in terms of the area *of* the cyclic loop, Δw , was derived by Jacobsen (1930) and is shown in Figure 4-4. In Figure 4-5 c, an example of λ versus γ_c curve is presented. Again, for convenience this relationship is customarily presented in a semi-log format.

4.3.5 Vertical Settlement Strain, ϵ_v , versus Number of Cycles, N

When cyclic loading is applied to an element of dry or partially saturated soil, the volume of the element will change due to the high compressibility of air in the voids. If the element is in a horizontally layered soil deposit and is subjected to vertically propagating seismic shear waves similar to that shown in Figure 4-1, radial strains will not develop and consequently the volume change will occur only in the vertical direction. This means that under such conditions the cyclic loading causes vertical settlement, which can be measured in term of accumulated vertical strain, ϵ_v . Figure 4-6 shows how a series of cyclic settlement tests with different constant cyclic shear strain can be presented.

Figure 4-7 illustrates applied cyclic shear strains, while Figure 4-8 illustrates the resulting variation of vertical strain with time. If several such cyclic strain controlled tests are conducted, a relationship between γ_c , ϵ_v and the number of cycles N, can be obtained.

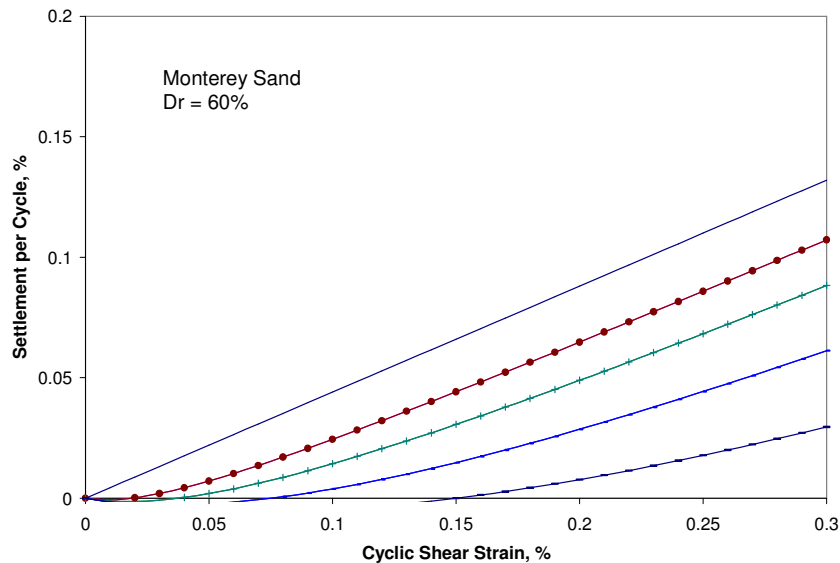


Figure 4-6 Incremental volumetric change versus number of cycles (Pyke 1975)

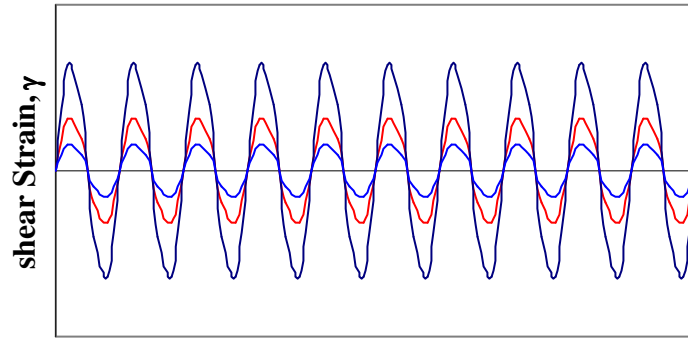


Figure 4-7 Applied shear strain history for three cyclic strain controlled tests

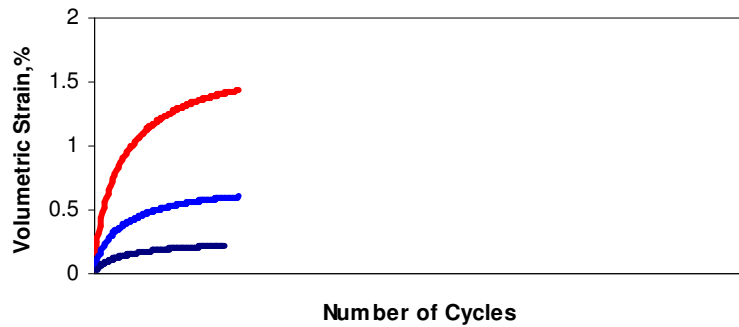


Figure 4-8 Variation of vertical strain with number of cycles

4.4 Scope of the Experimental Investigation

4.4.1 Soil Samples Tested and Analyzed

Two types of sands were tested in dry conditions for this investigation, while many previous results were collected, analyzed and compiled. A series of tests on 14 different types of sand developed by a UCLA research team were also compiled and analyzed. Details are provided in paragraph 4.9.

4.4.2 Types of Cyclic and Dynamic Direct Simple Shear Tests Conducted

A serie of direct simple shear (DSS) tests were conducted with respect to the applied level of cyclic shear strain amplitude, γ_c , using equipment in Professor Vucetic UCLA laboratory. They are labeled as DSS-L test.

The DSS-L tests were conducted in the standard NGI DSS device. Each test included a single cyclic stage with a an amplitude γ_c approximately between 0,1% and 0.3%. The volume change was allowed in this test, making it a cyclic settlement test. The main purpose of the test was to obtain the stress-strain properties of dry and partially saturated soils in the range of small cyclic shear strains. In conclusion, there is a total of 18 different cyclic simple shear tests conducted, where many soil samples were repeatedly tested in the same type of test but with different overconsolidation ratio. In some tests, the shape of cyclic straining was changed from sinusoidal to triangular to examine its effect on damping, which was found to be significant.

In some tests, the frequency of the cyclic loading was varied as well. This was done to examine its effect and the effect of the corresponding average rate of straining on both secant moduli and damping ratio.

4.4.3 Types of Classification of Tests Conducted

As shown in Table 4-1 through Table 4-3, the following classification tests were conducted on most of the oils samples in accordance with the ASTM standards:

ASTM D 4253, ASTM D 4254, ASTM D 422-63 (1992) and ASTM D 4318-90 (1992).

Sieve analysis tests were conducted to construct the grain size distribution curves. The Atterberg limits tests were conducted on the fines passing sieve #40 with the diameter of openings of 0.425 mm, and were used to determine the locations of the fines in the Unified Soil Classification System (USCS) plasticity chart. If the Atterberg limits tests could not be performed, the sample was labeled as nonplastic. The grain size distributions and the results of Atterberg limits tests were used jointly to determine the classification symbols of the soils tested according to the Unified Soil Classification System (USCS). The color of samples was also determined. It should be noted that $PI=0$ was assigned to non-plastic soils, although Atterberg limits tests could not and were not conducted on these soils. This was done to enable comparison of the non-plastic and plastic soils on the same charts and within the same frame.

4.4.4 Cyclic and Dynamic Testing Equipment

Cyclic simple shear tests were performed under drained conditions to evaluate vertical strain accumulation when uniform-amplitude cycles of shear strain are applied to the soil specimen. Commercially available wire-reinforced membranes were used to laterally confine the cylindrical soil specimens, which were prepared to a diameter of 102 mm and a height of 22 mm. These membranes minimized lateral expansion of the test specimens, while providing negligible shear stiffness. Since the effect of overburden pressure on vertical strain has previously been found to be minor (e.g., Silver and Seed 1971, Youd 1972, Pyke et al. 1975), all tests were performed under the same vertical stress of 101.2 kPa. A sinusoidal loading frequency of 1 Hz was used to induce cyclic shear strain amplitudes between $0.1\% \leq \gamma_c \leq 0.5\%$.

4.4.5 Standard NGI Direct Simple Shear Test

The NGI direct simple shear apparatus was developed in the 1960's (Bjerrum and Landva, 1966) for the testing of highly sensitive Norwegian quick clays. Since then, the device has been used throughout the world. The NGI device at the UCLA Soil Dynamics Laboratory is shown in Figure 4-9 and its components in Figure 4-10. The specimen setup is shown in Figure 4-11 and in Figure 4-12. It can be seen that the soil specimen is enclosed in a reinforced rubber membrane which prevents radial deformation during consolidation and shear, but allows the specimen to be deformed vertically and in simple shear, which is a unique feature of the NGI DSS test concept. The test can be performed under one of the following two conditions: (i) drained condition under which the specimen volume change is allowed, or (ii) constant volume conditions which are equivalent to undrained conditions. The drained test is appropriate for testing of cyclic settlement of dry and partially saturated soils, while the constant volume test is appropriate for testing of fully saturated soils. The undrained conditions are simulated in the constant volume test by continuously adjusting the vertical stress such that the specimen height is kept constant. Assuming that radial strains are close to zero or negligibly small, the change in vertical stress under such constant volume conditions is assumed to be equal to the change in pore water pressure that would have occurred in a truly undrained test. Such a pore water pressure simulation is the most fundamental principle of the NGI DSS test on fully saturated soils. Verification of this concept is described by Dyvik et al. (1987).

In the NGI DSS device different sizes of specimen can be tested, as shown in Fig. 4b. The specimens tested at UCLA had the diameter of 66.7 mm and height of approximately

18 to 19 mm. The monotonic and cyclic loads, or displacements, were applied and controlled by a servo hydraulic system operated via a computer, which was manufactured by the Instron company. The parameters were measured with electronic load cells and displacement transducers. The recorded data were processed with a data acquisition system. The cyclic tests were exclusively displacement-controlled, i.e., in any cyclic stage the cyclic strain amplitude, γ_c , was maintained approximately constant.

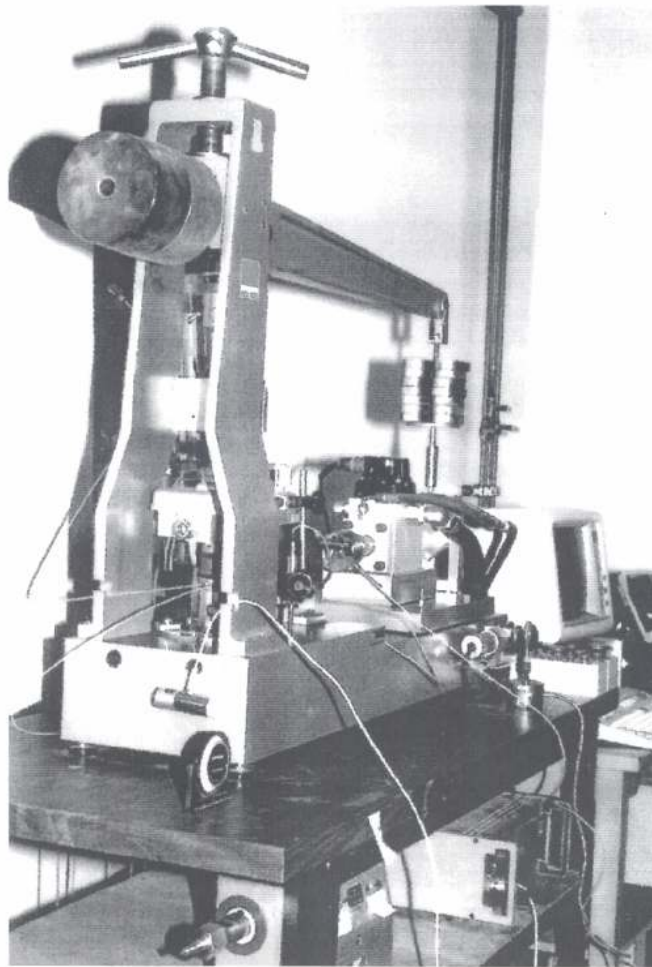


Figure 4-9 View of the NGI direct simple shear device with hydraulic actuator at the UCLA Soil Dynamics Laborator

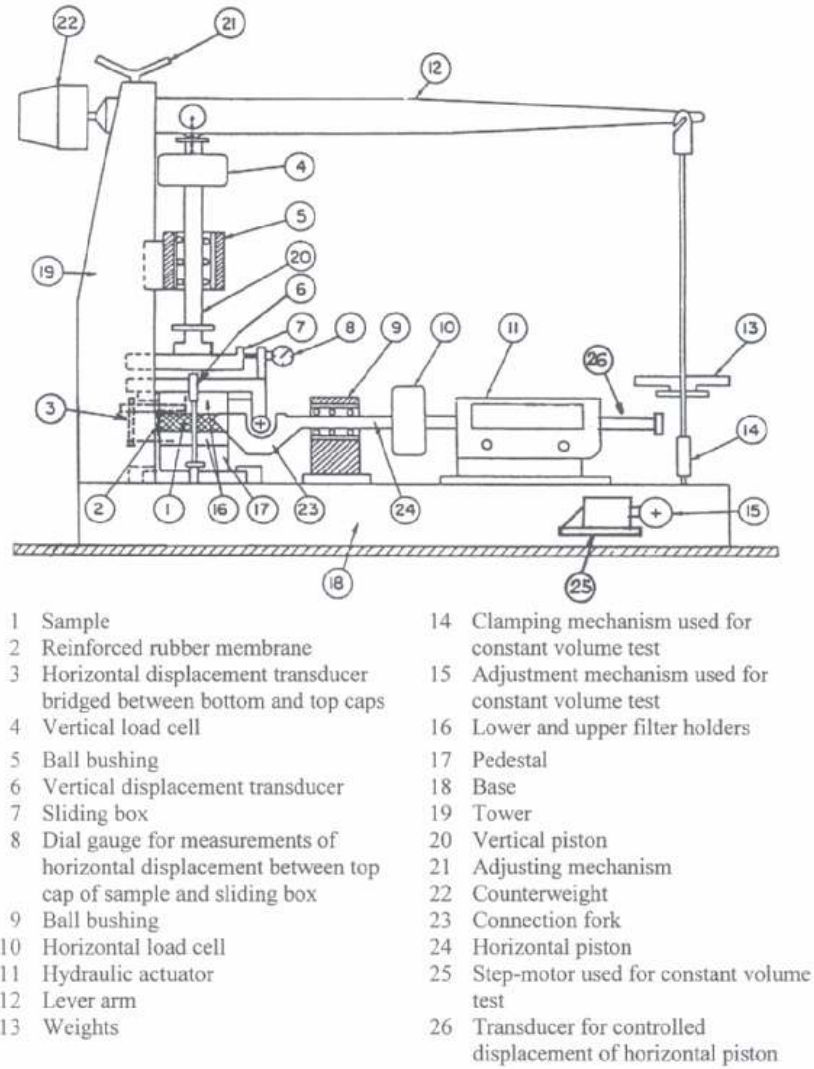


Figure 4-10 The NGI simple shear device at UCLA with the description of components

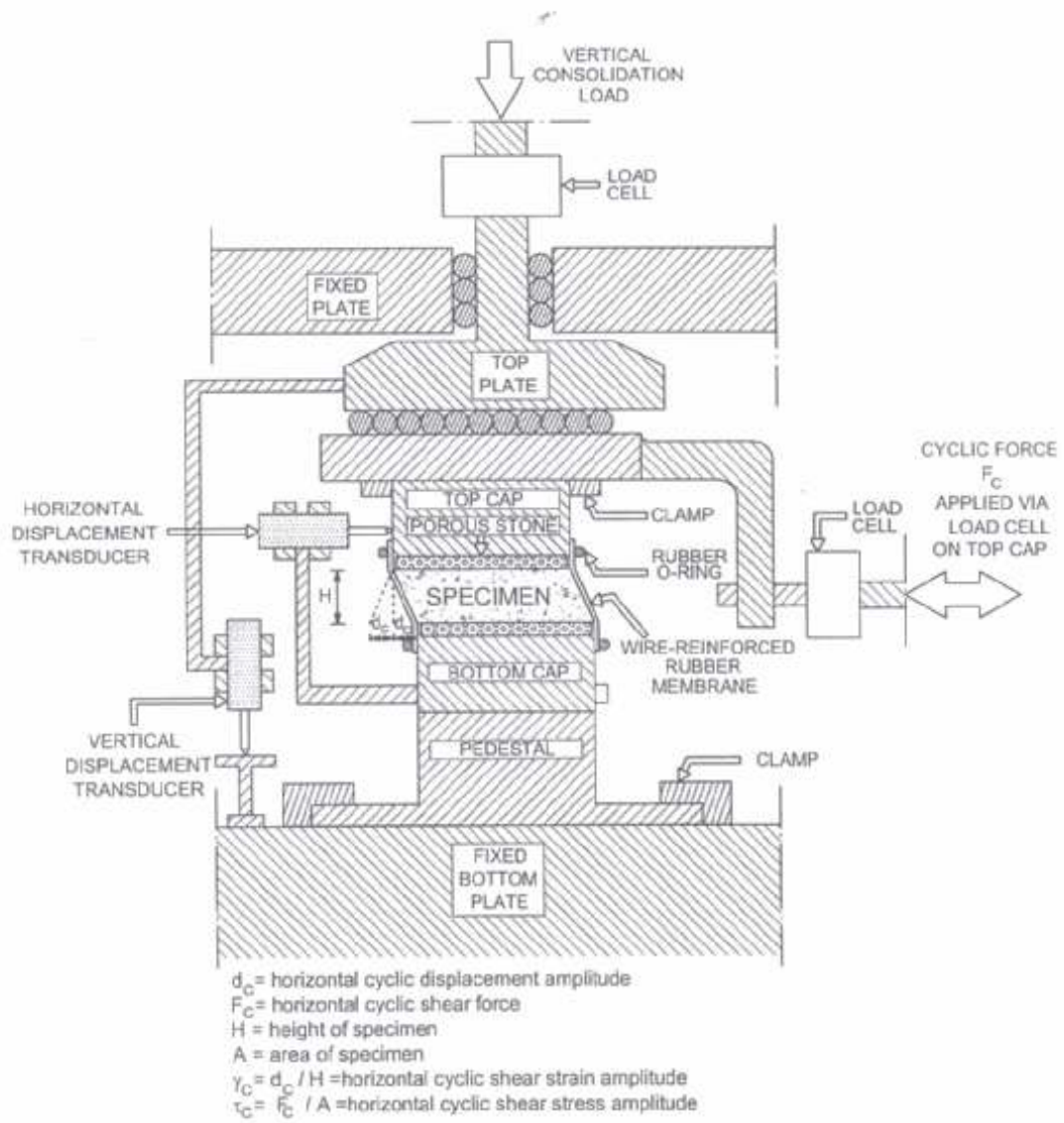


Figure 4-11 Illustration of the principles of testing with the NGI direct simple shear device

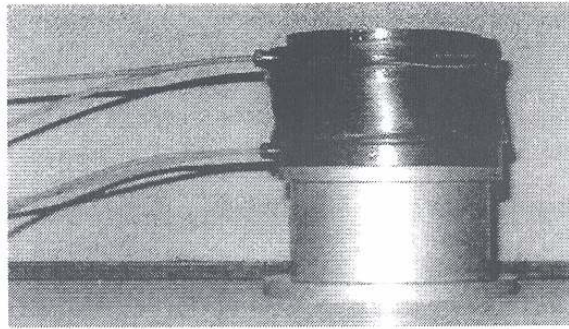


Figure 4-12 View of the specimen setup after shearing in a static test

4.4.6 Boundary Conditions in NGI Type Simple Shear Test

As already stated in Section 1.6, the simple shear test can only approximately reproduce field situations of pure shear state of stresses. The difference between the simple shear and pure shear state of stresses is sketched in Figure 4-13. The figure indicates that in the case of simple shear the distributions of stresses (and strains) on the specimen boundaries is nonuniform, with significant stress and strain concentrations along the edges of the test specimen. Such nonuniform distribution of stresses is presented in Figure 4-14. In the following both theoretical and experimental studies on this subject are briefly reviewed.

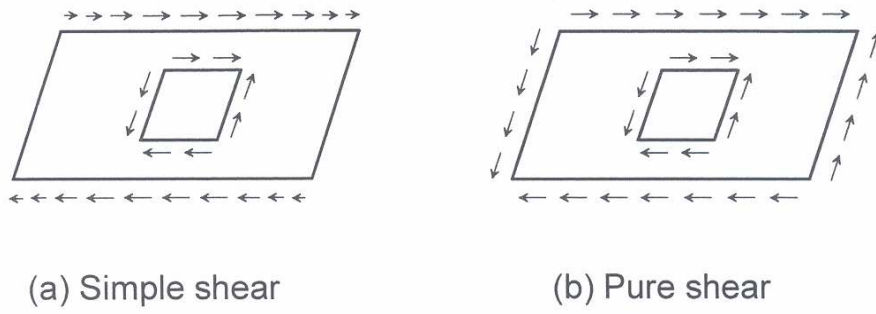


Figure 4-13 Simple shear and pure shear conditions

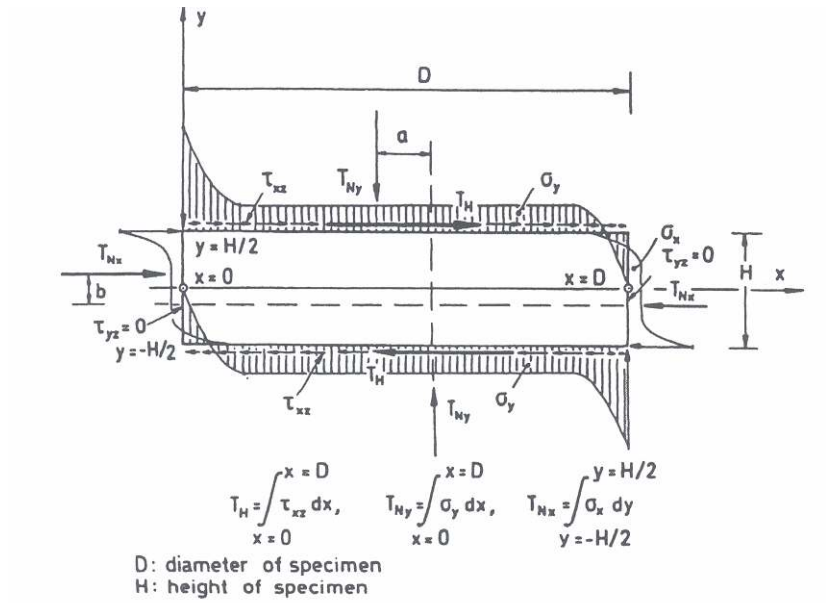


Figure 4-14 Stress distribution on the specimen boundaries and corresponding resultant forces (Vucetic and Lacasse, 1982)

4.5 Brief Review of two Theoretical Studies on the Stress and Strain Distributions in the Simple Shear Specimen

Lucks, et al. (1972) provided the first theoretical stress distribution in an NGI simple shear test. They presented an elastic three dimensional finite element solution for undrained tests. From analyses with axially symmetric elements loaded unsymmetrically, the researchers concluded that approximately 70% of the specimen has a remarkably uniform stress condition and that the average shear stress increment applied on the horizontal boundaries lies within 2% of the horizontal shear stress in the zone of uniformity within the specimen. Figure 4-15 presents the distribution of stresses for one of the specimen geometries analyzed.

Shen, et al. (1977; 1978) described very systematically the influences of various factors on the stress-strain distribution, including the effects of both height to diameter ratio and membrane stiffness. They predicted the stress-strain behavior of an idealized linear elastic solid specimen in the NGI device. The computations were performed with three-dimensional finite element analyses of a non-axisymmetrically loaded axisymmetric solid. Orthotropic elements were incorporated in the program to simulate the action of the wire-reinforced rubber membrane. Shen et al. (1977; 1978) also showed that the stress-strain distribution is nonuniform but acceptable for practical engineering analyses.

In conclusion, the described theoretical solutions show that the NGI simple shear test interprets pure shear stress-strain conditions rather well. The influence of the non-uniformities of stress-strain distribution on the shear strength of the specimen seems relatively small, if the disturbances due to sampling and trimming are taken into consideration. The above solutions are given for the linear elastic material. For the

elasto-plastic material concentrations of the stresses on the edges of the specimen would decrease due to yielding.

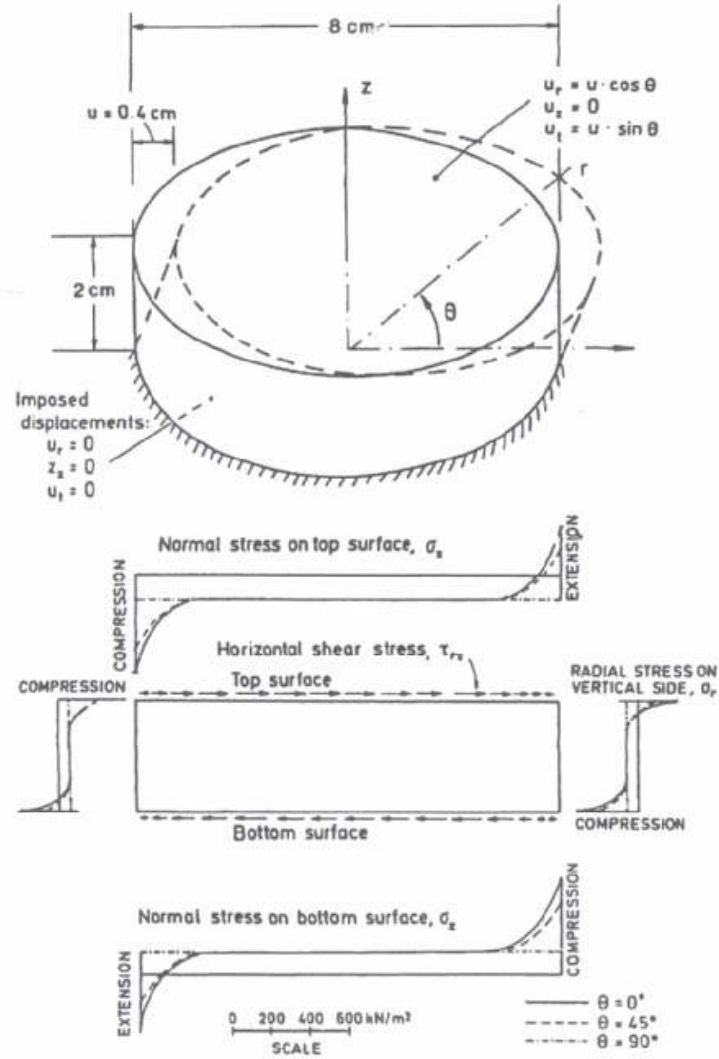


Figure 4-15 Normal stress distribution at specimen boundary (Lucks et al., 1972)

4.6 Review of Some Experimental Studies on Stress Distribution

There are several experimental studies published, dealing with the stress-strain distribution of specimens in the simple shear devices. Three of them are presented below:

Ladd and Edgers (1972) presented a comprehensive study of simple shear testing of clay in the NGI simple shear device. They described and compared the results of tests on seven clays with a wide range of plasticity. Based on experience and existing literature, they concluded that the stress and strains generally appear quite uniform, and that the measured values of shear strains, horizontal shear stress and vertical effective stress represent adequately the average conditions within the specimen. Budhu and Wood (1979) analyzed the results of NGI and Cambridge simple shear static tests. For both types of tests, the normal stresses, shear stresses and formations along the boundaries were measured. They showed that both apparatuses developed non-uniform boundary stresses on the sample. They concluded that the average ratio of shear stress to normal stress on the top and bottom horizontal boundaries underestimated the stress ratio in the center of the sample by about 12% in monotonic loading.

Based on the assumption that the no uniformities are greater if the specimen height to diameter ratio is larger (see Figure 4-15), Vucetic and Lacasse (1982) tested plastic clay specimens with three different ratios. The experimental results showed that the range of the height to diameter ratio tested has no significant influence on the static stress-strain behavior. The authors concluded that the direct simple shear test yields useful results and represents a valuable test to define the stress-strain behavior of soil in engineering practice.

4.7 Examples Direct Simple Shear (DSS-L) test results

In order to understand comprehensive results of the tests, selected results obtained in a DSS-L test are presented below and briefly discussed. The results presented below are from tests on Silica sand sample. The results obtained on silica sample in the DSS-L test are presented in Figure 4-16 through Figure 4-24. The DSS-L test was conducted in cyclic strain-controlled mode, with a magnitude of γ_c varying between 0.1% to around 0.5 %. The figures show the time histories of strains and stresses and settlement with time. The results show clearly that the settlement of sand with respect to time increases as the applied shear strain increases.

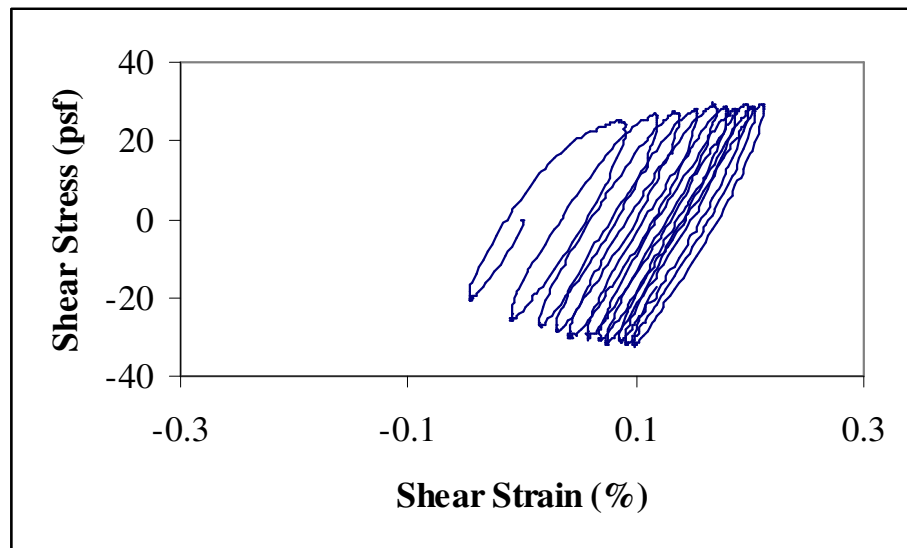


Figure 4-16 Typical stress- strain plot obtained with the DSS-L

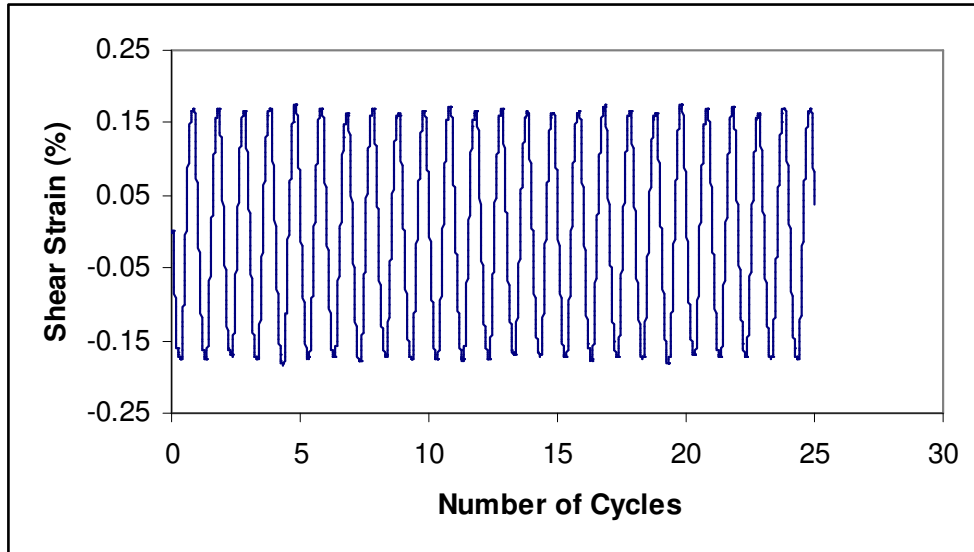


Figure 4-17 Example of shear strain time history results for Silica sand

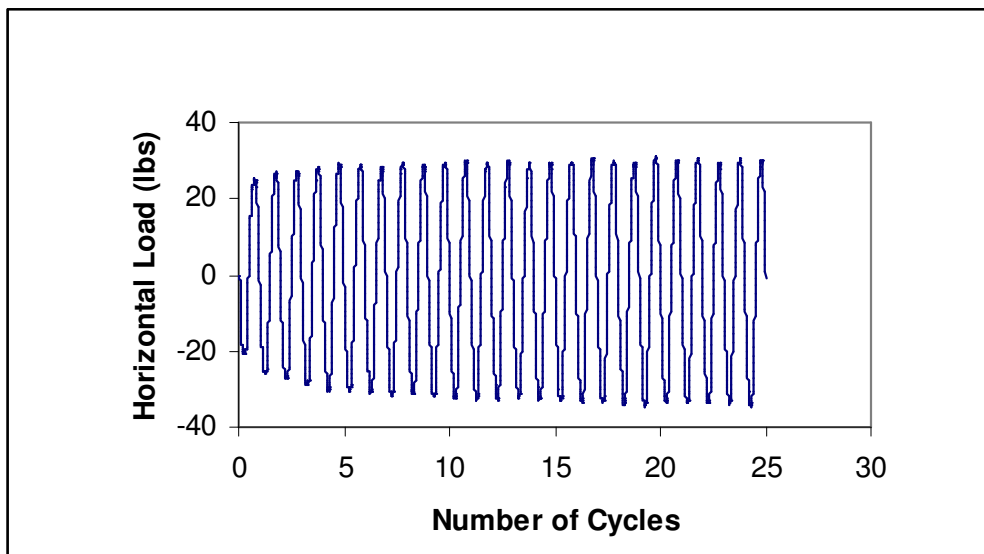


Figure 4-18 Example of shear stress time history results for Silica sand

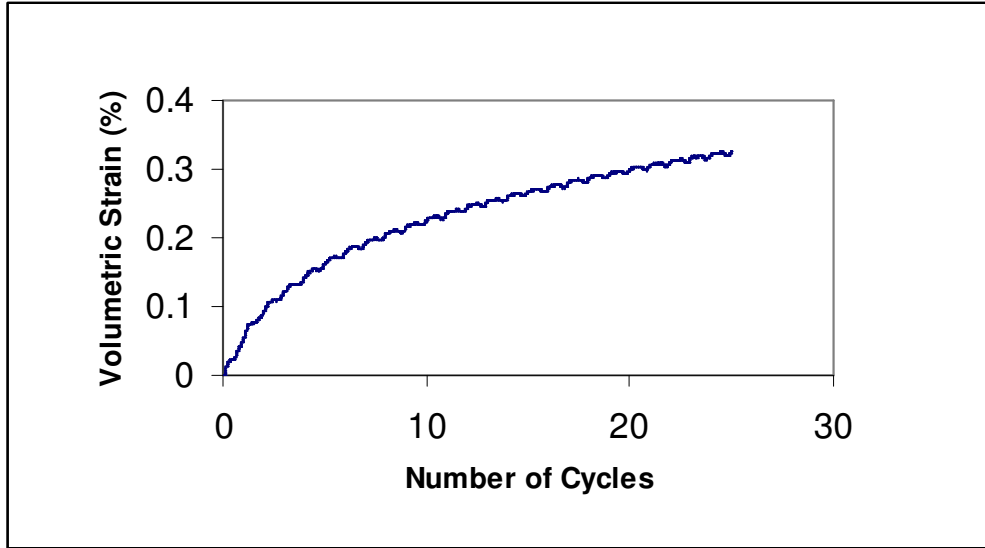


Figure 4-19 Example of volumetric strain time history results for Silica sand

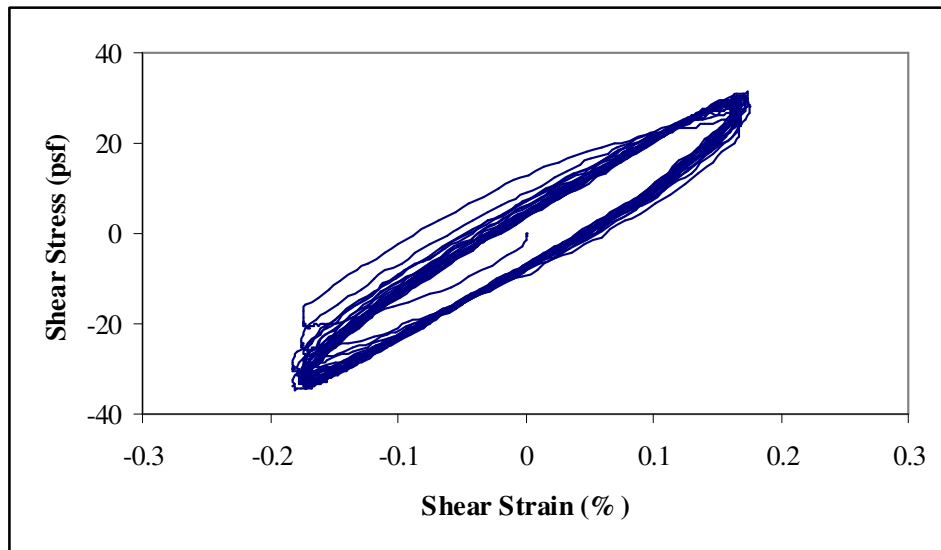


Figure 4-20 Example of cyclic loops for Silica Sand

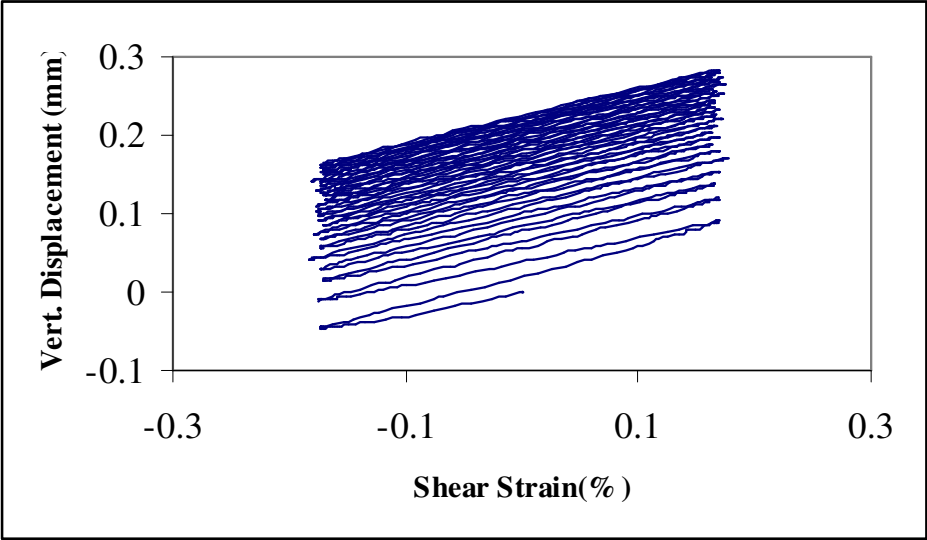


Figure 4-21 Example of shear strain versus vertical displacement

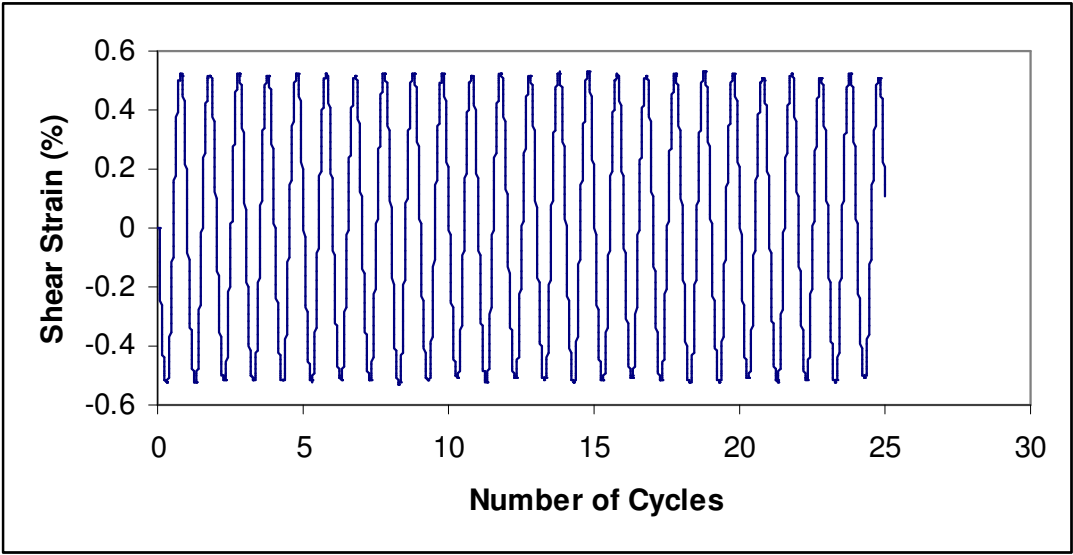


Figure 4-22 Example of shear strain versus number of cycles

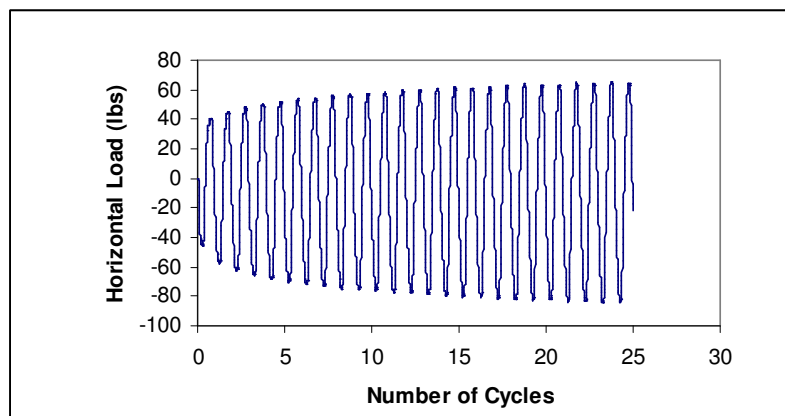


Figure 4-23 Example of horizontal load versus number of cycles

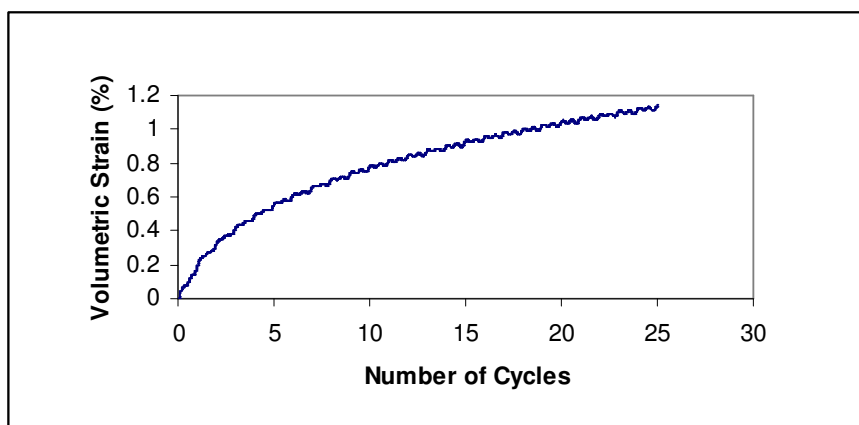


Figure 4-24 Example of vertical displacement versus number of cycles

4.7.1 Synthesis of Modulus Reduction and Damping Results From Tests

The modulus reduction and damping results from the DSS-L tests are synthesized in Figure 4-25. G/G_{max} versus γ_c It can be seen that the synthesis provides the G/G_{max} versus γ_c curve and λ versus γ_c curve for a wide range of cyclic shear strains. The γ_c curve is plotted from $\gamma_c = 0.0001\%$ to 1% , while λ versus γ_c curve is plotted from

$\gamma_c = 0.001\%$ to 1% . The modulus reduction and damping curves were also compared with the average curves for different sand types recommended by Seed et al. 1984; and Iwasaki, et al. 1978. The comparison shows good the agreement

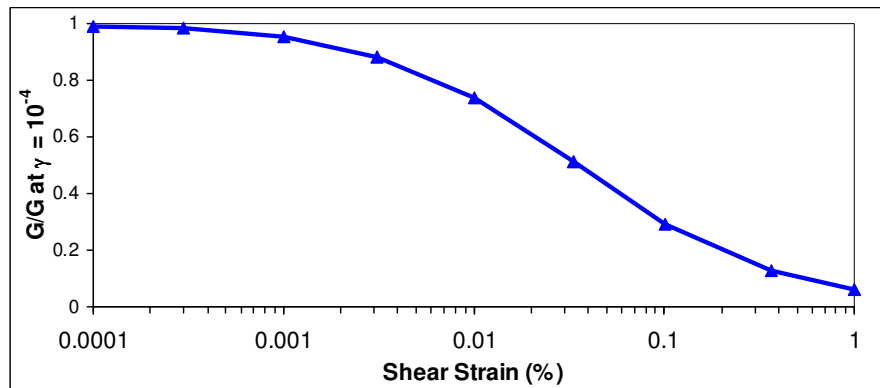


Figure 4-25 Degradation of G/G_{\max} versus shear strain

4.7.2 Identification and Inspection of The Cyclic Stress-Strain Loops

During the test, the analog electrical signals from testing device transducers are first amplified and then digitized with the help of the "LabTech Notebook" software. The frequency of digitization is usually set to 100 records per second, resulting in a large file of digitized data that needs to be processed. To identify, separate and inspect the cyclic loops from the recorded data the "Matlab" software was chosen for its computational ability and ease of programming.

Using the built-in artificial intelligence and boundary criteria, two "Matlab" language scripts, one tailored for the DSDSS device and the other for the NGI-DSS device, were programmed to read the recorded data processed by "LabTech Notebook" and display

them in a manner that allows easy identification and inspection of the cyclic loops. This step enable the user to graphically view the data loop by loop, verify its accuracy and integrity and either select or reject them for the input into the database. For the cyclic loops selected to be entered into the database the "Matlab" script automatically calculates secant shear modulus, damping ratio and other relevant parameters and outputs them to a "Microsoft Excel" compatible "Lotus" worksheet.

This identification and inspection step was designed mainly by Dr. Marco D'Elia, a former UCLA research fellow.

4.8 Organization of the Data Into the "Microsoft Excel" Worksheet Files

The next step is further organization and inspection of the data, and their arrangement for easy input into the database. For this purpose the data are transferred from the "Lotus" to a "Microsoft Excel" worksheet. The new arrangement in the "Microsoft Excel" worksheet format allows, for example, the viewing (and plotting) of the entire set of cyclic loops from a test or a step of the test. In this way the integrity and accuracy of the data can be verified further before the data are input into the database.

4.9 Input of the Data Into the Database

The "Microsoft Access" database software was selected to develop a complex and powerful database of the cyclic loop data. This database is the backbone of the 81' interpretation and analyses of cyclic soil behavior trends and relations presented in this thesis. The database consists of a complex structure of 10 separate tables and over

hundred fields with the data on the cyclic loops characteristics that are linked and can be related to each other. In spite of its complexity, the database is quite flexible and relatively easy to use. Using the prepared "Microsoft Excel" worksheet described in the above step, the database is also easily maintainable and updateable with the data from new tests. It was designed not just for handling the simple shear test results data, but also to accommodate the results of other types of tests that can be gathered from the literature. Manipulation and automatic graphical presentation of the data with "Microsoft Excel". In order to speed up the analysis of the large amounts of data contained in the database, the "Microsoft Excel" software is used again to link automatically the complex database queries to the database. Using the capabilities of the "Microsoft Excel" software, the multiple queries to the database are set up to define certain elaborate criteria by which the data should be selected from the database and automatically manipulated and plotted. The given structure and parameters of queries can be easily changed, allowing for the dynamic refreshment of the data meeting the new updated criteria. In this way one can observe the graphical results immediately, and repeat the same procedure with new criteria until appropriate and satisfactory results are obtained. Almost all of the behavioral trends and correlations obtained in this dissertation and presented in the following chapters are the product of this innovative procedure. This chapter discusses the details of the laboratory-testing program performed to clarify the manner in which sand's type affects the cyclic behavior susceptibility of sandy soils. First, the component of the soils and soil mixtures tested are discussed. This discussion focuses on the index testing program and the index properties of the soils.

Next, a brief review of cyclic simple shear testing is presented with an emphasis on the differences between in-situ and laboratory conditions and loadings. Last, and following an explanation of some of the testing parameters, which affect cyclic behavior of sands, a detailed test methodology is presented.

4.10 Soils Tested

The cyclic simple shear testing program considered in this study is based on 18 clean sand materials. The sands were selected to span a range of material gradation, particle size and particle shape. Compositional soil properties of the tested sands are presented in Table 4-1 through

Table 4-3, and the grain size distribution curves are shown in Figure 2.1. The maximum and minimum densities and void ratios of each of the sands were determined by using the Modified Japanese method and dry tipping and the standard ASTM D4253 and D4254. For 8 types of sand, both methods were used and the results were very comparable. Table 4-1 contains the two base sands tested for this study and their properties and Table 4-2 contains the sands tested previously by Silver and Seed (1971), by Martin et al.(1975), by Pyke (1975), by Bhatia (1980) and by Chung (2004) and their index properties while

Table 4-3 contains the sands tested by Stewart et al. (UCLA 2004) and their index properties. It should be mentioned that Nevada sand tested for this study and by Chung (2004) was also used and extensively in the VELACS program (Verification of Liquefaction Analyses by Centrifuge Studies Laboratory Program, 1992).

Sand	D₁₀ (mm)	D₃₀ (mm)	D₅₀ (mm)	C_u	C_c	e_{min}	e_{max}	e D_r=60%
Crystal Silica #30	0.5	1.5	1.6	1.5	0.89	0.689	1.016	0.820
Nevada	0.15	0.12	0.15	1.30	0.49	0.51	0.886	0.661

Table 4-1 Index properties of tested sand

Sand	D₁₀ (mm)	D₃₀ (mm)	D₅₀ (mm)	C_u	C_c	e_{min}	e_{max}	e D_r=60%
Crystal Silica (Silver & Seed, 1971, Martin et al. 1975)	0.5	0.60	0.63	1.5	0.96	0.633	0.973	0.777
Monterey (Pyke, 1975)	0.4	0.77	0.38	1.6	0.97	0.55	0.85	0.670
Ottawa C109 (Bhatia, 1980)	0.35	1.5	1.6	1.7	0.89	0.5	0.83	0.628
Nevada (Chung, 2004)	0.14	0.5	0.15	1.81	0.99	0.57	0.85	0.6

Table 4-2 Index Properties of previous history tested sands

Sand	D₁₀ (mm)	D₃₀ (mm)	D₅₀ (mm)	C_u	C_c	e_{min}	e_{max}	e D_r=60%
Crystal Silica	0.55	0.60	0.81	1.62	0.74	0.705	1.072	0.851
Silica #0	0.65	0.77	0.89	1.45	0.97	0.674	0.983	0.797
Silica #2	1.4	1.5	1.6	1.29	0.89	0.689	1.016	0.820
Flint 13	0.42	0.5	0.56	1.43	0.99	0.545	0.811	0.651
Flint 16	0.28	0.41	0.5	2.11	1.02	0.530	0.822	0.646
F-52	0.18	0.25	0.28	1.72	1.12	0.533	0.837	0.658
F – 110	0.08	0.10	0.13	1.90	0.84	0.616	0.884	0.722
Nevada	0.15	0.17	0.19	1.30	0.99	0.553	0.907	0.694
Irwindale	0.30	0.61	1.0	4.67	0.89	0.485	0.749	0.591
Post office	0.10	0.17	0.29	5.0	0.72	0.449	0.706	0.553
Pacoima #1	0.15	0.25	0.38	3.07	0.91	0.564	0.920	0.705
Pacoima #3	0.22	0.35	0.55	3.18	0.80	0.535	0.882	0.674
Vulcan	0.21	0.37	0.51	2.90	1.07	0.501	0.829	0.634
Newhall	0.08	0.18	0.37	4.28	0.41	0.546	0.945	0.705

Table 4-3 Index Properties of UCLA tested sands

4.10.1 Preparation of Specimen

Dry specimens ($S = 0\%$) were prepared using a dry pluviation method similar to that used by Silver and Seed (1971). A pre-weighed amount of oven-dried sand was poured into a wire-reinforced membrane that was pre-mounted to the bottom specimen cap with a screen placed at the base. Then, the screen was pulled up through the specimen to give each specimen essentially the same initial structure. After flattening the specimen and mounting the top specimen cap, a high frequency (60 Hz) vibrator was placed on the top cap to densify the specimen to a predetermined height that would achieve the target relative density. Other soil sand specimens were also prepared using tamping and kneading compaction methods to evaluate the effect of different specimen preparation techniques. In the tamping method, specimens were prepared in two lifts using the same wire reinforced membrane and compaction mold. A pre-weighed amount of oven-dried sand was loosely placed and gently tamped to a pre-determined height to achieve the target relative density after application of 1.0 atm of vertical stress. The kneading method uses a Harvard miniature compactor to induce shear strains during compaction and replicate what occurs in the field with a sheep foot roller. The kneading compaction technique is commonly used for soils with fines, but was adapted for clean sands in this study. This method is procedurally similar to the tamping method, with the exception of kneading rather than tamping to densify the specimen. A comparison of the results showed a reasonable agreement with the vibration compaction.

4.10.2 Grain Size Characteristics

The grain size distribution of each soil was determined in general accordance with ASTM D 422, Standard Test Method for Particle Size Analysis of Soils. The mean grain size D₅₀, the coefficient of uniformity, C_u, and the coefficient of curvature, C_c, for each sand were computed.

4.10.3 Maximum and Minimum Void Ratios

The vibratory table method (ASTM D 4252, Standard Test Method For Maximum Index Density Of Soils Using a Vibrating Table) shown in Figure 4-26 is limited to soils with maximum fines of 15 percent, while proctor tests do not always produce accurate, repeatable results for clean sands. Therefore, vibratory table as well as both Standard and Modified Proctor tests were performed for each sand. In agreement with the findings of Lee and Fitton (1968), the vibratory table tests yielded maximum dry densities similar to those produced by the Modified Proctor test. Because the vibratory table tests were found to give more repeatable results, they were used to define the maximum index densities and minimum index void ratios used in this study. Similarly, there is no ASTM procedure for determining minimum density for cohesionless soils which is applicable over the entire range of silt contents investigated in this study. The minimum density method (ASTM D- 4254, Standard Test Method for Minimum Index Density of Soils and Calculation of Relative Density) is limited to soils with maximum fines of 15 percent. Because our sands was clean sand, the maximum index void ratio and corresponding minimum index density for each soil mixture was determined in general accordance with the method presented in the specification. Both Method B and Method C of this standard were performed and found to give similar results. Method B consists of filling a tube, the

base of which is sitting within a mold of known weight and volume, with dry soil and then slowly lifting the tube so that the soil flows out and fills the mold. The soil is then struck level with the top of the mold, the mold and soil weighed, and the density determined. Method C consists of partially filling a glass cylinder with a known weight of dry soil and slowly inverting it. The height of the soil in the cylinder is then measured and the density determined. The values of minimum index density and maximum index void ratio determined by these two methods were similar. Those determined using Methods B were found to be slightly more consistent, and were used in the study.

4.10.4 Specific Gravity

Specific gravities were determined in general accordance with ASTM D 854, Standard Test Method for Specific Gravity of Soil for each sand.

4.10.5 Cyclic Simple Shear Testing

Cyclic simple shear tests attempt to model the loads applied to a soil mass by an earthquake. There are several differences between the loads applied to a soil mass in the field and those applied to a specimen in a cyclic simple shear test. Additionally, numerous factors can affect the cyclic behavior developed in a cyclic simple shear specimen and make it differ from that which might be developed in the field. These include the method of specimen preparation, the relative density of the specimen, the particle size and gradation of the soil, the size of the specimen, the shape of the loading function, and the frequency of application of the loading function.

Following a brief review of the basic theory behind cyclic simple shear testing, the differences between cyclic simple shear and in-situ loadings will be discussed. Next, the

factors that may affect a cyclic simple shear specimen are summarized, and lastly a review of the definition of cyclic behavior is presented.

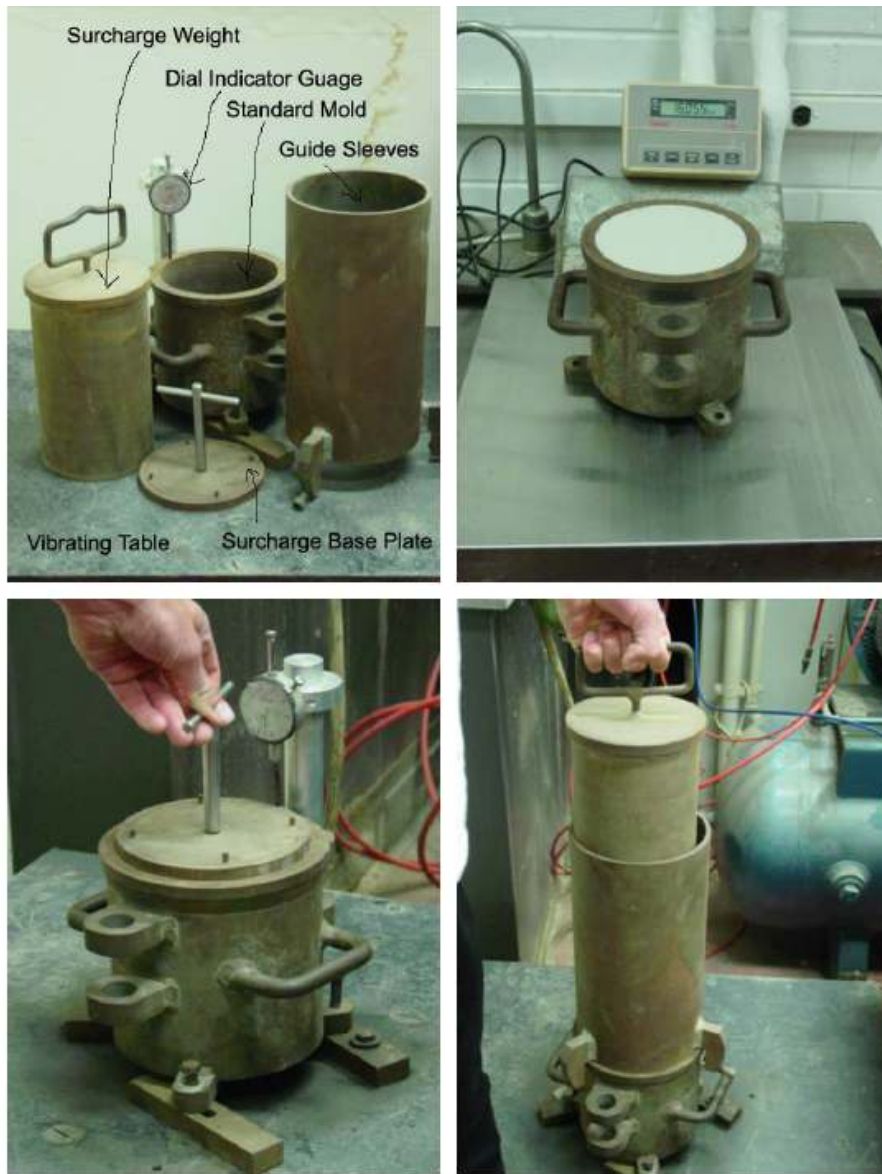


Figure 4-26 Vibrating Table and Mold used in computing e_{min} (ASTM 4353)

4.10.6 Uniformity of Loadings

The loading that a soil element in the ground receives during an earthquake is non-uniform, both in terms of its amplitude and their frequency. These variations would be very hard to model in the laboratory. To overcome this difficulty the concept of equivalent uniform cycles is applied (Seed and Idriss, 1971). The loading applied to a specimen during a cyclic simple shear is essentially constant in both amplitude and frequency and is most often applied in the form of a uniform, repeating sine wave. The cyclic stress ratio applied is usually assumed to be a function of some percentage (most frequently 65 percent) of the maximum acceleration of the design earthquake. Thus by assuming the applied stress (or acceleration) to be some percentage of the peak stress (or acceleration) the loading can be converted from the non-uniform, erratic loading seen in the field, to a uniform equivalent loading, easily applicable in the laboratory.

4.10.7 Components of Loadings

An actual earthquake would apply stresses to a soil element in the field in several directions simultaneously. Two perpendiculars horizontal and one vertical component were recorded. A cyclic simple shear test, however, only employs one component of loading. This is analogous to one horizontal component of the earthquake motion acting on the plane inclined at 45 degrees within the specimen. Studies by Seed and Pyke (1975) have shown that the difference in loading between the multi-component loading in the field and the single component loading in the lab results in the laboratory specimens failing at a stress which is approximately 10 percent higher than that required to cause failure in the field.

4.10.8 Factors Affecting Cyclic Response of Soil

Numerous factors affect the cyclic behavior measured in a cyclic simple shear specimen. These factors include the mean grain size of the soil, the void ratio and the relative density of the specimen, the method of specimen preparation, the size of the specimen, the shape of the loading function, the frequency of loading. Silver et al. (1976) and Townsend (1978) have provided excellent reviews of many of these factors.

For a given sand tested at a specified density, several of these factors, including mean grain size, void ratio, and relative density, are beyond the control of the test operator. The 44 remaining factors are a function of the test methodology and can be controlled by the operator. The operator-controlled factor that has the greatest effect on the cyclic behavior susceptibility of a specimen is the method used to form the specimen. Other factors include specimen size, the shape of the loading function, the frequency of loading, the ratio of principle stresses during consolidation, the degree of saturation in the specimen, and the membrane and area corrections applied to the test data. A brief discussion of the effects of each of the operator dependent parameters and how they were handled in this study follows.

4.10.9 Specimen Size

Lee and Fitton (1969) prepared and tested coarse and fine sands with different specimen diameters in order to determine the effects of specimen size on cyclic strength. The specimens tested were either 1.4 inches in diameter, were prepared to a constant relative density, and were tested at a constant confining pressure.

4.10.10 Shape of the Loading Pattern

Silver et al. (1976) and Mulilis, Townsend and Horz (1978) found that the cyclic strength of a soil is strongly influenced by the shape of the loading pattern. Several waveforms were examined including, in order of increasing cyclic strength produced, rectangular, degraded rectangular or triangular, and sine waves. Sine waves were found to produce cyclic strengths, which were 15 to 20 percent higher than those, produced under rectangular waves of the same maximum amplitude do. This strength increase is due to the severe velocity changes that occur during loading with the rectangular form and their effect on pore pressure. Additionally, a sine wave applies a lower average load than a rectangular wave with the same peak amplitude due to its longer rise time. This lower average stress results in a higher cyclic strength. The effects of varying wave shapes on cyclic stress can be seen in Figure 2-9 (after Silver et al. 1976) which plots cyclic resistance curves for Monterey #0 sand under various wave forms. While the testing system offers several options as to the shape of the loading function, a sinusoidal shaped function was used as recommended by Silver (1977).

CHAPTER 5

DEVELOPMENT OF DATA BASE

5.1 Introduction

During the past 36 years, the settlement of clean sands under earthquake induced loading has been studied and an understanding of its mechanisms and the parameters which affect it has been developed. The result of previous studies showed that settlement of sand is function of:

The relative density of the soil

The magnitude of the cyclic shear strains

The number of cycles or previous strain history.

Unfortunately, the understanding of the settlement of sands and how it varies with sand characteristics and over consolidation ratio is less complete. A review of the literature shows that there is no clear consensus as to what effect sand characteristics and an over-consolidation ratio have upon the settlement of sand.

The current study was undertaken in an attempt to clarify the uncertainties found in the literature, and to find parameters which control the settlement of sands. In order to achieve this goal, a series of simple cyclic shear tests were performed using two base clean sands. Tests were performed and evaluated using void ratio, relative density, and soil specific relative density as measures of density. Also used in this studies, the results of previous studies on Silica #20 sand (Silver and Seed, 1971, Martin et. al, 1975), on Monterey Sand

(Pyke, 1975), on Ottawa Sand (Bathia, 1980), on Nevada Sand (Chung, 2004) and data obtained from UCLA (Stewart et.al.) Consisting of series of simple cyclic shear tests on 8 clean sand, on 6 field sand materials and on sands (16 samples) with fine content. The sands span a range of material gradation, particle size and particle shape as well as mineral composition. Data on sands with fine content obtained from Stewart et al. were also analyzed and the role of fines in soils is also examined.

5.2 Data Presentation

5.2.1 Data Obtained From Previous Studies

Silver and Seed (1971) used Crystal Silica #20 sand to study the volume changes in sands during cyclic loading. The sand used was a uniform angular quartz sand having $D_{10} = 0.5$ mm and a uniformity coefficient of about 1.5. To analyze the effect of relative density, 45 %, 60 % and 80 % relative densities sand samples were used.

Martin et. al (1975) used the same Crystal silica sand with relative density of 45 % to analyze the change in volumetric strain and shear modulus during cyclic simple shear tests on dry sand. The results of these studies are shown in Figure 5-2 through Figure 5-4 in form of settlement versus the number of cycles for a uniform shear strain of 0.1 %.

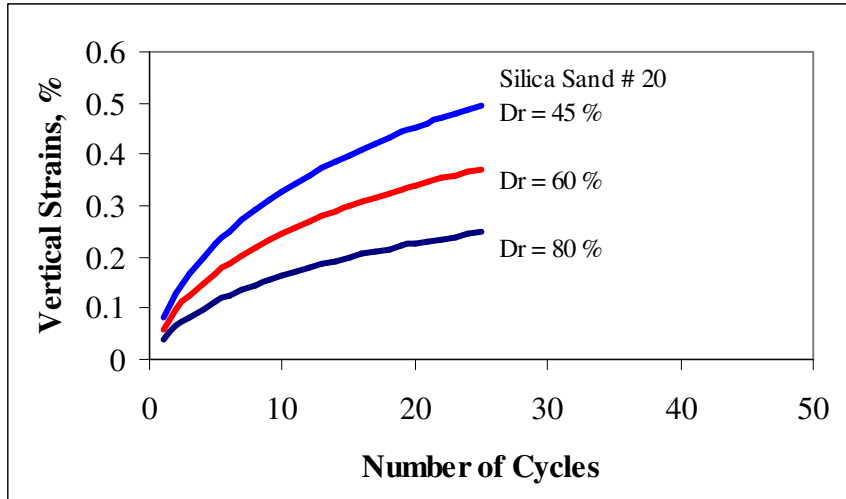


Figure 5-1 Vertical Settlement versus the number of Cycles (Silver and Seed 1971)

Pyke (1975) used the Monterey No. 0 sand with three different relative densities 40 %, 60 % and 80 % to study the settlement of sands under multidirectional shaking. It is a uniform medium quartz sand having $D_{10} = 0.4$ mm and a uniformity coefficient of 1.6. The result of his study is shown in Figure 5-2.

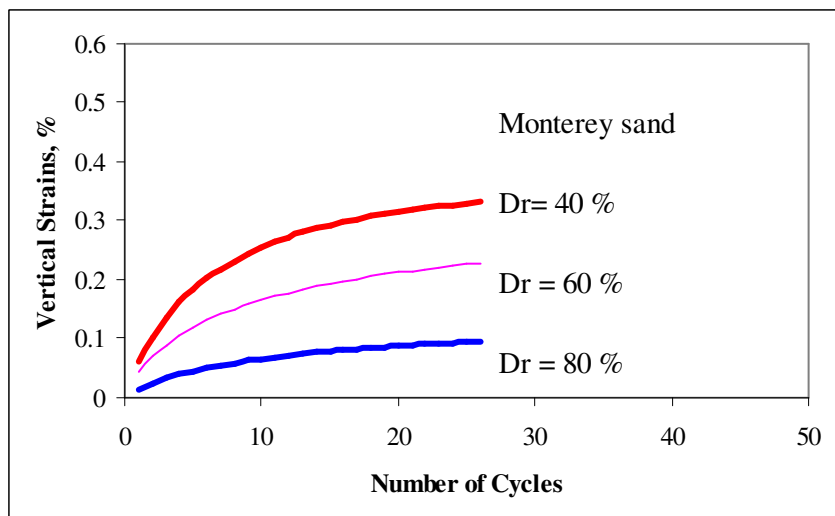


Figure 5-2 Vertical Settlement versus the number of Cycles (Pyke 1975)

Bhatia (1980) used the Ottawa C109 sand at three relative density, 40 %, 50 % and 60 % in her study of verification of relationships for effective stress method to evaluate liquefaction potential of saturated sands. It is a uniform quartz sand having $D_{10} = 0.35$ mm and a uniformity coefficient of 1.7.

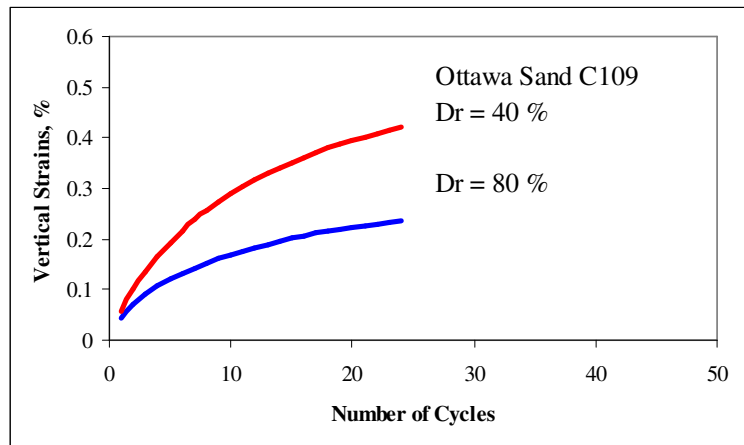


Figure 5-3 Vertical Settlement versus the number of Cycles (Bathia,1980)

Chung (2004) used the Nevada sand at 80 % relative density in his study to evaluate the dynamic and cyclic behavior of soils over the wide range of shear strains in NGI – type simple shear testing devices. The sand used was uniform quartz sand having $D_{10} = 0.15$ mm and a uniformity coefficient of 1.8.

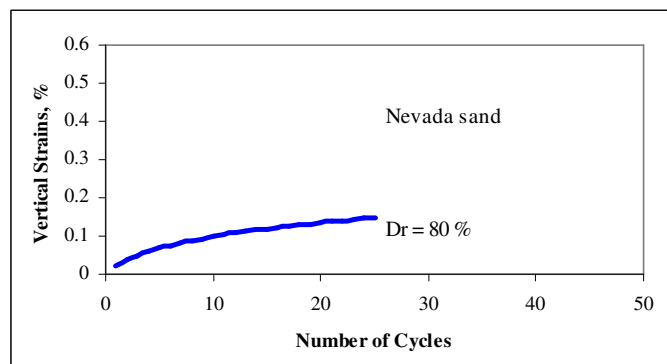


Figure 5-4 Vertical Settlement versus the number of Cycles (Chung 2004)

5.2.2 Tested Sands

Two sands were used for this study in tests conducted by the author. The first sand was Nevada sand and it was obtained from UC-Davis. This sand was extensively used in the Velacs project (Verification of Liquefaction Analysis by Centrifuge Studies). Nevada sand is uniform fine quartz sand. Its particles are angular to subangular in shape with a mean grain size of 0.14 mm and a coefficient of uniformity of 1.81. The soil was graded between U.S. No. 50 and 200 sieve sizes. The specific gravity of Nevada sand is 2.69. The maximum and minimum dry density are respectively 108.5 lb/ft^3 and 88.4 lb/ft^3 which were obtained by using respectively ASTM 4253 and 4254 and the Japanese Method and Dry Tipping developed by Lade. It should be mentioned that the maximum and minimum density for most of the sands used in this study were computed using the two methods mentioned above in order to eliminate any potential of error. The responses obtained by those two methods were comparable. The maximum and minimum void ratios for Nevada sand were 0.88 and 0.64, respectively. The second sand was Silica # 30 and it was obtained from UC-Berkeley and it was chosen because it is very similar to the sand used by Silver and Seed. This sand is a uniform angular having $D_{10}=0.5 \text{ mm}$ and a coefficient of uniformity of about 1.5. The maximum and minimum dry density are respectively 101.3 lb/ft^3 and 83.8 lb/ft^3 and the maximum and minimum void ratio are respectively 1.016 and 0.689. The size distribution curves for these sands are shown in Figure 5-5.

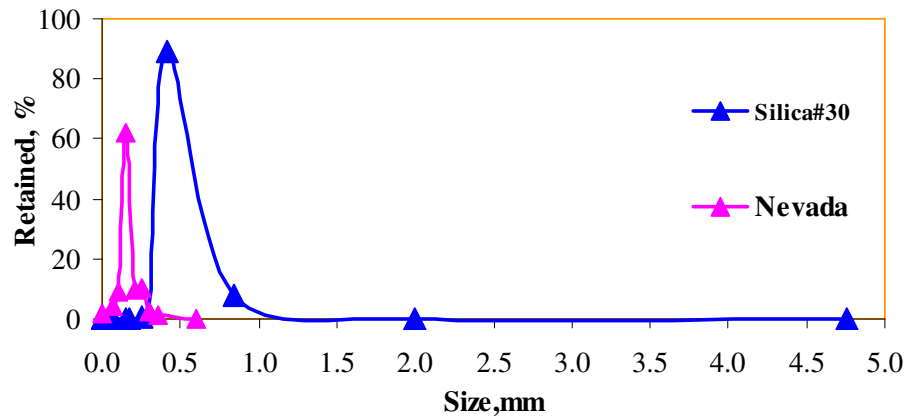


Figure 5-5 Size distribution of Nevada and Silica # 30 sands

Numerous laboratory tests were performed, consisting of nine tests on each sand using three different relative density, 40%, 60% and 80% and three different over consolidation ratio 1, 2 and 4. Results shown in Figure 5-6 to Figure 5-8 show that settlement of sand depends on the sand characteristics, on the over -consolidation ratio applied and on the relative density used in the testing. These results confirm the previous finding that settlement decrease with an increase in relative density, with an increase in over consolidation ratio and that settlements vary with sand characteristics.

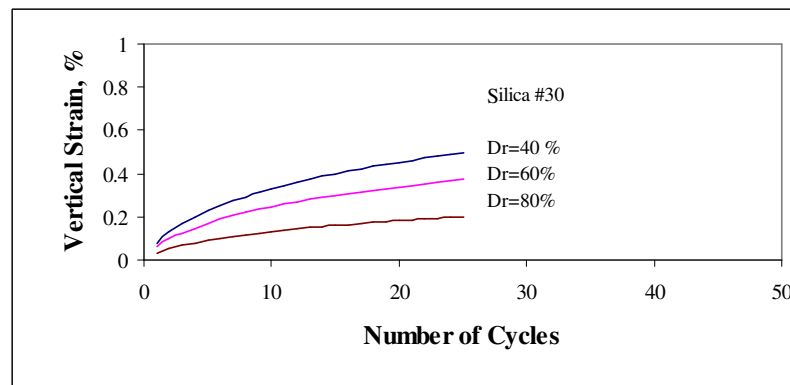


Figure 5-6 Vertical Settlement versus the number of Cycle (OCR=1, $\gamma=0.1\%$)

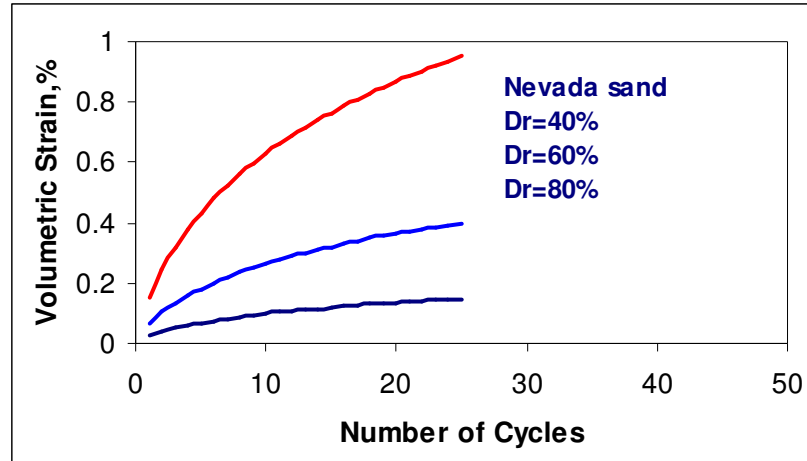


Figure 5-7 Vertical Settlement versus the number of Cycle (OCR=1, $\gamma=0.1\%$)

5.2.3 UCLA Test Program Data

Structural fills are earth structures that are placed to create level building pads for building construction. In hillside areas, these fills are generally constructed in wedge shape and placed along hillsides.

There are a number of processes that can lead to deformation of compacted structural fills. Static, long-term process includes hydro-compaction, consolidation and slope creep. Seismic process includes seismic slope instability and seismic compression.

The focus of the UCLA research team was on seismic compression, (which is defined as volumetric strain accumulation in unsaturated soil during earthquake shaking) and was largely motivated by the settlement of compacted fills which occurred in the Northridge earthquake. Seismic compression only occurs in compacted fills whose voids are not fully filled with water

(unsaturated soils); when such soils experience seismically induced shear deformations, the soil grains tend to settle into a denser configuration.

In order to achieve their objective and to provide insight into the seismic compression of sands, non-plastic silt mixtures, they performed laboratory simple shear testing on a total of 14 different clean sands and on 8 silty sands.

THE DATABASE COMPILED BY THE UCLA RESEARCH TEAM (STEWART ET AL.2004) WAS ANALYZED AND ADDED TO THE LABORATORY TESTS DATA PERFORMED FOR THIS STUDY. THE UCLA DATA BASE WHICH CONSISTED OF SIMPLE SHEAR TESTS ON 14 SANDS OF RELATIVE DENSITY ABOUT 60 % WAS ANALYZED, AND CURVE FITTING USED IN ORDER TO EVALUATE THE VARIATION OF SETTLEMENT OF THE SANDS WITH VARYING SHEAR STRAIN FOR A GIVEN UNIFORM NUMBER OF CYCLES AS SHOWN IN FIGURE 5-8. WHEN DATA ACCURACY CONCERNS WERE ENCOUNTERED, THE TESTS IN QUESTION WERE REPEATED BY THE UCLA TEAM IN ORDER TO RESOLVE CONCERNS. THE RAW DATA PROVIDED BY UCLA WERE IN THE FORM OF A CD WAS DISCUSSED IN CHAPTER 4 AND ARE SHOWN IN

APPENDIX C AND

Appendix D. Examples of the curve fitting are shown in Figure 5-9 to Figure 5-11.

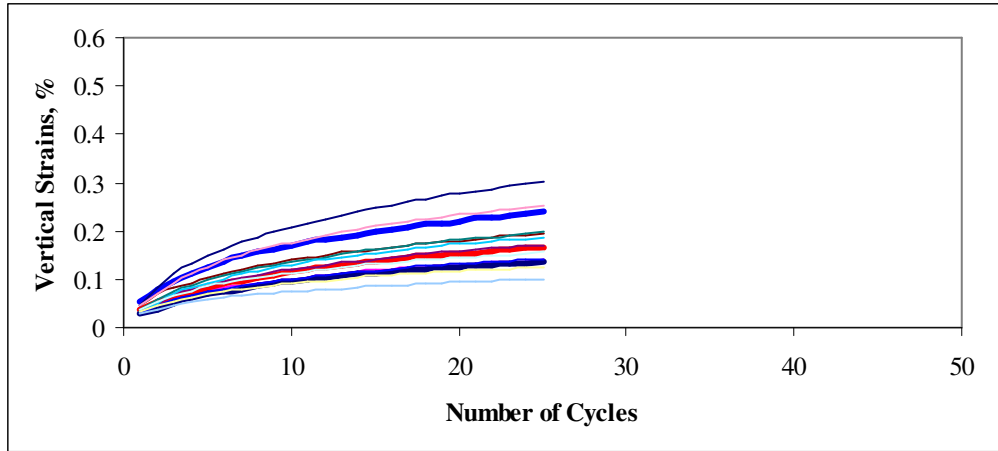


Figure 5-8 Vertical Settlement versus the number of Cycles (Stewart 2004)

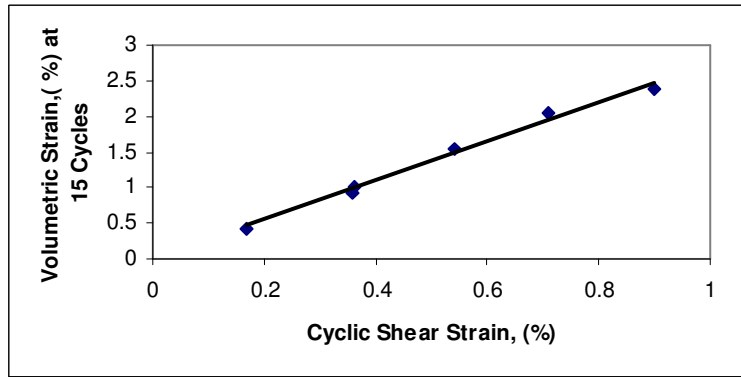


Figure 5-9 Variation of volumetric strain with cyclic shear strain for Newhall Sand

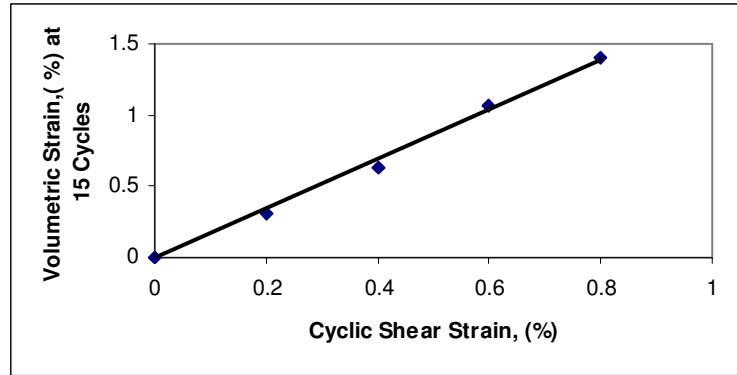


Figure 5-10 Variation of volumetric strain with cyclic shear strain for Pacoima 3 Sand

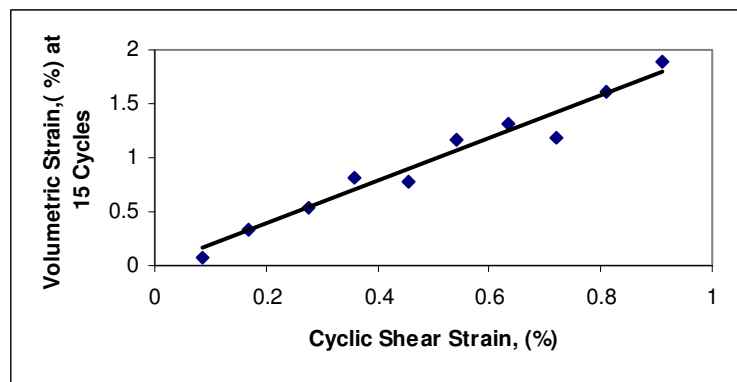


Figure 5-11 Variation of volumetric strain with cyclic shear strain for Flint 16 Sand

Also Stewart et.al (2004) performed cyclic simple shear tests on sand with fines content at two relative compaction values of 87 % and 92 % which corresponds to a relative density of 70 % and 80 %. They used two base clean sands, NSF and Silica #1 mixed with silt material (Sil-Co-Sil No. 52) in varying amount between 10 %, 20 %, 35 % and 50 %.

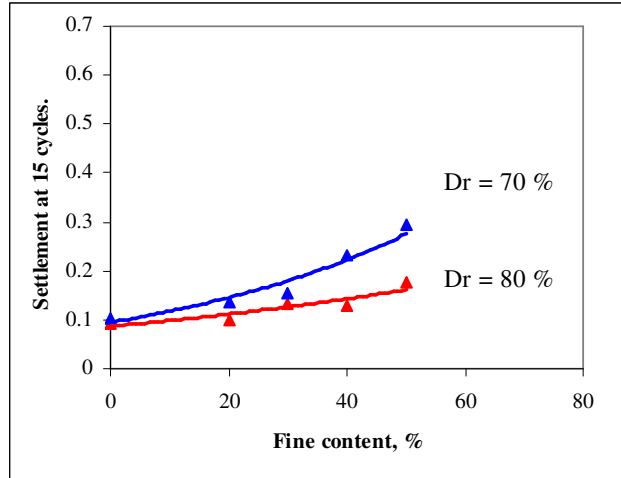


Figure 5-12 Effect of silt content on seismic compression of Silica host sand

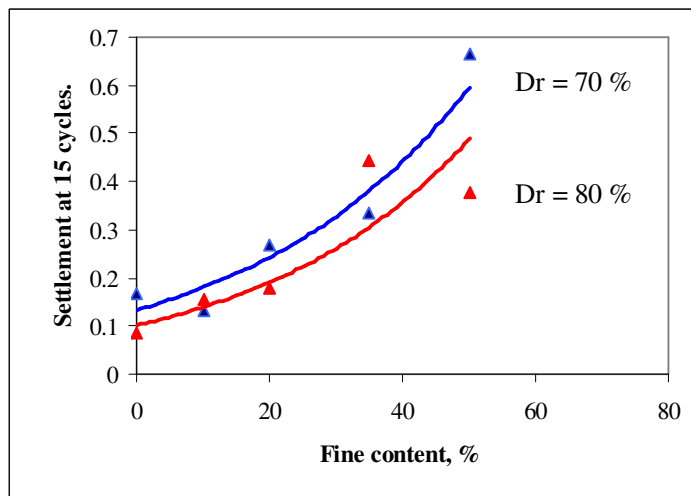


Figure 5-13 Effect of silt content on seismic compression of NSF host sand

CHAPTER 6

MINERALOGY AND PARTICLE CHARACTERISTICS ANALYSIS

6.1 Introduction

Preliminary analysis of the results discussed in Chapter 5 shows no significant trend in variation of vertical strain with soil compositional parameters such as Coefficient of Uniformity, C_u , median particle size, D_{50} . For this reason, It was decided to include in the study other soil parameters such as the mineral composition of the soils samples and the grains shape or texture. This study was done at the University of Southern California in the department of Earth Science under the supervision of Dr. Frank Corsetti.

Mineralogy and particle characteristics (texture) analysis of sand consists of determining the following:

- Mineral composition of sand
- Grain shapes by petrographic analysis
- Grain size distribution which can be determined by sieve analysis

Two methods were used to achieve the analysis, X-ray powder Diffraction for determining the minerals composition in the sand and petrographic analysis for determining the grains size and shape. The background to these analysis methods is described below.

6.2 X-Ray Powder Diffraction Method

Rocks, sediments, and precipitates are examples of geologic materials that are composed of minerals. Numerous analytical techniques are used to characterize these materials. One of these methods, X-ray powder diffraction (XRD), is an instrumental technique that is used to identify minerals, as well as other crystalline materials. In many geologic investigations, XRD complements other mineralogical methods, including optical light microscopy, electron microprobe microscopy, and scanning electron microscopy. XRD provides the researcher with a fast and reliable tool for routine mineral identification. XRD is particularly useful for identifying fine-grained minerals and mixtures or intergrowths of minerals, which may not lend themselves to analysis by other techniques. XRD can provide additional information beyond basic identification. If the sample is a mixture, XRD data can be analyzed to determine the proportion of the different minerals present. Other information obtained can include the degree of crystallinity of the mineral present, possible deviations of the minerals from their ideal compositions (presence of element substitutions and solid solutions), the structural state of the minerals (which can be used to deduce temperatures and (or) pressures of formation), and the degree of hydration for minerals that contain water in their structure. Some mineralogical samples analyzed by XRD are too fine grained to be identified by optical light microscopy. XRD does not, however, provide the quantitative compositional data obtained by the electron microprobe or the textural and qualitative compositional data obtained by the scanning electron microscope. The three-dimensional structure of nonamorphous materials, such as minerals, is defined by regular, repeating planes of atoms that form a crystal lattice. When a focused X-ray beam interacts with these planes of atoms, part of the beam is

transmitted, part is absorbed by the sample, part is refracted and scattered, and part is diffracted. Diffraction of an X-ray beam by a crystalline solid is analogous to diffraction of light by droplets of water, producing the familiar rainbow. X-rays are diffracted by each mineral differently, depending on what atoms make up the crystal lattice and how these atoms are arranged. In X-ray powder diffractometry, X-rays are generated within a sealed tube that is under vacuum. A current is applied that heats a filament within the tube, the higher the current the greater the number of electrons emitted from the filament. This generation of electrons is analogous to the production of electrons in a television picture tube. A high voltage, typically 15-60 kilovolts, is applied within the tube. This high voltage accelerates the electrons, which then hit a target, commonly made of copper. When these electrons hit the target, X-rays are produced. The wavelength of these X-rays is

When an X-ray beam hits a sample and is diffracted, we can measure the distances between the planes of the atoms that constitute the sample by applying Bragg's Law. Bragg's Law is:

$$n\lambda = 2d \sin \theta$$

where the integer n is the order of the diffracted beam, λ is the wavelength of the incident X-ray beam, d is the distance between adjacent planes of atoms (the d -spacing), and θ is the angle of incidence of the X-ray beam. Since we know λ and we can measure θ , we can calculate the d -spacing. The geometry of an XRD unit is designed to accommodate this measurement. The characteristic set of d -spacing generated in a typical X-ray scan provides a unique "fingerprint" of the mineral or minerals present in the sample. When properly interpreted, by comparison with standard

reference patterns and measurements, this "fingerprint" allows for identification of the material characteristics of the material.

These X-rays are collimated and directed onto the sample, which has been ground to a fine powder (typically to produce particle sizes of less than 10 microns). A detector detects the X-ray signal; the signal is then processed either by a microprocessor or electronically, converting the signal to a count rate. Changing the angle between the X-ray source, the sample, and the detector at a controlled rate between preset limits is an X-ray scan.

Powder X-ray Diffraction (XRD) is one of the primary techniques used by mineralogists and solid state chemists to examine the physico-chemical make-up of unknown solids. This data is represented in a collection of single-phase X-ray powder diffraction patterns for the three most intense D values in the form of tables of interplanar spacings (D), relative intensities (I/I_0) and mineral name . The XRD technique takes a sample of the material and places a powdered sample in a holder, then the sample is illuminated with x-rays of a fixed wave-length and the intensity of the reflected radiation is recorded using a goniometer. This data is then analyzed for the reflection angle to calculate the inter-atomic spacing value in Angstrom units (10^{-8} cm). The intensity is measured to discriminate using I ratios the various spacing and the results are compared to a table to identify possible matches.

Friedrich and Knipping first observed X-ray wave interference, commonly known as X-ray diffraction (XRD), in 1912 after a hint from their research advisor, Max von Laue, at the University of Munich. Bragg's Law greatly simplified von Laue's description of X-ray

interference. The Braggs used crystals in the reflection geometry to analyze the intensity and wavelengths of X-rays (spectra) generated by different materials. Their apparatus for characterizing X-ray spectra was the Bragg spectrometer. Laue knew that X-rays had wavelengths on the order of 1 \AA . After learning that Paul Ewald's optical theories had approximated the distance between atoms in a crystal by the same length, Laue postulated that X-rays would diffract, by analogy to the diffraction of light from small periodic scratches drawn on a solid surface (an optical diffraction grating). In 1918 Ewald constructed a theory, in a form similar to his optical theory, quantitatively explaining the fundamental physical interactions associated with XRD. Elements of Ewald's eloquent theory continue to be useful for many applications in physics. The results of the analysis are shown in

Diffraction can occur when electromagnetic radiation interacts with a periodic structure whose repeat distance is about the same as the wavelength of the radiation. Visible light, for example, can be diffracted by a grating that contains scribed lines spaced only a few thousand angstroms apart, about the wavelength of visible light. X-rays have wavelengths on the order of angstroms, in the range of typical interatomic distances in crystalline solids. Therefore, X-rays can be diffracted from the repeating patterns of atoms that are characteristic of crystalline materials.

6.2.1 Electromagnetic Properties of X-Rays

The role of X-rays in diffraction experiments is based on the electromagnetic properties of this form of radiation. Electromagnetic radiation such as visible light and X-rays can sometimes behave as if the radiation were a beam of particles, while at other times it behaves as if it were a wave. If the energy emitted in the form of photons has a

wavelength between 10^{-6} to 10^{-10} cm, then the energy is referred to as X-rays. Electromagnetic radiation can be regarded as a wave moving at the speed of light, c ($\sim 3 \times 10^{10}$ cm/s in a vacuum), and having associated with it a wavelength, λ , and a frequency, ν , such that the relationship $c = \lambda\nu$ is satisfied.

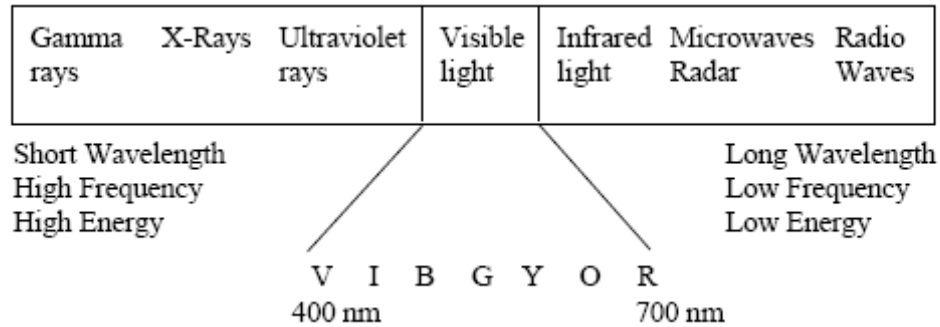


Figure 6-1 Electromagnetic spectrum. The colors of the visible range of the spectrum are abbreviated violet (V), indigo (I), blue (B), green (G), yellow (Y), orange (O), and red (R).

6.2.2 X-Rays and Crystalline Solids

In 1912, Maxwell von Laue recognized that X-rays would be scattered by atoms in a crystalline solid if there is a similarity in spatial scales. If the wavelength and the interatomic distances are roughly the same, diffraction patterns, which reveal the repeating atomic structure, can be formed. A pattern of scattered X-rays (the diffraction pattern) is mathematically related to the structural arrangement of atoms causing the scattering. When certain geometric requirements are met, X-rays scattered from a crystalline solid can constructively interfere, producing a diffracted beam. Sir Lawrence Bragg simulated the experiment, using visible light with wavelengths thousands of times

larger than those of X-rays. He used tiny arrays of dots and pinholes to mimic atomic arrangements on a much larger scale. Optical transform experiments, in which visible light is diffracted from arrays, yield diffraction patterns similar to those produced by shining X-rays on crystalline solids. However, the optical transform experiment is easier and safer than X-ray experiments and can be used in the classroom.

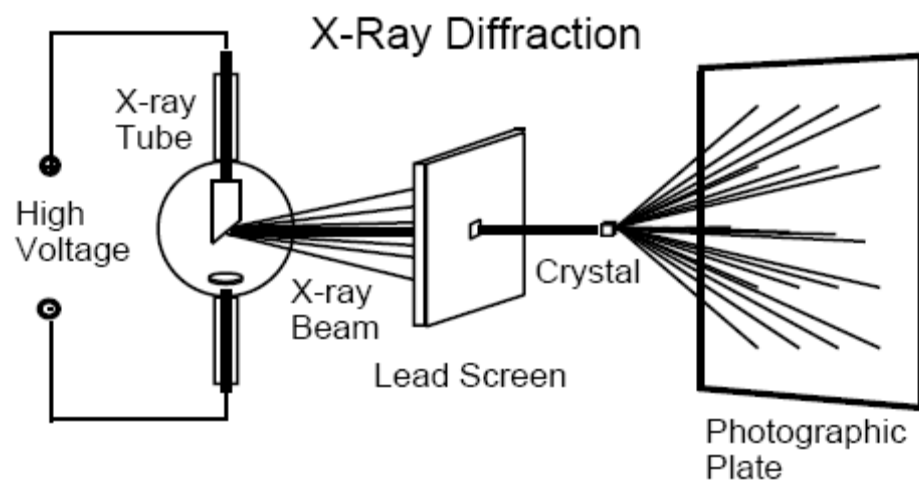


Figure 6-2 A schematic of X-ray diffraction

6.2.3 How Diffraction Patterns are Made

When electromagnetic radiation from several sources overlaps in space simultaneously, either constructive or destructive interference occurs. Constructive interference occurs when the waves are moving in step with one another. The waves reinforce one another and are said to be in phase. Destructive interference, on the other hand, occurs when the waves are out of phase, with one wave at maximum amplitude, while the other is at a minimum amplitude. Interference occurs among the waves scattered by the atoms when

crystalline solids are exposed to X-rays. The atoms in the crystal scatter the incoming radiation, resulting in diffraction patterns. Destructive interference occurs most often, but in specific directions constructive interference occurs.

6.2.4 Purpose of X-Ray Diffraction

Diffraction data has historically provided information regarding the structures of crystalline solids. Such data can be used to determine molecular structures, ranging from simple to complex, since the relative atomic positions of atoms can be determined. X-ray diffraction provided important evidence and indirect proof of atoms.

Diffraction patterns constitute evidence for the periodically repeating arrangement of atoms in crystals. The symmetry of the diffraction patterns corresponds to the symmetry of the atomic packing. X-ray radiation directed at the solid provides the simplest way to determine the interatomic spacing that exists. The intensity of the diffracted beams also depends on the arrangement and atomic number of the atoms in the repeating motif, called the unit cell. Thus, the intensities of diffracted spots calculated for trial atomic positions can be compared with the experimental diffraction intensities to obtain the positions of the atoms themselves.

X-rays are electromagnetic radiation of wavelength about 1 \AA (10^{-10} m), which is about the same size as an atom. They occur in that portion of the electromagnetic spectrum between gamma-rays and the ultraviolet. The discovery of X-rays in 1895 enabled scientists to probe crystalline structure at the atomic level. X-ray diffraction has been in use in two main areas, for the fingerprint characterization of crystalline materials and the determination of their structure. Each crystalline solid has its unique characteristic X-ray

powder pattern which may be used as a "fingerprint" for its identification. Once the material has been identified, X-ray crystallography may be used to determine its structure, i.e. how the atoms pack together in the crystalline state and what the interatomic distance and angle are etc. X-ray diffraction is one of the most important characterization tools used in solid state chemistry and materials science. We can determine the size and the shape of the unit cell for any compound most easily using the diffraction of x-rays.

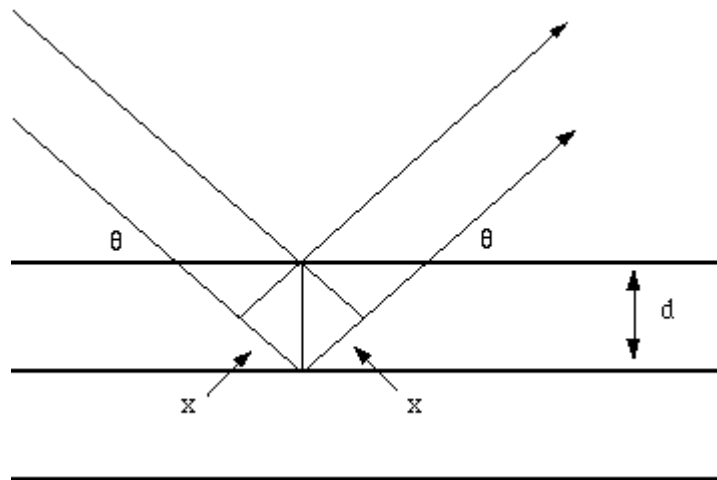


Figure 6-3 Reflection of x-rays from two planes of atoms in a solid

The path difference between two waves:

$$n\lambda = 2d \sin \theta$$

For constructive interference between these waves, the path difference must be an integral number of wavelengths:

$$n\lambda = 2x$$

This leads to the Bragg equation:

$$n\lambda = 2d \sin \theta$$

Figure 6-4 shows the x-ray diffraction pattern for Silica # 2 sand. Strong intensities can be seen for one number of values of n ; from this line we can calculate the value of d , the interplanar spacing between the atoms in the crystal.

Figure 6-5 shows the x-ray diffraction pattern for NSF sand. Strong intensities can be seen for a number of values of n ; from each of this line we can calculate the value of d , the interplanar spacing between the atoms in the crystal.

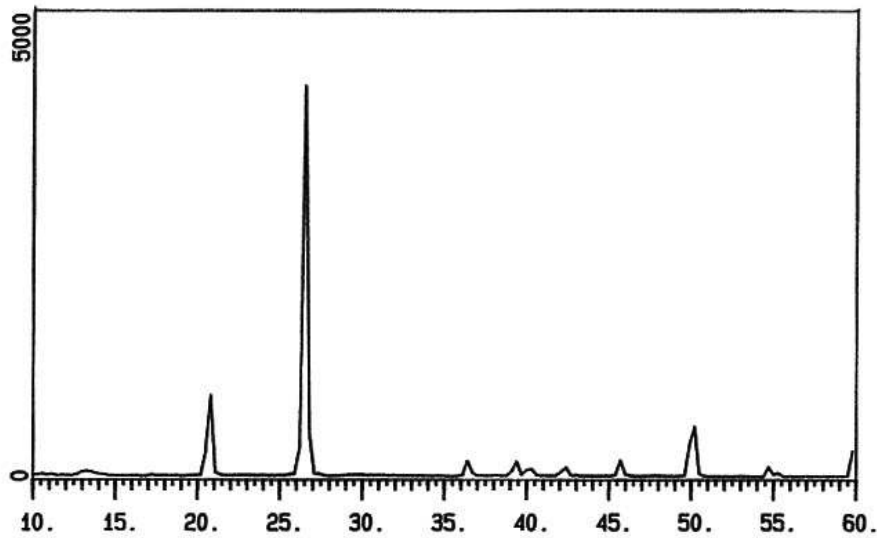


Figure 6-4 X-ray diffraction pattern for Silica #2 Sand

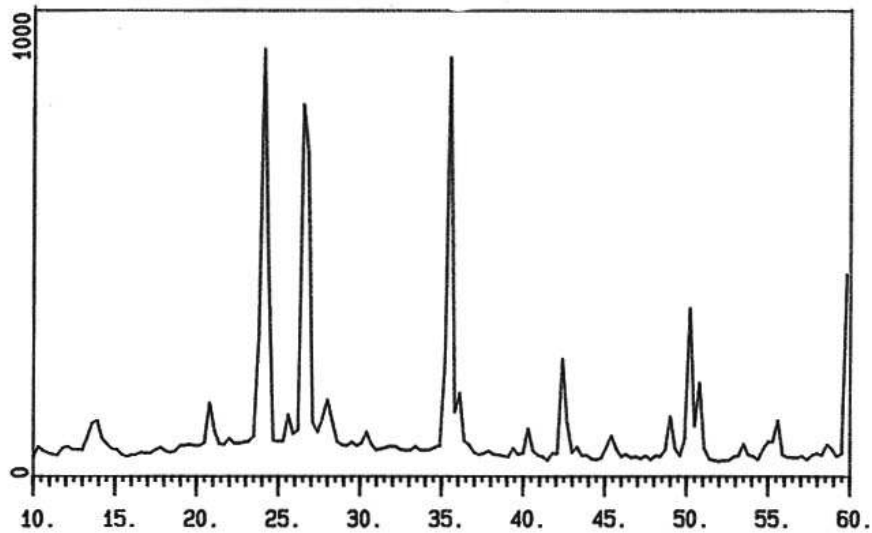


Figure 6-5 X-ray diffraction pattern for NSF Sand

Example of an X-ray powder diffractogram produced during an X-ray scan. The peaks represent positions where the X-ray beam has been diffracted by the crystal lattice. The set of d -spacing (the distance between adjacent planes of atoms), which represent the unique "fingerprint" of the mineral, can easily be calculated from the 2-theta (2θ) values shown. The use of degrees 2-theta in depicting X-ray powder diffraction scans is a matter of convention, and can easily be related back to the geometry of the instrument, shown in figure 1. The angle and the d -spacing are related by Bragg's Law, as described in the text.

6.2.5 Instrumentation

The X-ray diffraction experiment requires an X-ray source, the sample under investigation and a detector to pick up the diffracted X-rays. Figure 6-6 is a schematic diagram of a powder X-ray diffractometer.

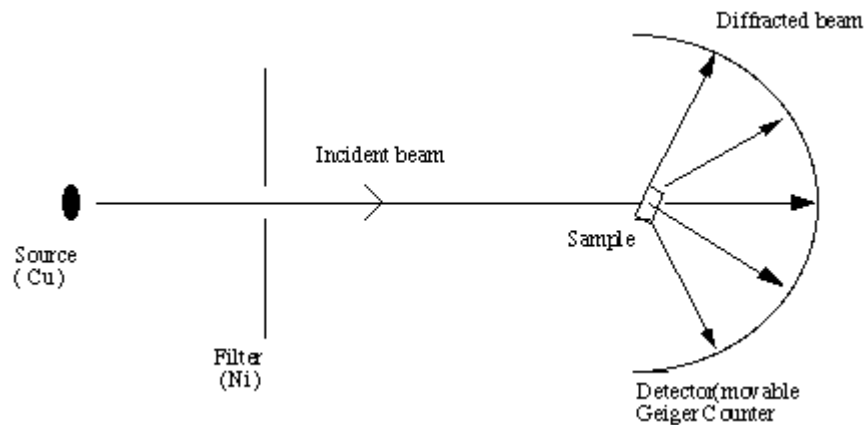


Figure 6-6 Schematic of an X-ray powder diffractometer

The X-ray radiation most commonly used is that emitted by copper, whose characteristic wavelength for the K radiation is $\lambda = 1.5418 \text{ \AA}$. When the incident beam strikes a powder sample, diffraction occurs in every possible orientation of 2θ . The diffracted beam may be detected by using a moveable detector such as a Geiger counter, which is connected to a chart recorder. In normal use, the counter is set to scan over a range of 2θ values at a constant angular velocity. Routinely, a 2θ range of 5 to 70 degrees is sufficient to cover the most useful part of the powder pattern. The scanning speed of the counter is usually 2θ of 2 degrees min^{-1} and therefore, about 30 minutes are needed to obtain a trace.

Bragg's Law refers to the simple equation:

$$n\lambda = 2d \sin\theta$$

derived by the English physicists Sir W.H. Bragg and his son Sir W.L. Bragg in 1913 to explain why the cleavage faces of crystals appear to reflect X-ray beams at certain angles

of incidence (theta, θ). The variable d is the distance between atomic layers in a crystal, and the variable lambda λ is the wavelength of the incident X-ray beam, n is an integer. This observation is an example of X-ray wave interference commonly known as X-ray diffraction (XRD), and was direct evidence for the periodic atomic structure of crystals postulated for several centuries. matter with any beam, e.g., ions, electrons, neutrons, and protons, with a wavelength similar to the distance between the atomic or molecular structures of interest.

6.2.6 Deriving Bragg's Law

Bragg's Law can easily be derived by considering the conditions necessary to make the phases of the beams coincide when the incident angle equals and reflecting angle. The rays of the incident beam are always in phase and parallel up to the point at which the top beam strikes the top layer at atom z (Figure 6-7). The second beam continues to the next layer where it is scattered by atom B . The second beam must travel the extra distance $AB + BC$ if the two beams are to continue traveling adjacent and parallel. This extra distance must be an integral (n) multiple of the wavelength (λ) for the phases of the two beams to be the same:

$$n\lambda = AB + BC$$

Recognizing d as the hypotenuse of the right triangle Abz , we can use trigonometry to relate d and θ to the distance $(AB + BC)$. The distance AB is opposite θ so,

$$AB = d \sin\theta$$

Because $AB = BC$, the equation above becomes,

$$n\lambda = 2AB$$

Substituting equation (3) in equation (4) we have,

$$n\lambda = 2 d \sin\theta$$

and Bragg's Law has been derived. The location of the surface does not change the derivation of Bragg's Law

$$n\lambda = 2 d \sin\theta$$

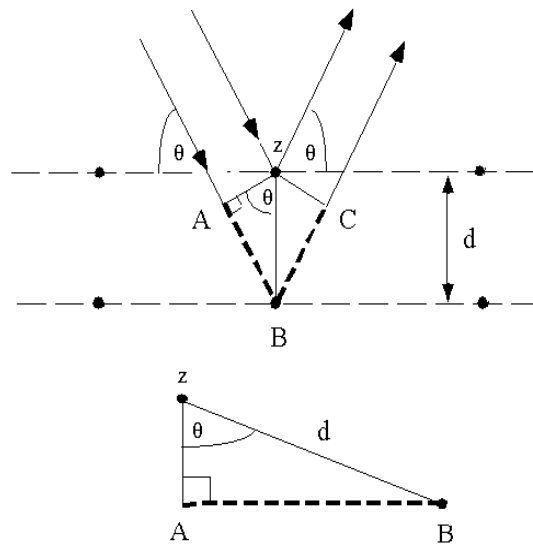


Figure 6-7 Deriving Bragg's Law using the reflection geometry and applying trigonometry. The lower beam must travel the extra distance (AB + BC) to continue traveling parallel and adjacent to the top beam.

Recognizing d as the hypotenuse of the right triangle Abz , we can use trigonometry to relate d and θ to the distance $(AB + BC)$. The distance AB is opposite θ so,

$$AB = d \sin\theta$$

Because $AB = BC$ eq. (2) becomes,

$$n\lambda = 2AB$$

Substituting eq. (3) in eq. (4) we have,

$$n\lambda = 2 d \sin\theta$$

and Bragg's Law has been derived. The location of the surface does not change the derivation of Bragg's Law.

6.3 Results of X-Ray powder Diffraction analysis

Sample	Quartz	Feldspar	Volcanic Fragments	Metamorphic Fragments	Accessory
Pacoima-1	34%	26%	16%	20%	4%
Pacoima-3	27%	21%	25%	25%	2%
Newhall	18%	19%	40%	18%	5%
Post Office	35%	21%	32%	9%	3%
Pat Irwindale	13%	21%	28%	28%	10%
NSF	24%	28%	15%	31%	1%

Table 6-1 Mineral composition of sands

100 grains per sample were counted on a grid using the 2.5x objective on a Zeiss petrographic microscope. Quartz was monocrystalline (polycrystalline quartz was considered a metamorphic rock fragment). Feldspar included plagioclase and orthoclase, including a minor amount of microcline. In these samples, the most common form of

feldspar was plagioclase. Most of the metamorphic fragments consisted of polycrystalline quartz plus muscovite, usually foliated. Volcanic fragments were not as consistent in mineralogy, but commonly contained a glassy or altered-glass groundmass with accessory phenocrysts such as plagioclase. Accessory grains included very minor amounts of hornblende, apatite, titanite, and in one case, a mollusk shell fragment.

Notes on individual samples:

- Pacoima-3 had trace amounts of biogenic CaCO₃ in the form of mollusk shell fragments--not sure where these might have come from, but it was the only sample with these grains.
- Newhall Sand accessories included some muscovite mica.
- Pat Irwindale Sand contained a significant amount of polycrystalline hornblende as an accessory mineral-in enough quantity to be considered in its own category. Some of the grains classified as metamorphic fragments could in fact be plutonic fragments, as some of them lacked a foliation.
- NSF Sand: Some of the grains classified as metamorphic fragments could in fact be plutonic fragments, as some of them lacked a foliation.

6.4 Petrographic Analysis

A thin section is made by grinding down a slice of rock which has been glued to a glass slide until it reaches a thickness of about 0.03mm (30 microns). At this thickness most minerals become more or less transparent and can therefore be studied by a microscope using transmitted light. A thin section is mounted on a microscope slide.

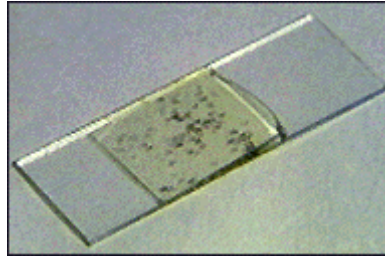


Figure 6-8 Thin Section

The petrographic microscope is a large apparatus with twin eyepieces and several extra attachments. To the naked eye, a thin section is nearly transparent, and that's true under the microscope too. Even dark minerals like are clear. The stage with the thin section on it can be rotated and as you do that some of the minerals wink bright, then dark. That's because underneath the stage is a polarizing filter, and any mineral that itself is polarizing interferes with that polarized light. Where polarizers cross each other, you get darkness, and where they both have the direction you get brightness. when you flip in the microscope's second polarizer, which is mounted above the stage and is crossed relative to the first polarizer. Then bright turns to dark across the whole field of view, and the different minerals take on interference colors that sometimes are quite vivid. Basically, those colors tell the observer a lot about a mineral's identity and composition, and the angles that can be measured using the rotating stage tell more. For good measure, there's also a very thin wedge of quartz that the microscopist can slide in and out of the light path to gauge the effect on the interference colors.

Polarized Light Microscope Configuration

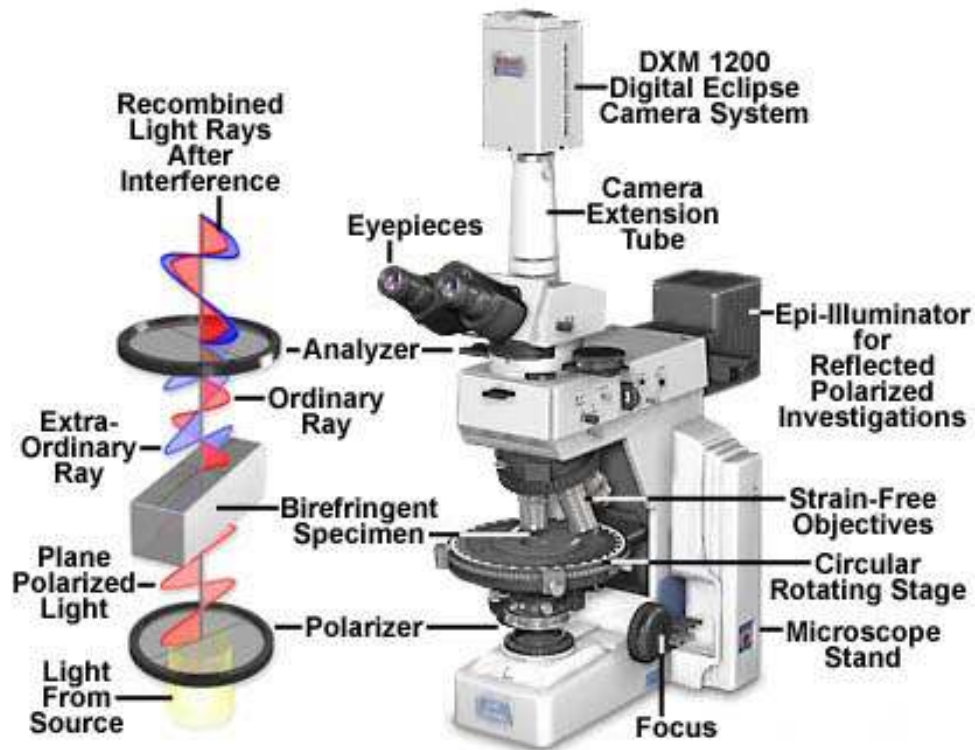


Figure 6-9 The Polarising Microscope

6.4.1 The Nature of Polarised Light

Light travels as electro-magnetic vibrations in which the vibration direction is transverse to the direction of propagation. Transverse wave-motions of this type are said to be plane polarised when all the vibrations lie in one plane. Light from the sun is unpolarised but when it reflects off a surface it becomes partly polarised as shown opposite.

6.4.2 Double Refraction

Most crystalline substance is anisotropic - their physical properties (including refractive index) differ if measured in different directions. Crystals belonging to the cubic system are the exception and are said to be isotropic - their physical properties do not vary with direction. When a ray of ordinary (unpolarised) light enters an anisotropic crystal it is in general split into two rays - this is called double refraction

6.4.3 Common Minerals in Igneous Rocks:

6.3.3.1 Optical Properties of Quartz

Uniaxial positive; first order interference colors (gray to pale yellow); undulant extinction; clear in plane polarized light; conchoidal fracture; no visible cleavage or twinning. In intrusive rocks, quartz is typically a late-forming mineral and therefore interstitial to other minerals. The photos on this page are under crossed polarizers: on the left above is strained quartz in granite; on the right is a quartz phenocryst in rhyolitic glass, showing conchoidal fracture. The photos below show quartz grains in a sedimentary rock, conglomerate. On the left, Boehm lamellae in the grains indicate a high stress regime; the grains on the right show sutured grain boundaries and internal strain, indicating a probable metamorphic origin.

6.3.3.2 Occurrence:

Many intrusive rocks, such as granite, quartz monzonite, granodiorite, tonalite, etc; extrusive rocks such as rhyolite, dacite, etc., and many metamorphic and sedimentary rocks.

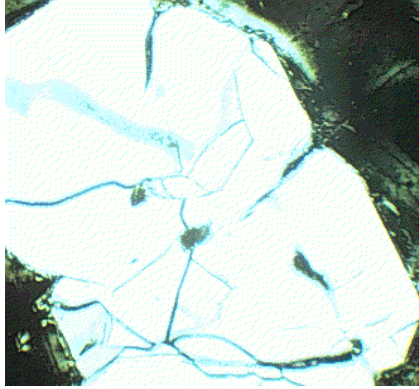


Figure 6-10 Quartz

6.3.3.3 Optical Properties of Plagioclase

Biaxial + or -, first order gray to very pale straw yellow interference colors; low relief; polysynthetic twinning is very common, as in the photos on the left, which helps distinguish plagioclase from orthoclase; twins are typically continuous, with parallel sides, unlike microcline. Plagioclase also may be strongly zoned, as in the photos at the right above: normal zoning when the center of the grain is more Ca-rich than the edges, and oscillatory zoning when the composition alternates from Ca- to Na-richer zones.

Plagioclase is the most abundant mineral in Earth's crust, occurring in most igneous and metamorphic rocks.



Figure 6-11 Plagioclase

6.3.3.4 Optical Properties of Calcite

Uniaxial -; extreme birefringence, high order colors; common polysynthetic twinning; rhombohedral cleavage; symmetrical extinction; colorless in plane polarized light. The photos above (left is plane polarized light, right under crossed polarizers) show the high birefringence, twinning, and cleavage typical of calcite.

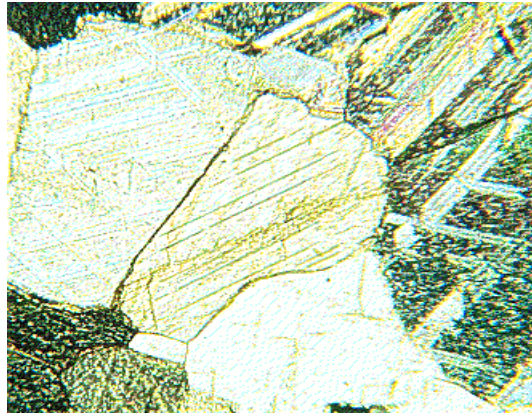


Figure 6-12 Calcite

6.5 Results of Petrographic Analysis

The results of the petrographic analysis on 15 samples shown in Appendix I indicated that 10 of them have a rounded to subrounded shape and these 10 samples are: F-110, F-52, Flint 13, Flint 16, Nevada, Pacoima 1, Pacoima 3, Pat Irwindale , Post Office and NSF. sand the rest of the samples have an angular to subangular shape and they are: S0, S1. S2. S30, and Newhall.

Although it is evident that the mechanical properties of sand depend on the grain shape as well as grain size distribution, it is rather difficult to quantify irregular grain shapes. The

indices for grain shape have been proposed by some researchers in various areas not only in geotechnical engineering. An index widely used in soil mechanics is Roundness R proposed by Wadell (1932). Since roundness is, however, inadequate for grain with sharp corners such as crushed stones, Lee (1964a,b) proposed an alternative concept, angularity A . Yoshimura and Omega (1993) demonstrated a unique negative correlation between Roundness and Angularity with the aid of a coefficient of form unevenness FU , which can be obtained by image analysis proposed by him. Roundness can be estimated by visual comparison with charts, such as the one shown in Figure 2-b (Folk 1955, Barrett 1980). Differences in estimated roundness and sphericity by different assessors is in the order of 0.1 and does not exceed 0.2. Digital image analysis facilitates the systematic evaluation of mathematical descriptors of particle shape including Fourier analysis, fractal analysis and other hybrid techniques (e.g., Meloy 1977, Clark 1987, Hyslip and Vallejo 1997, Bowman et al. 2001).

Figure 6-14 to Figure 6-21 show the grain shape for different sands and Table 6-2 shows the values of Roundness, R , Sphericity, S and Regularity, ρ for all sands.

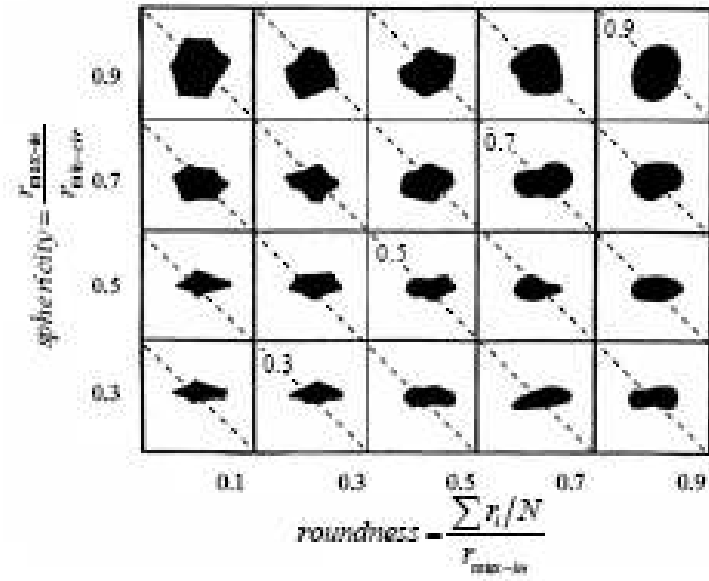


Figure 6-13 Sphericity and Roundness chart Diagonal dotted line correspond to constant particle regularity $\rho = (R+S)/2$ (Santamarina et al.2004)

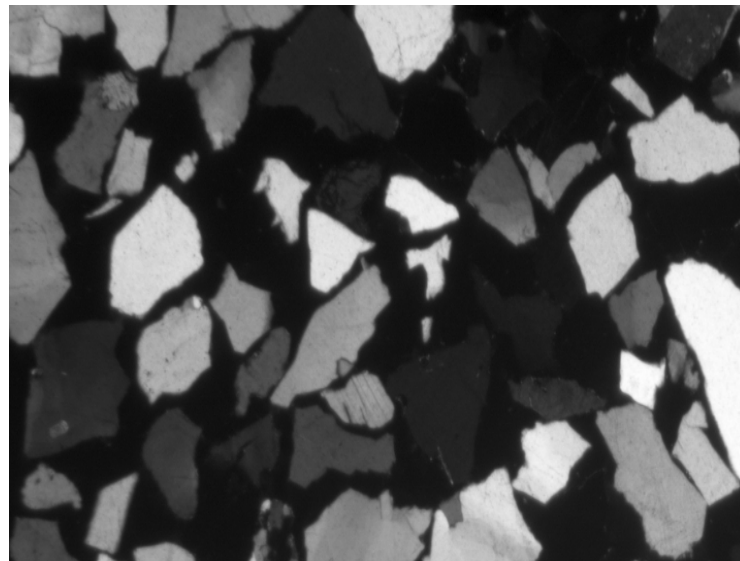


Figure 6-14 Silica 0 Sand

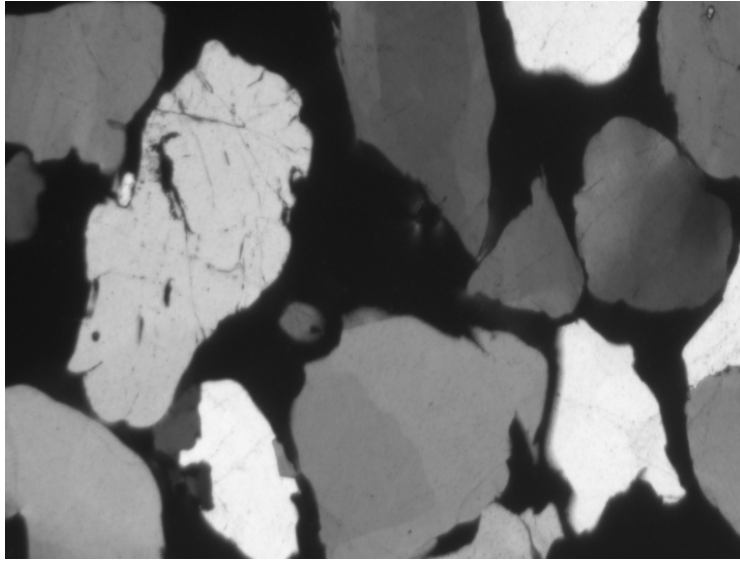


Figure 6-15 Silica 1 Sand

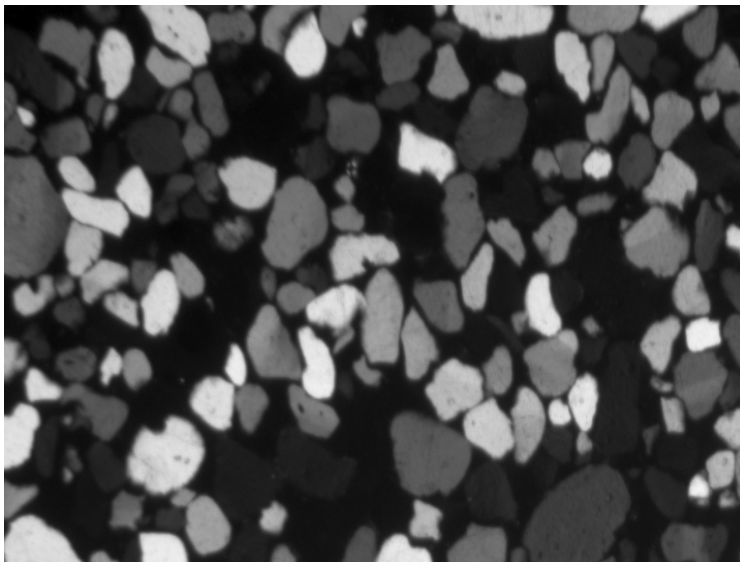


Figure 6-16 F-110 Sand

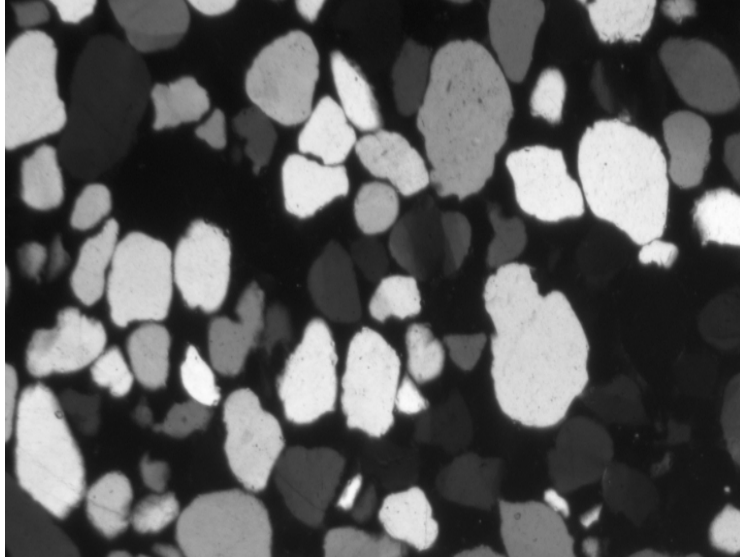


Figure 6-17 Flint 16 Sand

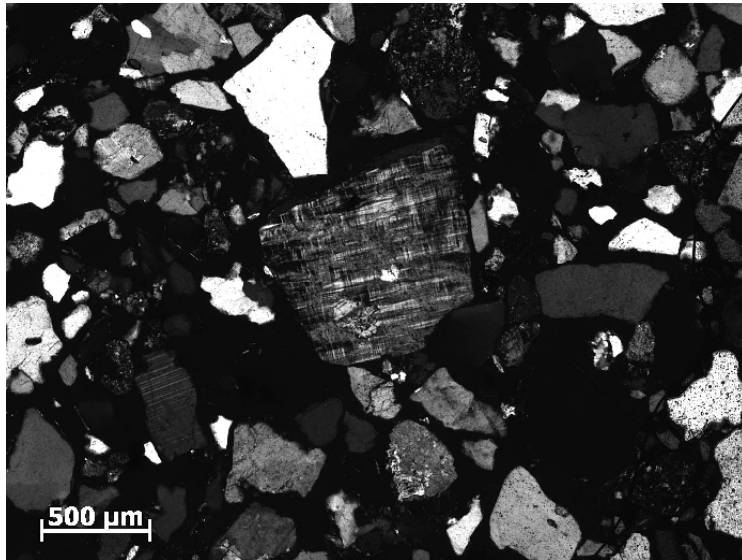


Figure 6-18 Pacoima 1 Sand, Microcline Feldspar Grain

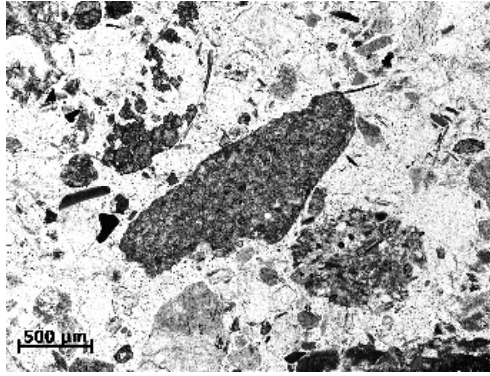


Figure 6-19 Newhall Volcanic Fragments Sand

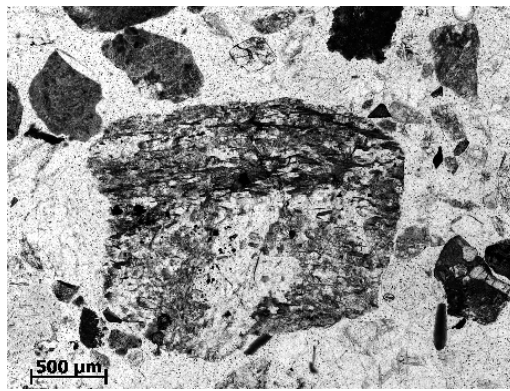


Figure 6-20 NSF Metamorphic Fragment Foliation Sand

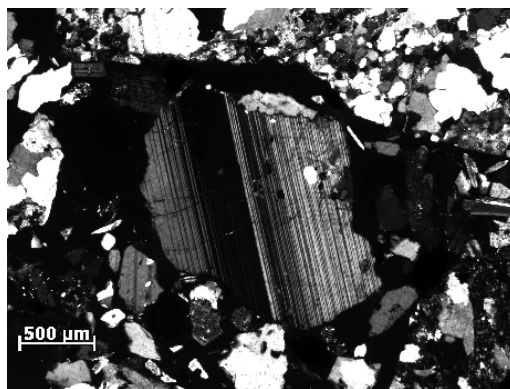


Figure 6-21 Post Office Feldspar Sand

Sample	R	S	□
S0	0.51198	0.717939	0.61496
S1	0.45766	0.678778	0.56821
S2	0.367536	0.613805	0.49067
S30	0.61278	0.781224	0.69700
F-110	0.671333	0.832821	0.75207
F-52	0.746963	0.887345	0.81715
Flint 13	0.789314	0.917878	0.85359
Flint 16	0.770502	0.904315	0.83740
Nevada	0.633089	0.80525	0.71917
Pacoima-1	0.612553	0.790445	0.70149
Pacoima-3	0.673692	0.834522	0.75410
NSF	0.743753	0.885031	0.81439
Pat	0.889498	0.990103	0.9398
Post Office	0.958373	0.989757	0.97406
Newhall	0.572446	0.761531	0.66698

Table 6-2 Mineral composition of sands

CHAPTER 7

GRAIN PACKING OF SPHERES

7.1 Introduction

A preliminary analysis of the results obtained in Chapter 5 shows no significant trend in variation of vertical strain with soil mineral composition and their grains shapes. In fact, while most of the sands samples have the same mineral composition (Quartz), their vertical strain behavior is different, and while several sands samples have the same mineral composition and the same grains shape, their vertical strain behavior is still different. For these reasons mentioned above, it was decided to examine the problem from pure geometry point of view by examining how grain packing of soil particles could influence volume change when subjected to shaking.

Packing of spheres and other solids has been studied since at least 1611. For spheres, scientists have determined packing efficiencies, known as the packing fraction ϕ , which is a ratio of the total volume occupied by the spheres to the total volume of the container. The packing efficiency for various methods of sphere packing, including structured and random packing has been considered. Besides the random packing of spheres, the study of packing efficiencies of other solids has been studied. Specifically, the effect of increasing the magnitude of deviation from a spherical figure is of great interest. Being roughly the same shape and size, When poured randomly and lightly shaken, the oblate spheroid (a squashed spheroid in which the polar radius is greater than the equatorial radius), pack more densely than randomly packed spheres. It has a larger random packing efficiency ($\phi \approx 0.685$) than randomly packed spheres ($\phi \approx 0.64$).

The study of how particles pack was believed to be first considered by Johannes Kepler in 1611. He suggested that the densest possible arrangement of spheres fills 74.04% of the total space of a container. This remained unproven until 1998.

When discussing how particles pack, a specific ratio is considered. Represented by ϕ , the packing efficiency is defined to be the ratio of volume occupied by some solid to the total volume of the container in which the solids have been placed. Packing efficiencies vary as a function of the shape of a particular solid.

By first examining the extensive research and study concerning spherical packing, a comparison can be made to aspherical shapes. The packing fraction of spheres for various crystal lattice structures has been found through various experimentations.

Specifically, a simple cubic lattice structure (Figure 7-1, a) has a packing efficiency of 52%, while another known as body centered cubic (Figure 7-1, b) has a packing efficiency of about 68%. The lattice structure with the most efficient packing fraction is the face-centered cubic (Figure 7-1, c), in which $\phi \approx 0.74$. As evidenced by the packing fractions, varying the lattice structure of the spheres greatly alters its packing efficiency.

Another area of concern regards the packing efficiency of randomly packed spheres, as well as other similar surfaces. Through experimentation, scientists have found that randomly packed spheres poured into a container and lightly shaken have a packing fraction approximately equal to 0.64, which is the arrangement with the largest random packing fraction for spheres and receives a special term known as random close packing.

A similar concept, known as random loose packing, yields a packing fraction of 0.56, in which spheres are packed in a liquid in order to eliminate the effect of gravity. However,

this packing technique represents the lowest packing fraction in which spheres are locked in place. Although these figures and techniques have theoretical importance, spheres are rarely the shape used in packing. Recently, experiments have been performed to evaluate the random packing tendencies of spheroids, as well as ellipsoids. By deviating from a spherical shape, the packing efficiency for randomly packed objects is greatly altered. Through experimentation with (oblate spheroids) and other shapes, scientists begin to interpret the relationship between packing density and particle shape, as well as consider the impact of various methods of shaking and pouring. The exploration of packing efficiencies of various shapes reveals pertinent information in the field of mathematics in regards to theoretical formulations and in the field of science in regards to particle behavior, which has many practical applications.

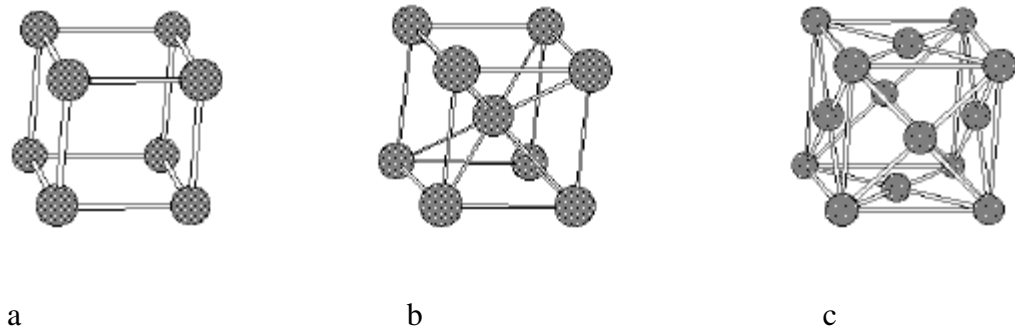


Figure 7-1 (a) Simple Cubic, Packing fraction=0.52; (b) Body Centered Cubic, Packing fraction=0.68; (c) Face Centered Cubic Packing fraction=0.74

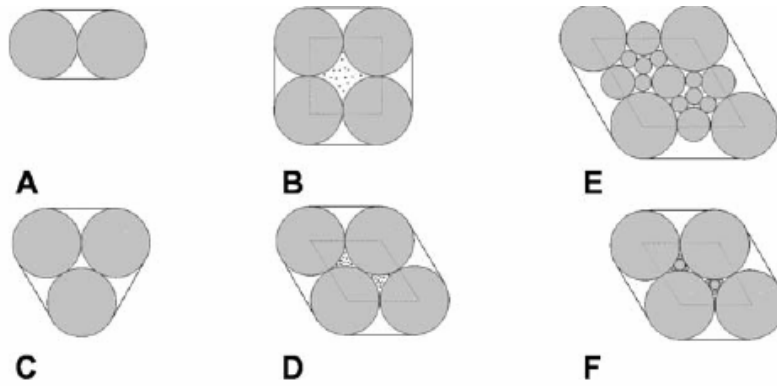


Figure 7-2 Envelope geometries and elementary cells for different types of spheromodels. A: and B: Cubic densest packing (density of elementary cell approx. 0.78). C: and D: Hexagonal densest packing (density of elementary cell approx. 0.91). E: Continuous three-size densest packing (density of elementary cell approx. 0.78). F: Fractal three-size densest packing (density of elementary cell approx. 0.96); (A to D after Leppmeier, 1997)

7.2 Theory

The density achieved by random packing is dependent on the average number of items that come in contact with any one item in the packing. The relation is shown in the following graphs:

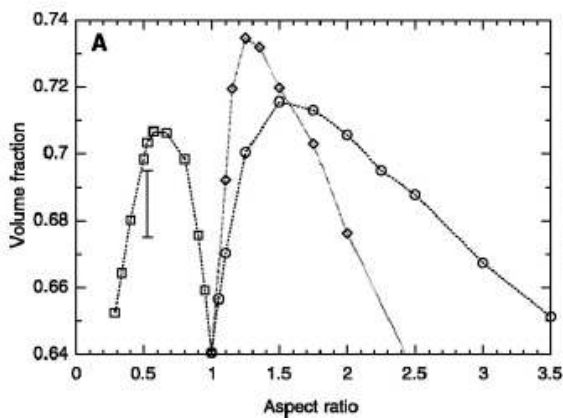


Figure 7-3 Volume fraction vs. aspect ratio for points vs. prolate (○), oblate (□), and aspherical (◇) oblate (□) ellipsoids

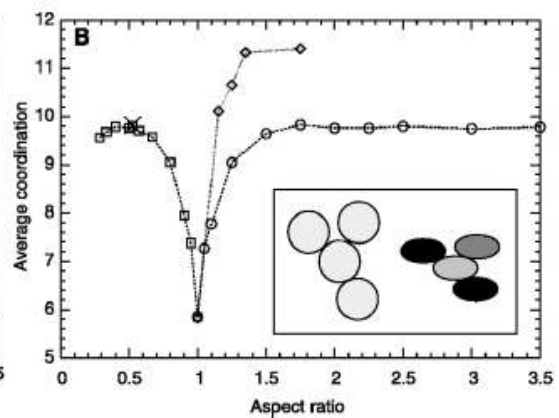


Figure 7-4 Number of contact aspect ratio for prolate (○), and aspherical (◇) ellipsoids

The graph includes data for both prolate (\circ) and oblate (\square) ellipsoids as well as fully aspherical (\diamond) ellipsoids. Figure 7-3 shows that the maximum volume fraction is achieved when the items deviate from a sphere with its aspect ratio of about 1.25 where the aspect ratio $\alpha = b/a$, for ellipsoids: $x^2/a + y^2/b + z^2/c = 1$. For this aspect ratio, the average coordination is about 11.3. This means that for the greatest volume fraction, the average number of contact points is about 11. An aspherical ellipsoid and using the graph of volume fraction vs. aspect ratio and assuming the aspect ratio is between 1.3 and 2.2, the random packing should yield a volume fraction between 0.7 and 0.715. These volume fractions are greater than the volume fraction of an oblate shape. These fractions imply that the more a figure deviates from a sphere to a specific point, the greater the packing efficiency. The increased packing efficiency associated with aspherical shapes results from the increased number of contact points between the particles. Because of its shape, ellipsoids have more degrees of freedom, or an increased number of directions in which the particle can move. Each surrounding object that touches the central particle applies a force on that particle. In order for that particle to be in equilibrium, these forces in each direction must sum to be zero. In the case of spheres, exerted forces can cause the sphere to move but not rotate, whereas in the case of ellipsoids, exerted forces can cause it to move and rotate. In order to stabilize the particles, more contact points are required in order to eliminate the increased number of degrees of freedom. The increased amount of contact points results in a more compact packing and larger packing efficiency. More specifically, the exact volume fraction of a particular shape can be found by first determining the values for a and b , where a = length of the radius on the

horizontal axis, while b = length of the radius on the horizontal axis. The aspect ratio (α) for any solid can then be computed according to the following: $\alpha=b/a$. This value of α can then be used to determine the volume fraction or packing efficiency for that particular solid by locating the aspect ratio on Figure 7-3.

In summary, the result of the experiment is that packing efficiency is a factor of the shape only when dealing with a homogeneous model.

7.3 Maximum and Minimum Dry Densities of Cohesionless Soils

The properties and characteristic behavior of sands are related to it's relative density, D_r . This quantity indicates the relative position of the field ratio, e , between the maximum and minimum void ratios, e_{\max} and e_{\min} for a given sand:

$$D_r = \frac{e_{\max} - e}{e_{\max} - e_{\min}} \cdot 100$$

These two values are not unique, but they depend on the method used for the determination. These two methods had produced comparable results. The two extreme void ratios for sand can be determined by procedures such as ASTM tests Methods D4253 and D4254 and such as The Japanese Method and Dry Tipping for Max and Min densities. Lade et al. (1998) and Ishihara et al. (2002) studied the effect of non-plastic fines on minimum and maximum void ratios of sand and concluded that values of minimum and maximum void ratios are expected to depend on factors such as (Fraser 1935):

- The shape of the grain-size distribution curve
- The fines content

- The grain size
- The grain shape

Their study was limited to the two first points. But the conclusion of their study was that the grain shape and size as well as the shape of the grain size distribution curve were very important factors.

7.4 Homogeneous Sphere Models

Spherical grains having the same diameter can be arranged in five idealized packing corresponding to different void ratios. These ratios are independent of the grains diameter, and they can all be calculated using pure geometry. Figure 7-5 shows these five configurations and they are:

The loosest possible packing or the simple cubic packing in which the grains are stacked on top of each other (centroid over centroid), the void ratio for simple cubic is:

$$e = \frac{6 - \pi}{\pi} = 0.909$$

The next packing is called single stagger packing. In this packing, each sphere touches six neighboring spheres in its own layer and the spheres in different layers are stacked directly on top of each other. The void ratio for single stagger is : $e = \frac{3\sqrt{3} - \pi}{\pi} = 0.653$

- The next packing is the double stagger in which each sphere in one layer has slid over and down to contact two spheres in the second layer. The void ratio for this packing is :

$$e = \frac{9 - 2\pi}{2\pi} = 0.432$$

- The face-centered cubical or pyramidal packing where each sphere in one layer sits in the depression between and is in contact with four spheres forming a square in the layer below.
- The close- packed hexagonal or tetrahedral packing where each sphere in one layer sits in the depression between and is in contact with three spheres forming an equilateral triangle in the layer below. The void ratio for the last two packing is :

$$e = \frac{3\sqrt{2} - \pi}{\pi} = 0.350$$

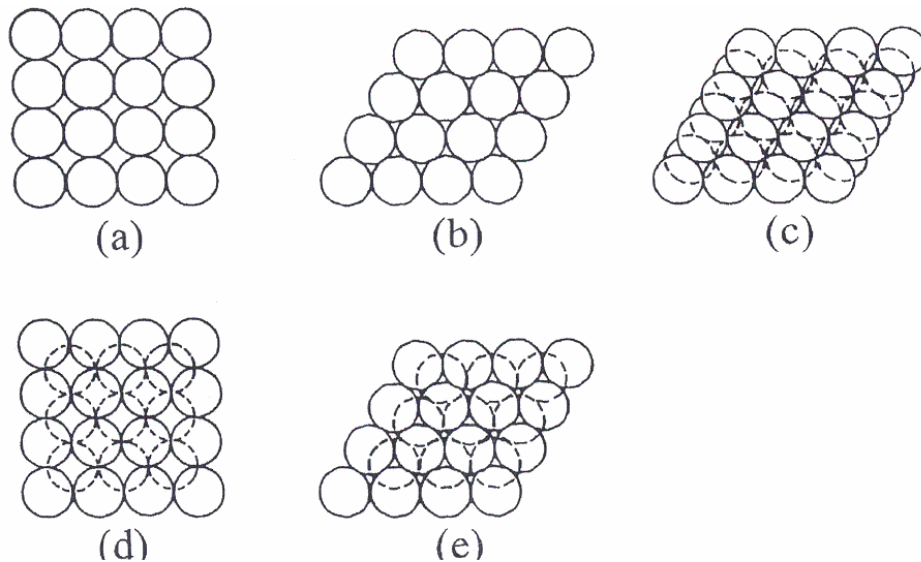


Figure 7-5 Theoretical packing of mono-sized spheres, (a) simple packing, (b) single stagger, (c) double stagger, (d) tetrahedral

7.5 Heterogeneous Sphere Models

Densities and their variations for mixtures of two grain sizes have also been studied theoretically and experimentally (Furnas 1928; Fraser 1935; White and Walton 1937; McGear 1961). Both grains are assumed to be spherical, and their minimum void ratios (or maximum densities) are assumed to be independent of the grain diameter, i.e., the theoretical densities are entirely a matter of geometrical considerations. Thus, differences in specific gravity between the grains are not included in the considerations. Consequently, the expressions presented below are in terms of volumes. Two issues emerge in connection with mixing a binary system of spheres: One relates to the void ratio variation with % fines by weight, i.e., as the mixture of grains varies from 100% large grains to 100% small grains. The other issue relates to the effect of the ratio between the two grain sizes on the void ratio variation. Both issues are addressed below.

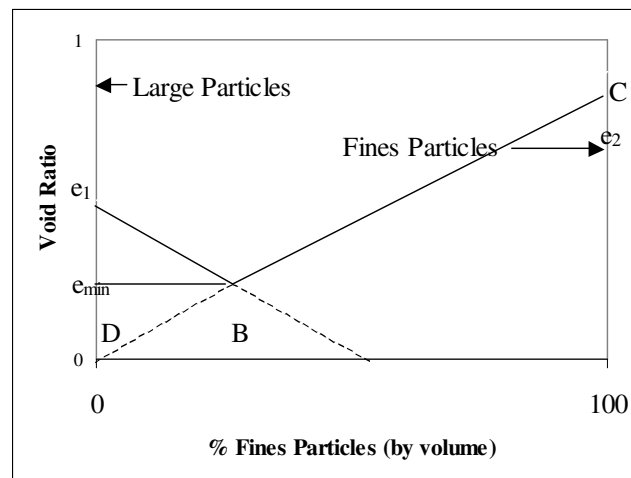


Figure 7-6 Schematic diagram of theoretical variation of minimum void ratio in binary packing with % fines (Lade, 1998)

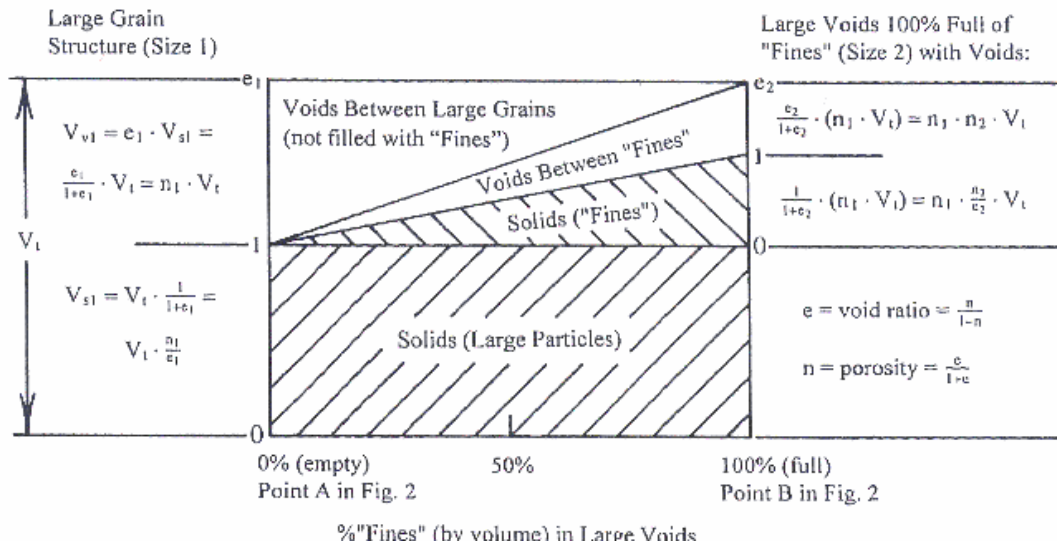


Figure 7-7 Schematic diagram of filling void between large particles with smaller particles (Lade 1998)

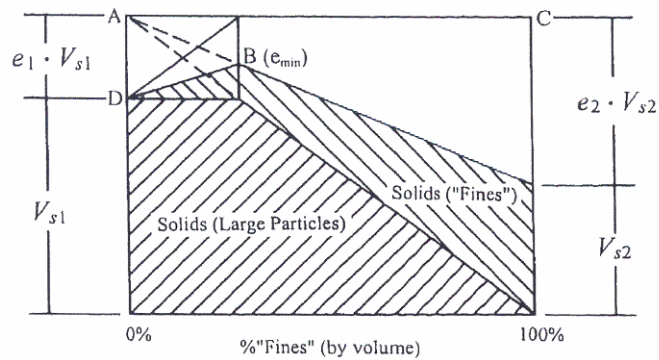


Figure 7-8 Schematic diagram of increasing % fines from B to C, (Lade 1998)

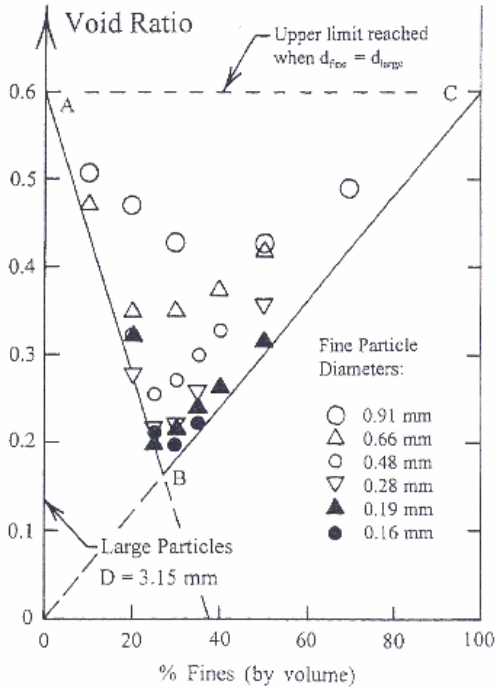


Figure 7-9 Effect of % fines and ratio of diameters of large and small spherical steel shot on e_{min} (Lade 1998)

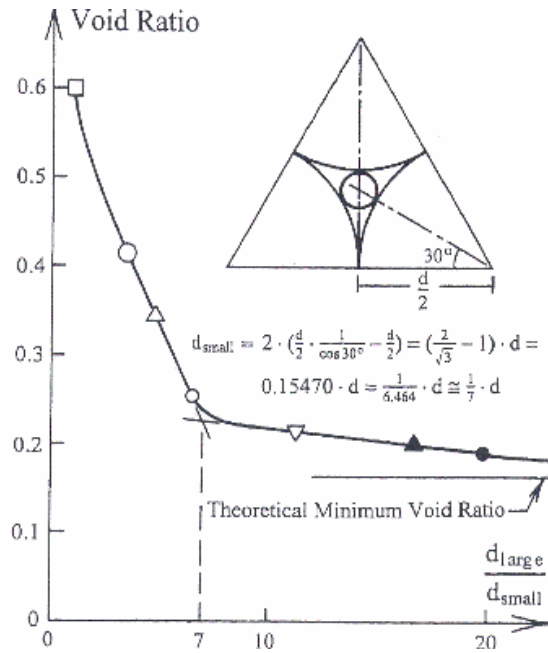


Figure 7-10 Minimum void ratio versus the ratio of large diameter to the small diameter (Lade 1998)

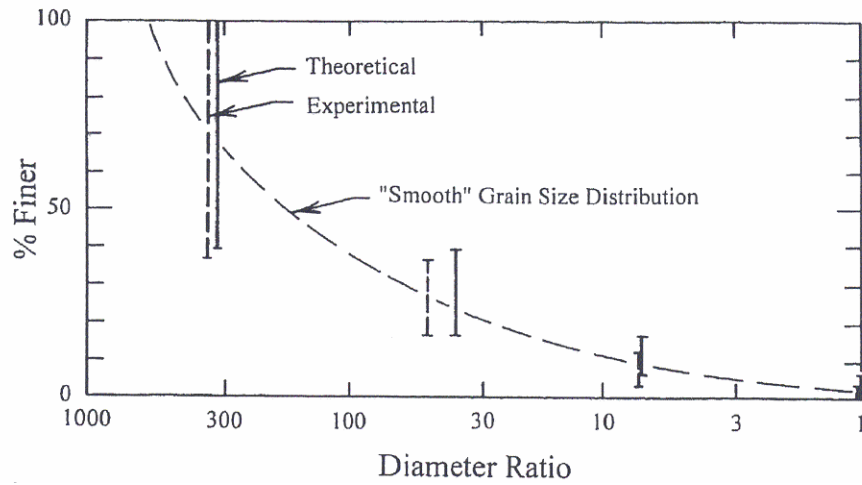


Figure 7-11 Theoretical and experimental grain size distribution to produce the densest possible quaternary packing of spherical particles (Mc Geary 1961).

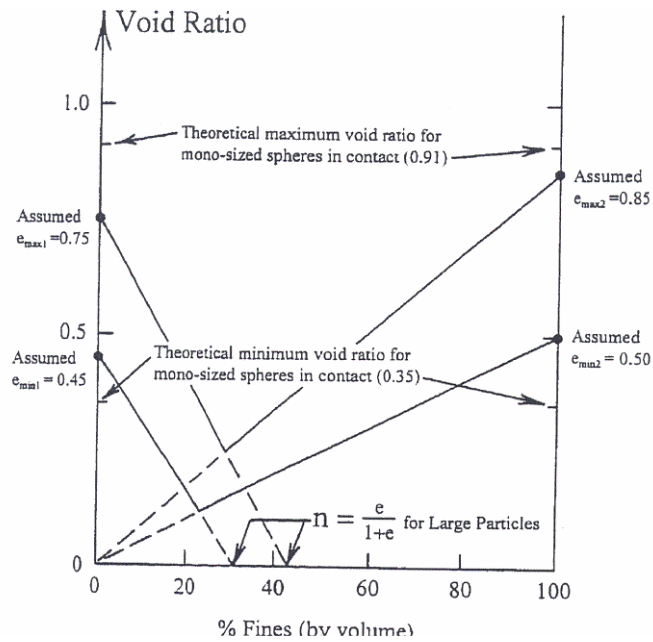


Figure 7-12 Variation of maximum and minimum void ratio for binary mixtures of particles (Lade 1998)

7.6 Theoretical Packing

The theoretical variation of void ratio with % fines is shown schematically in Figure 7-6. In derivation of the two lines (AB and BC), it is assumed that the smaller 'filler' spheres have much smaller diameters than the large spheres, thus avoiding the second issue mentioned above. As seen in Figure 7-6, the largest void ratios occur in a deposit of uniformly sized spheres, whether large or small.

At the end with 0% fines, the large particles (Size I) form a structure with an initial void ratio e_1 , say one of those reviewed above. Small particles (Size 2) are then dropped into the primary fabric of large particles. Thus increasing the weight without changing the overall volume, as indicated on the second inserted sketch in Figure 7-6. This increases the % fines while the overall void ratio decreases. The minimum void ratio is reached when the voids in the primary fabric are completely full of small particles with void ratio e_2 . The filling process occurs along a straight line from A to B in Figure 7-6, and if all voids between the large spheres were filled with solids, then a void ratio of zero would be reached at a point on the horizontal axis (indicating % fines) corresponding to the porosity of the large grains, as shown in the diagram. The schematic diagram in Fig. 3 illustrates the variation in void ratio with % fines. The minimum void ratio at Point B, e_{tot} in Figure 7-6 may be calculated from the void ratios of the parts. i.e. e_1 for the primary fabric and e_2 for the filler spheres (the secondary particles) (Figure 7-7):

$$e_{tot} = \frac{V_{voids}}{V_{solids}} = \frac{n_1 \cdot n_2}{\frac{n_1}{e_1} + n_1 \cdot \frac{n_2}{e_2}}$$

The % fines at which the minimum void ratio is reached (Point B in Figure 7-6) may also be obtained from Figure 7-7 :

$$\% \text{ fine} = \frac{e_{tot}}{e_2} \cdot 100$$

As the % fines increases beyond the point of minimum void ratio for the binary mixture, the large particles in the primary fabric are pushed apart, as shown in Figure 7-6 . Upon reaching 100 % fines (Point C in Figure 7-6), there are no large grains left in the mixture, and the void ratio of the fines is obtained at this point. From B to C the void ratio increases linearly with % fines as the large grains are spread apart and finally disappear at the end with 100% fines. This is shown in the void ratio e_2 at point C may be different from or the same as e_1 at point A, depending on the type of packing. There is a tendency for smaller grains to pack with higher void ratios, as discussed later, and to be general, this is indicated in Figure 7-6 to Figure 7-8.

As the % large grains increases to the left of Point B, i.e., along the dotted line from B to D in Figure 7-6, the larger grains will overlap, and at 100% large grains the mixture consists of solid material. This branch is obviously imaginary, but the entire line from 0% fines at Point D to 100% fines at Point C is described as a straight line.

7.7 Experimental Packing

In the analyses presented above, it was assumed that the small filler spheres had much smaller diameters than the large spheres, corresponding to a very large ratio between the large diameters and the small diameters. However, if the ratio between the two grain sizes becomes smaller, the issue of fitting the small grains into the voids between the

large grains emerges. This issue has been addressed experimentally by, e.g., McGeary (1961). He found that the most efficient method to produce these mixtures was to begin depositing the large particles first into a large container until they formed their densest configuration. The smaller particles were then added from the top while the container was vibrated. The smaller particles would then, little by little, migrate down through the voids and finally reach a saturation point at which time further addition of smaller particles was not possible. McGeary also found that blending the particles before vibration was not nearly as effective in achieving the smallest void ratios. In fact, pre-blending and vibrating the particles would lead to segregation rather than regular packing arrangements with low void ratios.

Figure 7-9 shows a diagram of void ratio versus % fines for binary mixtures consisting of one large particle size and smaller particles with six different diameters. If the minimum void ratio for the spherical fines is assumed to be the same as that for the larger grains (it would be if the same type of packing were obtained for the two sizes of spherical grains), the possible minimum void ratios in the entire range of % fines are described by the broken, solid line ABC shown in Figure 7-9. The diagram also shows that the fines with the smallest diameters produce mixtures that are closest to the theoretical mixtures. However, even for the smallest diameter filler grains, the lowest void ratio at Point B is not reached. In fact, to reach this theoretical point, the diameter of the filler grains would have to be infinitely small. As the sizes of the filler grains increase, the experimental results are increasingly removed from the theoretical line ABC, and the lowest void ratios that can be reached in practice increases with increasing diameter of the filler grains. This

is due to the increasing misfit of filler grains into the voids between the large grains, The upper limit of the lowest minimum void ratio (corresponding to Point B) is reached when the diameters of the large and small spheres are equal in magnitude, This corresponds to the horizontal line AC in Figure 7-9,

7.8 Ternary and Quarternary Packing

The minimum void ratios that can be obtained for ternary and quarternary packing of spherical grains can also be calculated theoretically. In derivation of the expressions for the void ratio and the % fine, the formulas are built up by adding one component at a time. In fact, the pattern in the developments given above can be expanded to any number of components. The above expressions are valid if the specific gravity is the same for each component, or if the % fines are expressed in terms of volumes, as indicated on the diagrams. If the specific gravity varies with the size of the components (as it sometimes does for real soils), this would have to be factored into the derivations because this would affect the relative weight of each component in the packing.

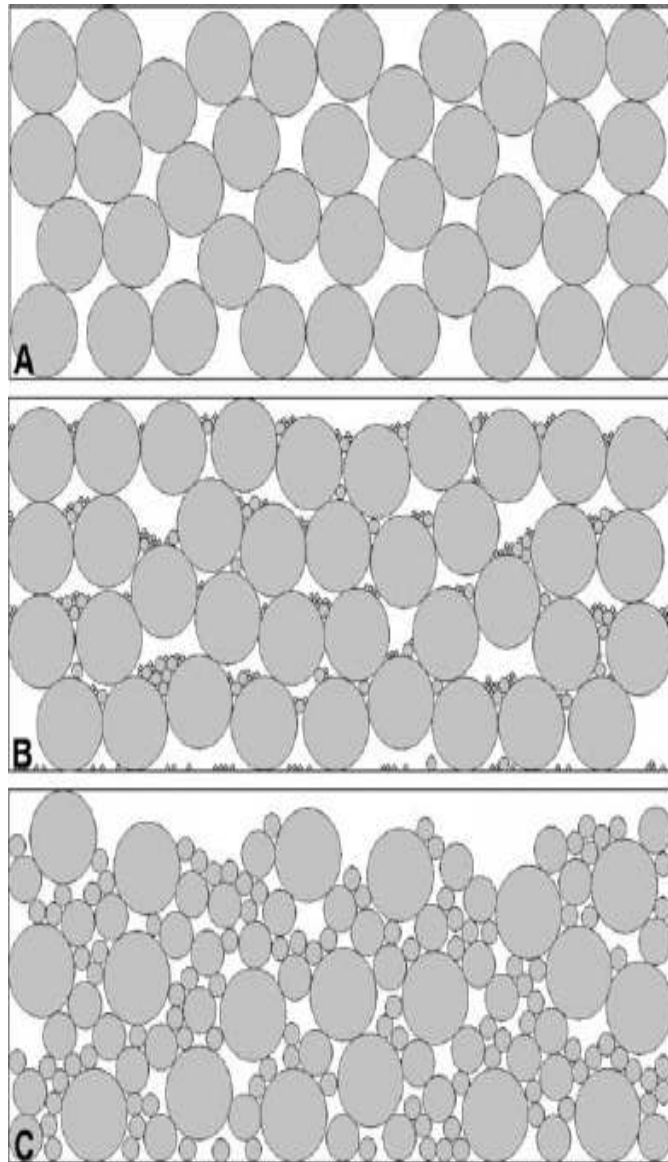


Figure 7-13 Random homogeneous single-layer sphere models after a volume increase of 10%: A: Random single-size sphere model. B: Random fractal three-size sphere model, showing the incomplete filling of the interstitial spaces with the use of the same number of spheres as the symmetric fractal model. C: Random continuous three-size sphere model. Note the similar occupation of the available volume of models A, and B, and the settlement effect of model C in the same available volume.

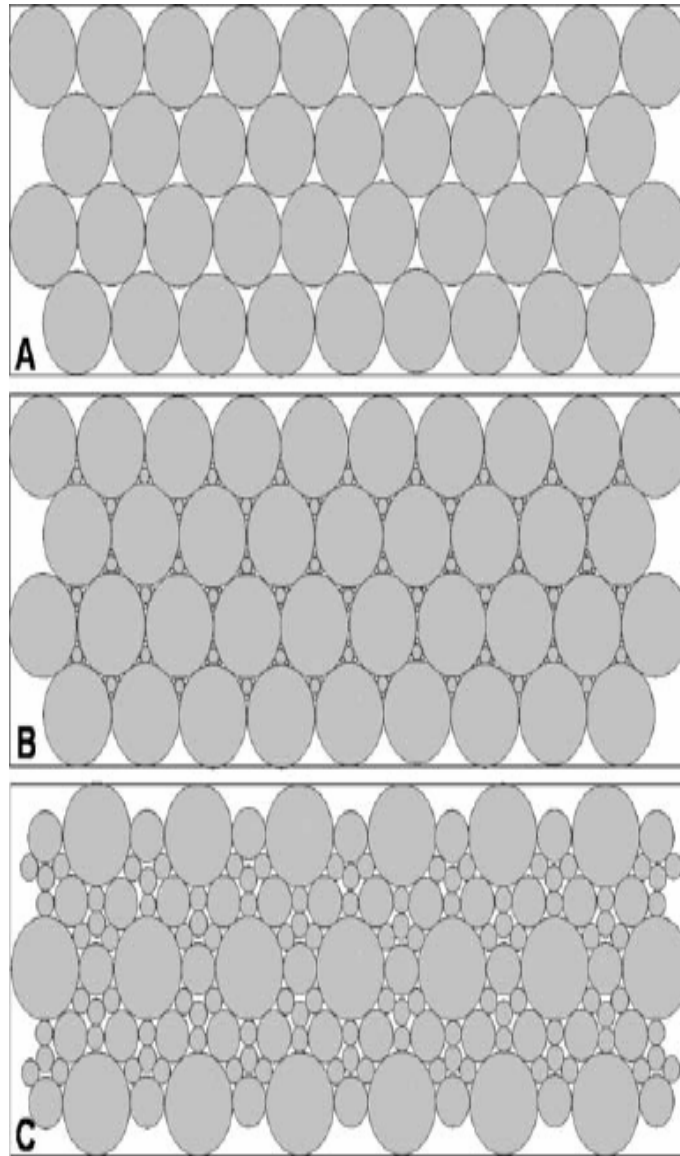


Figure 7-14 Symmetric single-layer sphere models for densest packing within a constant volume. A: Hexagonal densest packing, single-size sphere model. B: Fractal three-size sphere model (Apollonian Packing). C: Continuous three-size sphere model.

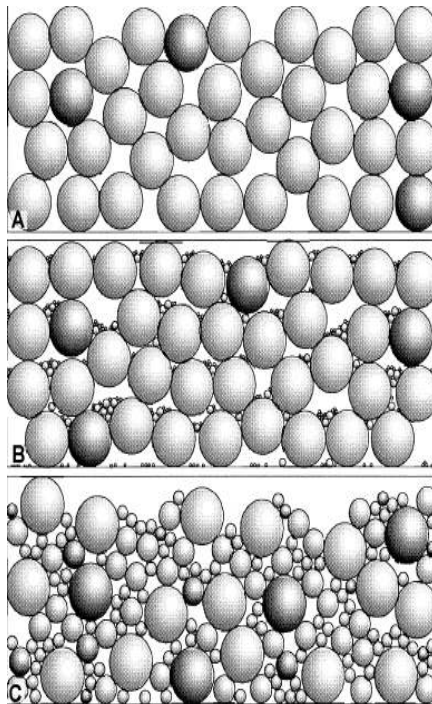


Figure 7-15 Random heterogeneous single-layer sphere models with 10% of weak spheres (dark colour). The weak grains are distributed randomly. Models A, B, and C compare to Figure 7-13.

7.9 Optimum Grain-Size Relations for Dense Packing

The minimum void ratios for the binary packing shown in Figure 7-9 are plotted in Figure 7-10 for each ratio of large to small grain diameter. This diagram shows that the minimum void ratio decreases sharply in the beginning as the diameter ratio increases. At larger diameter ratios, beyond approximately 7, the additional reduction in minimum void ratio due to further decreases in the small grain size is much less pronounced. Thus, the most efficient and largest reduction in minimum void ratio is obtained for packing of

spheres with diameter ratios near 7. Larger ratios will produce even lower minimum void ratios, but at a much lower rate. The reason that a transition in packing efficiency occurs at a diameter ratio near 7 is that the fine grains can still migrate and fit through pore paths formed between the larger grains. The insert in Figure 7-10 shows a calculation of the diameter of a spherical grain that can just fit through the triangular pore path between three mono-sized spherical grains. For smaller ratios, the fine grains are larger and they begin to push the large grains apart, thus increasing the minimum void ratios.

Based on the expressions for minimum void ratios and proportions of each component in a packing, as presented above, as well as a diameter ratio of 7, it is possible to produce a theoretically most efficient arrangement of spheres of prescribed sizes and proportions. Thus, a grain-size distribution curve to achieve minimum void ratio and maximum density may be composed for a quarternary packing. The experimental minimum void ratio of 0.60 for packing of single-sized spheres indicated in Figure 7-9 will be assumed for each of the four sizes:

Diameter ratio:	34.4	49	7	1
Volume composition:	63.76%	23.91%	8.97%	3.36%

The calculated minimum void ratio for this packing is 0.0202. McGeary (1961) performed an experiment to produce the densest possible quarternary packing of spherical grains. He did not have available four grain sizes with diameter ratios of exactly 7, but obtained results as follows:

Diameter ratio:	316	38	7	1
Volume composition:	60,7%	23,0%	10,2%	6,1 %

McGeary achieved an overall void ratio of 0,0515 for this experimental packing, Considering the difficulties in producing minimum void ratios, this experimental packing is reasonably close to the theoretical composition calculated above,

The theoretical and experimental grain-size distributions are compared in Figure 7-11. The distributions are shown by discrete vertical lines indicating the four grain sizes on a diagram similar to a conventional grain-size distribution diagram of % finer versus $\log(\text{diameter ratio})$. The dashed trend line through the midpoints of the vertical lines indicates an expected equivalent smooth optimum grain-size distribution.

It should be recalled that McGeary (1961) produced his packing by first vibrating the largest particles in a container, then adding the next size and vibrating and finally ending up adding the finest size. It may therefore not be possible to achieve the small void ratios indicated above for blended mixtures or for mixtures with smoothly varying grain-size distributions. Consequently, the theoretical calculations may only serve as goals towards which the void ratios of real mixtures of discrete spherical grains may converge, but never reach,

7.10 Maximum Void Ratios of Spherical Particles

The largest void ratio that can be achieved for mono-sized spherical grains in contact with each other is that of the cubical packing reviewed above. However, this arrangement is not stable in a gravitational field. But it may be supported in small regions of a larger assembly of spherical grains. It is also possible that honeycomb structures, in which not all spheres are in contact, may exist in some regions of loose assembly. Thus, it is not possible to model theoretically the maximum void ratio that may be achieved in

a packing of mono-sized spheres. It may be expected, however, that the maximum void ratios obtained in mixtures of large and small spheres will follow a pattern somewhat similar to that achieved for the minimum void ratios. Thus, if the maximum void ratios for two grain sizes were known, they could be expected to combine with a similar chevron-shaped variation as indicated for the minimum void ratios in Figure 7-6 and in Figure 7-9. This would occur if the small particles would fill the pores between the large particles and thus reduce the maximum void ratio, while further increases in the % fines would serve to push the large particles apart, and at 100% fines, the maximum void ratio of the fine particles would be obtained. Figure 9 indicates a speculative variation of minimum and maximum void ratios of binary packing of spherical grains under these conditions.

If, however, the fines do not all enter the pores between the larger particles, but some are lodged between the large grains, the large grains will be pushed apart, and this may occur even at low fines contents. This would cause the void ratio of the large grains, the so-called "skeleton" void ratio, to increase. The skeleton void ratio may be determined from the last two equations mentioned above by solving these equations for e_1 , the skeleton void ratio of the large grains:

$$e_{skeleton} = \frac{fines - e_{tot}}{1 - fines}$$

in which the fines are expressed as a pure number, and e_{tot} is the overall void ratio of the mixture. For the case that the skeleton void ratio stays constant and equal to the maximum void ratio at zero % fines, the relation between % fines and the maximum void

ratio follows the straight line indicated on the left hand side in Figure 7-12. However, if the fines get lodged between the large particles, then the maximum void ratios will be higher than those shown in Figure 7-12. This will be further illustrated in connection with the experimental study described below.

7.11 Effects of Fines in Sands with Non-Spherical Particles

The extreme void ratios shown on the diagrams discussed above are those obtained from calculations or measured in experiments with spherical particles of sizes in the gravel and coarse to medium sand range. Forces other than gravitational become important when the sizes decrease into the fine sand and silt regions. This is especially true for real, non-spherical particles. Friction, adhesion, and bridging between the fine particles cause these to form structures that are controlled by inter-particle forces. The importance of the inter-particle forces increase with decreasing particle size. Fraser (1935) pointed out that irregularly shaped particles can, in principle, be either more tightly or more loosely packed than those obtained for spherical grains. Thus, if an initially solid rock is fractured into grains, but these remain in place, then void ratio will be very low. But if the same fractured grains are removed from their tight positions and re-deposited, it will be impossible to get them into their tight structure again. In fact, a deposit of very angular grains such as those produced by fracturing will easily bulk up to fill more than a mixture of equivalent spheres. For particles formed by fracture, the smaller-sized particles are increasingly unable to withstand the mechanical wear necessary to produce more rounded particles. The smaller particles are continuously being broken without becoming rounded. There is therefore a tendency to obtain increasing angularity with decreasing

particle size. This angularity enhances the particle bridging effects, and angular particles consequently tend to produce higher void ratios than equivalent spheres. Ellis and Lee (1919) found that the void ratios for sands increased with decreasing particle size. This increase became more pronounced as the grain sizes decreased towards fine sandy loam, the smallest range in their experiments.

Fine sand and silt have sufficiently small particle sizes that van der Waals attraction and double layer repulsion begin to compete with gravitational forces for control of packing mechanisms and arrangements. These attractive and repulsive forces depend on the distance between the particles, and they begin to play a role for grain sizes near the No. 200 sieve (Cadle 1965). As the grain sizes decrease below the No. 200 sieve they become more influential relative to the gravitational forces. This effect is further enhanced in water where the particles are buoyed and will pack more loosely than under dry conditions. The effects of the inter-particle forces are that fine particles tend to adhere to each other, and externally they appear to exhibit cohesion. Thus, evidence shows that the angle of repose increases with decreasing particle size for particles in the fine sand and silt range as well as for many powders. The angle of repose for such granular materials is well above that expected on the basis of friction alone. The consequence of the inter-particle forces are that, rather than slipping into the voids and fitting between the larger particles and producing deposits with low void ratios, as described above, the fine particles tend to stick together, and with the help of frictional effects, they form loose chains and honeycomb structures with high void ratios. Mixtures of sand with fines will consequently tend to exhibit increasing void ratios with increasing fines content.

7.12 Experimental Study

The study of minimum and maximum void ratios of mixtures of spherical particles presented above is used as background and guide for an experimental study of the effect of fines content on the void ratios of clean sand with non-spherical particles and smooth grain size distribution curve. It is expected that the behavior of real sands will follow the same pattern outlined above, but actual values of maximum and minimum void ratios are expected to depend on factors such as (Fraser 1935):

- The shape of the grain-size distribution curve and their variation (Figure 7-16)
- The fines content
- The grain size
- The grain shape
- The method of deposition



Figure 7-16 Variation of grains particle size and shape – important factors for packing density

7.13 Procedures for Minimum and Maximum void ratios

As previously discussed in paragraph 7.3, the minimum and maximum void ratios may be determined using the ASTM (D 4253) and (D 4254) Methods. But when fines are present, the ASTM method is not reliable. An alternative procedure was developed by Lade et al. (1998).

This was especially important for the fine sand because its extreme void ratios were sensitive to small variations in methods and care in execution of procedures. To avoid any particle breakage during the tests, it was decided not to employ any type of surcharge in the densification procedures. Thus, after some experimentation the procedure for determination of the minimum void ratio consisted of spooning 822 g of sand into a 2000 mL graduated cylinder. After three spoonfuls (approximately 50 g), the cylinder was tapped eight times with the rubber handle of a screwdriver, twice each on opposite sides. This procedure was continued until all sand had been deposited into the smallest possible volume. This volume was then read on the graduated cylinder to the nearest cubic centimeter, corresponding to a variation in void ratio of approximately 0.003. It is estimated that the overall accuracy on determination of the void ratio is within 0.01. This is sufficiently accurate for the study of extreme void ratios for sand. For the fine Nevada sand, this method produced lower minimum void ratios than dry pluviation from any height.

Following the determination of e_{\min} the maximum void ratio was found by first covering the opening of the graduated cylinder with a piece of latex membrane. The cylinder with the 822 g of sand inside was then turned upside down very slowly (approximately 45 to

60 s to rotate 180°). The new greater sand volume was then read on the graduated cylinder, after which the rotation was repeated until the maximum volume was reproduced five times. Care was taken to avoid segregation of grains during this procedure.

7.14 Santamarina et.al Studies(2004)

Santamarina et al. studied the effect of particle shape on maximum and minimum void ratio of soils and found that both e_{\max} and e_{\min} and the void ratio difference $e_{\max} - e_{\min}$ increase as roundness and sphericity decrease as shown in Figure 7-17. His study consisted of determining the two extremes void ratio following standard procedures (ASTM C136 D4254, and D1557). The tested soils included 17 crushed sands from Georgia (granite and carbonate) and 16 natural sands from various places around the world, and some other materials such as glass beads, granite powder and syncrude tailings. Soils are made of grains. Grain size distribution plays a pivotal role in determining soil behavior. However, particle shape emerges as a significant parameter. Similar observations can be found in Fraser (1935), Shimobe and Moroto (1995), Miura et al. (1998), Cubrinovski and Ishihara (2002), Dyskin et al. (2001), and Jia and Williams (2001). Clearly, irregularity hinders particle mobility and their ability to attain minimum potential energy configurations. In the extreme case of low-sphericity, platy mica particles bridge gaps between grains and create large open voids (Guimaraes 2002).

In his analysis, Santamarina purposely removed The relevance of grain size distribution and the coefficient of uniformity C_u on packing density by considering soils having $C_u \leq 2.5$ (see Youd 1973).

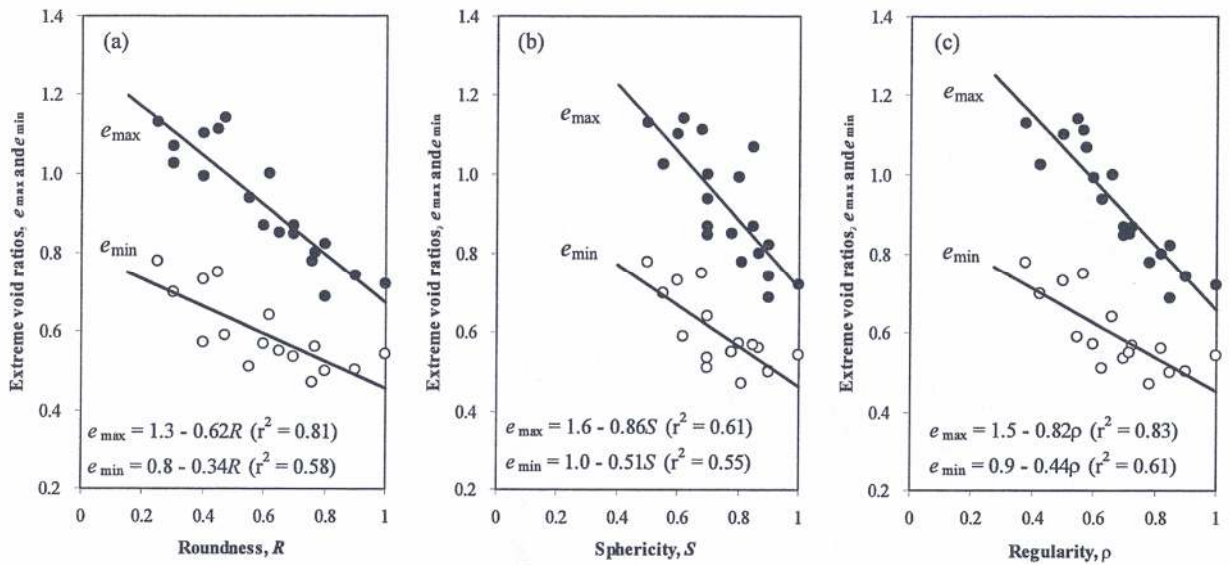


Figure 7-17 Effect of particle shape on extreme void ratios (natural sands with $C_u \leq 2.5$).

CHAPTER 8

DATA ANALYSIS PROCEDURE AND RESULTS

In this chapter, the results of laboratory tests on settlement of sands presented in Chapter 5 are analyzed. In the following section, the cumulative results of all tests results are compiled together to develop a simplified analysis procedure for estimating ground settlements of cohesionless soils caused by cyclic loading.

Preliminary evaluations suggested that the settlement of sands depends on:

Mineral composition of the sand (Quartz, Feldspar, Plagioclase, Rock fragment, Volcanic Rock, etc)

The shape of the grains,

The size of the grains or the gradation curve,

The relative density

The overconsolidation ratio

The induced cyclic shear strain,

The earthquake time history

The results of the current study will be presented in terms of the various measures examined. First, the results of the tests evaluated in terms of sand type will be presented, and subsequently in terms of mineral composition, grain shape and size, followed evaluation in terms of over consolidation ratio. Finally, the results of the tests evaluated in terms of a new parameter ($e-e_{\min}$) will be presented.

Following the analysis, recommendations for revised design analysis procedures using time history approaches and parameters reflecting the influence of sand type and overconsolidation ratio were documented.

8.1 Tests Evaluated in Terms of Sand Type or Characteristics

The settlement of sand was first examined in term of sand type. As expected, settlements of sands are not unique, different sands other than Crystal Silica #20 used by Silver and Seed behave differently as shown in Figure 8-1 where 18 types of sands at relative density of 60% were subjected to a 25 uniform cyclic shear strain of 0.1%. The settlement of these sands varies from 0.1% to 0.36 %. It should be mentioned that the settlement of Crystal Silica sand used by Silver and Seed is about 0.21%.

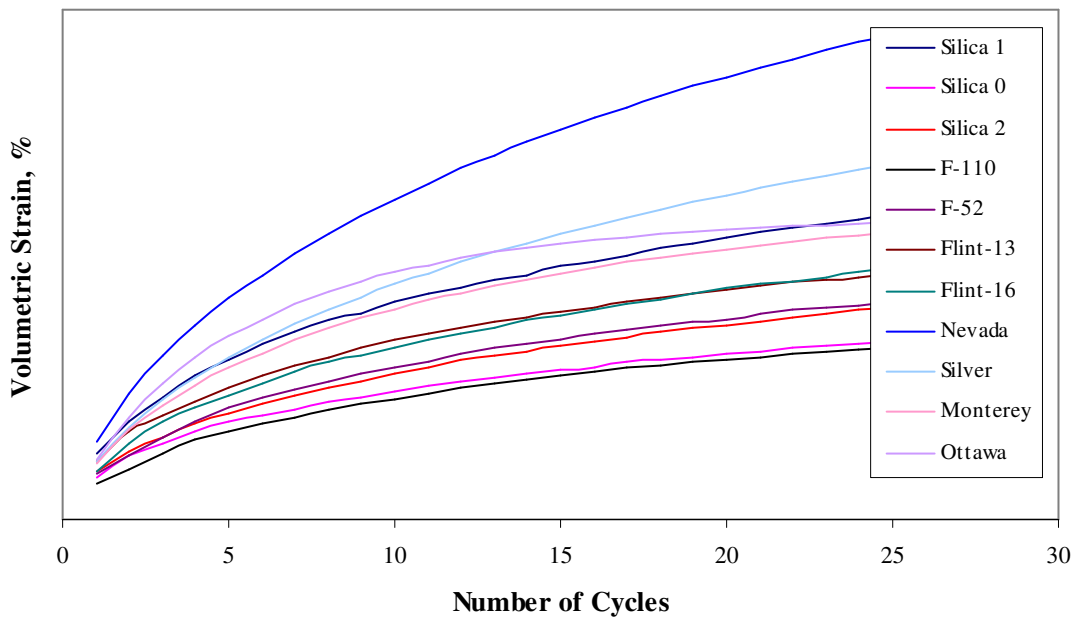


Figure 8-1 Settlement of 18 types of sands under uniform cyclic loading.

8.2 Tests Evaluated in Terms of the Mineral Composition of Sand

The settlement of sands was first examined in terms of the mineral composition of the sands. The results of all tests on sands performed by the author on Nevada and Silica #30 sands which were all prepared to a void ratio corresponding to relative density of 60% and tests results collected from previous studies on Silica #20 sand (Silver and Seed, 1971), on Monterey sand (Pyke, 1975), on Ottawa sand (Bhatia, 1980), on Flint-13 &16, F-52 &10, Silica 0,1 and 2 (Stewart et al.2004), are presented Figure 8-2 and show that settlement of sands are not sensitive to sand mineralogy. All the sands shown in Figure 8-2 are made out of 99.9 % quartz but differ from each by the size and the shape of the grains. Their gradation curves are shown in Figure 8-3. The behavior of the 8 other materials sands obtained from UCLA which are a mixtures of quartz, feldspar, plagioclase metamorphic and volcanic rock fragments, and organic material are shown in Figure 8-4.

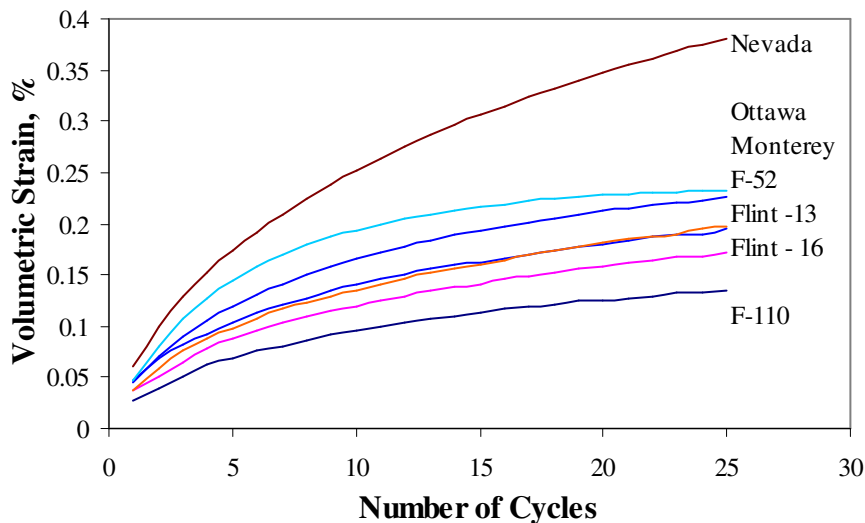


Figure 8-2 Settlement of sands under uniform cyclic loading

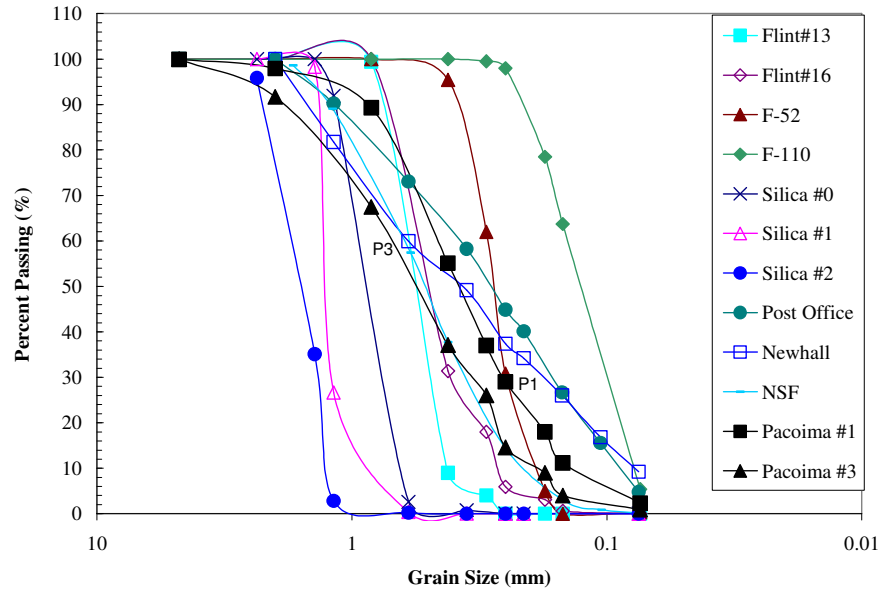


Figure 8-3 Grain size distribution

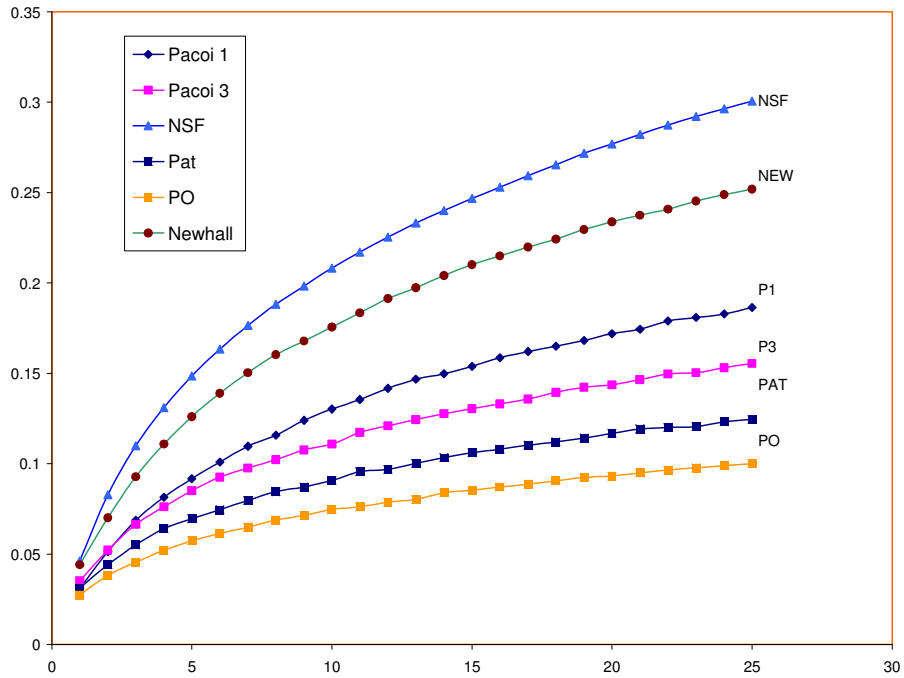


Figure 8-4 Settlement of sands under uniform cyclic loading

8.3 Tests Evaluated in Terms of Grains Size and Shape

The results of all tests show that settlements are sensitive to the grains size and shape.

Among the sands that were tested, they are rounded to subrounded and angular to subangular shape. The gradation curves cover a wide range and the sands vary from poorly to well graded. Despite the fact that Silica sand #0, #1 ,2 and #30 are all quartz and their grain shape are angular to subangular , their settlement under uniform cyclic loading are all different as shown in Figure 8-5. The grains sizes are shown in Figure 8-3.

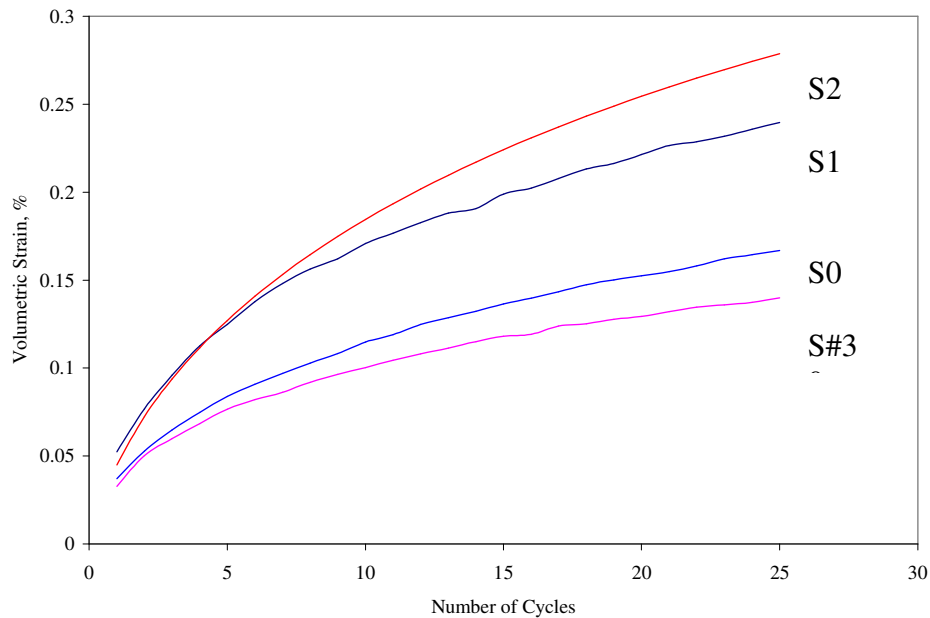


Figure 8-5 Settlement of sands under uniform cyclic loading

Figure 8-6 shows the settlement of sands type that are rounded to subrounded in shape. Again, these sands were similar in mineral composition, they are all quartz but they differ in sizes, gradation curves. The settlement versus number of cycles is different except for

Flint 13 and Flint 16. A look at the gradation curves for Flint 13 and Flint 16 shown Figure 8-7 how that they are very similar.

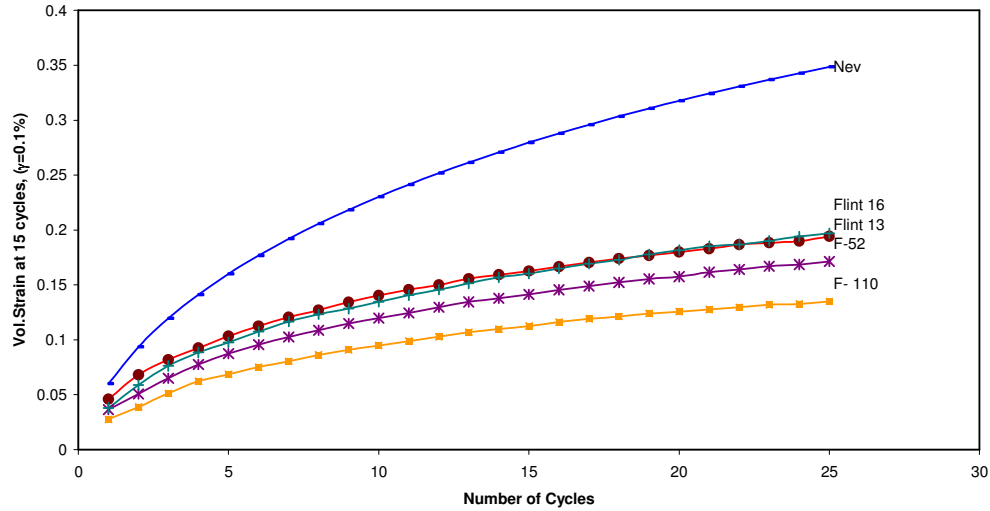


Figure 8-6 Settlement of sands under uniform cyclic loading

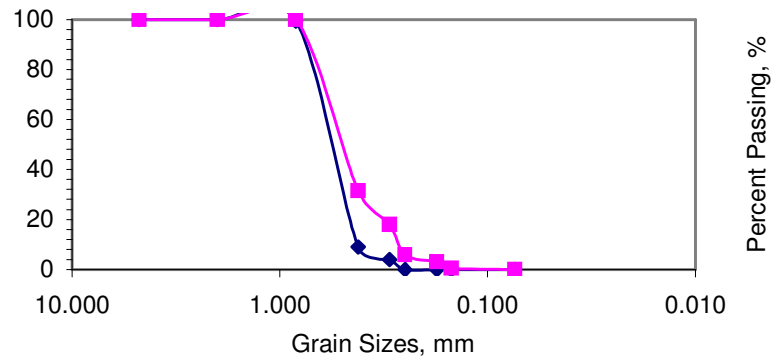


Figure 8-7 Grain distribution curves for Flint 13 and 16

8.4 Grain Size Distribution and Grain Shape.

The grain size distributions of samples were obtained by sieving the samples through a set of sieves that have progressively smaller opening. Although it is evident that the mechanical properties of sand depend on the grain shape as well as grain size distribution, it is rather difficult to quantify irregular grain shapes. The indices for grain shape have been proposed by some researchers in various areas not only in geotechnical engineering. An index widely used in soil mechanics is Roundness R proposed by Wadell (1932). Since roundness is, however, inadequate for grain with sharp corners such as crushed stones, Lee (1964a,b) proposed an alternative concept, angularity A. Yoshimura and Omega (1993) demonstrated a unique negative correlation between Roundness and Angularity with the aid of a coefficient of form unevenness FU, which can be obtained by image analysis proposed by him. Roundness can be estimated by visual comparison with charts, such as the one shown in Figure 2-b (Folk 1955, Barrett 1980). Differences in estimated roundness and sphericity by different assessors is in the order of 0.1 and does not exceed 0.2. Digital image analysis facilitates the systematic evaluation of mathematical descriptors of particle shape including Fourier analysis, fractal analysis and other hybrid techniques (e.g., Meloy 1977, Clark 1987, Hyslip and Vallejo 1997, Bowman et al. 2001). Figure 8-8 shows the grain shape for three different sands.

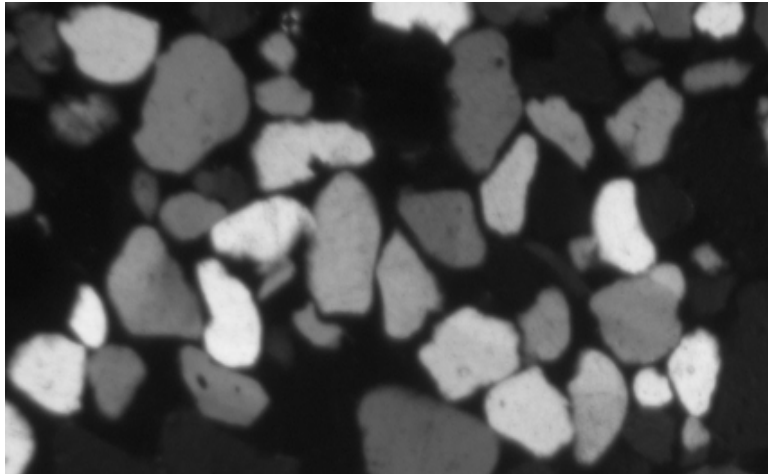
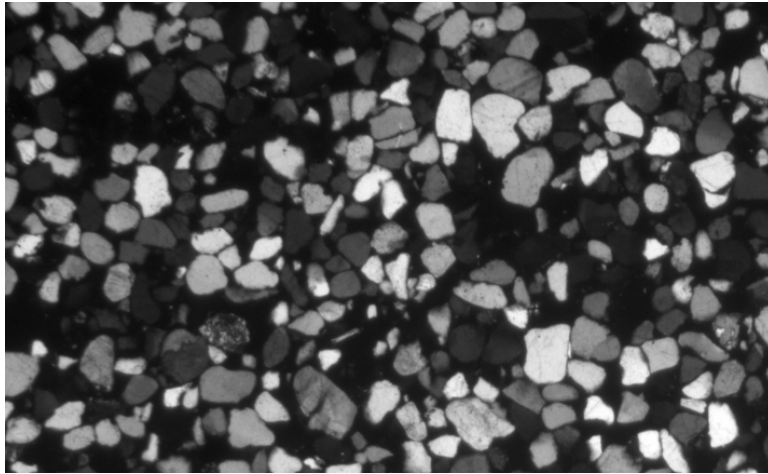
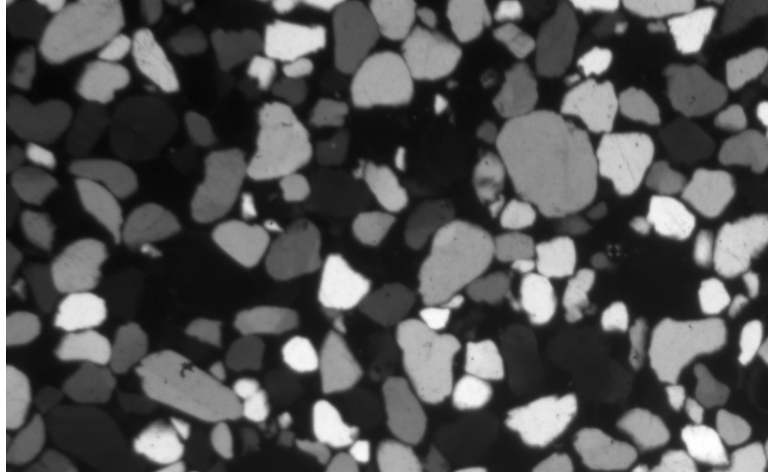


Figure 8-8 F-110 (top), Nevada (middle) and F-110 (bottom)

8.5 Tests Evaluated in Terms of Soil Relative Density

Finally, the data were evaluated in terms of their soil relative densities. The relative

density for given sand is:

$$D_r = \frac{e_{\max} - e}{e_{\max} - e_{\min}} \cdot 100$$

Where e is the void ratio of the sample, e_{\max} and e_{\min} are respectively the maximum and the minimum void ratio. The soil relative density is the relative density of the specimen based upon its gross void ratio and the maximum and minimum index void ratios for that particular sand. When the settlements are plotted in terms of the soil relative density, clear patterns emerge. There is a clear trend between increasing soil relative density and decreasing settlement. These plots for the Silica #30 sand, Nevada Sand, Silica Sand #20, Monterey sand, Ottawa sand are presented in Chapter 5.

These two values e_{\min} and e_{\max} can be determined using ASTM D 4253 for Maximum Index Density and Unit Weight of Soils Using a Vibratory Table and ASTM D 4254 Test Method for Minimum Index Density and Unit weight of Soils and Calculation of Relative Density. However, other methods have been employed and these often produce different values than those obtained by ASTM procedures. In order to avoid this error, and knowing that Stewart et al. used a procedure other than ASTM in order to compute these extreme void ratios, it was decided to recompute these two values using the standard ASTM procedure. The two extreme void ratios are then computed as:

$$e_{\max} = \frac{\rho_s}{\rho_{d \min}} - 1, \quad e_{\min} = \frac{\rho_s}{\rho_{d \max}} - 1$$

Where ρ_s is the specific gravity of the soil?

8.5.1 Tests Evaluated in Terms of Soil Overconsolidation Ratio

Loose sands, whose behavior under earthquake loading may be of interest, are unlikely to be naturally overconsolidated, but may in some cases be preloaded to reduce settlements under static loading. It is known that overconsolidation increases the coefficient of lateral earth pressure, K_0 , of sands. All the samples shown in fig. 11 were cyclically sheared under a vertical stress of 2000 psi. In order to obtain an overconsolidation ratio of 2 and 4, similar samples were loaded respectively to 4000 psi and 8000 psi, unloaded to zero and reloaded to 2000 psi before testing. It should be mentioned that the volume changes caused by overconsolidation were relatively small and all samples were close to the relative density at the commencement of shearing. The effect of overconsolidation is quite clear and the results suggest that preloading loose sands reduces their settlement potentials. The sensitivity of settlement of Nevada and Silica #1 sand to sand type and over consolidation ratio are shown in Figure 8-9 and in Figure 8-10

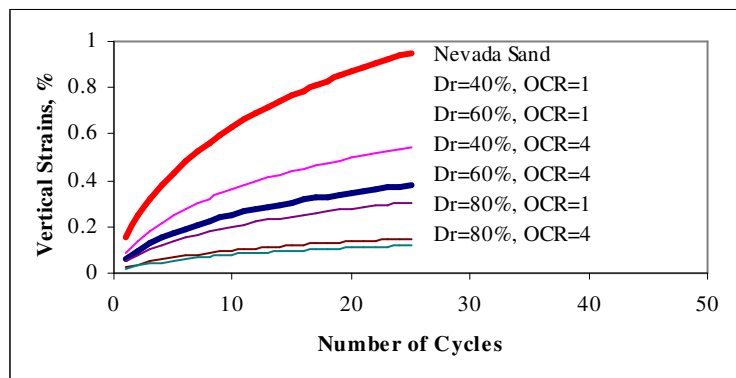


Figure 8-9 Settlement of Nevada sand under uniform cyclic loading and with OCR =1 and OCR = 4.

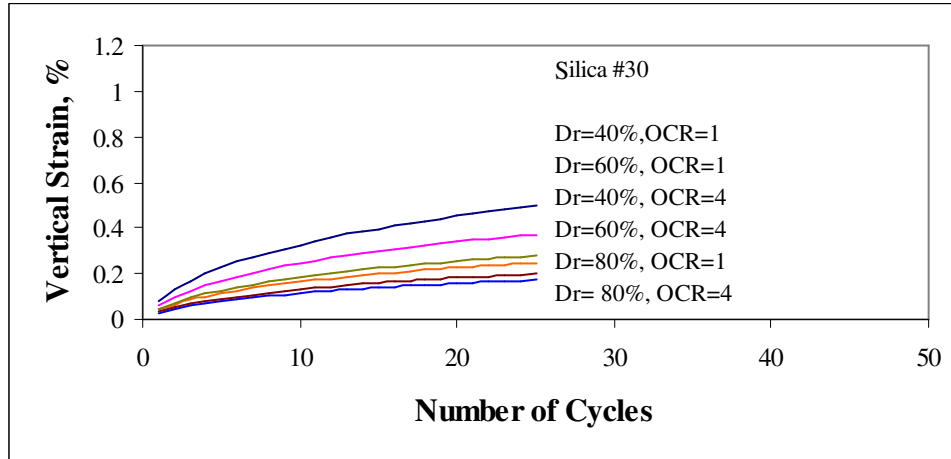


Figure 8-10 Settlement of Silica # 30 sand under uniform cyclic loading and OCR =1 and OCR= 4.

8.5.2 Tests Evaluated in Terms of Applied Shear Strain

The results show that settlement of sand increases with higher shear strain amplitude and that this increase occurs during the first few cycles. Figure shows the vertical volumetric strain versus the cyclic shear strain.

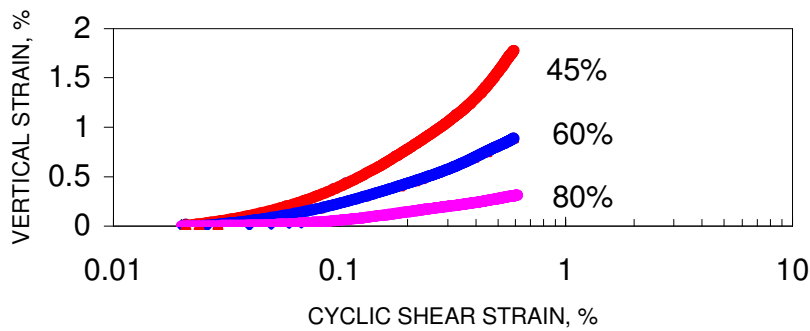


Figure 8-11 Settlement versus shear strain, %

The objective of this research is to develop analysis parameters to reflect the above factors leading to recommendations for revised design analysis procedures using time history approaches and parameters reflecting influence of sand characteristics and overconsolidation ratio. It seems that settlements of sands under cyclic loading are sensitive to the sand type. Sands differ from each other by mineral composition, shape and sizes or grain distribution. We have seen in Figure 8-2 that all pure quartz sands, behave differently under cyclic loading, so it seems that settlement of sands under cyclic loading is primarily a function of grain shape and grain size.

8.6 Overall Evaluation of the Results

The conclusion of Santamarina study is that the maximum and minimum void ratio of a particular sand are function of the grain shape (sands with $C_u \leq 2.5$) and grain shape and grain distribution ($C_u > 2.5$). It seems logical to assume that the variation of the void ratio from maximum to minimum as shown in Figure 8-12 is also function of the grain shape and grain size.

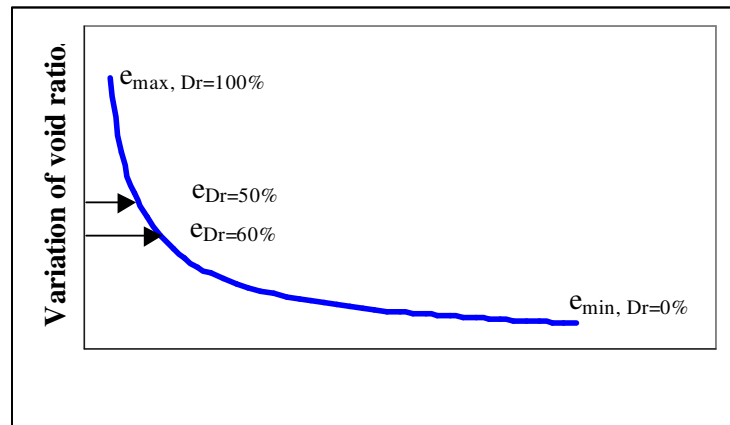


Figure 8-12 Typical Variation of Void ratio

Each sand has its own maximum and minimum void ratio which reflect the grain shapes and grain sizes of that sand, the void ratio difference, $I_e = (e_{\max} - e_{\min})$ is a characteristic of that sand. Settlement of sand under cyclic loading and for a given relative density, would be expected to increase as I_e gets larger and decrease as I_e gets smaller. In comparing the result of the studies and because the relative density was not always the same, we will use the difference between the void ratio of the tested sample and the minimum void ratio instead of I_e , as a parameter reflecting potential settlement behavior under cyclic loading.

8.7 Settlement of Sands in Term of Mineral Composition

The settlement of all sands having relative density of 60 % and that are pure quartz are plotted in term of $(e - e_{\min})$ and is shown in Figure 8-13. The plot confirms that settlement of sands under cyclic loading could be represented in terms of $(e - e_{\min})$ by a linear relationship. We also plot the settlement of material sands contributed by the UCLA research team, having relative density around 60 %, which are field sands containing volcanic and metamorphic rock fragments and organic materials besides quartz and plagioclase, etc. Again the plot shown in Figure 8-14 confirm the finding mentioned above. Last we plot the settlement of all the above sands versus $(e - e_{\min})$. The result of the plot presented in Figure 8-15 shows that settlement of sands under cyclic loading is independent of the mineral composition of the sands and dependent only on grain shape and grain size distribution which can be represented by the difference between the void ratio of the sand and the minimum void ratio. The linear relationship can be represented by an equation of the form:

$$\text{Settlement (at 15 cycles and shear strain amplitude of 0.1 \%)} = 1.2 (e - e_{\min})$$

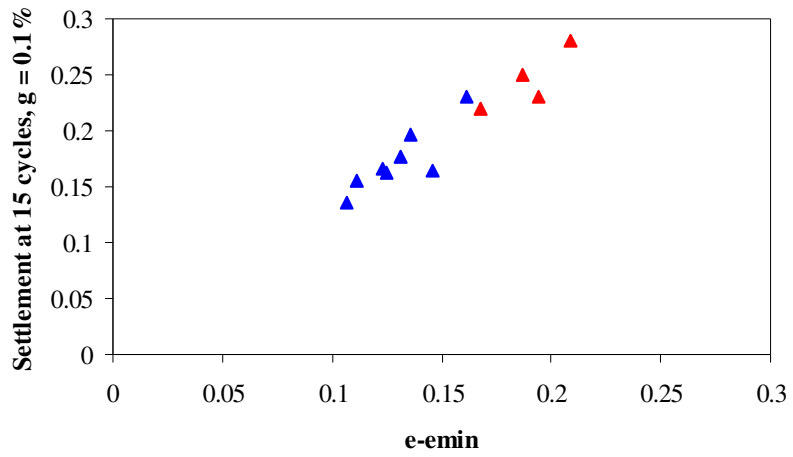


Figure 8-13 Settlement of pure quartz sand ($Dr = 60\%$) versus $e - e_{min}$

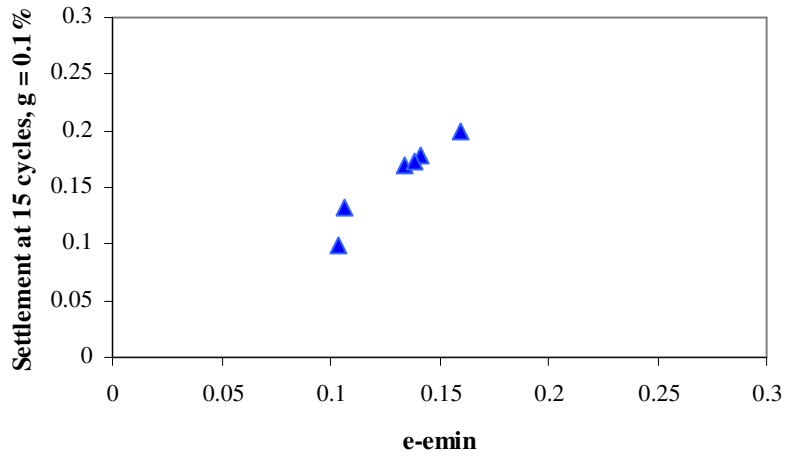


Figure 8-14 Settlement of materials sand ($Dr = 60\%$) versus $e - e_{min}$

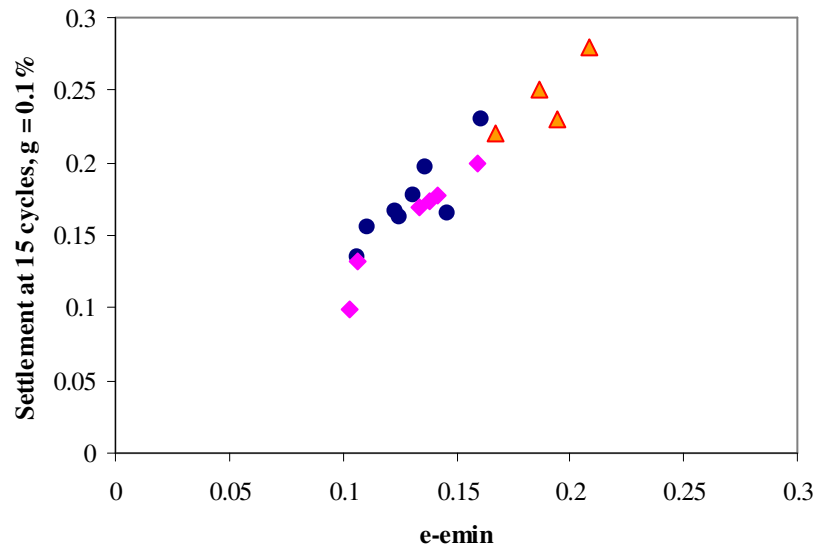


Figure 8-15 Settlement of all sands ($D_r = 60\%$) versus(e_{-min})

8.8 Settlement of Non-Plastic Silty Sands

Sands with fines content were not originally intended to be a part of this study. But given the fact that the raw data obtained from UCLA contained data on sands with fine content, it was decided to check the applicability of the finding of this study to sands with fine content.

Compacted fill soils usually contain a fine-grained fraction (i.e., soil particles smaller than the #200 sieve opening). It has long been understood that the presence of fines in soil significantly changes ordinary mechanical properties such as shear strength relative to clean sands (e.g., Casagrande, 1932). With respect to dynamic properties, numerous recent laboratory studies have investigated the effects of non-plastic fines on the undrained behavior of saturated sands (e.g., Troncoso, 1990; Polito and Martin, 2001; Xenaki and Athanasopoulos, 2003).

The UCLA research team investigated the effects of non-plastic fines on volumetric strains associated with seismic compression. They compared the results to the findings of previous studies of the undrained response of silty sands (i.e., liquefaction studies), and found similar trends related to the effects of fines observed in the liquefaction testing.

The soil materials that they tested were artificial mixtures of sand and silt materials. Two sand materials and one silt material were used. Sand #1 is termed “Vulcan sand,” which is commercially available from Vulcan Materials in Irwindale, California. Vulcan sand has no fines, is well-graded, and has approximately 57.5% and 2.8% passing the No. 30 (0.6 mm) and No. 100 (0.15 mm) sieves, respectively. Vulcan sand has a mean grain size, D₅₀, of 0.51 mm and particle shapes that range from subangular to subrounded. Sand #2 is termed “Silica No. 2,” which is commercially available from US Silica Company. Silica No. 2 has no fines and is poorly graded (approximately 35.1% and 2.8% passing the No. 10 (2.0 mm) and No. 20 (0.84 mm) sieves, respectively). Silica #2 sand has a mean grain size, D₅₀, of 1.6 mm and subrounded particles. The silt used in their study was Sil-Co-Sil No. 52 obtained from US Silica Company. The gradation curve for this silt material was established from hydrometer testing. The silt material is non-plastic, being comprised of Quartz particles of very small size (i.e., rock flour). These materials have immeasurable liquid limit based on ASTM procedures, but LL is estimated as $C_u < 17$. For each sand material, four different sand-silt mixtures were created with silt contents varying from 10 to 50% (Table 8-1). Index testing performed on these mixtures include gradation (ASTM 2487, D4221), modified Proctor compaction (ASTM D1557), minimum/maximum void ratio. The maximum and minimum dry densities and void

ratios of each sand-silt combination were determined using the Modified Japanese method and dry tipping, respectively (these techniques are comparable to those in ASTM D4253 and D4254). The minimum and maximum void ratios for the two soil mixtures are plotted as a function of fines content (FC) in Figure 8-16. The dip in these void ratio quantities at mid-level FC is typical of non-plastic sand-silt mixtures, which has been explained by Polito and Martin (2001) utilizing the concept of limiting silt content (FCL). The parameter FCL is defined as the maximum amount of silt that can be contained in the void space between sand particles while maintaining a contiguous sand skeleton. For $FC < FCL$, the addition of silt merely fills in inter-grain void space, thus decreasing void ratio. For $FC > FCL$, sand grains float within a silt matrix, and increasing FC increases the overall void ratio because intra-fines void ratios are relatively high. Hence, FCL can be identified as the FC corresponding to lowest possible minimum void ratio. Using Figure 4.3, values of FCL are identified as approximately 20% and 30% for the Vulcan-silt and Silica-silt mixtures, respectively. These are typical values for FCL based on data compiled by Polito (1999).

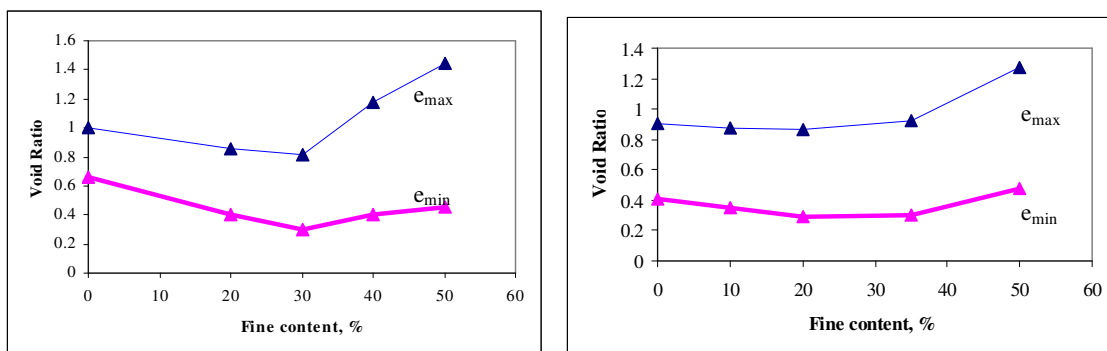


Figure 8-16 Variation of Index Void Ratios with Silt Content, Vulcan Host Sand (right) Silica #2 Host Sand (left)

8.9 Effect of Fines Content

Thevanayagam (1998) postulated that a soil mixture is a delicate matrix comprised of two submatrices, a coarser-grain matrix and finer-grain matrix. For $FC < FCL$, the finer-grain matrix does not actively participate in the transfer of contact frictional forces, or their contribution is secondary. It follows that the coarser-grain matrix at $FC < FCL$ can be described by the intergranular void ratio, e_s (Thevanayagam, 1998):

where FC is in percent. At $FC > FCL$, the soil force chain is governed primarily by the contacts within the finer matrix and the coarser grains float in the finer-grain matrix. Consequently, the finer-grain matrix at $FC > FCL$ can be described by the interfine void ratio, e_f , as follows Using the above definitions, void ratio terms e_s and e_f .

Void ratios corresponding to relative densities intermediate between 0 and 100% (corresponding to e_{max} and e_{min} , respectively) have similar variations with FC . The observed increase in seismic compression with increasing FC below FCL can be explained using the conceptual framework of Thevanayagam (1998) presented above. In particular, for $FC < FCL$, the increase of intergranular void ratio (e_s) with FC explains the observed increase in $\varepsilon_{v,N=15}$ values, because e_s is the void ratio that controls the soil behavior for this range of FC . For $FC > FCL$, the interfine void ratio, e_f , decreases with increasing FC which would suggest a reduction in $\varepsilon_{v,N=15}$ values with increasing FC above FCL . However, the opposite occurs, that is, $\varepsilon_{v,N=15}$ increases with FC . This could be explained by the fact that $(e - e_{min})$ increase with increase FC even beyond FC_L as shown in Figure 8-17 and in

Figure 8-18.

Soil	FC(%)	emax	emin	emax- emin	e RC=87%	e RC=92%	Cu
Vulcan	0	0.904	0.412	0.492	0.549	0.464	2.9
	10	0.872	0.352	0.52	0.524	0.441	9.6
	20	0.87	0.289	0.581	0.467	0.387	33.3
	35	0.92	0.297	0.623	0.513	0.430	45.83
	50	1.271	0.474	0.797	0.640	0.550	52.0
Silica # 2	0	1.006	0.662	0.344	0.774	0.677	1.29
	20	0.86	0.405	0.455	0.501	0.419	68
	30	0.819	0.298	0.521	0.478	0.398	88
	40	1.177	0.398	0.779	0.573	0.488	151
	50	1.442	0.457	0.985	0.682	0.591	160

Table 8-1 Sand- Silt mixtures used by in the UCLA testing program

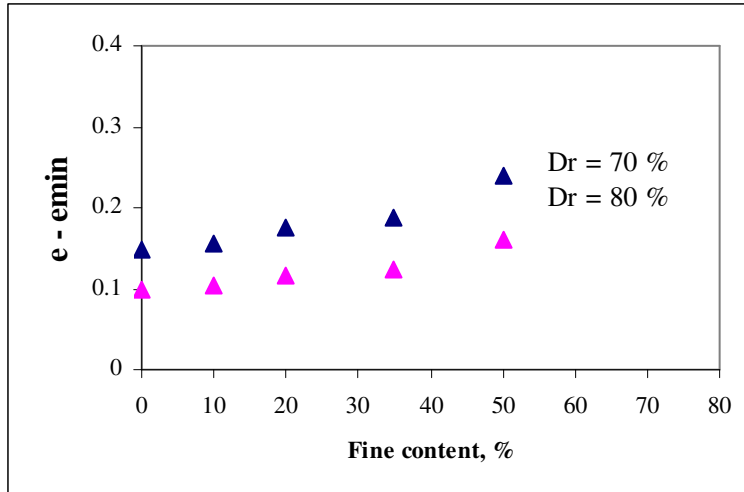


Figure 8-17 $e - e_{min}$ versus fine content for Vulcan Host Sand (Stewart et.al, 2004)

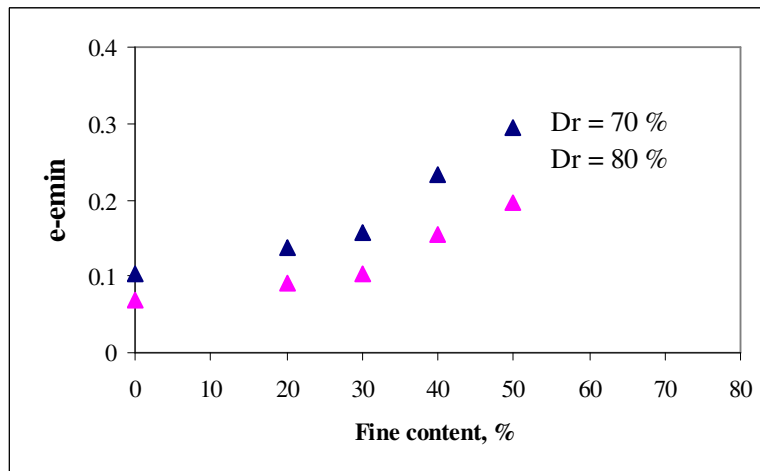


Figure 8-18 $e - e_{min}$ versus fine content for Silica #2 Host sand (Stewart et.al, 2004)

Figure 8-19 Shows the variation of settlement of the Vulcan Host Sand and Silica #2 Host Sand with variable fines content as a function of $(e-e_{min})$.

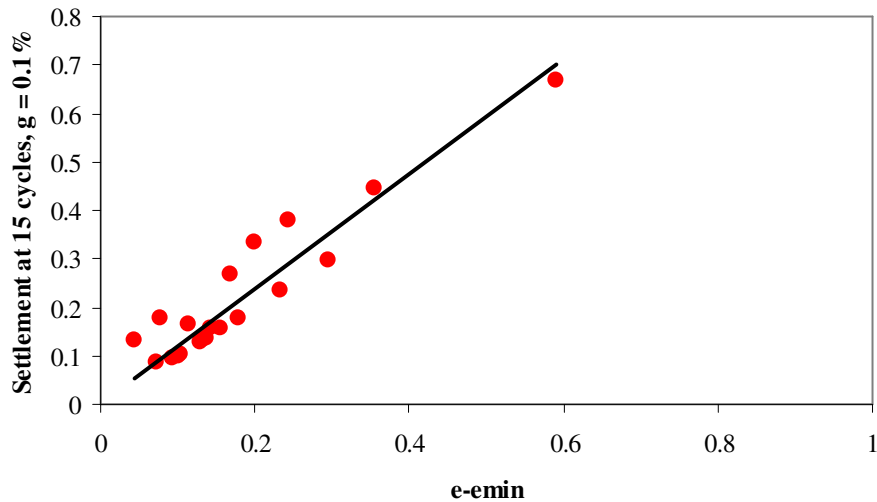


Figure 8-19 Settlement of sands versus $(e-e_{min})$ for Vulcan Host sand and For Silica #2 Host Sand

The UCLA research team performed a total of 20 tests on the two host sands and with two different relative densities, $D_r = 70\%$ and $D_r = 80\%$. Figure 8-19 shows that by adopting the concept of $(e-e_{min})$, we can express settlement of all sands including sands with fine content by using the concept mentioned above. Figure 8-20 shows the settlement of all sands as a function of $(e-e_{min})$ for normally consolidated sands, ($OCR = 1$). Figure 8-20 includes the results on clean sand with variable relative densities and it also includes the results on sands with fines content with variable relative densities. It indicates that settlement of all sands has the same shape but they differ in the quantity. That quantity is a function of the value $(e-e_{min})$, which implies that the larger $(e-e_{min})$,

The data in Figure 8-20 contains a total of 48 tests on different clean sands and sands with fines content with variable relative densities all normally consolidated more empty voids to be filled and the larger the settlement is going to be observed.

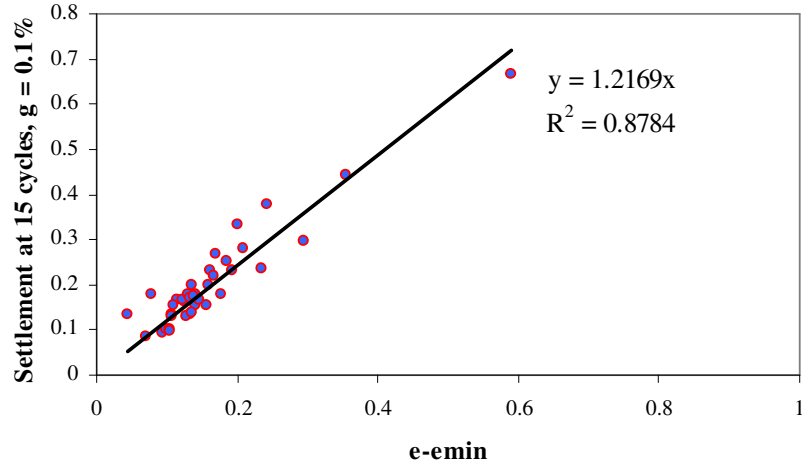


Figure 8-20 Settlement of sands versus $(e-e_{min})$

8.10 Effect of Over Consolidation Ratio

The result of liquefaction studies show that overconsolidated sands have a greater resistance to liquefaction and that the resistance increase with overconsolidation ratio, OCR (Seed and Peacock, 1971). The process of overconsolidation increases the coefficient of lateral earth pressure, K_0 , of sand hence mean effective stress. It is generally considered that the increase in liquefaction potential is caused by higher mean effective stress. The higher mean effective stress results in increased shear modulus and lower shear strain.

The lower shear strain result in smaller volumetric strain and lower porewater pressure for saturated sand. Martin et al (1975) showed that volumetric change in dry or partially saturated sand is related to the generation of porewater pressure in saturated sand, so it is reasonable to assume that volumetric change of dry sand subjected to cyclic loading would decrease with increasing overconsolidation ratio, OCR. As part of this study, two sands were tested with three different OCR as mentioned in Chapter 5 and data from previous studies on Monterey sand, (Pyke, 1975) and on Ottawa sand (Bathia, 1980) were compiled in order to analyze the effect of OCR on settlement of sands. In summary, four sands at 40 % relative density were tested using an OCR = 1, then the tests were repeated using OCR= 2 and 4 while keeping the relative density for each sand the same. Thus, the line in Figure 8-20 is going to be used as the base line or reference line. The results are shown in Figure 8-21 which confirm that an increase in overconsolidation ratio would result in decrease in settlement. This decrease is a function of $(e-e_{min})$, which means that for a larger $(e-e_{min})$, this decrease is significant.

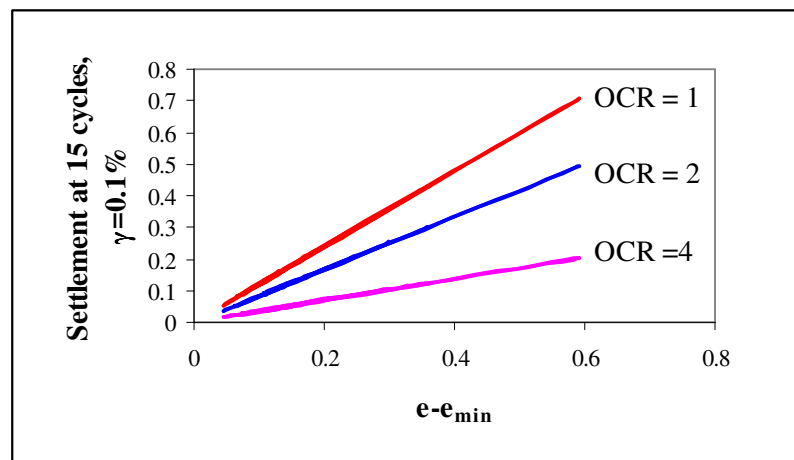


Figure 8-21 Settlement of sands versus $(e-e_{min})$ for OCR= 1,2 and 4.

CHAPTER 9

PARAMETRIC ANALYSES USING DESRA-MUSC

9.1 Introduction

Silver and Seed (1971) tested only the Crystal Silica sand to develop their charts which were subsequently used by Tokimatsu and Seed (1984). However, as shown from this study, results from a total of 50 tests on clean sand and on sand with fines were evaluated to define the volumetric behavior of these sands at three relative densities of 40%, 60 % and 80 %. The settlement of sand is a function of the soil characteristics, which can be defined by the grain size distribution and the grains shape. Using the procedure developed by Martin et al (1975), the volumetric constants that define the behavior of several of these sands were computed. Using the new available experimental data, the response of the sands to a constant shear strain of 0.1% was computed. The result shows clearly that the volumetric behavior of these different sands is not the same. For example, the response of four different types of sand normally consolidated ($OCR = 1$) at relative density of 40% and subjected to a constant shear strain of 0.1% shown in Figure 9-1, indicates that the Nevada sand settles twice as much as the Monterey sand. The Silica sand represents the sand used by Silver and Seed (1971).

The paragraphs below examine errors in the Tokimatsu and Seed (1984) procedure arising from variation in settlement behavior of different sands and earthquake time histories by using the computer program DESRA-MUSC. Following this study, a recommended design procedure is documented.

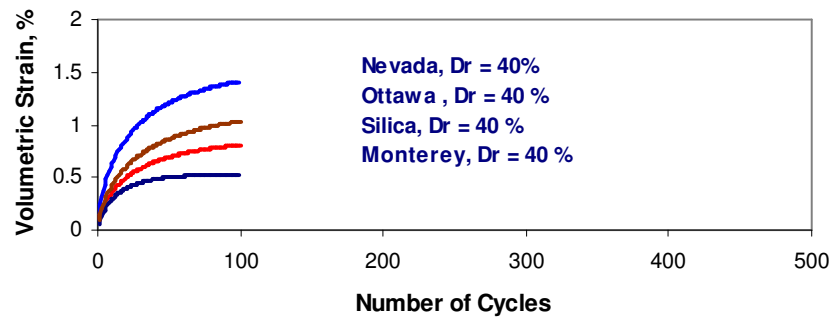


Figure 9-1 Volumetric Strain curves versus Number of Cycles for constant shear strain amplitude of 0.1 %.

9.2 Settlement Analysis using the Computer Program DESRA-MUSC.

In order to be able to compare the results obtained by DESRA-MUSC to that obtained using the Tokimatsu and Seed procedure, , the soil deposit (50 ft) shown in Figure 9-2 composed of Crystal Silica sand at a relative density of 45 % was subjected to S740 W component of the record obtained at Pacoima Dam (1971 San Fernando Earthquake) after scaling it to yield a maximum base acceleration of 0.35g and a surface acceleration of 0.45g, in order to compare the analysis to that performed by Tokimatsu and Seed. The shear modulus degradation with shear strain used is that used by Tokimatsu and Seed, which is the middle curve in Figure 9-3. The results are shown in

Figure 9-5, where the computed settlements for one-directional ground shaking obtained by DESRA-MUSC was 2.05 in. compared to that obtained by the Tokimatsu and Seed procedure which was 1.68 in.

The same soil profile was then analyzed but with two different relative densities, 60 % and 80%. The volumetric strain constants and the hardening parameters were computed

using the experimental data furnished by Silver and Seed, 1971 shown in Figure 9-4 and using Finn and Byrne analytical expression in order to compute the constants volumetric change used in DESRA-MUSC.

$$(\Delta\varepsilon_{vd})_{Dr_2} = R(\Delta\varepsilon_{vd})_{Dr_1}$$

$$R = 0.00031(100 - D_r)^2 + 0.062$$

$$45 \leq D_r \leq 80$$

Where R is a constant that varies with the relative density, and $(\Delta\varepsilon_{vd})_{Dr_1}$ is the volumetric strain increment computed for relative density of 45%.

The results shown in Figure 9-5, Figure 9-6 and Figure 9-7 show reasonably good agreement between DESRA-MUSC and the simplified procedure of Tokimatsu and Seed, 1984. The reasonable agreement is based on the fact that the sand and the ground motion used in the analyses were the same as used by Tokimatsu and Seed. Note that hardening parameters were not used in these analyses.

D_r (%)	C_1	C_2	$C_3=C_1C_2C_4$	C_4
Silica Sand				
45	0.80	0.725	0.35	0.6
60	0.45	1.30	0.63	1.08
80	0.15	3.6	1.56	2.9

Table 9-1 Values of C_1 , C_2 , C_3 and C_4 for the three relative densities

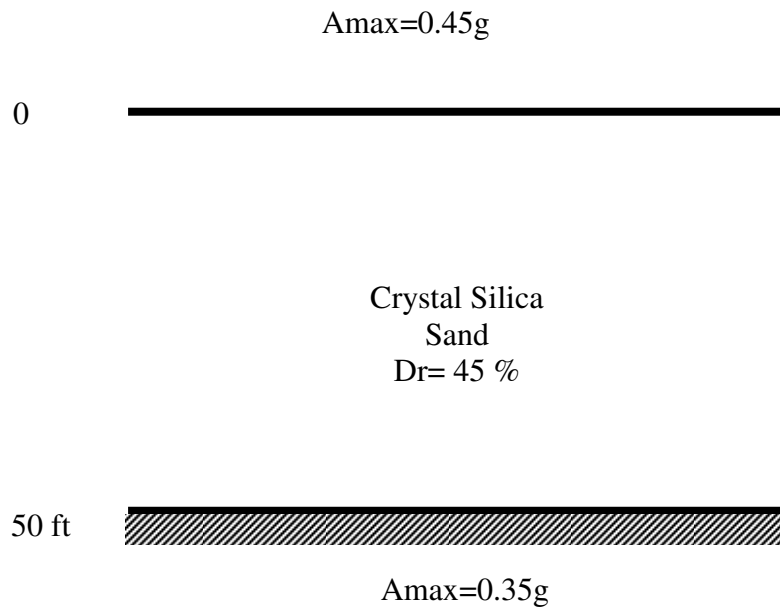


Figure 9-2 Soil profile Analyzed by Tokimatsu and Seed (1987)

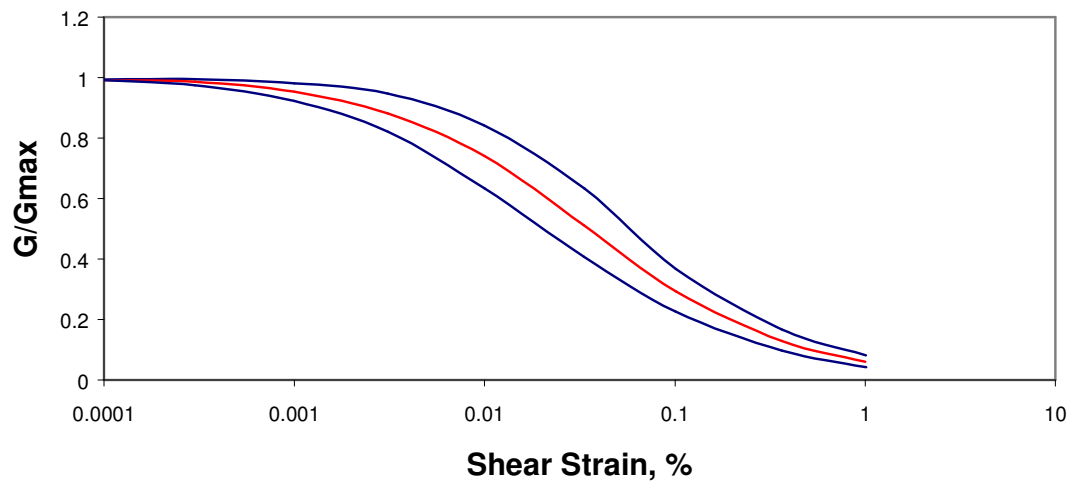


Figure 9-3 Relationship between shear modulus and shear strain for sand (Seed et al.1984)

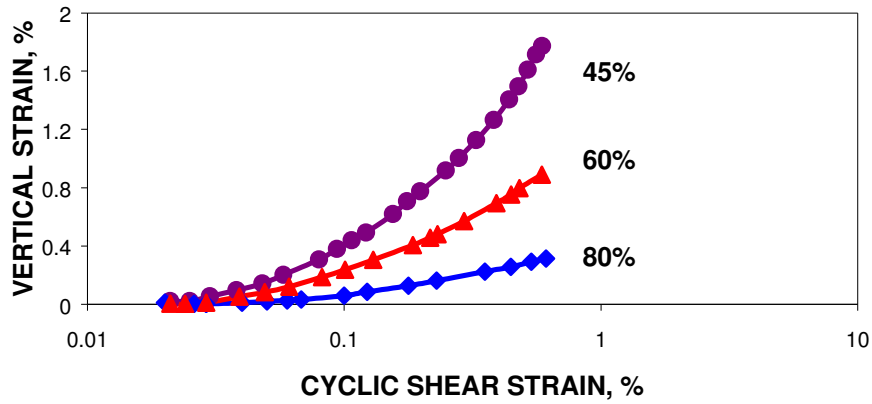


Figure 9-4 Effect of Relative Density on Settlement in 10 Cycles (Silver and Seed 1971)

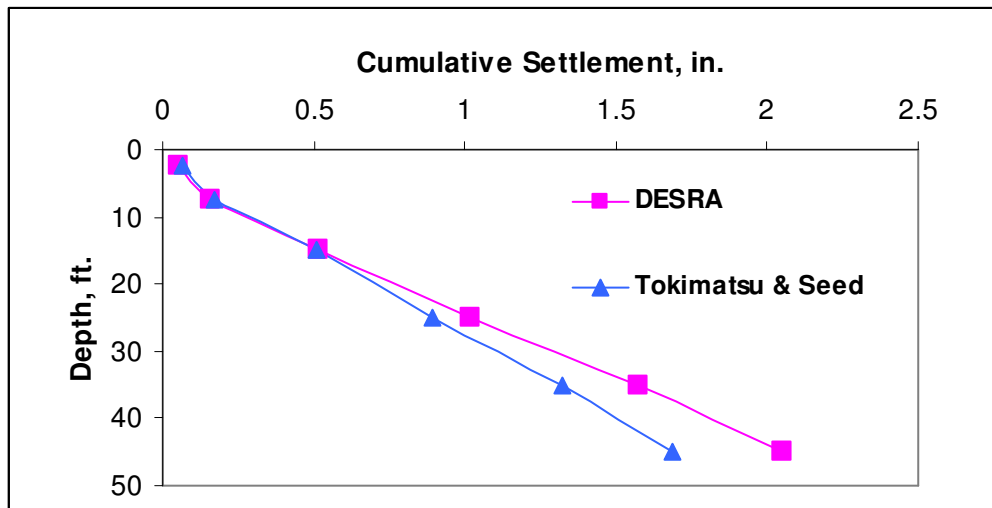


Figure 9-5 Settlement versus depth for relative density ($D_r=45\%$)

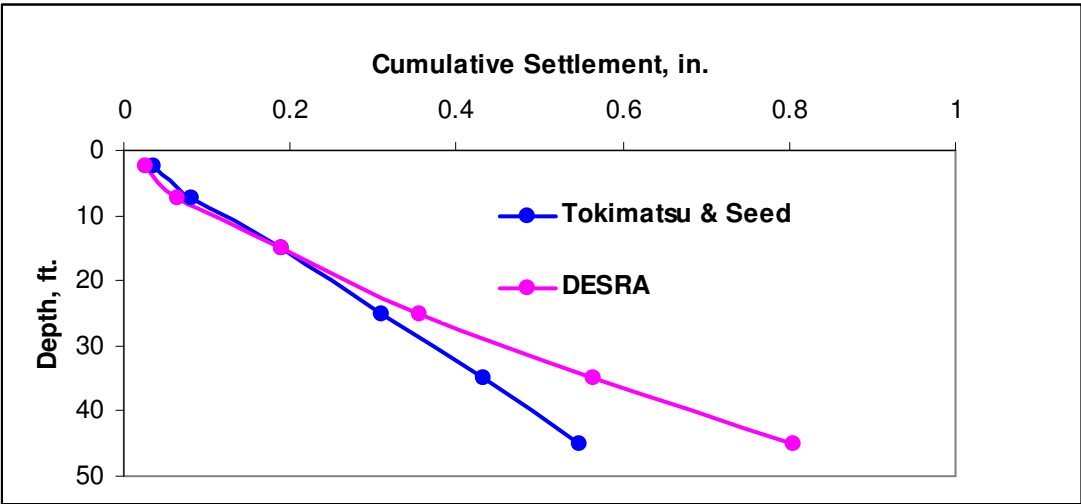


Figure 9-6 Settlement versus depth for relative density (Dr=60%)

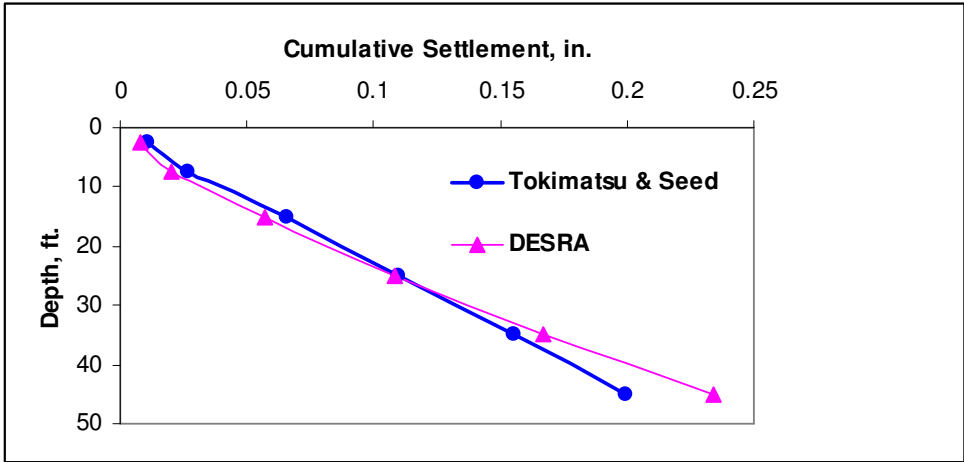


Figure 9-7 Settlement versus depth for relative density (Dr=80%).

9.3 Errors in Tokimatsu and Seed Procedure

9.3.1 Effect of Sand Type or Characteristics

DESRA-MUSC was also used to compute the settlement of the same soil profile analyzed above but with three different sand types and three different ground motion records. The sands used were Silica #1, F-110 and NSF at relative density of 45%. Silica #1 and F-110 are pure quartz and the grains shape is respectively angular-subangular to rounded-subrounded. NSF is a mixture of quartz, plagioclase and volcanic rock fragments.

Figure 9-8 shows their grain size distribution. The ground motion records used were the El Centro (1940), Pacoima San Fernando (1971) and Northridge (1994) earthquakes. The recorded earthquake magnitudes for these three ground motion were respectively 7.1, 6.6 and 6.7. The number of equivalent uniform number of strain cycles for these three ground motion are respectively 12, 10 and 10 cycles. These values are based on the empirical correlation develop by Seed et al (1975) relating earthquakes magnitude and equivalent number of uniform cycles as shown in Figure 9-9 . The three earthquakes ground motions are shown in Figure 9-10.

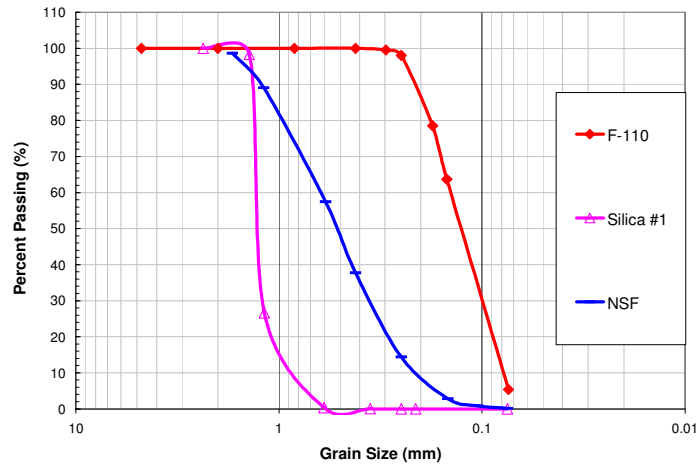


Figure 9-8 Grain size distribution

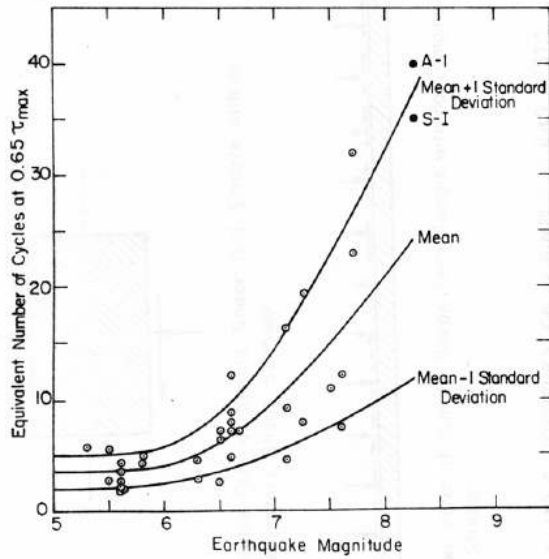


Figure 9-9 Earthquake magnitude versus equivalent number of cycles (Seed et al. 1975)

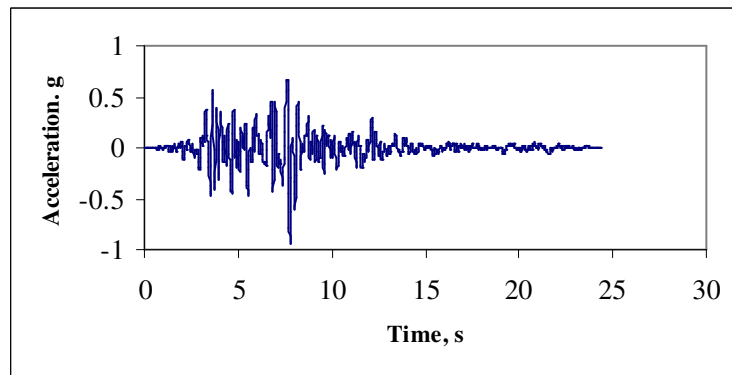
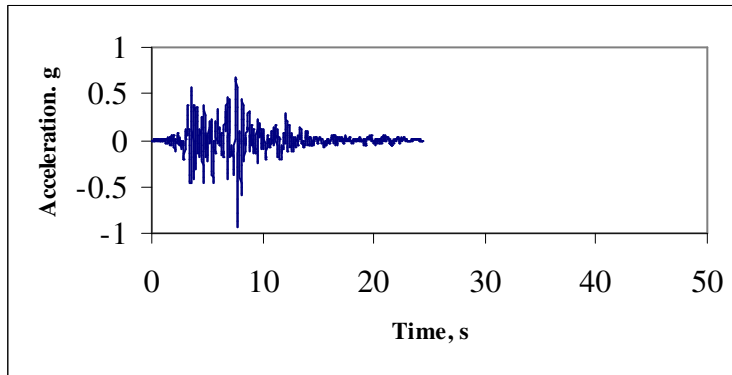
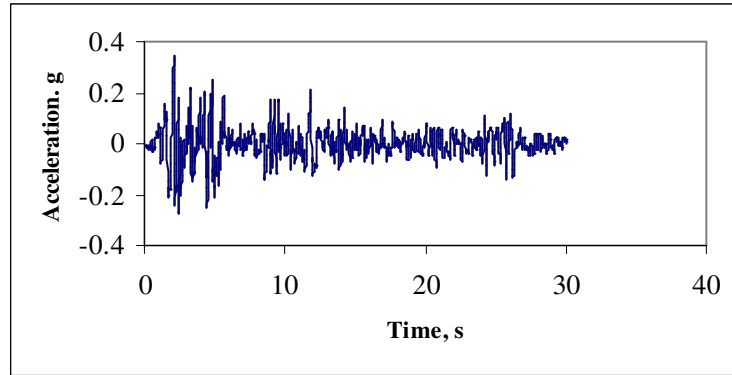


Figure 9-10 Three ground motion used in the parametric studies, El-Centro (top), Pacoima Dam (middle) and Northridge (bottom)

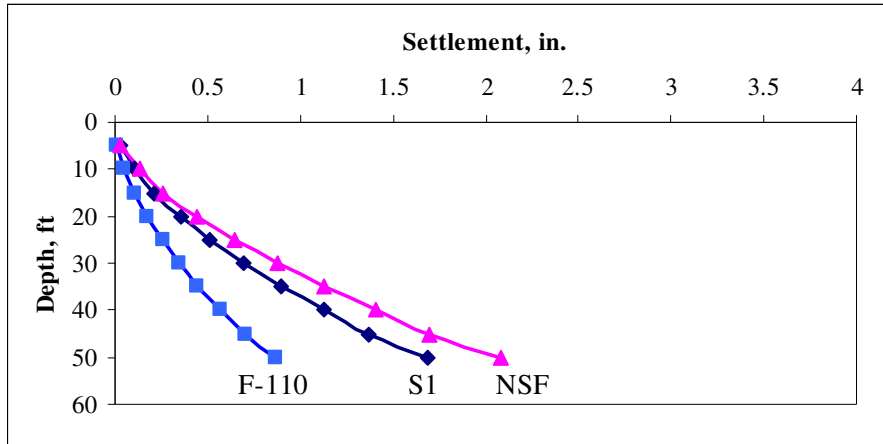


Figure 9-11 Settlement versus depth using El Centro earthquake (Dr=60%)

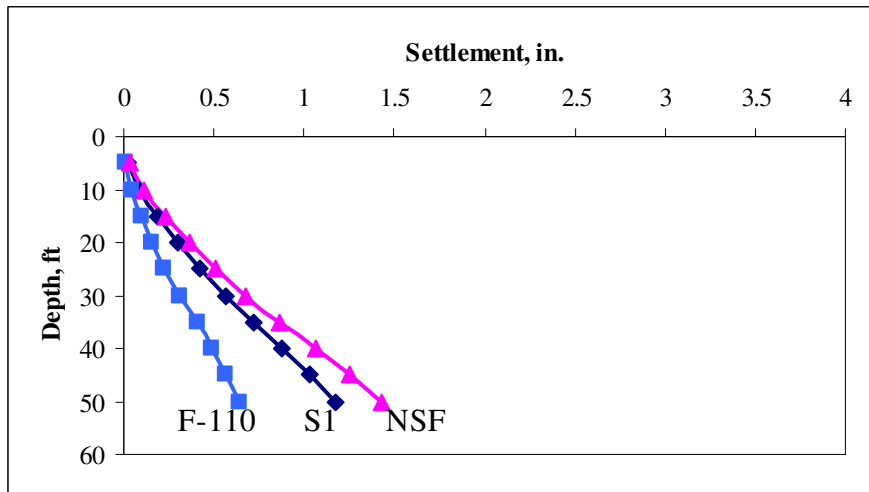


Figure 9-12 Settlement versus depth using San Fernando earthquake (Dr=60%).

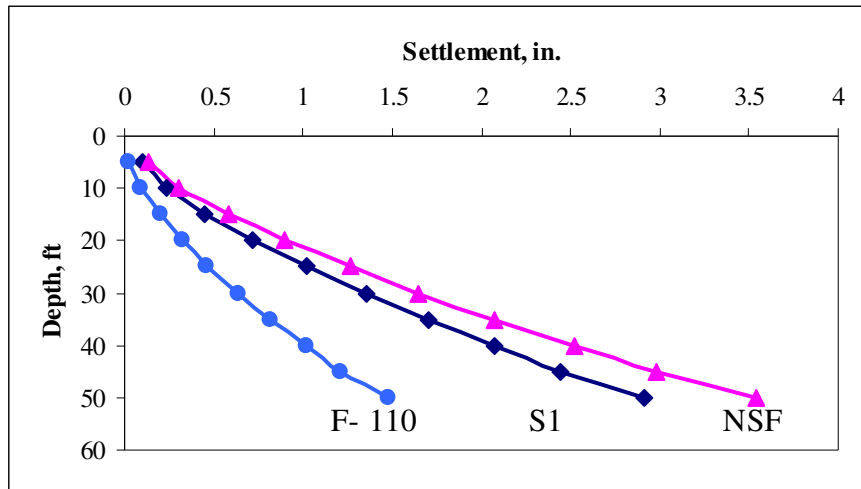


Figure 9-13 Settlement versus depth using Northridge earthquake ($D_r = 60\%$)

The results of the analyses are shown in Figure 9-11 to Figure 9-13, which indicate clearly that the charts developed by Silver and Seed (1971) are not valid for all types of sand. For the sands used in the example, the maximum settlement is about 2.5 times the minimum settlement.

9.3.2 Effect of the Equivalent Number of Cycles Concept

The Tokimatsu and Seed simplified procedure requires the use of equivalent number of shear strain cycles that was developed by Seed et al. (1975) which relate that value to the magnitude of the earthquake. The three earthquake records chosen in this study were El Centro, San Fernando and Northridge earthquakes having a magnitude of 7.1, 6.6 and 6.7 respectively. The resulting equivalent number of cycles would be 12, 10 and 10 respectively.

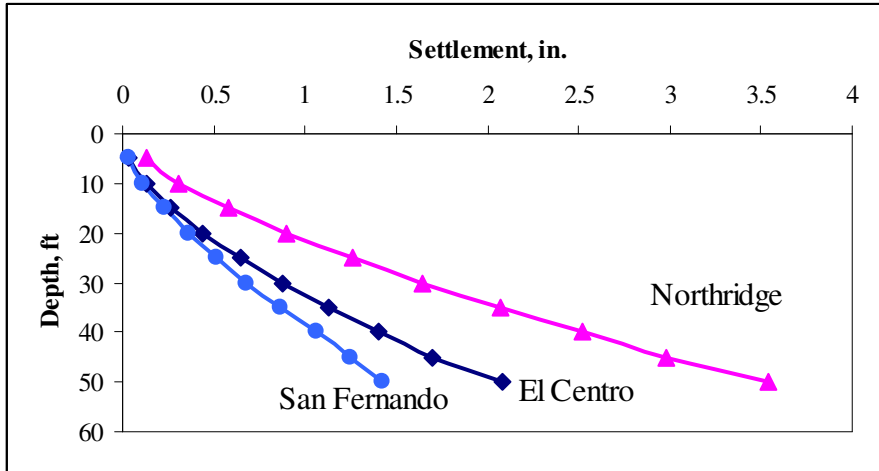


Figure 9-14 Settlement versus depth for NSF sand ($D_r = 60\%$)

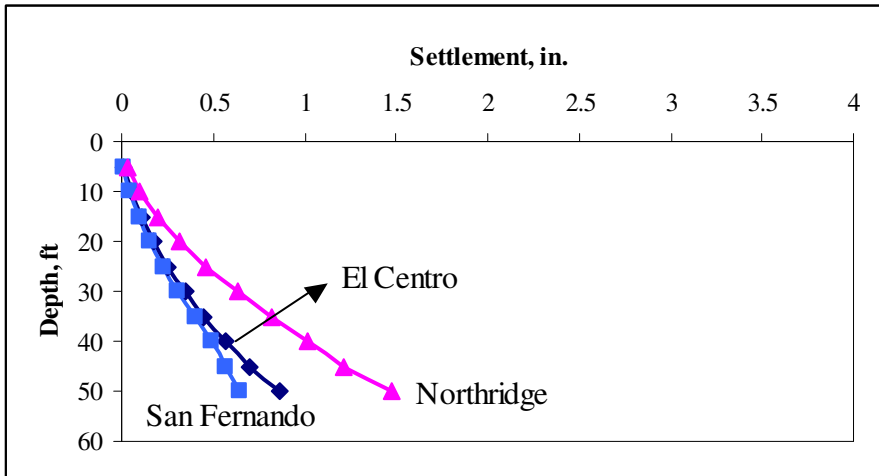


Figure 9-15 Settlement versus depth for F-110 sand ($D_r = 60\%$)

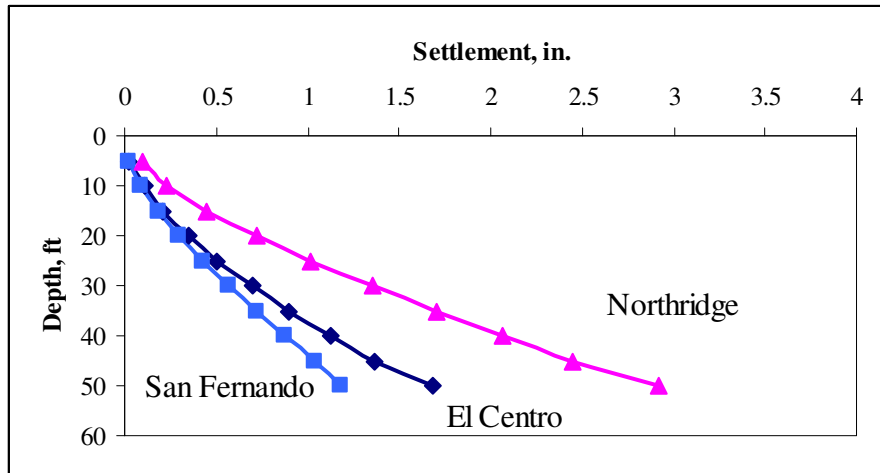


Figure 9-16 Settlement versus depth for S1 sand ($D_r=60\%$)

The results of the analyses shown in Figure 9-14 to Figure 9-16, indicates that the response predicted by using the Northridge earthquake is 3 times larger than the response predicted by using the San Fernando earthquake despite the fact that these two earthquakes have the same magnitude, 6.7 and the same peak acceleration. The Tokimatsu and Seed simplified procedure would have predicted the same response. In summary, the errors that can occur using the concept of equivalent number of cycles may be significant.

9.4 Discussion on Implications for Liquefaction Analysis

9.4.1 Pore-Water Pressure Increase During Undrained Tests

As previously discussed, Martin et al., (1975) presented a detailed study of the volumetric changes in sand subjected to cyclic shear strains and proposed an empirical function to compute the incremental volumetric strain $\Delta\varepsilon_{vd}$ in dry sand as follows:

$$\Delta\varepsilon_{vd} = c_1(\gamma - c_2\varepsilon_{vd}) + \frac{c_3\varepsilon_{vd}^2}{(\gamma + c_4\varepsilon_{vd})}$$

Where c_1 , c_2 , c_3 and c_4 are four constant to be determined from two or three constant strain amplitude cyclic tests. $\Delta\varepsilon_{vd}$, ε_{vd} and γ are respectively the incremental volumetric strain, the accumulated volumetric strain and the shear strain all expressed as percentage.

They also proposed an analytical function to express the incremental pore water pressure in saturated sand under undrained conditions as a function of the incremental volume change under drained conditions, which can be described as follows:

Let us assume that a sample of saturated sand is subjected to one cycle of loading in a drained simple shear test, and let us assume that $\Delta\varepsilon_{vd}$ is the net volumetric strain increment due to slip at grain contacts and corresponding to the decrease in volume occurring during that cycle. For undrained conditions, it is reasonable to assume that slip at grain contacts resulting in volumetric strain increment $\Delta\varepsilon_{vd}$ will also occur. However, the slip deformation must transfer some of the vertical stress carried by the intergranular forces to the more incompressible water. The increase in pore water pressure will result in decrease in vertical effective stress, which result in the release of recoverable volumetric $\Delta\varepsilon_{vr} = \frac{\Delta u}{E_r}$ strain stored by elastic deformation at grain contacts. For

volumetric compatibility, we must have:

Change in volume of voids = net change in volume of sand structure.

$$\frac{\Delta u \cdot n_e}{K_w} = \Delta\varepsilon_{vd} - \frac{\Delta u}{E_r}$$

$$\Delta u = \frac{\Delta \varepsilon_{vd}}{\frac{1}{E_r} + \frac{n_e}{K_w}}$$

Where Δu = residual pore water pressure increment; K_w = bulk modulus of water; n_e = porosity of the sample; E_r = tangent modulus of the one-dimensional unloading curve at a point corresponding to the initial vertical effective stress.

For saturated samples and assuming incompressible water, the equation becomes:

$$\Delta u = E_r \Delta \varepsilon_{vd}$$

Where the unloading modulus was fitted to a function of the form:

$$E_r = \frac{(\sigma'_v)^{1-m}}{mk(\sigma'_{vo})^{n-m}}$$

Where E_r is the unloading modulus of 1-D unloading curve at a point corresponding to the initial vertical effective stress and m, n, k are three controlling parameters.

9.4.2 Liquefaction Resistance of Sands

As the liquefaction characteristics of sand are relatively insensitive to sand types (grading and grain shape characteristics), one could question the observed sensitivity of volume change to sand type. Based on above discussion, one could expect that sands at a given relative density but having different volume change characteristics would have different liquefaction strengths. However, if the unloading modulus in the equation $\Delta u = E_r \Delta \varepsilon_{vd}$ may adversary such as when linked with the associated volume changes to establish liquefaction behavior, the two effects tend to compensate leading to insensitivity to pore pressure increases. This reflect the importance of establishing a fundamental understanding of volume change behavior as a prerequisite of developing robust

constitutive models for the undrained cyclic behavior of sand. This is examined in the following discussion.

9.4.3 Settlement and Liquefaction of Four Types of Sands

In order to evaluate the above disussion, four sands of different settlement characteristics were chosen. They were Nevada sand, F110, Silica #20 and Monterey sand. Their settlements characteristics are presented in Figure 9-18. The unloading curve for each sand was computed in 1-d consolidation tests as shown in Figure 9-17 for Nevada sand. The unloading curves for all four sands are presented in Figure 9-18. While the settlement behavior of these sands vary from 0.1% to 0.4 % at 25 consecutive cycles and at shear strain of 0.1 %, their corresponding liquefaction strength curves computed using the procedure described in Martin et al., 1975 tare somewhat similar as shown in Figure 9-20.

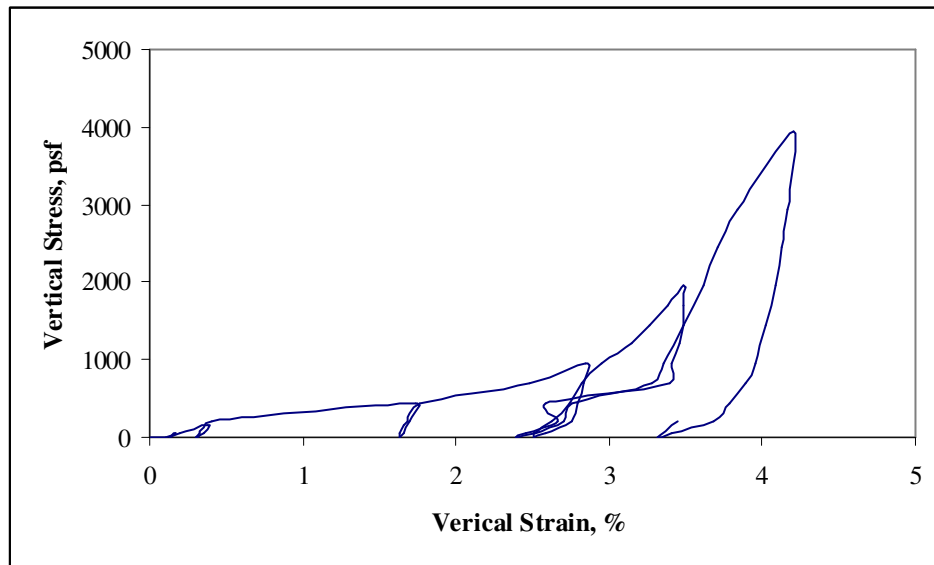


Figure 9-17 Experimental Loading-Unloading Curve for Nevada Sand

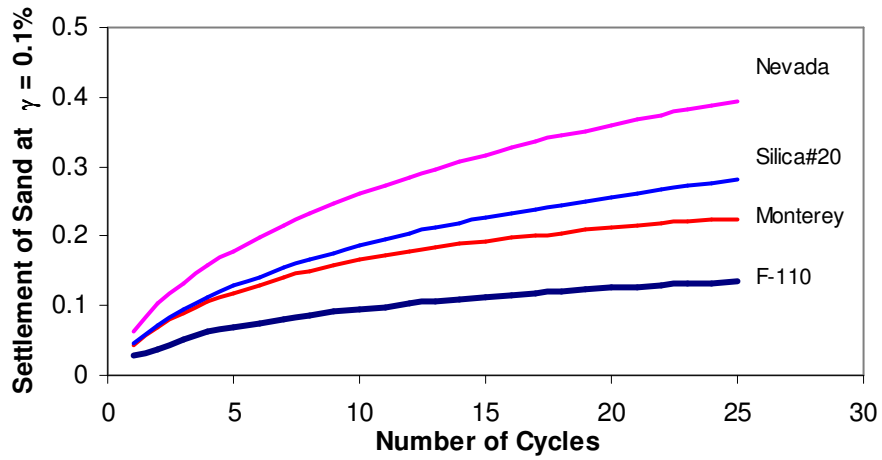


Figure 9-18 Settlement of Four Types of Sands

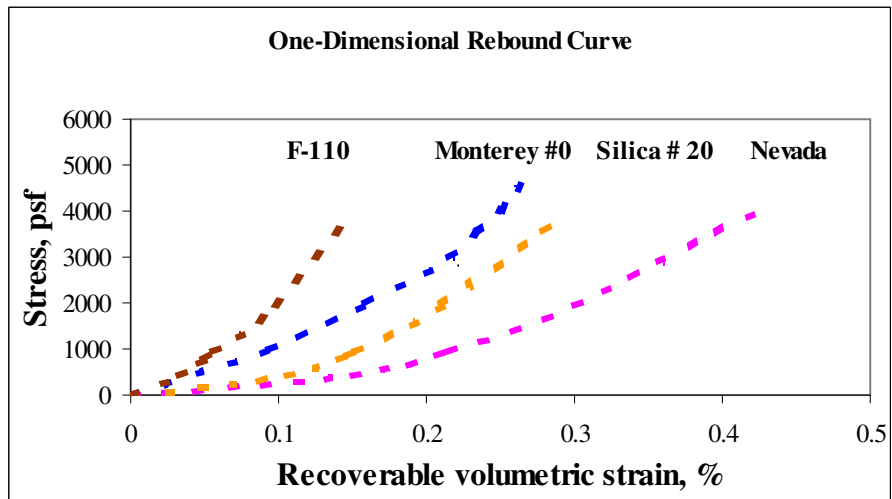


Figure 9-19 One- Dimensional Unloading Curves for Four Types of Sands

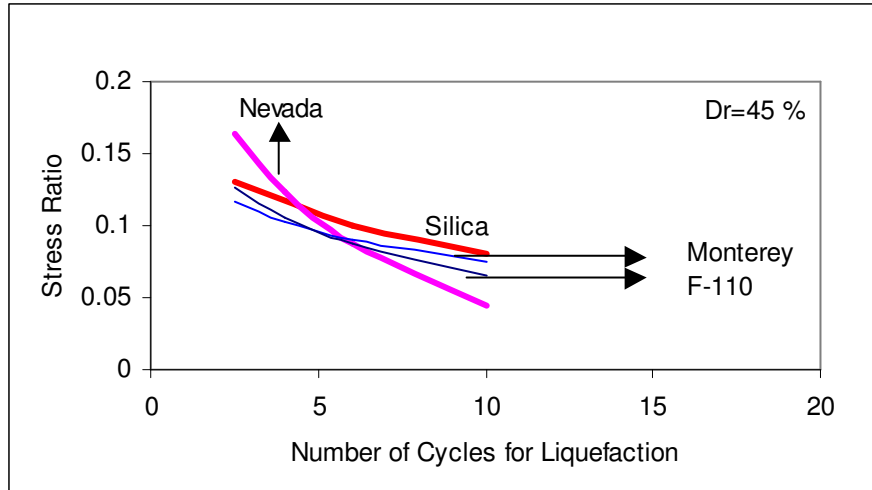


Figure 9-20 Computed Results for Number of Cycles causing Liquefaction for Four Types of Sands

9.5 Recommendations for a Settlement Design Approach

Both DESRA and DESRA-MUSC can be used to compute the settlement of a cohesionless soil deposit using a real earthquake time history. However, based on the finding of this study, the volume change characteristics can be determined from the parameters e , (the void ratio of sand in each layer) and e_{min} , (the minimum void ratio for that sand), as discussed below.

9.5.1 Design Approach Using DESRA or DESRA-MUSC With Time History Input

The design approach can be summarized as follow:

- Obtain normalized standard penetration test values $(N_1)_{60}$ for each layer of the soil deposit

- Use $(N_1)_{60}$ to compute D_r using the empirical equation proposed by Byrne (1991):

$$D_r = 15 (N_1)_{60}^{1/2}$$
- Obtain a soil sample for each layer and determine e_{\min} and e_{\max} from standard laboratory tests.
- Compute e from the equation : $D_r = \frac{e_{\max} - e}{e_{\max} - e_{\min}} \cdot 100$
- Use the factor $\alpha = \frac{(e - e_{\min})_{Field}}{(e - e_{\min})_{CrystalSilica}}$ to evaluate the volume change parameters to

be used in DESRA.

$$C1 = C'1 * \alpha$$

$$C2 = C'2 / \alpha$$

$$C3 = C'3 / \alpha$$

Where $C'1$, $C'2$ and $C'3$ are the volume change constant for Crystal Silica Sand as documented in paragraph 3.4.

Other nonlinear site response programs could also be adopted for analyses by adopting the DESRA volume change constitutive model, and the use of the $(9e - e_{\min})$ parameter. This approach is recommended as it provides a means of properly including time history effects and sand volumetric change characteristics. A modified form of the Tokimatsu and Seed approach could be adopted to at least reflect sand type variations, as described below.

- Use DESRA or DESRA-MUSC with the appropriate time histories and nonlinear backbone curve to compute earthquake induced settlements.

9.5.2 Design Approach Using a Modified Tokimatsu and Seed Procedure

The design approach can be summarized as follow:

- Obtain normalized standard penetration test values $(N_1)_{60}$ for each layer of the soil deposit
- Use $(N_1)_{60}$ to compute D_r using the empirical equation proposed by Byrne (1991):
$$D_r = 15 (N_1)_{60}^{1/2}$$
- Obtain a soil sample for each layer and determine e_{\min} and e_{\max} from standard laboratory tests.

- Compute e for each layer from the equation : $D_r = \frac{e_{\max} - e}{e_{\max} - e_{\min}} .100$

- Use Tokimatsu and Seed simplified procedure to compute the settlement of the soil deposit using the same relative density variations as the field sample.
- Apply a factor α to the settlement value obtained for each layer with

Tokimatsu and Seed procedure, where $\alpha = \frac{(e - e_{\min})_{Field}}{(e - e_{\min})_{CrystalSilica}}$.

e_{\max} and e_{\min} for Crystal Silica sand are presented in Table 4-2.

CHAPTER 10

SUMMARY AND CONCLUSIONS

Settlement of unsaturated cohesionless soil deposit has been recognized as a major cause of seismically induced damage (e.g, Stewart et al.2001, Wartman et al.2003). As a result, there has been an increasing demand within the engineering profession for seismic settlement analysis procedures as evidenced by the California Geological Survey's (CGS) recent requirement that analysis of seismic settlement be included as part of the design process for critical projects such as schools and hospital structures (CGS. 2004). Among the most widely used existing methods for estimating settlement of cohesionless soil deposits is the Tokimatsu and Seed, 1987 procedure. However, this procedure based on cyclic laboratory test data for only one clean sand as documented by Silver and Seed, 1971, and incorporated simplifying assumption on the effect of earthquake time history input. Consequently, This analysis procedure has a number of uncertainties as to its accuracy.

10.1 The objective of Research

The principal objective of this study was to perform additional cyclic tests on a variety of sand types and also to compile other available laboratory cyclic simple shear testing data to provide insight into the settlement of sands of varying characteristics, and to develop a volumetric strain material model encompassing variability in soil characteristics.

All cyclic simple shear tests were performed under drained conditions to evaluate the vertical strain accumulation under varying cyclic strain amplitudes. Tests were performed by the author also to evaluate the effect of overconsolidation ratio on

settlement. The results of a total of 18 different clean sands and 8 silty sands were used for this study. The sands were selected to span a range of material gradation, particle size and particle shape. Specimens were prepared to varying levels of relative density ($D_r = 45, 60, 80 \%$). The database include the following:

- The original Silver tests by Silver and Seed (1971)
- Pyke (1975) and Martin (1975)
- Ottawa Sand tested by Bhatia (1980)
- Fourteen clean sands tested by Stewart et. al (2004)
- Eight silty sands tested by Stewart et. al(2004)
- Two sands, Nevada and Silica #30, tested by the author.

A further objective of the study was to develop an improved design method including the effect of variation in time history. For this purpose, the computer program DESRA-MUSC (Qui, 19) is recommended together with the constitutive model for volume change by Martin (1975). This study demonstrate that the required volume change parameters could be obtained using the $(e - e_{min})$ parameter, hence avoiding the need for laboratory testing on samples.

10.2 Research Findings and Recommendations

The laboratory test results provide significant new insights into factors that affect settlement of sand subjected to cyclic loading. These include:

- 1) Significant sand-to-sand variability of vertical strains (up to a factor of three) was observed for all clean sands prepared to a similar relative density for a common set of loading conditions.

- 2) For clean sands, no statistically significant trends in the variation of vertical strains with soil compositional parameters such as Coefficient of Uniformity ($CU = D_{60}/D_{10}$), median particle size (D_{50}) and particle shape were observed.
- 3) For all sands, including sands with fines, there was a significant trend relating the settlement and value of the parameter ($e - e_{min}$), where e is the void ratio and e_{min} is the minimum void ratio. Tests results show that settlements increase as the ($e - e_{min}$) increases. The parameter ($e - e_{min}$) reflects the combined effect of particle size and gradation.
- 4) The result of the study shows that settlement can be expressed in a linear function in term of ($e - e_{min}$) as follow: Settlement = 1.216 ($e - e_{min}$).
- 5) Vertical strains were also found to decrease with increasing secant shear modulus, sometimes by a factor of three for a similar set of baseline conditions. The dependence of vertical strain on shear modulus is likely associated with the same compositional factors that decrease seismic settlement susceptibility.
- 6) For non-plastic silty sands, the effect of increasing FC was observed to increase the settlement susceptibility when using constant RC (relative compaction) as a basis for comparison.
- 7) The effect of overconsolidation ratio was significant for sand at low relative density. With increasing overconsolidation ratio, a decrease in settlement was observed.
- 8) This study confirm that liquefaction characteristics of sand are relatively insensitive to sand types (grading and grain shape characteristics), and that the

observed sensitivity of volume change to sand type and be explained by the change of the unloading modulus in the equation $\Delta u = E_r \Delta \varepsilon_{vd}$.

- 9) A new design method using DESRA-MUSC and a modified Tokimatsu and Seed (1987) method were presented.

10.3 Recommendations for Future Research

The studies summarized in this report have identified a number of aspects of settlement of sand that warrant additional research. These include:

- Continued experimental database to further validate the conclusion on effect of particle shape and gradation
- Development of design examples using DESRA and recommendations to obtain volume change constants for all relative density.
- A study of the potential effect of the modulus hardening parameter on analyses.

REFERENCES

- American Society for Testing and Materials, ASTM (1994). Standard Test Method for Measurement of Soil Potential (Suction) Using Filter Paper, ASTM D5298, ASTM International, West Conshohocken, Pa.
- American Society for Testing and Materials, ASTM (1999). Standard Test Method for Dispersive Characteristics of Clay Soil by Double Hydrometer, ASTM D4221, ASTM International, West Conshohocken, Pa.
- American Society for Testing and Materials, ASTM (2000). Standard Classification of Soils for Engineering Purposes (Unified Soil Classification System), ASTM D2487, ASTM International, West Conshohocken, Pa.
- American Society for Testing and Materials, ASTM (2000). Standard Test Methods for Maximum Index Density and Unit Weight of Soils Using a Vibratory Table, ASTM D4253, ASTM International, West Conshohocken, Pa.
- American Society for Testing and Materials, ASTM (2000). Standard Test Methods for Minimum Index Density and Unit Weight of Soils and Calculation of Relative Density, ASTM D4254, ASTM International, West Conshohocken, Pa.
- American Society for Testing and Materials, ASTM (2000). Standard Test Methods for Liquid Limit, Plastic Limit, and Plasticity Index of Soils, ASTM D4318, ASTM International, West Conshohocken, Pa.
- American Society for Testing and Materials, ASTM (2002). Standard test methods for laboratory compaction characteristics of soil using modified effort, ASTM D1557, ASTM International, West Conshohocken, Pa.
- Ang, A.H. and Tang, W.H. (1975). Probability concepts in engineering planning and design, John Wiley and Sons, Vol. 1.
- Bhatia S.(1980), "The verification of relationships for effective stress method to evaluate liquefaction potential of saturated sands" Dissertation, the university of British Columbia.
- Boulanger, R. W., Chan, C. K., Seed, H. B., and Sousa, J. (1993). "A low-compliance bidirectional cyclic simple shear apparatus," Geotech. Testing J., ASTM, 16 (1). 36-45.
- Brandon, T.L., Duncan, J.M., and Gardner, W.S. (1990). "Hydrocompression settlement of deep fills," J. Geotech. Engrg., ASCE, 116(10), 1536-1548.
- Bragg W.L., 1913, The Diffraction of Short Electromagnetic Waves by a Crystal, Proc. Cambridge Phil. Soc., 17, 43-57. For details, see P. P. Ewald, 1962, IUCr

Byrne P., "A Cyclic Shear-Volume Coupling and pore Pressure Model for sand" Proceeding: Second International Conference on Recent Advances in Geotechnical Earthquake Engineering and Soil Dynamics, March 11-15, 1991, St. Louis, Missouri, Paper No. 1.24

Bray, J.D., Sancio, R.B., Riemer, M.F. and Durgunoglu, T. (2004). "Liquefaction susceptibility of fine-grained soils," Proc. 11th International Conf. on Soil Dynamics and Earthquake Engineering and 3rd International Conf. on Earthquake Geotechnical Engineering, Berkeley, CA, Jan. 7-9, Vol. 1, 655-662.98

California Geological Survey, CGS (2004). "Engineering geology and seismology for public schools and hospitals in California," Report to Accompany California Geological Survey Note 48 Checklist, Robert H. Sydnor (ed.).

Casagrande, A. (1932). "The Structure of clay and its importance in foundation engineering," Contributions to Soil Mechanics, Boston Society of Civil Engineers, Boston, 72-112.

Chang S. W., Bray, J. D., and Seed, R. B. (1996). "Engineering implications of ground motions from the Northridge Earthquake," Bull. Seism. Soc. Am., 86 (1B), S270-S288.

Chu, H.-H. and Vucetic, M. (1992). "Settlement of compacted clay in a cyclic direct simple shear device," Geotech. Testing J., 15(4), 371-379.

Darendeli M. B. and Stokoe, K. H. (2001). "Development of a new family of normalized modulus reduction and material damping curves," Geotechnical Engineering Report GD01-1, University of Texas, Department of Civil Engineering.

Dobry, R.M. and Ladd, R.S. (1980). Discussion to "Soil liquefaction and cyclic mobility evaluation for level ground during earthquakes," by H.B. Seed and "Liquefaction potential: science versus practice," by R.B. Peck, J. Geotech. Engrg., ASCE, 106 (6), 720-724.

Duncan J. M., Williams G. W., Sehn A. L., and Seed R. B. (1991). "Estimation of earth pressure due to compaction," J. Geotech. Engrg., ASCE, 117 (12), 1833 – 1847.

Grant, R., Christian, J.T., and Vanmarcke, E.H. (1974). "Differential settlement in buildings," J. Geotech. Engrg., ASCE, 100 (9), 973-991.

Gye-Chun Cho, Jake Dodds and J.C. Santamarina. "Particle Shape Effects on Packing Density, Stiffness, and Strength: Natural and Crushed Sands" J. Geotech. and Geoenviron. Engrg., Volume 132, Issue 5, pp. 591-602 (May 2006)

Houston, S.L., Houston, W.N., and Spadola, D.J. (1988). "Prediction of field collapse of soils due to wetting," *J. Geotech. Engrg., ASCE*, 114 (1), 40-58.

Hsu, C.C. (2002). "Dynamic and cyclic behavior of soils over the wide range of shear strains in NGI-type simple shear testing devices" Dissertation, UCLA.

Hsu, C.C. and Vucetic, M. (2004). "Volumetric threshold shear strain for cyclic settlement," *J. Geotech. & Geoenv. Engrg., ASCE*, 130 (1), 58-70.

Ishihara, K., and Koseki, J., (1989). "Discussion on the cyclic shear strength of fines-containing sands," *Proc. of the Eleventh Inter. Conf. on Soil Mechanics and Foundation Engrg., Rio de Janeiro, Brazil*, 101-106.

Iwasaki, I., Tatsuoka, F., and Takagi, Y. (1978). "Shear modulus of sands under cyclic torsional shear loading," *Soils and Foundations*, 18 (1), 39-50.

Kokusho, T., Hara, T., and Hiraoka, R. (2004). "Undrained shear strength of granular soils with different particle gradations," *J. Geotech. & Geoenv. Engrg., ASCE*, 130 (6), 621-629.

Kuerbis, R. H., Negussey, D. and Vaid, Y. P. (1988). "Effect of gradation and fines content on the undrained response of sand," in *Hydraulic Fill Structures*, ASCE Geotechnical Special Publication No. 21, Dirk Van Zyl (ed.), 330 – 345.99

Lade PV (1998). "Effect of non-plastic fines on minimum and maximum void ratios of sand." *Geotechnical Testing Journal*, Vol. 4, Issue 21

Ladd, R.S. (1974). "Specimen preparation and liquefaction of sands," *J. Geotech. Engrg., ASCE*, 100 (10), 1180-1184. Lawson, A.C., ed. (1908). "Minor geologic effects of the earthquake," *California earthquake of April 18, 1906*, Publ. 87, Vol. 1, Part 2, Carnegie Institute of Washington, D.C., 384-409.

Laue M. (1912). *Eine quantitative Prüfung der Theorie für die Interferenz-Erscheinungen bei Röntgenstrahlen*. *Sitzungsberichte der Kgl. Bayer. Akad. der Wiss* 363--373, reprinted in *Ann. Phys.* (1913), 41, 989-1002 where he interpreted and indexed the first diffraction diagram (Friedrich, W., Knipping, P., and Laue, M. (1912). *Interferenz-Erscheinungen bei Röntgenstrahlen*, *Sitzungsberichte der Kgl. Bayer. Akad. der Wiss*, 303--322, reprinted in *Ann. Phys.*, (1913), 41, 971-988, taken with zinc-blende, ZnS

Lawton, E., Fragaszy, R.J., and Hardcastle, J.H. (1989). "Collapse of compacted clayey sand" *J. Geotech. Engrg., ASCE*, 115 (9), 1252-1266.

Lee, K.L., and Fitton, J.A., (1968). "Factors affecting the cyclic loading strength of soil," *Vibration Effects of Earthquakes on Soils and Foundations*, ASCE STP 450, 71-95.

Liu A. H., Stewart J. P., Abrahamson N. A. and Moriwaki, Y. (2001) "Equivalent number of uniform stress cycles for soil liquefaction analysis," J. Geotech. & Geoenv. Engrg., ASCE, 127(12), 1017-1026.

Lee K.W., and Finn W.D.L., "DESRA – 2, Dynamic Effective Stress Response Analysis of Soil Deposits with Energy Transmitting Boundary Including Assessment of Liquefaction Potential". University of British Columbia, June 1978

Martin, G.R., W.D.L.Finn and H.B.Seed (1974)," Fundamentals of Liquefaction Under Cyclic Loading," Journal of Geotechnical Division, ASCE, Vol.101, No. GT5, pp. 423-438.

McClure, F.E. (1973). Performance of single family dwellings in the San Fernando earthquake of February 9, 1971. NOAA, U.S. Dept. of Commerce, May.

Mulilis, P.J., Seed, H.B., Chan, C., Mitchell, J.K., and Arulanandan, K. (1977). "Effect of sample preparation on sand liquefaction," J. Geotech. Engrg., ASCE, 103 (2), 91-109.

Polito, C.P. (1999) "The effects of non plastic and plastic fines on the liquefaction of sandy soils," PhD Thesis. Virginia Polytechnic Institute and State University, Blacksburg, VA.

Polito, C.P., and Martin, J.R. (2001) "Effects of nonplastic fines on the liquefaction resistance of sands," J. Geotech & Geoenv. Engrg., ASCE, 127 (5), 408-415.

Pradel, D. (1998). "Procedure to evaluate earthquake-induced settlements in dry sandy soil," J.Geotech. & Geoenv. Engrg., ASCE, 124 (4), 364-368.

Pyke, R., Seed, H.B., Chan, C.K. (1975). "Settlement of sands under multidirectional shaking," J. Geotech. Engrg., ASCE, 101 (4), 379-398.

Seed, H.B. and Idriss, I.M. (1971). "Simplified procedure for evaluating soil liquefaction potential," J. Soil Mech. & Found. Div., ASCE, 97 (9), 1249-1273.

Seed, H.B. and Silver, M.L. (1972). "Settlement of dry sands during earthquakes," J. Soil Mech.& Found. Div., ASCE, 98 (4), 381-397.

Seed, H.B., Idriss, I.M., Makdisi, F., and Banerjee, N. (1975). "Representation of irregular stress time histories by equivalent uniform stress series in liquefaction analyses," Rpt. No. UCB/EERC-75/29, U.C. Berkeley,100.

Seed, R. B., Cetin, K. O., Moss, R. E. S., Kammerer, A. M., Wu, J., Pestana, J. M., and Riemer, M. F. (2001). "Recent advances in soil liquefaction engineering and seismic site response evaluation," Proc. 4th Int. Conf. on Recent Advances in Geotech. Eqk. Engrg. Soil Dyn., Paper No. SPL-2.

Silver, M.L. and Seed, H.B. (1971). "Volume changes in sands due to cyclic loading," J. SoilMech. & Found. Div., ASCE, 97 (9), 1171-1182.

Stewart, J.P., and Whang, D.H. (2003). "Simplified procedure to estimate ground settlement from seismic compression in compacted soils," Proc. of the 2003 Pacific Conference on Earthquake Engrg., New Zealand Society for Earthquake Engrg., Paper No. 046

Stewart, J.P., Bray, J.D., McMahon, D.J., Smith, P.M., and Kropp, A.L. (2001). "Seismic performance of hillside fills," J. Geotech. & Geoenv. Engrg., ASCE, 127 (11), 905-919.

Stewart, J.P., Smith, P.M., Whang, D.W., and Bray, J.D. (2004). "Seismic compression of two compacted earth fills shaken by the 1994 Northridge earthquake," J. Geotech. & Geoenv. Engrg., ASCE, 130 (5), 461-476.

Thevanayagam, S. (1998). "Effect of fines and confining stress on undrained shear strength of silty sands," J. Geotech. & Geoenv. Engrg., ASCE, 124 (6), 479 – 491.

Tokimatsu, K. and Seed, H.B. (1987). "Evaluation of settlements in sands due to earthquake shaking," J. Geotech. Engrg., ASCE, 113 (8), 861-878.

Troncoso, J. H. (1988). "Evaluation of seismic behavior of hydraulic fill structures," in Hydraulic Fill Structures, ASCE Geotechnical Special Publication No. 21, Dirk Van Zyl (ed.), 475 – 491.

Tsukamoto, Y., Ishihara, K., Sawada, S., and Kanno, T. (2004) "Residual deformation characteristics of partially saturated sandy soils subjected to seismic excitation," Proc. 11th International Conf. on Soil Dynamics and Earthquake Engineering and 3rd International Conf. on Earthquake Geotechnical Engineering, Berkeley, CA, Jan. 7-9, Vol. 1, 694-701.

Vaid, Y.P., Sivathayalan, S., and Stedman, D. (1999). "Influence of specimen reconstitution method on the undrained response of sand," Geotech. Testing J., ASTM, 22 (3), 187-196.

Vucetic, M. (1994). "Cyclic threshold shear strains in soils," J. Geotech. Engrg., ASCE, 120(12), 2208-2228.

Vucetic, M. and Dobry, R. (1991). "Effect of soil plasticity on cyclic response," J. Geotech.Engrg., ASCE, 117 (1), 89-107.

Whang, D. (2001). "Seismic compression of compacted fills," Ph.D. Thesis, University of California, Los Angeles, Civil & Environmental Engineering Department.
101

Whang, D.W., Stewart, J.P., and Bray, J.D. (2004). "Effect of compaction conditions on the seismic compression of compacted fill soils," Geotech. Testing J., ASTM, 27 (4).

Xenaki, V.C., and Athanasopoulos, G.A., (2003). "Liquefaction resistance of sand-silt mixtures: an experimental investigation of the effect of fines," Soil Dynamics and Earthquake Engrg., 23,183-194.

Yasuda, S., Wakamatsu, K., and Nagase, H., (1994). "Liquefaction of artificially filled silty sands," in Ground Failures Under Seismic Conditions, ASCE Geotechnical Special PublicationNo. 44, S. Prakash and P. Dakoulas (eds.), 91 – 104.

Youd, T.L. (1972). "Compaction of sands by repeated shear straining," J. Soil Mech. & Found.Div., ASCE, 98 (7), 709-725.

Zettler, T.E., Frost, J.D., and DeJong, J.T. (2000). "Shear-induced changes in HDPE geomembrane surface topography," Geosynthetics International, 7 (3), 243-267

APPENDICES

APPENDIX A

DATABASE FOR NEVADA SAND

SETTLEMENT (%) VS NUMBER OF CYCLES

Cycles	Dr=40%, OCR=1	Dr=40%, OCR=4	Dr=60%, OCR=1	Dr=60%, OCR=4	Dr=80%, OCR=1	Dr=80%, OCR=4
1	0.1536	0.0614	0.0880	0.0492	0.0239	0.0191
2	0.2469	0.0988	0.1415	0.0790	0.0384	0.0307
3	0.3197	0.1279	0.1832	0.1023	0.0498	0.0398
4	0.3805	0.1522	0.2180	0.1218	0.0592	0.0474
5	0.4333	0.1733	0.2483	0.1387	0.0675	0.0540
6	0.4802	0.1921	0.2751	0.1537	0.0747	0.0598
7	0.5224	0.2090	0.2993	0.1672	0.0813	0.0651
8	0.5608	0.2243	0.3213	0.1795	0.0873	0.0698
9	0.5964	0.2385	0.3417	0.1908	0.0928	0.0743
10	0.6292	0.2517	0.3605	0.2013	0.0979	0.0784
11	0.6597	0.2639	0.3780	0.2111	0.1027	0.0822
12	0.6883	0.2753	0.3944	0.2203	0.1071	0.0857
13	0.7152	0.2861	0.4098	0.2289	0.1113	0.0891
14	0.7405	0.2962	0.4243	0.2370	0.1153	0.0922
15	0.7645	0.3058	0.4380	0.2447	0.1190	0.0952
16	0.7874	0.3150	0.4511	0.2520	0.1226	0.0981
17	0.8091	0.3236	0.4635	0.2589	0.1259	0.1008
18	0.8296	0.3319	0.4753	0.2655	0.1291	0.1033
19	0.8492	0.3397	0.4865	0.2717	0.1322	0.1058
20	0.8680	0.3472	0.4973	0.2778	0.1351	0.1081
21	0.8861	0.3544	0.5077	0.2835	0.1379	0.1103
22	0.9034	0.3613	0.5176	0.2891	0.1406	0.1125
23	0.9199	0.3679	0.5270	0.2944	0.1432	0.1146
24	0.9358	0.3743	0.5361	0.2995	0.1457	0.1165
25	0.9510	0.3804	0.5448	0.3043	0.1480	0.1184

APPENDIX B

DATABASE FOR SILICA #30 SAND

SETTLEMENT (%) VS NUMBER OF CYCLES

Cycles	Dr=40 %, OCR=1	Dr=40 %, OCR=4	Dr=60 %, OCR=1	Dr=60 %, OCR=4	Dr=80 %, OCR=1	Dr=80 %, OCR=4
1	0.08	0.045	0.06	0.04	0.032	0.02758621
2	0.128648649	0.0723375	0.09645	0.0643	0.05144	0.0443616
3	0.166537605	0.09365625	0.124875	0.08325	0.0666	0.05742676
4	0.198222993	0.1114875	0.14865	0.0991	0.07928	0.06835276
5	0.225709705	0.12695625	0.169275	0.11285	0.09028	0.07783093
6	0.250103388	0.14068125	0.187575	0.12505	0.10004	0.08624255
7	0.272093796	0.15305625	0.204075	0.13605	0.10884	0.09382545
8	0.292146735	0.16430625	0.219075	0.14605	0.11684	0.10074025
9	0.310594803	0.1747125	0.23295	0.1553	0.12424	0.10710166
10	0.327685547	0.18433125	0.245775	0.16385	0.13108	0.11299502
11	0.343609229	0.193275	0.2577	0.1718	0.13744	0.11848594
12	0.358515896	0.20165625	0.268875	0.17925	0.1434	0.12362617
13	0.372526392	0.20953125	0.279375	0.18625	0.149	0.12845738
14	0.385739767	0.21695625	0.289275	0.19285	0.15428	0.13301371
15	0.398238422	0.2239875	0.29865	0.1991	0.15928	0.13732359
16	0.410091787	0.23068125	0.307575	0.20505	0.16404	0.14141096
17	0.421359017	0.2370375	0.31605	0.2107	0.16856	0.14529621
18	0.432091003	0.24305625	0.324075	0.21605	0.17284	0.1489969
19	0.442331901	0.24879375	0.331725	0.22115	0.17692	0.15252824
20	0.452120323	0.25430625	0.339075	0.22605	0.18084	0.15590356
21	0.461490259	0.25959375	0.346125	0.23075	0.1846	0.15913457
22	0.470471819	0.26465625	0.352875	0.23525	0.1882	0.16223166
23	0.479091823	0.26949375	0.359325	0.23955	0.19164	0.16520408
24	0.487374284	0.2741625	0.36555	0.2437	0.19496	0.1680601
25	0.495340802	0.27860625	0.371475	0.24765	0.19812	0.17080717

APPENDIX C

DATABASE FOR CLEAN SAND, (QUARTZ, DR= 60%)

SETTLEMENT (%) VS NUMBER OF CYCLES

Cycles	Silica 1	Silica 0	Silica 2	F-110	F-52	Flint-13	Flint-16	Nevada
1	0.05232	0.03274	0.03706	0.02772	0.03646	0.04608	0.03792	0.04
2	0.07672	0.05016	0.05273	0.03876	0.05063	0.0683	0.05887	0.06235
3	0.09593	0.05983	0.06487	0.05138	0.06495	0.08195	0.0762	0.07966
4	0.11258	0.06841	0.07477	0.06224	0.07757	0.09244	0.08855	0.09412
5	0.12486	0.07658	0.0838	0.06871	0.08746	0.1032	0.09762	0.10667
6	0.13773	0.08209	0.09066	0.07528	0.0956	0.11263	0.10744	0.11783
7	0.14814	0.08623	0.09696	0.0805	0.10273	0.12059	0.11656	0.12792
8	0.15622	0.09192	0.10279	0.0864	0.10884	0.12724	0.12331	0.13713
9	0.16213	0.09636	0.10817	0.09078	0.11494	0.13433	0.12843	0.14563
10	0.1707	0.10035	0.11478	0.09476	0.11983	0.14051	0.13474	0.15353
11	0.17665	0.10437	0.11899	0.09889	0.12429	0.14565	0.14064	0.1609
12	0.18256	0.10811	0.12474	0.1029	0.12962	0.14988	0.14574	0.16782
13	0.18804	0.1113	0.12859	0.10688	0.13454	0.15568	0.15134	0.17434
14	0.19059	0.11502	0.13228	0.10974	0.13795	0.15922	0.15693	0.18051
15	0.19892	0.11809	0.13641	0.11249	0.14138	0.16257	0.16027	0.18635
16	0.20223	0.11916	0.13979	0.11623	0.14559	0.16673	0.16484	0.19191
17	0.20775	0.12391	0.14345	0.11911	0.14893	0.17054	0.16939	0.19721
18	0.21319	0.12528	0.14734	0.12117	0.15237	0.17394	0.17275	0.20226
19	0.21629	0.12778	0.15015	0.12407	0.15538	0.17674	0.1779	0.2071
20	0.2213	0.12942	0.1524	0.12559	0.15751	0.17987	0.18157	0.21174
21	0.22652	0.13206	0.15474	0.12764	0.16148	0.18291	0.18523	0.21619
22	0.22861	0.13456	0.15804	0.12968	0.16405	0.18678	0.18699	0.22047
23	0.23171	0.13595	0.16203	0.13189	0.16697	0.18842	0.19006	0.22458
24	0.23575	0.13732	0.16437	0.13269	0.16859	0.18996	0.19418	0.22854
25	0.23953	0.13994	0.16682	0.13504	0.17126	0.1943	0.19697	0.23236

APPENDIX D

DATABASE FOR CLEAN MATERIALS SAND (DR =60%)

SETTLEMENT (%) VS NUMBER OF CYCLES

Cycles	Pacoi 1	Pacoi 3	NSF	Pat	PO	Newhall	NSF
1	0.03114	0.03523	0.0463	0.03119	0.02736	0.04417	0.03307
2	0.05135	0.05221	0.08291	0.04419	0.03826	0.07015	0.05922
3	0.0687	0.06644	0.10985	0.05514	0.04555	0.09277	0.07847
4	0.08148	0.07625	0.13105	0.06412	0.05205	0.11089	0.0936
5	0.09172	0.08519	0.14857	0.06955	0.05735	0.12609	0.10612
6	0.10091	0.09254	0.16342	0.07444	0.0615	0.13894	0.11673
7	0.10966	0.09758	0.17653	0.07962	0.0649	0.15037	0.1261
8	0.11575	0.10221	0.18821	0.08456	0.06887	0.16036	0.13444
9	0.12398	0.10763	0.1983	0.08722	0.0714	0.16791	0.14164
10	0.13024	0.1109	0.20828	0.09071	0.07476	0.17559	0.14877
11	0.13551	0.11734	0.21703	0.09562	0.07622	0.18349	0.15502
12	0.14177	0.12098	0.22541	0.09688	0.0787	0.19137	0.16101
13	0.14676	0.12442	0.23312	0.10027	0.08029	0.19739	0.16652
14	0.14978	0.12772	0.2401	0.10335	0.08394	0.20412	0.1715
15	0.15381	0.13039	0.24669	0.10616	0.0854	0.21008	0.17621
16	0.15859	0.13311	0.2529	0.1081	0.08714	0.21498	0.18064
17	0.16205	0.13568	0.25933	0.11033	0.08868	0.21988	0.18524
18	0.16506	0.13947	0.26533	0.11204	0.09056	0.22428	0.18952
19	0.16814	0.1423	0.27175	0.11427	0.09244	0.22958	0.1941
20	0.17191	0.14364	0.27683	0.11681	0.09316	0.23381	0.19774
21	0.1744	0.14647	0.2822	0.11921	0.09491	0.23745	0.20157
22	0.179	0.14967	0.28728	0.12004	0.0966	0.24079	0.2052
23	0.18094	0.15037	0.29208	0.12057	0.09772	0.24532	0.20863
24	0.18283	0.15309	0.29632	0.12326	0.09886	0.24886	0.21166
25	0.18635	0.15543	0.30066	0.12449	0.10013	0.25192	0.21475

APPENDIX E

DATABASE FOR SEVERAL SAND (DR =40%)

SETTLEMENT (%) VS NUMBER OF CYCLES

Cycles	Nevada	Ottawa	Silica	Monterey
1	0.1536	0.0913	0.088	0.056
2	0.24691	0.15393	0.14146	0.09964
3	0.31968	0.2041	0.18315	0.13567
4	0.38054	0.24669	0.21802	0.16638
5	0.43334	0.28401	0.24827	0.19312
6	0.48019	0.31738	0.27511	0.21675
7	0.52243	0.34764	0.29931	0.23786
8	0.56083	0.37538	0.32131	0.25689
9	0.59635	0.40102	0.34166	0.27416
10	0.62918	0.42487	0.36047	0.28992
11	0.65971	0.44718	0.37796	0.30438
12	0.68832	0.46813	0.39435	0.31769
13	0.7152	0.48789	0.40975	0.32998
14	0.74054	0.50659	0.42427	0.34137
15	0.76454	0.52433	0.43802	0.35195
16	0.78739	0.5412	0.45111	0.36181
17	0.80909	0.55728	0.46354	0.371
18	0.82963	0.57264	0.47531	0.3796
19	0.84922	0.58733	0.48653	0.38764
20	0.86803	0.60142	0.49731	0.39519
21	0.88608	0.61493	0.50765	0.40227
22	0.90336	0.62792	0.51755	0.40894
23	0.91987	0.64042	0.52701	0.4152
24	0.93581	0.65245	0.53614	0.42111
25	0.95098	0.66406	0.54483	0.42668

APPENDIX F

SOILS WITH FINES PARAMETERS

FC(%)	e_{max}	e_{min}	e	e	e_s	e_s	$e-e_{min}$	$e-e_{min}$
0	0.904	0.412	0.549	0.464	0.549	0.464	0.137	0.052
10	0.872	0.352	0.524	0.441	0.693333	0.601111	0.341333	0.249111
20	0.87	0.289	0.467	0.387	0.83375	0.73375	0.54475	0.44475
35	0.92	0.297	0.513	0.43	1.327692	1.2	1.030692	0.903
50	1.271	0.474	0.64	0.55	2.28	2.1	1.806	1.626

NSF

RC=87%

RC=92%

RC=87%

RC=92%

FC(%)	e_{max}	e_{min}	e	e	e_s	e_s	$e-e_{min}$	$e-e_{min}$
0	1.006	0.662	0.774	0.677	0.774	0.677	0.112	0.015
20	0.86	0.405	0.501	0.419	0.87625	0.77375	0.47125	0.36875
30	0.819	0.298	0.478	0.398	1.111429	0.997143	0.813429	0.699143
40	1.177	0.398	0.573	0.488	1.621667	1.48	1.223667	1.082
50	1.442	0.457	0.682	0.591	2.364	2.182	1.907	1.725

Silica

e_s =Intergranular

Void

Ratio

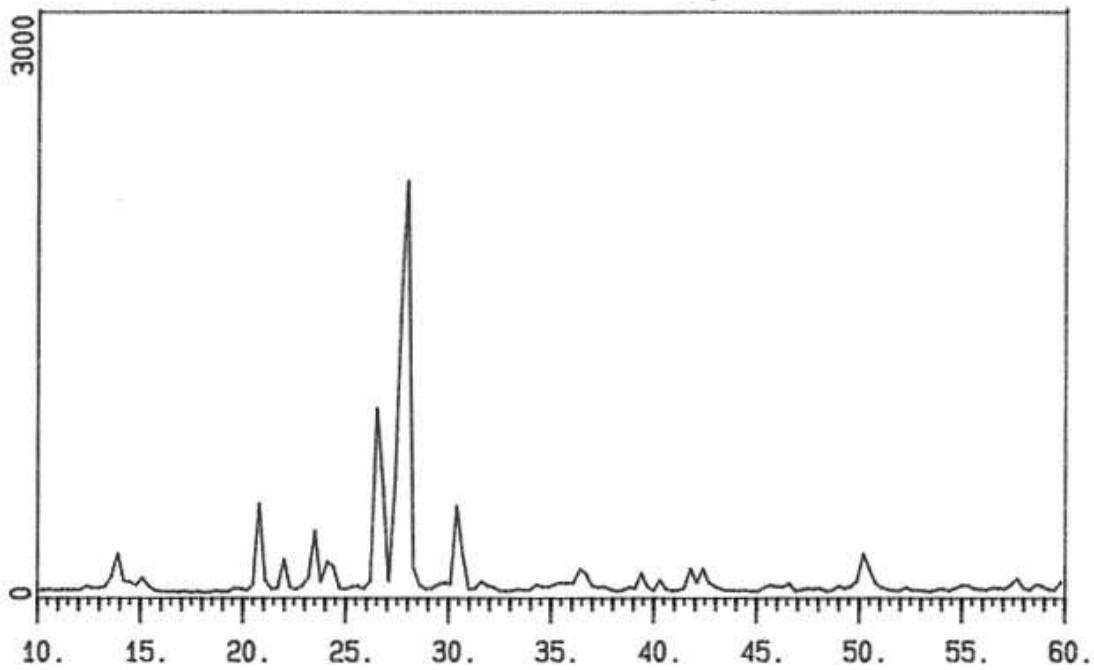
RC = Relative compaction

APPENDIX G

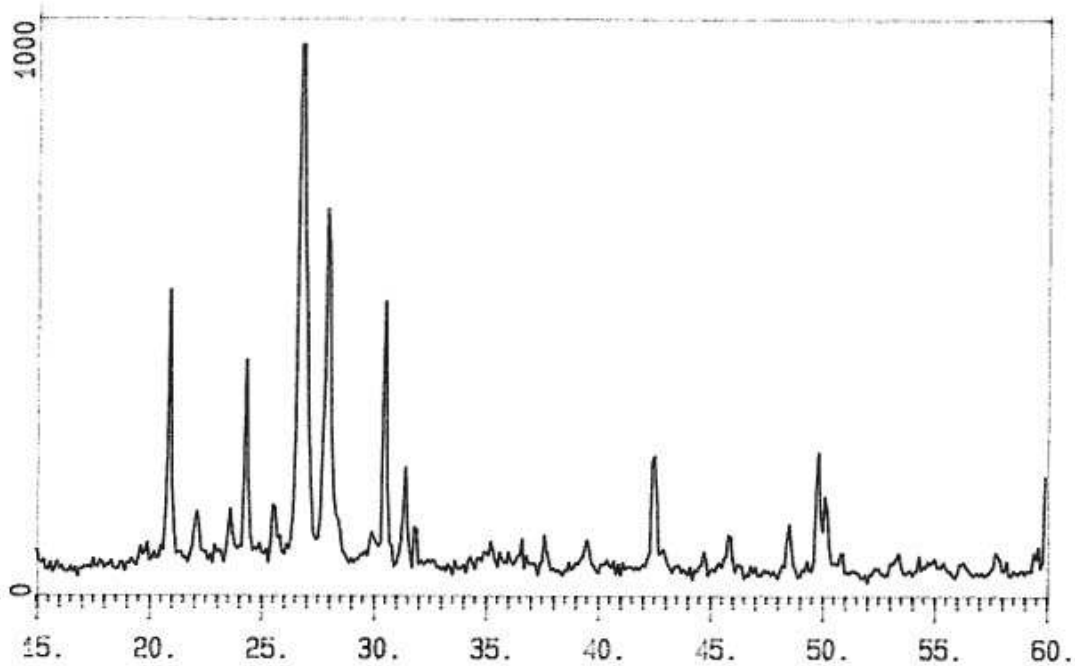
VOLUME CHANGE CONSTANTS

C1	C2	C3	e-e_{min}	Sand
0.45	1.4	1.08	0.131	Silica 1
0.263158	2.394	1.8468	0.123	Silica 0
0.28125	2.24	1.728	0.146	Silica 2
0.221675	2.842	2.1924	0.107	F-110
0.319149	1.974	1.5228	0.125	F-52
0.365854	1.722	1.3284	0.106	Flint 13
0.367647	1.7136	1.32192	0.116	Flint 16
0.266272	2.366	1.8252	0.141	Nevada
0.350195	1.799	1.3878	0.141	Pacoi 1
0.292018	2.1574	1.66428	0.139	Pacoi 3
0.565327	1.1144	0.85968	0.134	NSF
0.233888	2.6936	2.07792	0.106	Pat
0.188127	3.3488	2.58336	0.103	PO
0.473684	1.33	1.026	0.160	Newhall

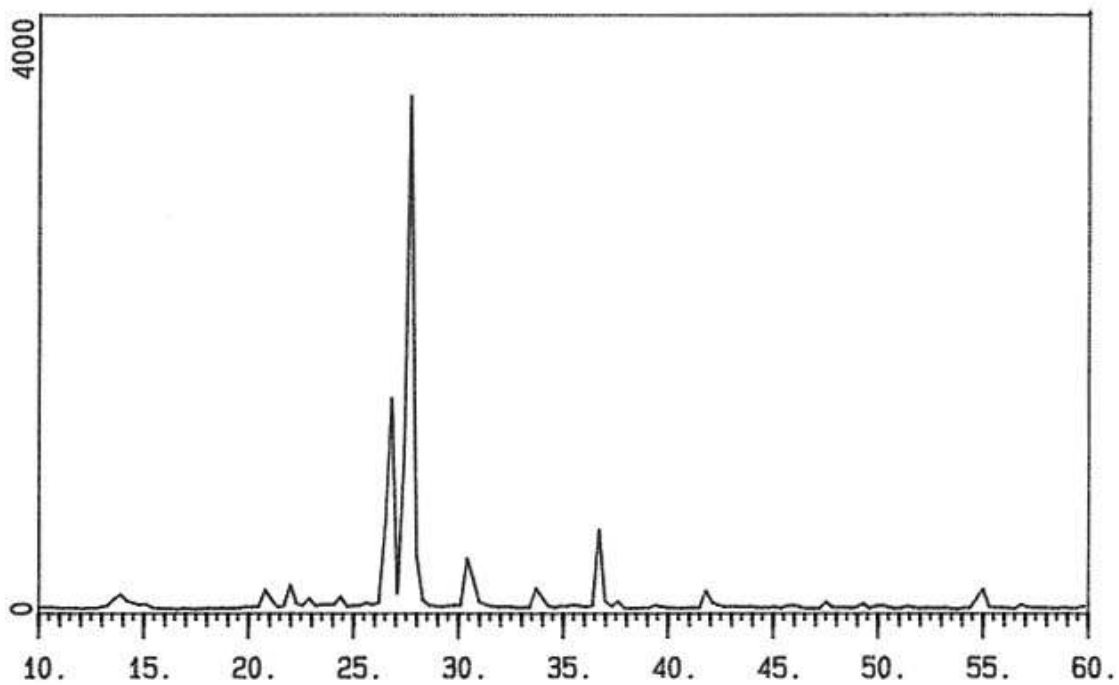
APPENDIX H
X-RAY DIFFRACTION RESULTS



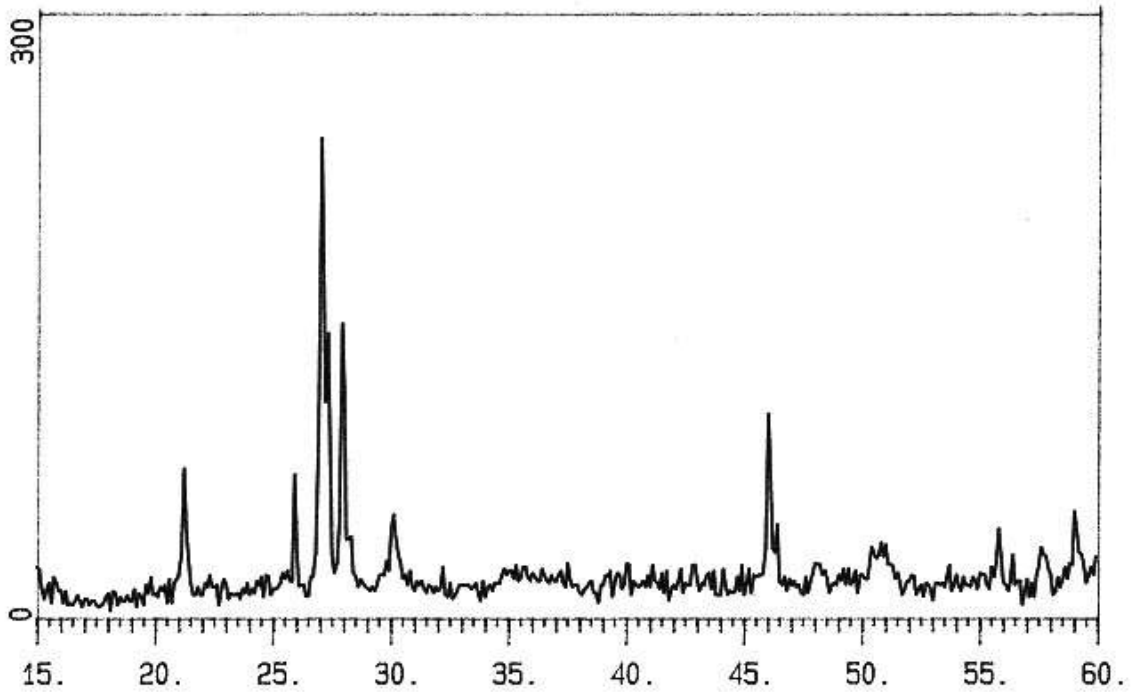
Post Office



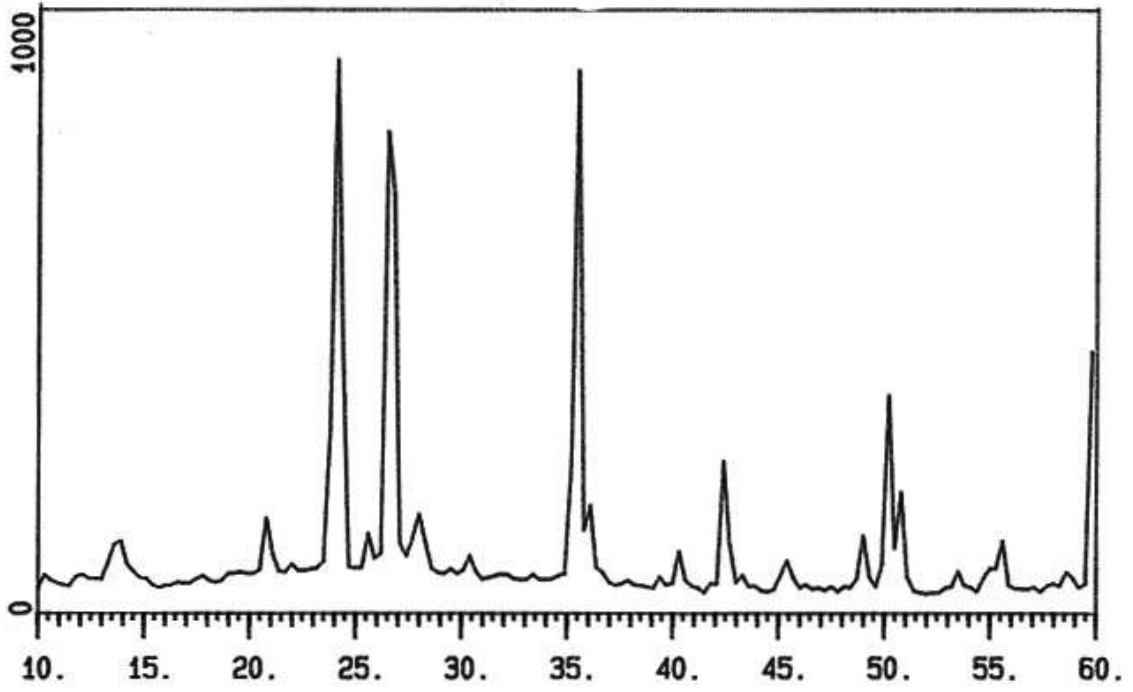
Newhall



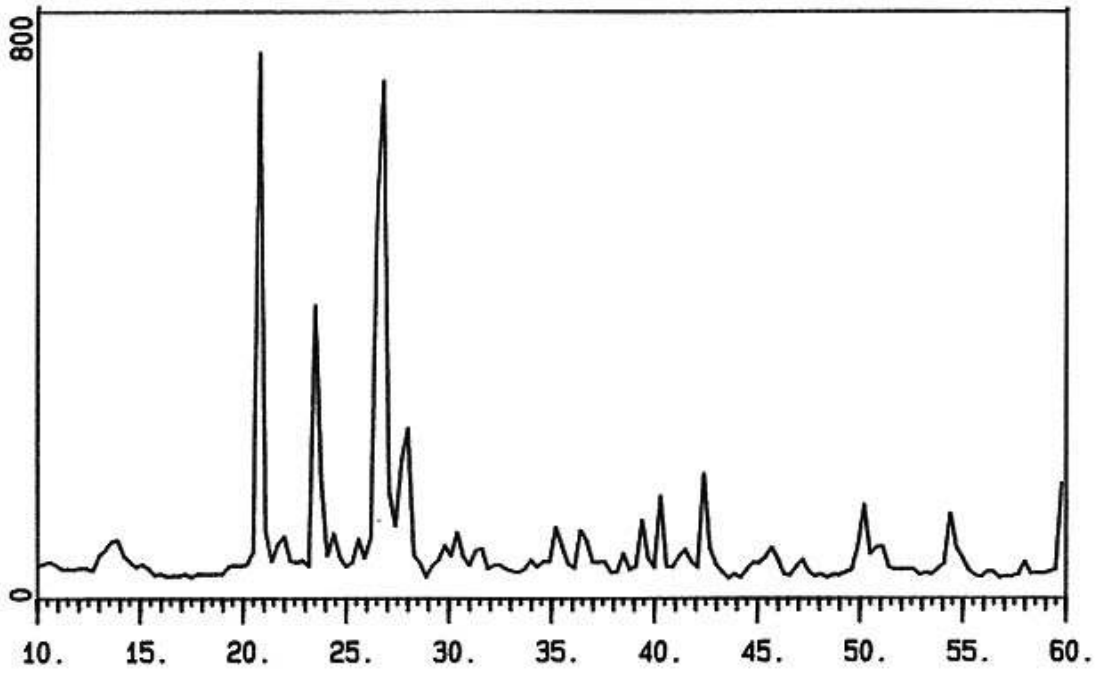
Pacoima 3



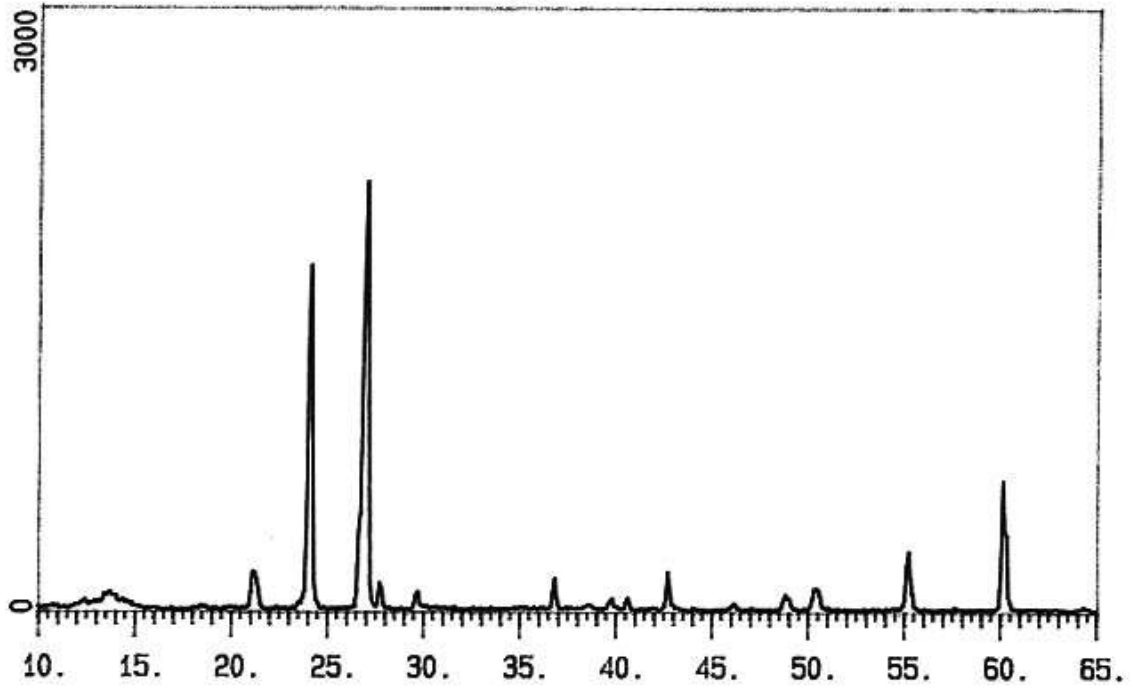
Pacoima 1



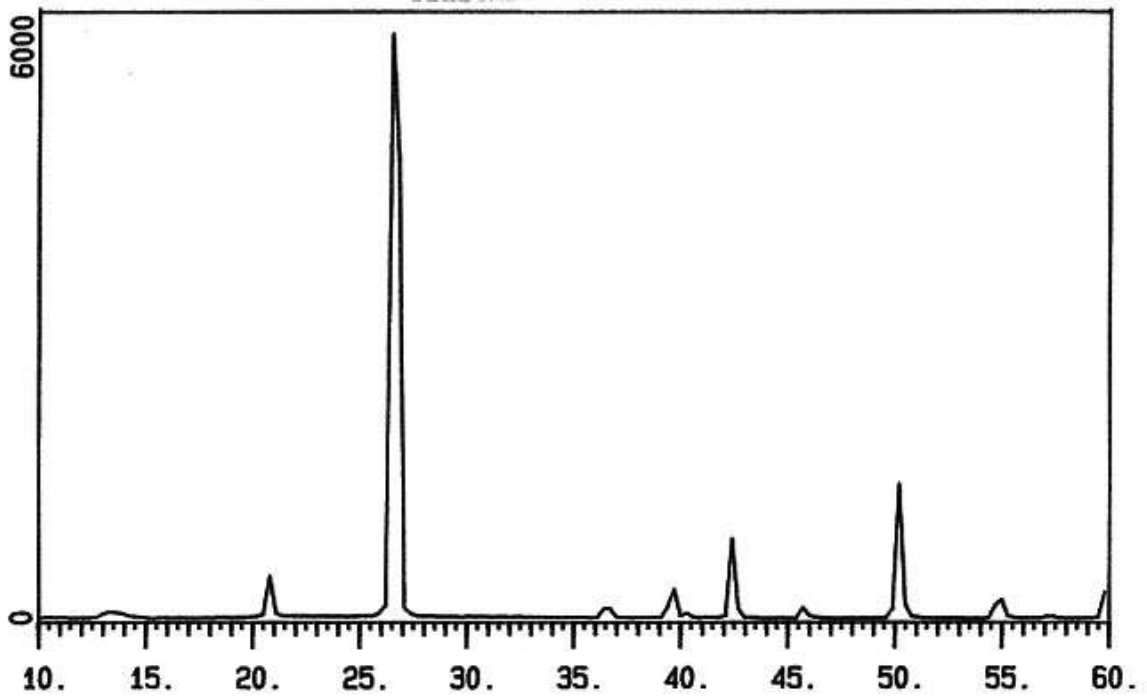
NSF



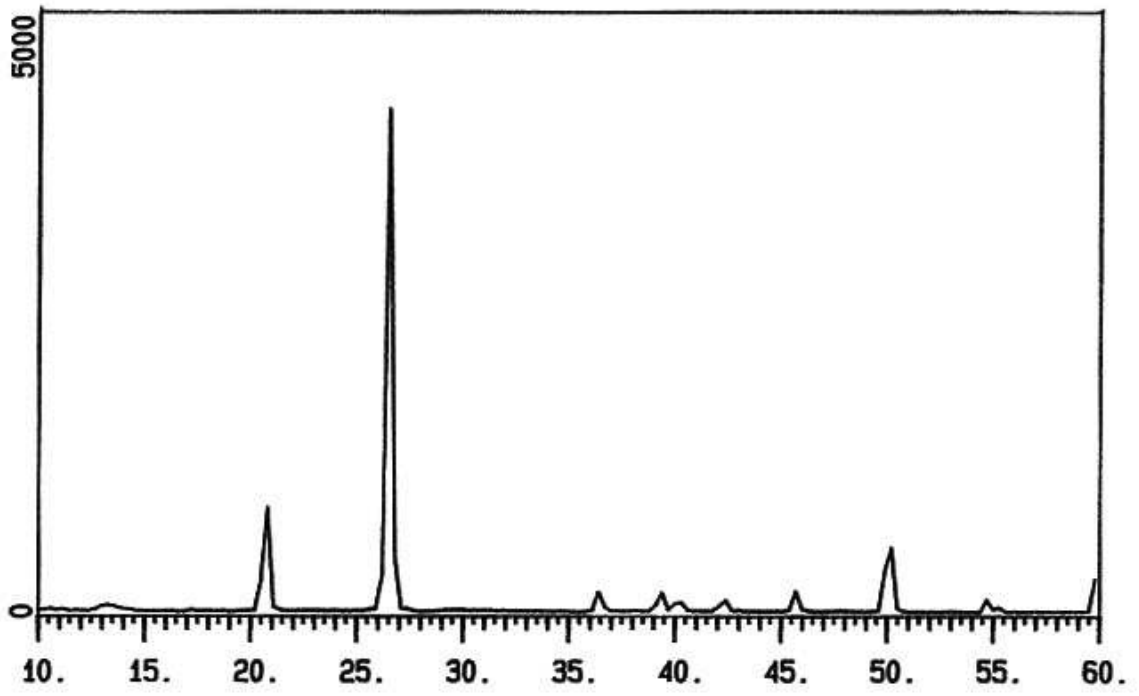
Pat Irwindale



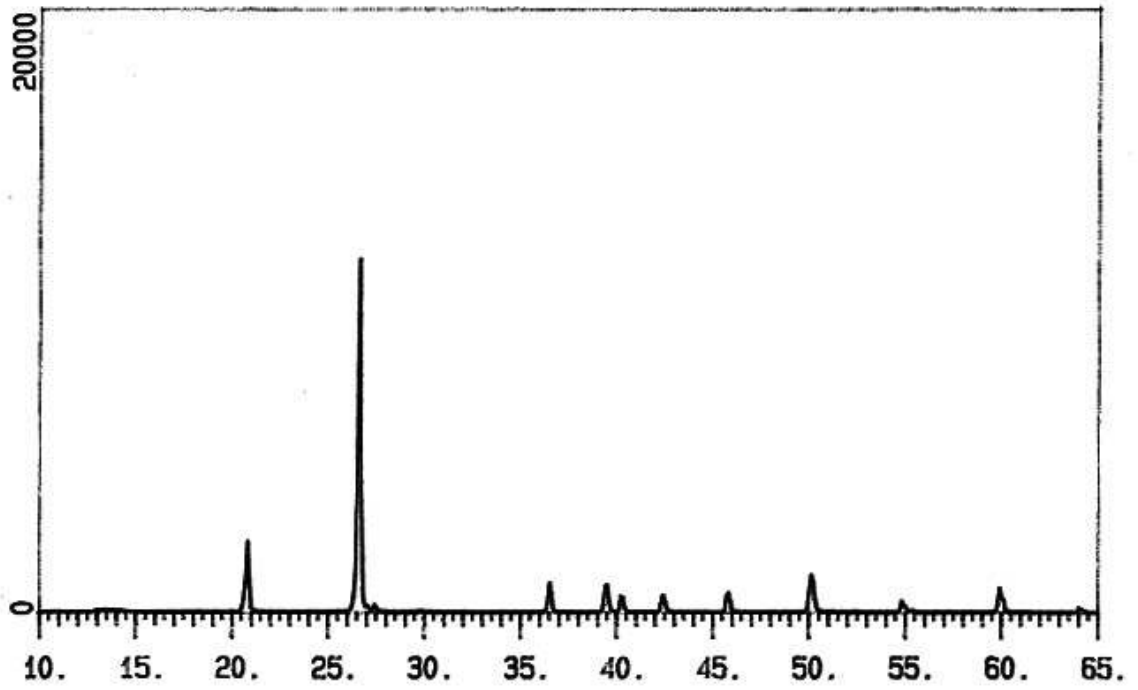
Silica # 30



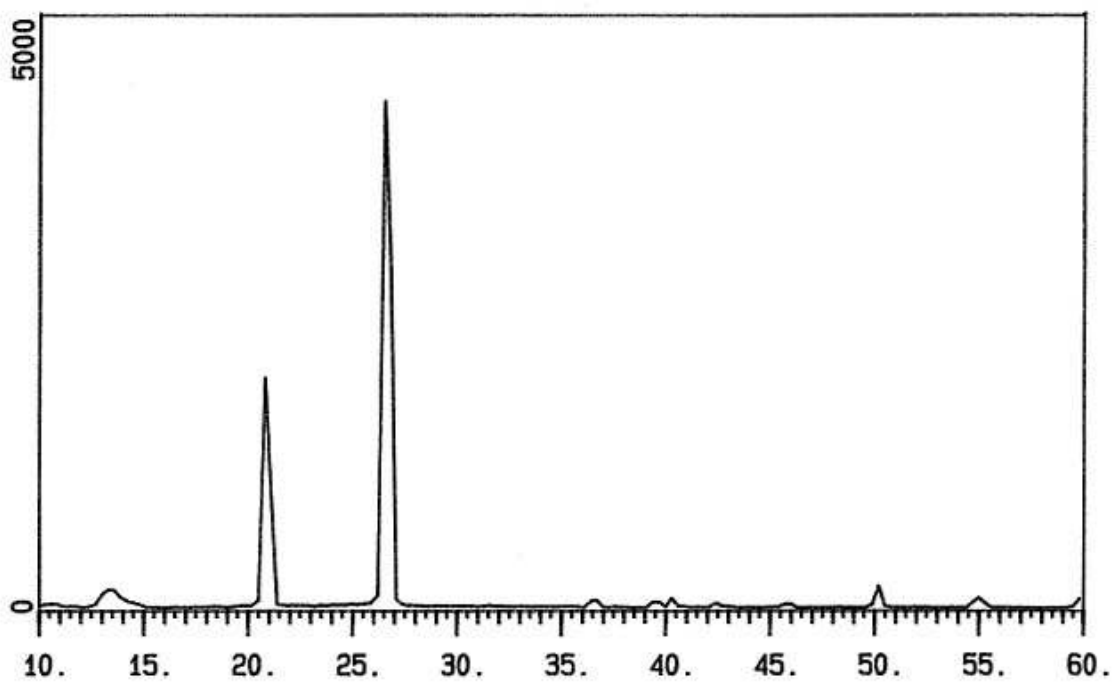
Silica # 1



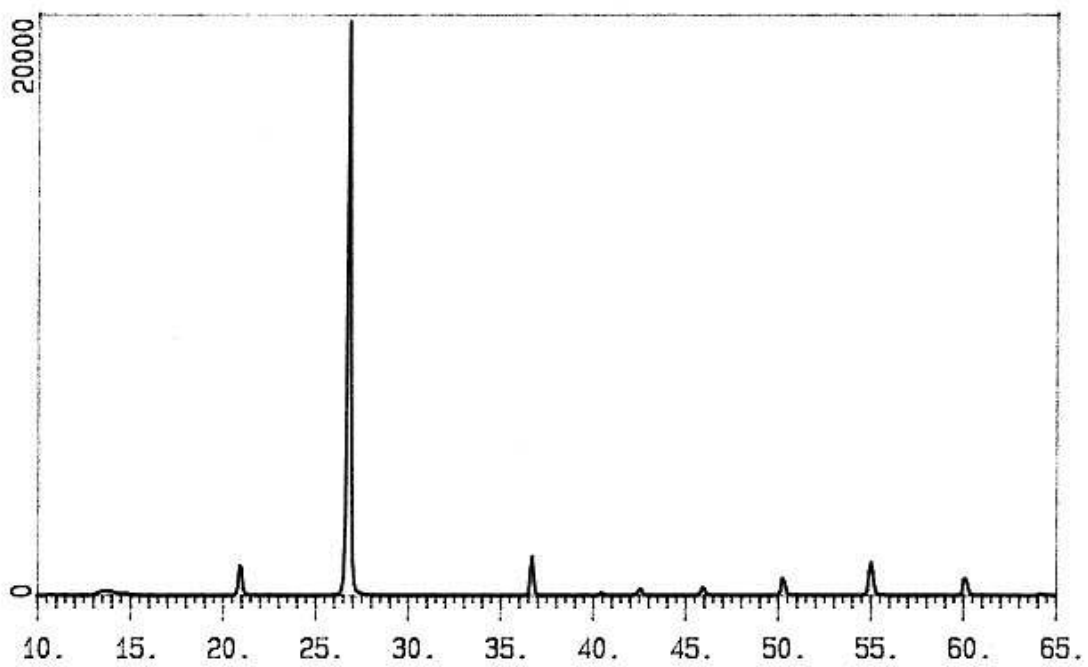
Silica # 2



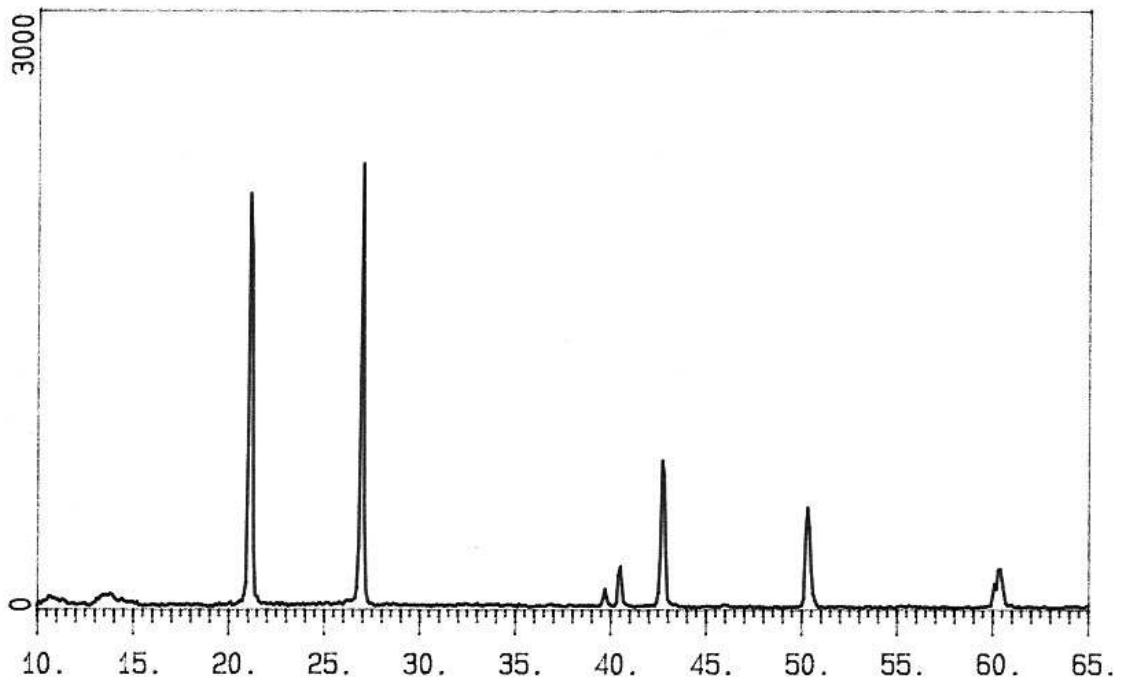
Nevada



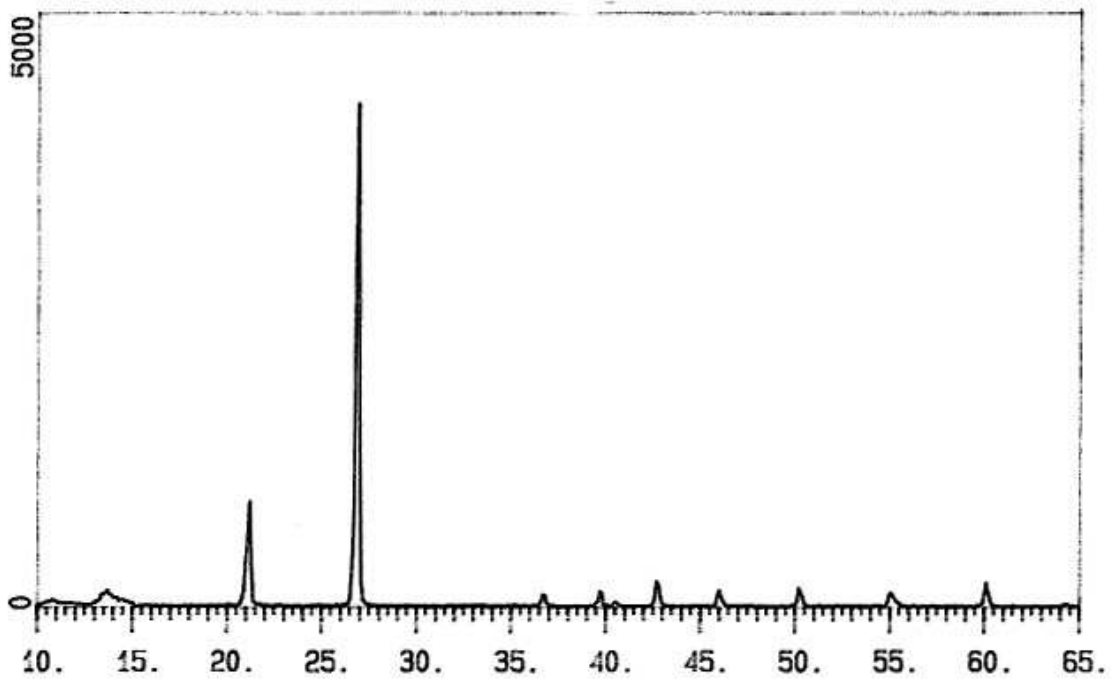
F-52



F-110

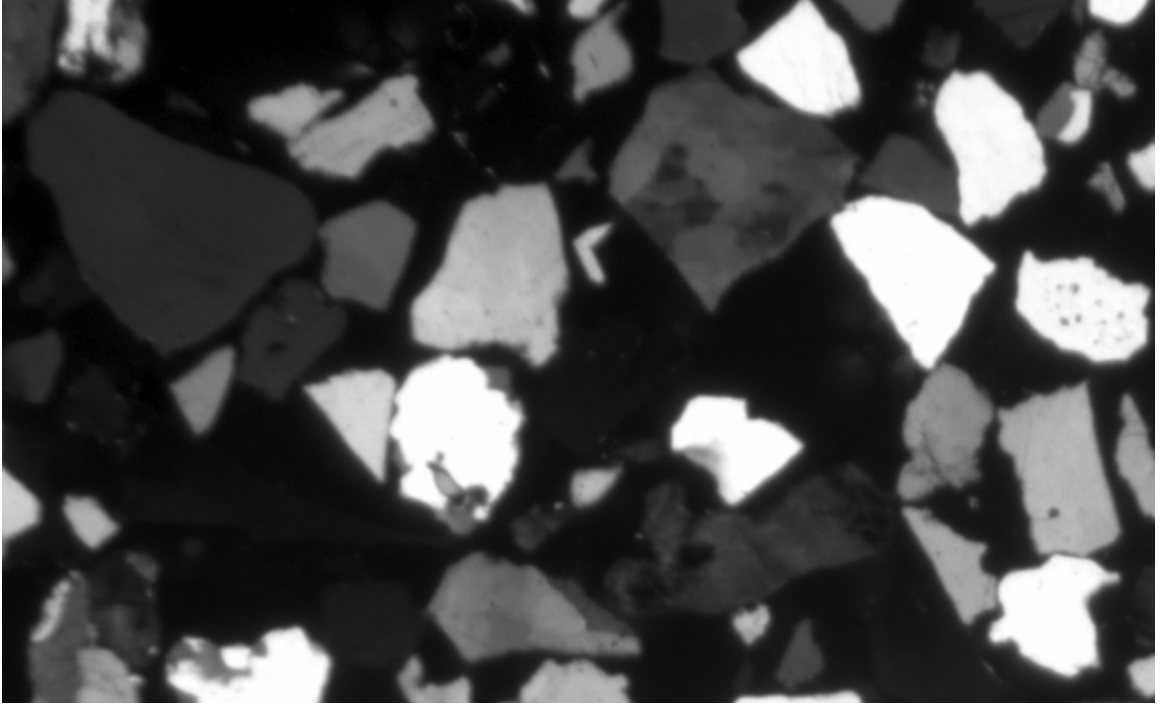


Flint # 13

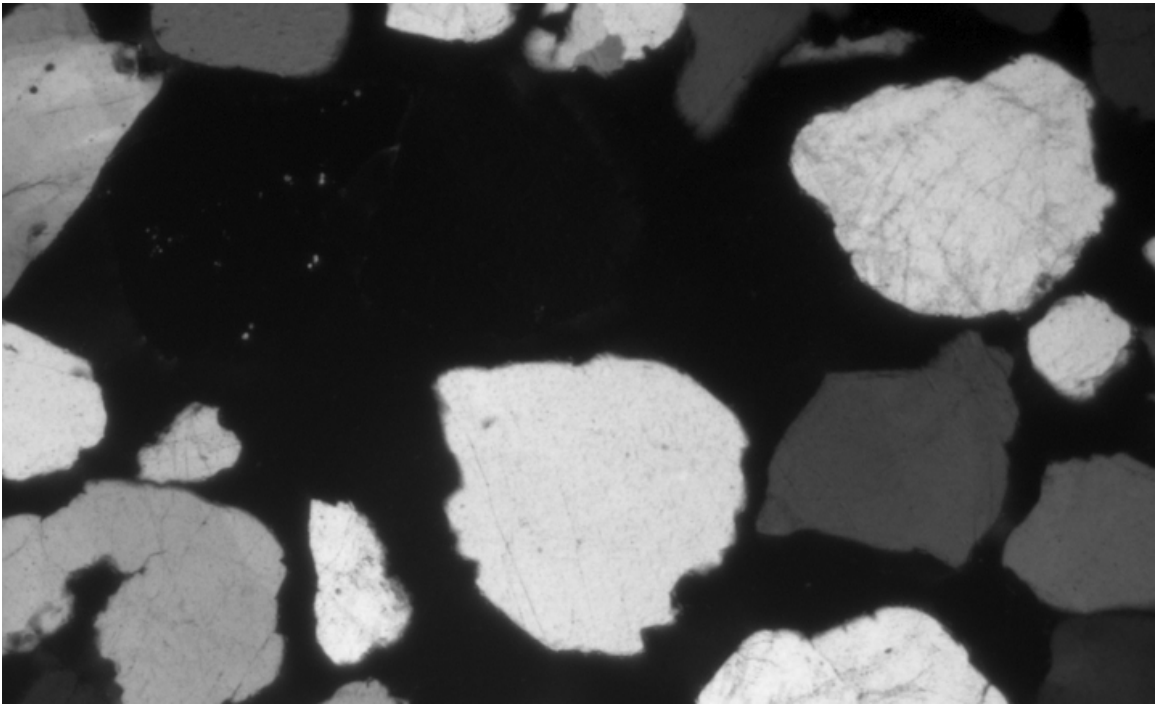


Flint #16

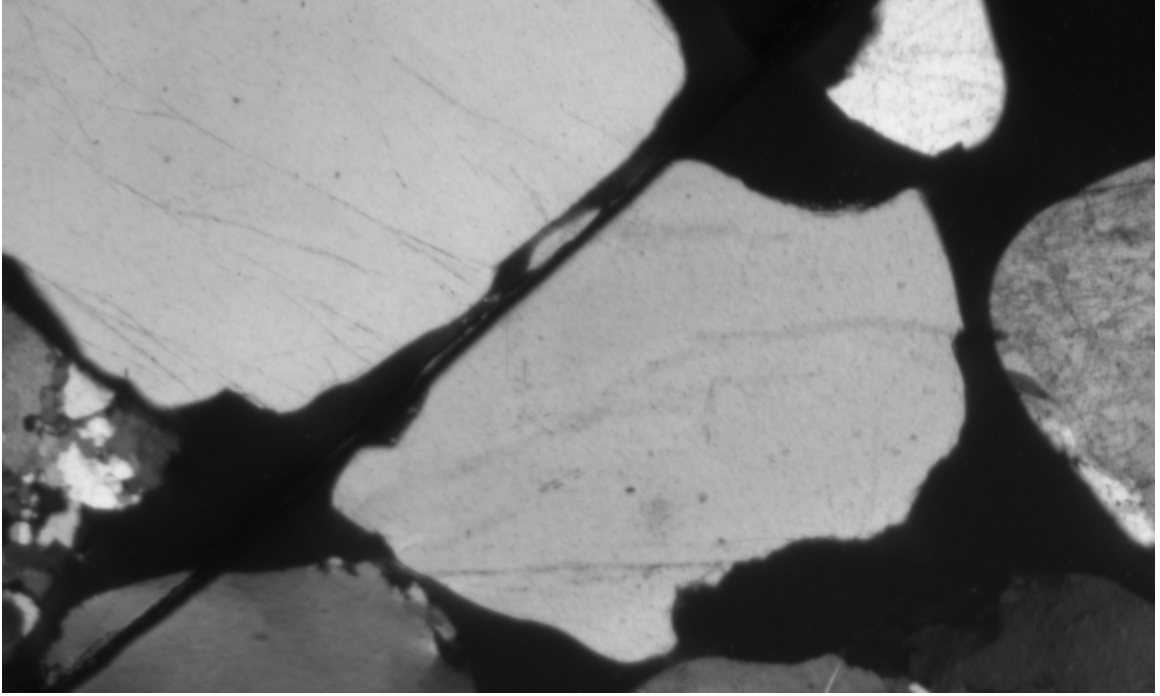
APPENDIX I
THIN SECTION RESULTS



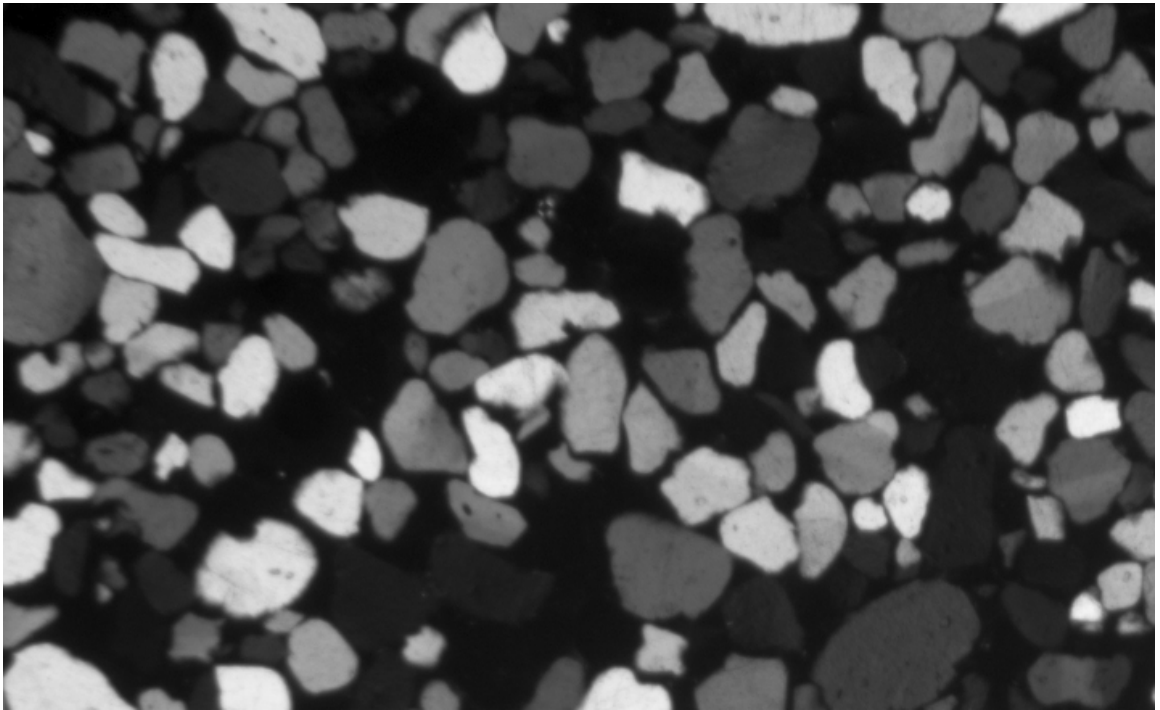
Silica 0



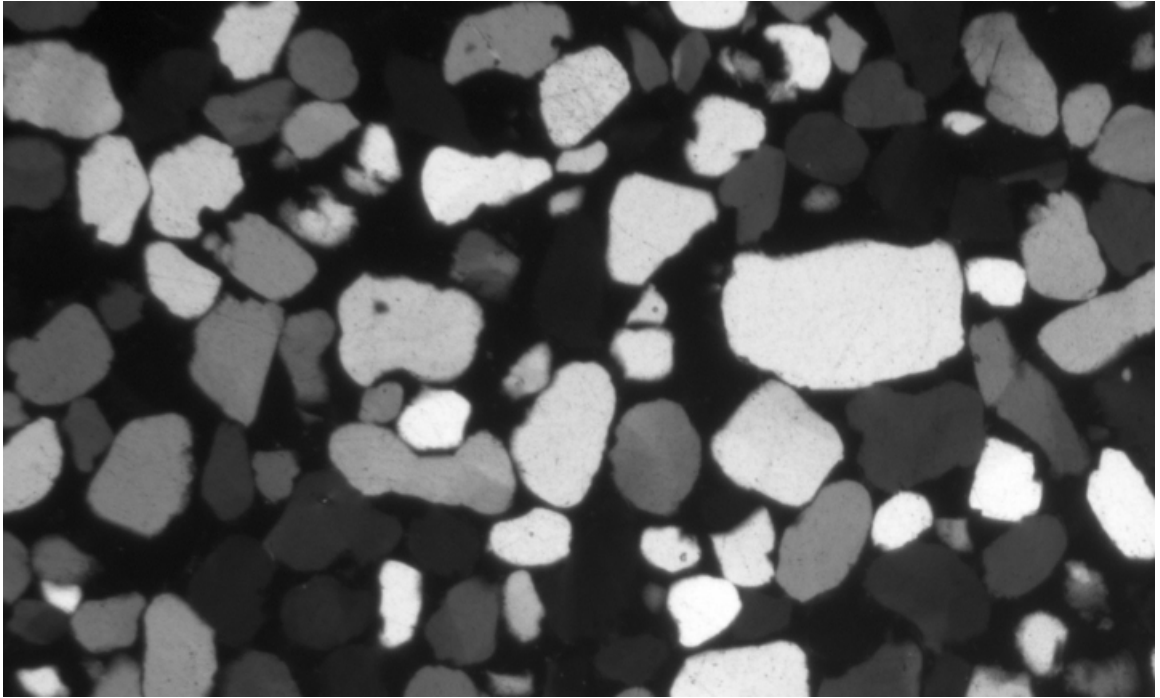
Crystal Silica 1



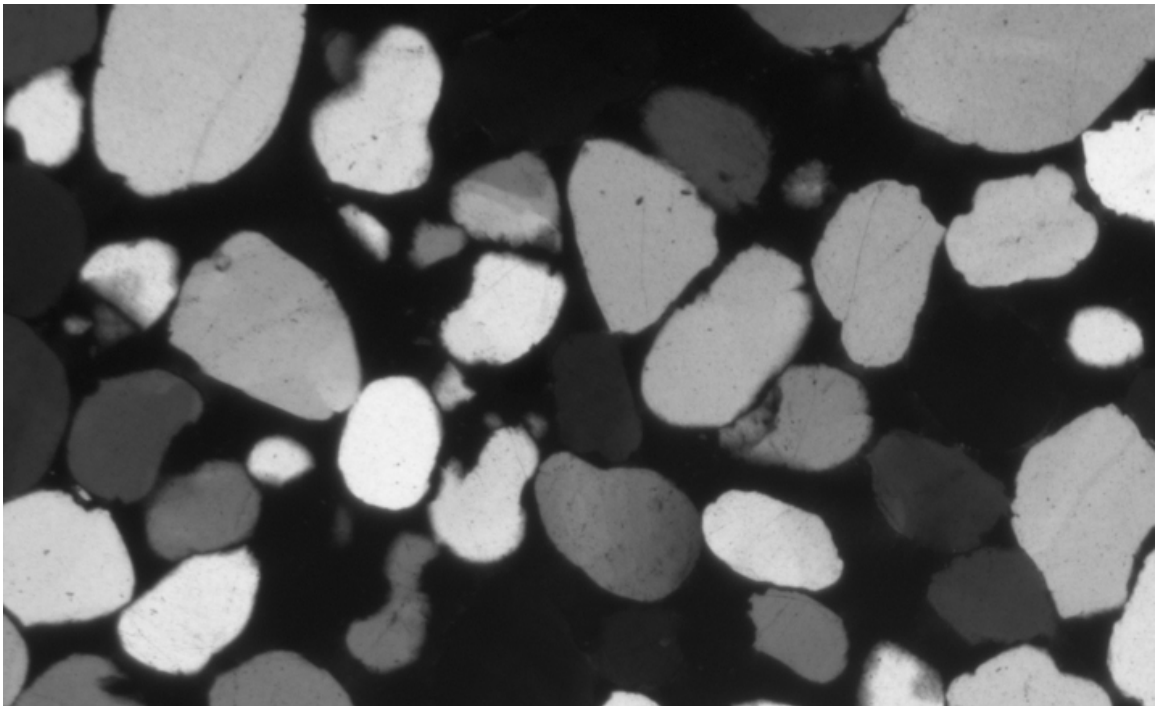
Silica 2



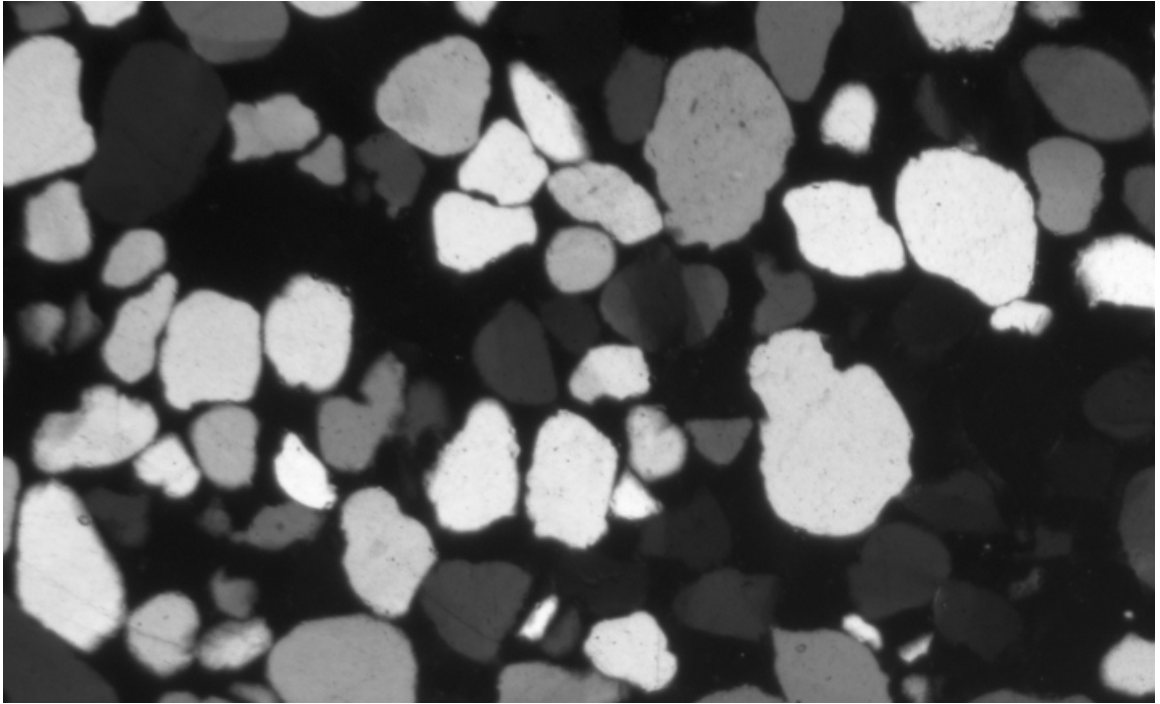
F-110



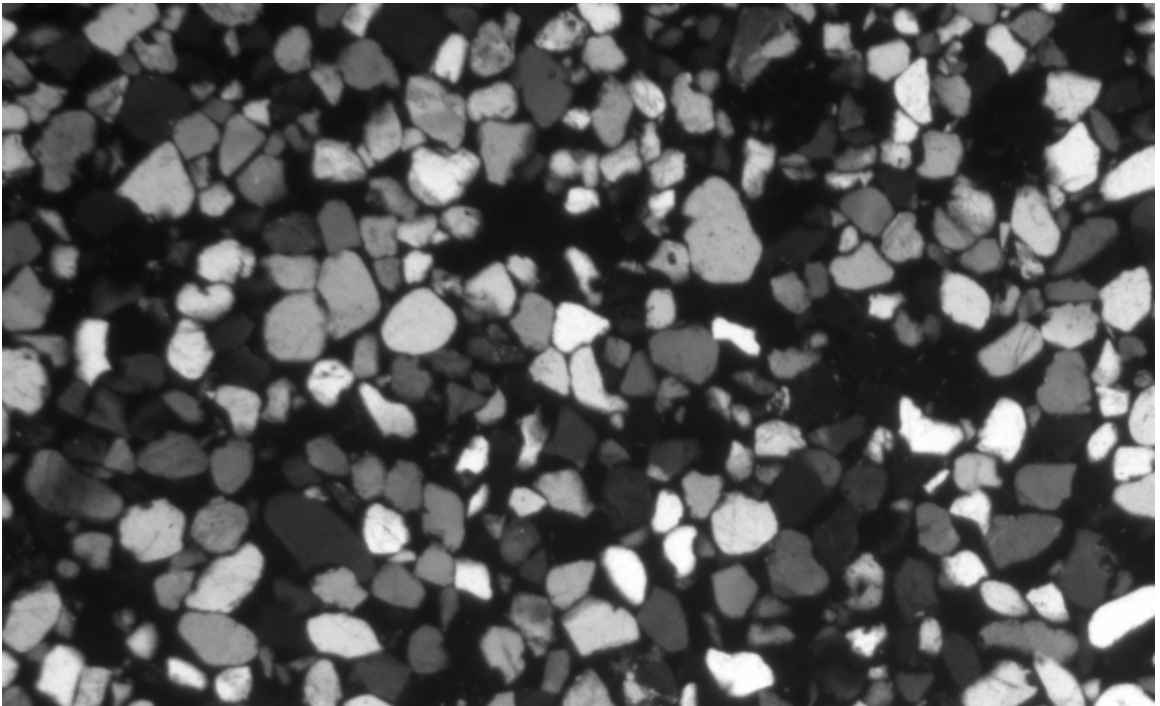
F-52



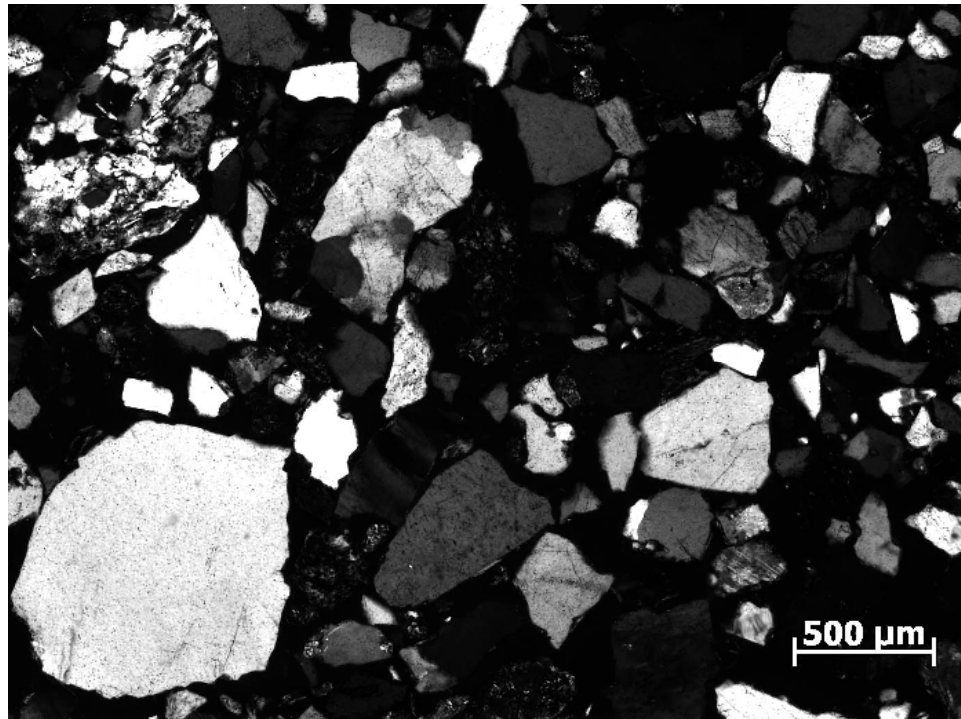
Flint - 13



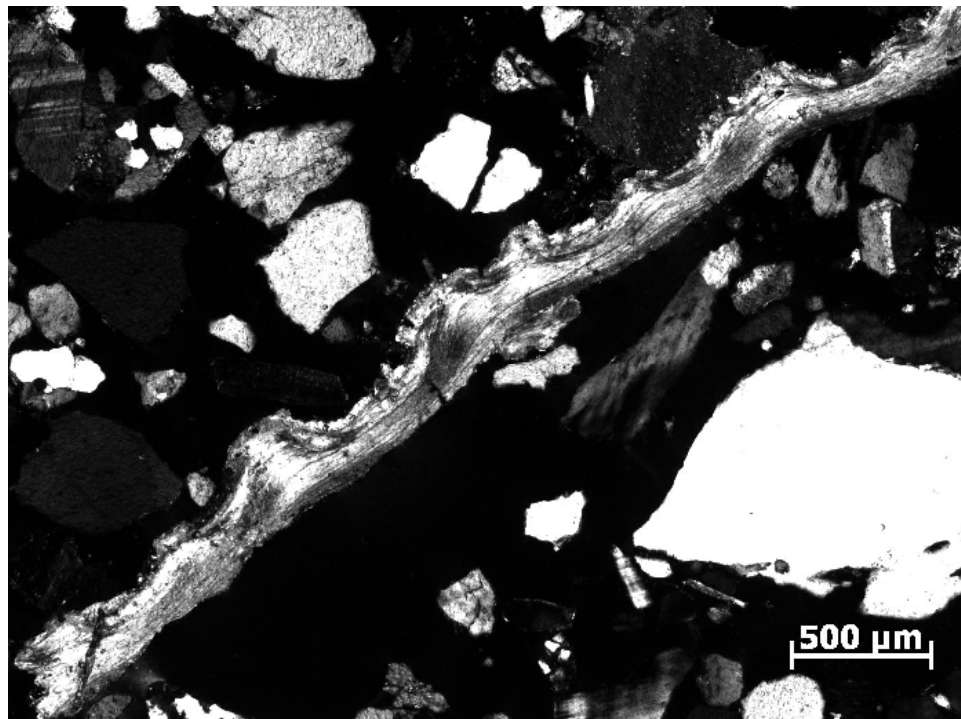
Flint - 16



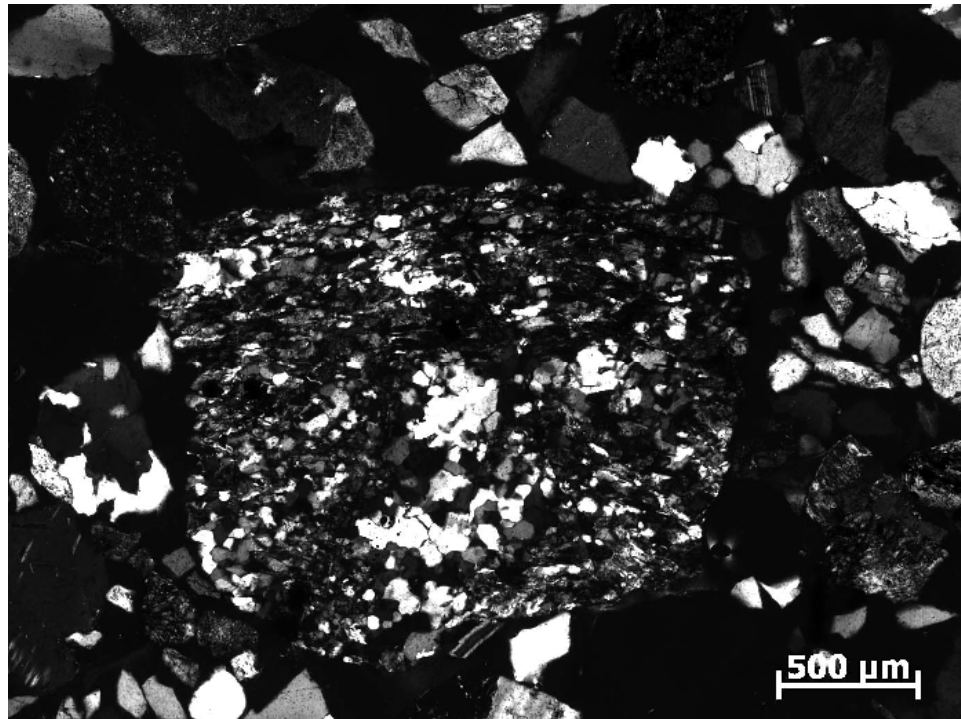
Nevada



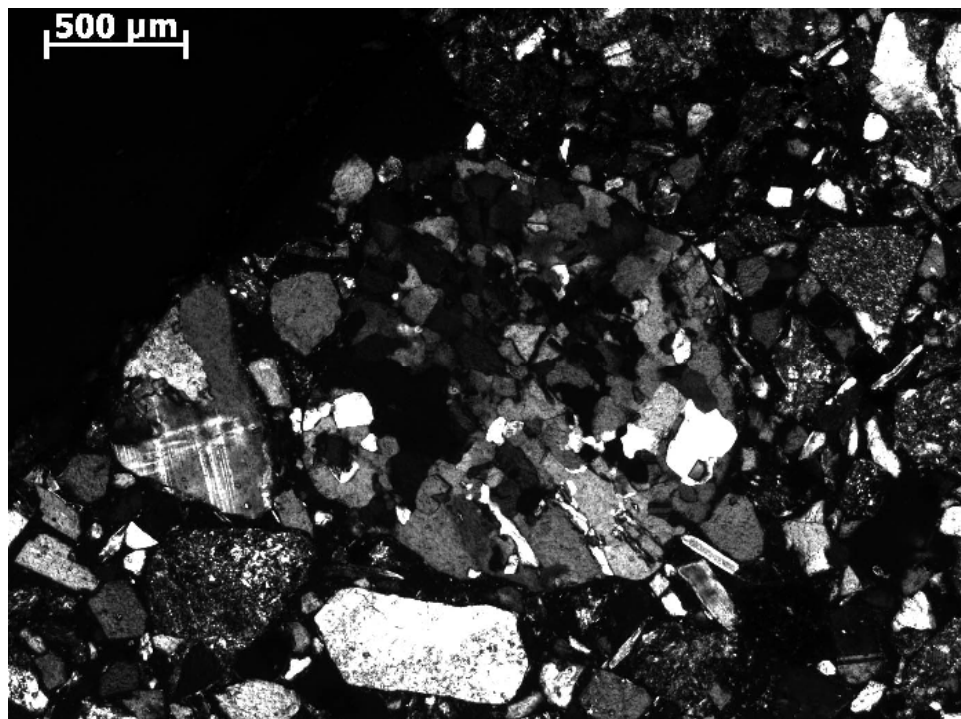
Pacoima 1



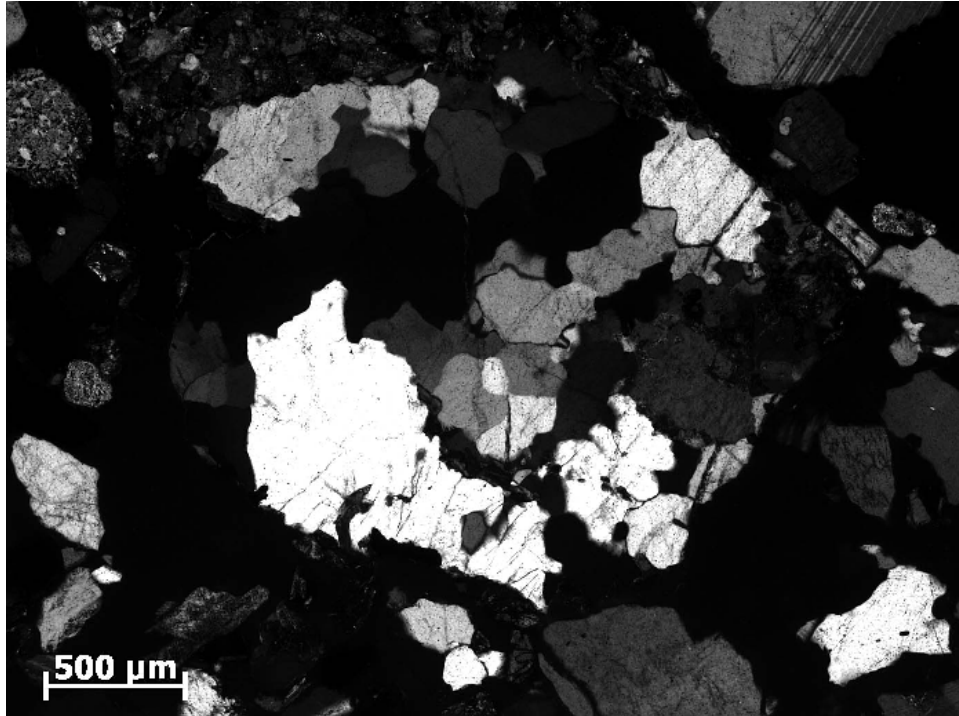
Pacoima 3



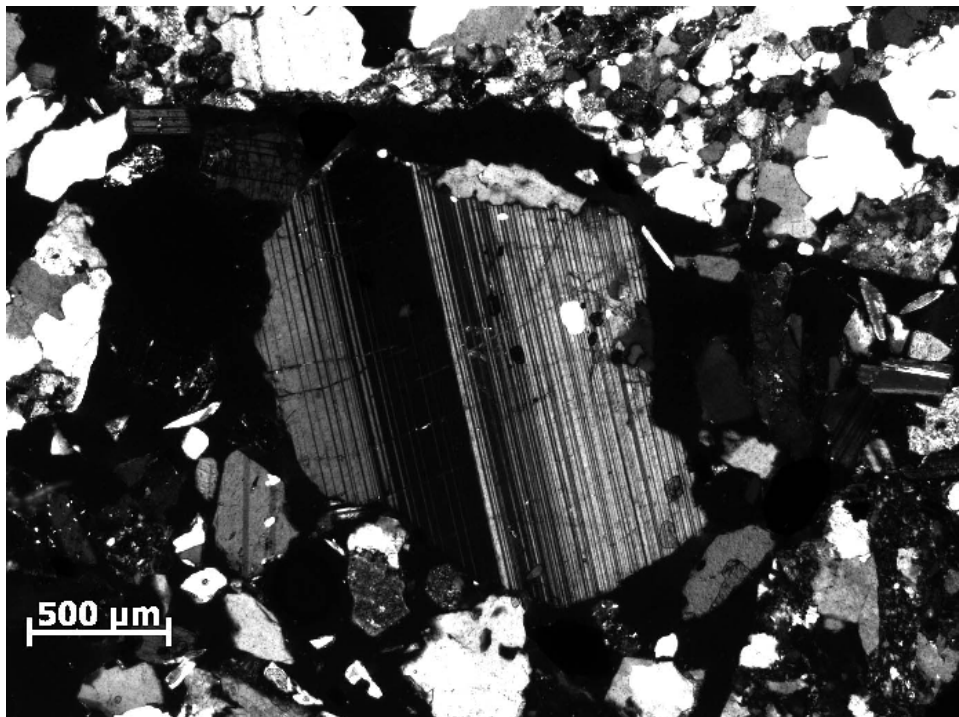
NSF



Newhall



Pat Irwindale



Post office